ISSN 1948-0210 (online)

World Journal of *Stem Cells*

World J Stem Cells 2020 January 26; 12(1): 1-99

Published by Baishideng Publishing Group Inc

WJSC

World Journal of Stem Cells

Contents

Monthly Volume 12 Number 1 January 26, 2020

World Journal of Stem Cells
Volume 12 Number 1 January 26, 2020

Contents

NAME OF JOURNAL
World Journal of Stem Cells

ISSN
ISSN 1948-0210 (online)

LAUNCH DATE
December 31, 2009

FREQUENCY
Monthly

EDITORS-IN-CHIEF
Tong Cao, Shengwen Calvin Li, Carlo Ventura

EDITORIAL BOARD MEMBERS
https://www.wjgnet.com/1948-0210/editorialboard.htm

EDITORIAL OFFICE
Jin-Lei Wang, Director

PUBLICATION DATE
January 26, 2020

INSTRUCTIONS TO AUTHORS
https://www.wjgnet.com/bpg/gerinfo/204

GUIDELINES FOR ETHICS DOCUMENTS
https://www.wjgnet.com/bpg/GerInfo/287

GUIDELINES FOR NON-NATIVE SPEAKERS OF ENGLISH
https://www.wjgnet.com/bpg/gerinfo/240

PUBLICATION MISCONDUCT
https://www.wjgnet.com/bpg/gerinfo/208

ARTICLE PROCESSING CHARGE
https://www.wjgnet.com/bpg/gerinfo/242

STEPS FOR SUBMITTING MANUSCRIPTS
https://www.wjgnet.com/bpg/GerInfo/239

ONLINE SUBMISSION
https://www.f6publishing.com

World Journal of Stem Cells

Submit a Manuscript: https://www.f6publishing.com

World J Stem Cells 2020 January 26; 12(1): 1-7

DOI: 10.4252/wjsc.v12.i1.1

ISSN 1948-0210 (online)

EDITORIAL

Adipose stromal/stem cells in regenerative medicine: Potentials and limitations

Leandra Santos Baptista

ORCID number: Leandra Santos Baptista (0000-0001-9998-8044).

Author contributions: Baptista LS drafted the article, contributed to the conception and design of the manuscript, wrote the manuscript and approved the final version of the article.

Supported by the Carlos Chagas Filho Foundation for Research Support of the State of Rio de Janeiro (FAPERJ), No. E-26/202.682/2018.

Conflict-of-interest statement: The author declares no conflict of interest.

Manuscript source: Invited manuscript

Received: June 4, 2019
Peer-review started: June 5, 2019
First decision: August 1,2019
Revised: October 11, 2019
Accepted: November 14, 2019
Article in press: November 14, 2019

Leandra Santos Baptista, Multidisciplinary Center for Biological Research (Numpex-Bio), Federal University of Rio de Janeiro (UFRJ) Campus Duque de Caxias, Duque de Caxias, RJ 25245-390, Brazil

Leandra Santos Baptista, Post-graduate Program in Biotechnology, National Institute of Metrology, Quality and Technology (INMETRO), Duque de Caxias, RJ 25250-020, Brazil

Leandra Santos Baptista, Post-graduate Program in Translational Biomedicine (Biotrans), Unigranrio, Campus I, Duque de Caxias, Duque de Caxias, RJ 25250-020, Brazil

Leandra Santos Baptista, Laboratory of Tissue Bioengineering, Directory of Metrology Applied to Life Sciences, National Institute of Metrology, Quality and Technology (INMETRO), Duque de Caxias, RJ 25250-020, Brazil

Corresponding author: Leandra Santos Baptista, PhD, Associate Professor, Laboratory of Tissue Bioengineering, Directory of Metrology Applied to Life Sciences, National Institute of Metrology, Quality and Technology (INMETRO), Duque de Caxias, RJ 25250-020, Brazil. leandrabaptista@xerem.ufrj.br

Abstract

This article presents the stem and progenitor cells from subcutaneous adipose tissue, briefly comparing them with their bone marrow counterparts, and discussing their potential for use in regenerative medicine. Subcutaneous adipose tissue differs from other mesenchymal stromal/stem cells (MSCs) sources in that it contains a pre-adipocyte population that dwells in the adventitia of robust blood vessels. Pre-adipocytes are present both in the stromal-vascular fraction (SVF; freshly isolated cells) and in the adherent fraction of adipose stromal/stem cells (ASCs; *in vitro* expanded cells), and have an active role on the chronic inflammation environment established in obesity, likely due their monocytic-macrophage lineage identity. The SVF and ASCs have been explored in cell therapy protocols with relative success, given their paracrine and immunomodulatory effects. Importantly, the widely explored multipotentiality of ASCs has direct application in bone, cartilage and adipose tissue engineering. The aim of this editorial is to reinforce the peculiarities of the stem and progenitor cells from subcutaneous adipose tissue, revealing the spheroids as a recently described biotechnological tool for cell therapy and tissue engineering. Innovative cell culture techniques, in particular 3D scaffold-free cultures such as spheroids, are now available to increase the potential for regeneration and differentiation of mesenchymal lineages. Spheroids are being explored not only as a model for cell differentiation, but also as powerful 3D cell culture tools to maintain the stemness and expand the regenerative and differentiation capacities

Published online: January 26, 2020

P-Reviewer: Garg M, Hernanda PY, Musumeci G
S-Editor: Dou Y
L-Editor: A
E-Editor: Zhang YL

of mesenchymal cell lineages.

Key words: Mesenchymal stromal/stem cells; Subcutaneous adipose tissue; Stromal-vascular fraction; Adipose stromal/stem cells; Regenerative medicine; Cell therapy; Tissue engineering; Spheroids

Core tip: Adipose tissue, notably subcutaneous, has a population of CD34-positive progenitor cells functionally known as pre-adipocytes. The pre-adipocytes have molecular and functional identities with the monocytic-macrophagic lineage and are altered in metabolic diseases such as obesity. To what extent will new 3D tools in cell culture, such as spheroids, be able to overcome the limitations imposed by 2D monolayer culture and unravel dormant capabilities of adipose stromal/stem cells?

Citation: Baptista LS. Adipose stromal/stem cells in regenerative medicine: Potentials and limitations. *World J Stem Cells* 2020; 12(1): 1-7
URL: https://www.wjgnet.com/1948-0210/full/v12/i1/1.htm
DOI: https://dx.doi.org/10.4252/wjsc.v12.i1.1

INTRODUCTION

Mesenchymal stromal/stem cells (MSCs) were first described and isolated from bone marrow as adherent colony-forming units of fibroblasts (CFU-F), and the primary role attributed to MSCs was to form niches for hematopoietic cells, supporting hematopoiesis[1]. In 1999, Pittenger *et al*[2] first described the *in vitro* multipotential nature of human bone marrow MSCs, introducing their use in cell therapy approaches, by delivering MSC suspensions to injury sites. The hypothesis was that MSCs were capable of tissue repair through grafting and differentiation into tissue-resident cells[3,4]. A few years later, an adipose tissue MSC population was described that shared some properties with MSCs isolated from the bone marrow, but had important unique characteristics[5,6].

Currently the widely accepted mechanism for tissue repair using bone marrow and adipose tissue sources (based on data from preclinical studies) is that MSCs interact with injured cells, creating tissue microenvironments or temporary niches that facilitate repair[7]. Thus, tissue regeneration by MSC transplantation may not rely exclusively on MSC differentiation, and the potential of MSCs to differentiate into multiple lineages is yet to be confirmed *in vivo*. In regenerative medicine approaches, the paracrine activity of MSCs fits well with cellular therapy protocols, while there *in vitro* multilineage potential is beneficial for tissue engineering. Furthermore, the "stemness" of MSCs and their *in vitro* multilineage potential can be optimized by cell culture conditions. The aim of this editorial is to reinforce the peculiarities of the stem and progenitor cells from subcutaneous adipose tissue, revealing the spheroids as a recently described biotechnological tool for cell therapy and tissue engineering. Spheroids are a 3D cell culture approach where cell clusters are formed in the absence of a scaffold (scaffold-free), optimizing cell-cell and cell-extracellular matrix interactions[8,9]. Recent studies have shown that culture as spheroids can be used to optimize the stemness and multilineage potential of MSCs[10], unraveling unknown characteristics of these cells, as well as opening new avenues for MSC use in regenerative medicine.

REVEALING THE POTENTIAL OF STROMAL CELL POPULATIONS IN SUBCUTANEOUS ADIPOSE TISSUE

The subcutaneous adipose tissue is composed of adipocytes and of a heterogeneous "stromal-vascular fraction" (SVF). These two main cell compartments can be separated by a centrifugation approach that results in the adipocytes floating as a layer, while SVFs sediment to the bottom of the tube. Previously, the SVF was known as a compartment containing cells capable of accumulating intracytoplasmic lipids *in vitro*[11]. Currently, the SVF is defined as a heterogeneous population containing pre-

adipocytes, endothelial mature cells, macrophages and fibroblasts. Furthermore, the SVF contains stem and progenitors cells showing different degrees of differentiation[12]. Due to their cell heterogeneity, the SVF is a major contributor to the unique molecular identity of the different depots of adipose tissue[13].

In 2001, Zuk *et al*[5] first described an MSC population in human subcutaneous adipose tissue isolated from the SVF. In 2013, the International Federation for Adipose Therapeutics and Science and the International Society for Cellular Therapy established the minimal definitions for stromal cells derived from subcutaneous adipose tissue[14]. The stromal cells within the SVF comprise heterogeneous cell types not amenable to culture *in vitro*, and a population of adherent, stromal/stem cells that can be culture *in vitro*. The latter are referred to as "adipose tissue derived stromal/stem cells" (ASCs), and this term will be used throughout this manuscript.

While ASCs were initially described as having the same *in vitro* multipotential nature, clonogenic potential (CFU-F) and similar surface markers as human bone marrow MSCs[15], differences between bone marrow and adipose MSCs emerged in subsequent publications (Table 1). Importantly, the tissue microenvironment differs significantly between the bone marrow and white adipose tissue. In these tissues, MSCs interacts with different neighboring cells, including an osteoblastic niche in the bone marrow[16] and cells from the more vascularized microenvironment in the white adipose tissue[6]. Consequently, bone marrow MSCs shows an intrinsic capacity to form bone and to support hematopoiesis after *in vivo* transplantation to ectopic sites[17], while ASCs have a superior angiogenic capacity[18]. Intriguingly, adipose tissue is also capable of supporting hematopoiesis (in a specific form), despite the remarkable differences in tissue microenvironment relative to the bone marrow[21]. In comparison with the MSC population derived from bone marrow after *in vitro* expansion, MSCs derived from subcutaneous adipose tissue can be distinguished by being positive for CD36 and negative for CD106[14]. Given the differences between bone marrow MSCs and ASCs, different morphogens are required and commonly used to induce the full range of multipotential differentiation of these cells *in vitro*.

Importantly, uncultured SVFs from subcutaneous adipose tissue contain a unique cell population: The pre-adipocytes[14]. These cells dwell in the adventitia of robust blood vessels and are identified as negative for the pan hematopoietic surface marker (CD45), the mesenchymal stem cell surface marker (CD146) and for the mature endothelial cell surface marker (CD31), being positive only for CD34[6]. Pre-adipocytes had already been identified in adipose tissue even before the discovery of the MSC population[11,22]. In mice, pre-adipocytes and macrophages both originate from the monocytic lineage (CD14 positive cells)[23]. In line with this observation, pre-adipocytes share some surface markers with macrophages, as well as having the capacity to acquire certain macrophage properties[24].

Macrophages, especially the tissue resident population (M2), have a crucial role in adipose tissue homeostasis[22]. This role is highlighted in obesity, where chronic inflammation leads to macrophage polarization from an M2 to an M1 phenotype, disrupting adipose tissue homeostasis[25]. This disruption also alters the behavior of pre-adipocyte, as well as increasing their frequency in early stages of obesity[26]. In our hands, the subcutaneous adipose tissue samples from obese individuals do not present alterations in the pre-adipocyte population *per se*, but have increased frequency of mesenchymal precursors in the SVF, and ASCs with altered behavior *in vitro*[27].

Our research group first showed that the frequency and size of blood vessels are increased in subcutaneous adipose tissue from ex-obese donors that have been subjected to bariatric surgery[28]. In addition to blood vessels alterations, we described a significant increase in the number of pre-adipocytes cells in the SVF, together with a more heterogeneous population of ASCs, containing pre-adipocytes[27]. The increase in pre-adipocyte frequency can be linked to the increase in the size of blood vessels, since robust vessels have the adventitia layer, where pre-adipocytes dwell[6]. Thus, adipose tissue from ex-obese individuals appears to keep a cellular "memory" of the inflammatory microenvironment of obese tissue, despite relevant clinical improvement in obesity[29].

Both fractions of subcutaneous adipose cells - SVF and ASCs - have been extensively used in clinical trials, mainly due their paracrine and immunomodulatory potentials; however some discrepancies between studies have emerged, mainly due donor-to-donor variability combined with differences between the protocols for cell isolation and expansion *in vitro*, highlighting the need to better characterize even the ASCs[30]. In spite of their apparent homogeneity *in vitro*, ASCs contain a population of pre-adipocytes whose true potential has not yet been fully elucidated, especially in obese and ex-obese subcutaneous adipose tissue samples.

Table 1 Differences of mesenchymal stromal/stem cell niche, cell subpopulations, mesenchymal stromal/stem cell surface *in vitro* markers and multipotentiality between bone marrow and adipose tissue

Tissue	MSC niche	Cell subpopulations	MSC *in vitro* surface markers	Multipotentiality
Bone marrow	Subendosteal and vascular	Osteoblasts, Endothelial progenitor and mature cells, Macrophages, MSCs	Positive: CD44, CD71, CD73, CD90, CD105, CD106, CD120a and	Adipogenic, Chondrogenic, and Osteogenic. Pre-committed into osteogenic lineage.
		Hematopoietic stem and progenitor cells, lymphocytes, megakaryocytes, erythrocytes, monocytes, neutrophils, basophils, eosinophils	CD124	
			Negative: CD14, CD34 and CD45	
Adipose tissue	Vascular	Adipocytes	Positive: CD13, CD29,	Adipogenic, Chondrogenic, and Osteogenic. Pre-committed into adipogenic lineage.
			CD44, CD73, CD34, CD36, CD90 and CD105	
		SVF: Pre-adipocytes, endothelial progenitor and mature cells, macrophages, fibroblasts, MSCs	Negative: CD31, CD45, CD235a and CD106	

MSCs: Mesenchymal stromal/stem cells; SVF: Stromal-vascular fraction.

ARE MULTIPOTENTIALITY AND PLURIPOTENTIALITY DEPENDENT ON CELL CULTURE CONDITIONS?

ASCs has been extensively described in the scientific literature as having their embryonic origin in a mesodermal progenitor population[31]. As a consequence, the typical multilineage capacity of ASCs represents their ability to form adipose tissue, bone and cartilage *in vitro*[14]. The multilineage capacity of ASCs has been extensively explored in tissue engineering, mainly by scaffold-based approaches. Recently, non-classical, scaffold-free approaches to tissue engineering have emerged that often rely on the production of 3D cell clusters called "spheroids"[32]. Spheroids mimic the embryonic stages of tissue development, optimizing the multilineage differentiation capacity of ASCs and MSCs (Figure 1). Moreover, spheroids are currently used not only as 3D culture models of cell differentiation *in vitro*, but also as a powerful cell culture tool to maintain the stemness and increase the regenerative, anti-inflammatory and angiogenic potentials of ASCs and MSCs[33]. The increase in the stemness of ASC and MSC spheroids (compared with 2D culture) is indicated by their higher multilineage potential, increased expression of pluripotency genes and late senescence[10], which reflect the cytoskeletal reorganization and expressive changes in cell morphology observed in spheroids[34]. However, the limitations of ASC and MSC spheroids comprise the low proliferation rate, causing *in vitro* cell expansion to still occur by monolayer culture. Furthermore, part of tissue engineering approaches intends to repair tissue critical-sized defects, requiring a scaffold.

Embryonic development in mammals starts with a cluster of epiblast stem cells[35]. Therefore, *in vitro* culture as spheroid-like cell clusters is used not only for embryonic stem cells, which are isolated from the early blastocyst stage, but also for induced pluripotent stem cells (iPSC) obtained by "reprogramming" adult somatic cells. Recapitulating embryogenesis, iPSCs initially form cell clusters that eventually become 3D cell aggregates representing spheroids.

A population of cells recently isolated from mesenchymal human tissue, named multilineage-differentiating stress enduring cells (Muse), is capable of forming pluripotent spheroid-like cell clusters[36] in the absence of *in vivo* tumorigenic capacity[37]. The differentiation of Muse cells for non-mesenchymal lineages relies on cell culture as clusters or spheroids, as well as on the use of a lower percentage of serum (or even on serum deprivation) during cell culture[38]. Human ASCs cultured in early passage under a lower percentage of autologous serum formed floating 3D spheroid-like cell clusters spontaneously[39]. Adipose-Muse cells differentiate into mesodermal, ectodermal and endodermal lineages, without teratoma formation[40].

The capacity of mature adipocytes to dedifferentiate and to differentiate into multiple cell lineages was already described before the identification of Adipose-

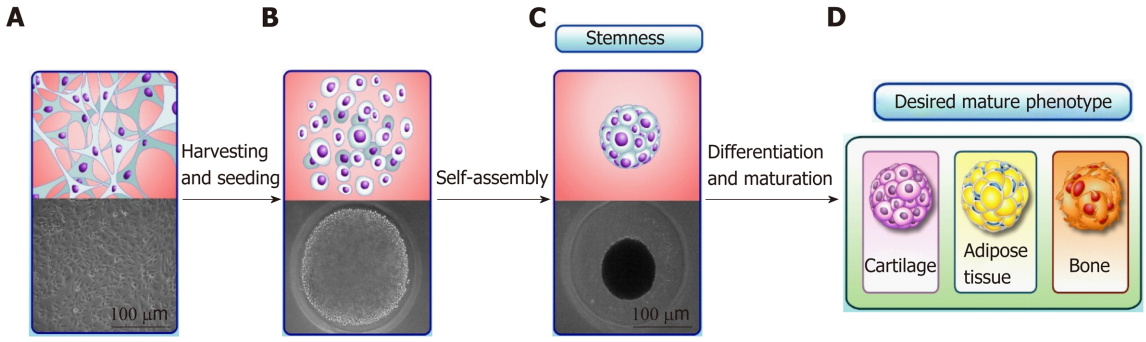

Figure 1 Spheroids mimic the embryonic stages of tissue development, optimizing the multilineage differentiation capacity of Adipose stromal/stem cells and mesenchymal stromal/stem cells. A: Adipose stromal/stem cells (ASCs) and mesenchymal stromal/stem cells (MSCs) can be harvested from monolayer and seeded into 3D culture plate dishes; B: The cell suspension starts to establish cell-cell interaction in a process known as self-assembly; C: The resulting spheroids containing cells and extracellular matrix components, are described for optimizing the stemness; D: Multilineage differentiation capacity of ASCs and MSCs under appropriate morphogens.

Muse cells[41,42], with some signs of pluripotency[36]. Accordingly, it is not surprising that spheroid-based culture, which is known to increase the stemness capacity of cells, may increase the potential of ASC differentiation beyond that expected for mesenchymal lineage cells. The major advantage in exploring the pluripotency of ASC spheroids will be their safety in regenerative medicine protocols, since some studies show the absence of teratoma formation after Adipose-Muse transplantation[40].

CONCLUDING REMARKS

In 2001, ASCs emerged as an accessible source of adult multipotent stem cells, showing high angiogenic and regenerative potential. The *in vitro* expansion of ASCs as monolayers may mask the multipotency and anti-inflammatory capacities of ASCs from obese and ex-obese donors. Embryonic development is marked by the formation of spheroid-like cell clusters, which can be mimicked *in vitro* by 3D culture as spheroids. Spheroid culture promises to reveal features of ASCs that were masked by culture in monolayers, including their pluripotency. In conclusion, ASC spheroids can be delivered into the injury site in an undifferentiated state due their regenerative potential or even as a tissue engineered construct, while allowing the use of obese and ex-obese ASCs in regenerative medicine protocols.

FUTURE DIRECTIONS

The transition from 2D monolayer culture of ASCs to 3D culture as spheroids brought previously unimaginable advantages. The next step is to translate the advantages of spheroid culture into novel therapeutic uses of ASCs in tissue regeneration and tissue engineering.

REFERENCES

1 **Friedenstein AJ**, Deriglasova UF, Kulagina NN, Panasuk AF, Rudakowa SF, Luriá EA, Ruadkow IA. Precursors for fibroblasts in different populations of hematopoietic cells as detected by the in vitro colony assay method. *Exp Hematol* 1974; **2**: 83-92 [PMID: 4455512]
2 **Pittenger MF**, Mackay AM, Beck SC, Jaiswal RK, Douglas R, Mosca JD, Moorman MA, Simonetti DW, Craig S, Marshak DR. Multilineage potential of adult human mesenchymal stem cells. *Science* 1999; **284**: 143-147 [PMID: 10102814 DOI: 10.1126/science.284.5411.143]
3 **Popp FC**, Piso P, Schlitt HJ, Dahlke MH. Therapeutic potential of bone marrow stem cells for liver diseases. *Curr Stem Cell Res Ther* 2006; **1**: 411-418 [PMID: 18220884 DOI: 10.2174/157488806778226759]
4 **Ohnishi S**, Ohgushi H, Kitamura S, Nagaya N. Mesenchymal stem cells for the treatment of heart failure. *Int J Hematol* 2007; **86**: 17-21 [PMID: 17675261 DOI: 10.1532/ijh97.07041]
5 **Zuk PA**, Zhu M, Mizuno H, Huang J, Futrell JW, Katz AJ, Benhaim P, Lorenz HP, Hedrick MH. Multilineage cells from human adipose tissue: implications for cell-based therapies. *Tissue Eng* 2001; **7**: 211-228 [PMID: 11304456 DOI: 10.1089/107632701300062859]
6 **Zimmerlin L**, Donnenberg VS, Pfeifer ME, Meyer EM, Péault B, Rubin JP, Donnenberg AD. Stromal vascular progenitors in adult human adipose tissue. *Cytometry A* 2010; **77**: 22-30 [PMID: 19852056 DOI: 10.1002/cyto.a.20813]

7 **Murphy MB**, Moncivais K, Caplan AI. Mesenchymal stem cells: environmentally responsive therapeutics for regenerative medicine. *Exp Mol Med* 2013; **45**: e54 [PMID: 24232253 DOI: 10.1038/emm.2013.94]

8 **Musumeci G**, Mobasheri A, Trovato FM, Szychlinska MA, Graziano AC, Lo Furno D, Avola R, Mangano S, Giuffrida R, Cardile V. Biosynthesis of collagen I, II, RUNX2 and lubricin at different time points of chondrogenic differentiation in a 3D in vitro model of human mesenchymal stem cells derived from adipose tissue. *Acta Histochem* 2014; **116**: 1407-1417 [PMID: 25307495 DOI: 10.1016/j.acthis.2014.09.008]

9 **Achilli TM**, Meyer J, Morgan JR. Advances in the formation, use and understanding of multi-cellular spheroids. *Expert Opin Biol Ther* 2012; **12**: 1347-1360 [PMID: 22784238 DOI: 10.1517/14712598.2012.707181]

10 **Cesarz Z**, Tamama K. Spheroid Culture of Mesenchymal Stem Cells. *Stem Cells Int* 2016; **2016**: 9176357 [PMID: 26649054 DOI: 10.1155/2016/9176357]

11 **Glick JM**, Rothblat GH. Effects of metabolic inhibitors on the synthesis and release of lipoprotein lipase in cultured cells derived from the stromal-vascular fraction of rat adipose tissue. *Biochim Biophys Acta* 1980; **618**: 163-172 [PMID: 7378429 DOI: 10.1016/0005-2760(80)90063-6]

12 **Casteilla L**, Charrière G, Laharrague P, Cousin B, Planat-Benard V, Péricaud L, Chavoin JP. [Adipose tissue, plastic and reconstructive surgery: come back to sources]. *Ann Chir Plast Esthet* 2004; **49**: 409-418 [PMID: 15518941 DOI: 10.1016/j.anplas.2004.08.001]

13 **Peinado JR**, Jimenez-Gomez Y, Pulido MR, Ortega-Bellido M, Diaz-Lopez C, Padillo FJ, Lopez-Miranda J, Vazquez-Martínez R, Malagón MM. The stromal-vascular fraction of adipose tissue contributes to major differences between subcutaneous and visceral fat depots. *Proteomics* 2010; **10**: 3356-3366 [PMID: 20706982 DOI: 10.1002/pmic.201000350]

14 **Bourin P**, Bunnell BA, Casteilla L, Dominici M, Katz AJ, March KL, Redl H, Rubin JP, Yoshimura K, Gimble JM. Stromal cells from the adipose tissue-derived stromal vascular fraction and culture expanded adipose tissue-derived stromal/stem cells: a joint statement of the International Federation for Adipose Therapeutics and Science (IFATS) and the International Society for Cellular Therapy (ISCT). *Cytotherapy* 2013; **15**: 641-648 [PMID: 23570660 DOI: 10.1016/j.jcyt.2013.02.006]

15 **Fraser JK**, Schreiber RE, Zuk PA, Hedrick MH. Adult stem cell therapy for the heart. *Int J Biochem Cell Biol* 2004; **36**: 658-666 [PMID: 15010330 DOI: 10.1016/j.biocel.2003.10.018]

16 **Balduino A**, Mello-Coelho V, Wang Z, Taichman RS, Krebsbach PH, Weeraratna AT, Becker KG, de Mello W, Taub DD, Borojevic R. Molecular signature and in vivo behavior of bone marrow endosteal and subendosteal stromal cell populations and their relevance to hematopoiesis. *Exp Cell Res* 2012; **318**: 2427-2437 [PMID: 22841688 DOI: 10.1016/j.yexcr.2012.07.009]

17 **Charbord P**, Livne E, Gross G, Häupl T, Neves NM, Marie P, Bianco P, Jorgensen C. Human bone marrow mesenchymal stem cells: a systematic reappraisal via the genostem experience. *Stem Cell Rev Rep* 2011; **7**: 32-42 [PMID: 20198518 DOI: 10.1007/s12015-010-9125-6]

18 **Casteilla L**, Planat-Bénard V, Dehez S, De Barros S, Barreau C, André M. Endothelial and cardiac regeneration from adipose tissues. *Methods Mol Biol* 2011; **702**: 269-287 [PMID: 21082409 DOI: 10.1007/978-1-61737-960-4_20]

19 **Lucas D**. The Bone Marrow Microenvironment for Hematopoietic Stem Cells. *Adv Exp Med Biol* 2017; **1041**: 5-18 [PMID: 29204826 DOI: 10.1007/978-3-319-69194-7_2]

20 **Polymeri A**, Giannobile WV, Kaigler D. Bone Marrow Stromal Stem Cells in Tissue Engineering and Regenerative Medicine. *Horm Metab Res* 2016; **48**: 700-713 [PMID: 27871114 DOI: 10.1055/s-0042-118458]

21 **Cousin B**, Casteilla L, Laharrague P, Luche E, Lorsignol A, Cuminetti V, Paupert J. Immuno-metabolism and adipose tissue: The key role of hematopoietic stem cells. *Biochimie* 2016; **124**: 21-26 [PMID: 26107410 DOI: 10.1016/j.biochi.2015.06.012]

22 **Cousin B**, Munoz O, Andre M, Fontanilles AM, Dani C, Cousin JL, Laharrague P, Casteilla L, Pénicaud L. A role for preadipocytes as macrophage-like cells. *FASEB J* 1999; **13**: 305-312 [PMID: 9973318 DOI: 10.1096/fasebj.13.2.305]

23 **Luche E**, Cousin B, Garidou L, Serino M, Waget A, Barreau C, André M, Valet P, Courtney M, Casteilla L, Burcelin R. Metabolic endotoxemia directly increases the proliferation of adipocyte precursors at the onset of metabolic diseases through a CD14-dependent mechanism. *Mol Metab* 2013; **2**: 281-291 [PMID: 24049740 DOI: 10.1016/j.molmet.2013.06.005]

24 **Charrière G**, Cousin B, Arnaud E, André M, Bacou F, Penicaud L, Casteilla L. Preadipocyte conversion to macrophage. Evidence of plasticity. *J Biol Chem* 2003; **278**: 9850-9855 [PMID: 12519759 DOI: 10.1074/jbc.M210811200]

25 **Chinetti-Gbaguidi G**, Staels B. Macrophage polarization in metabolic disorders: functions and regulation. *Curr Opin Lipidol* 2011; **22**: 365-372 [PMID: 21825981 DOI: 10.1097/MOL.0b013e32834a77b4]

26 **Martyniak K**, Masternak MM. Changes in adipose tissue cellular composition during obesity and aging as a cause of metabolic dysregulation. *Exp Gerontol* 2017; **94**: 59-63 [PMID: 27939445 DOI: 10.1016/j.exger.2016.12.007]

27 **Silva KR**, Liechocki S, Carneiro JR, Claudio-da-Silva C, Maya-Monteiro CM, Borojevic R, Baptista LS. Stromal-vascular fraction content and adipose stem cell behavior are altered in morbid obese and post bariatric surgery ex-obese women. *Stem Cell Res Ther* 2015; **6**: 72 [PMID: 25884374 DOI: 10.1186/s13287-015-0029-x]

28 **Baptista LS**, da Silva KR, da Pedrosa CS, Claudio-da-Silva C, Carneiro JR, Aniceto M, de Mello-Coelho V, Takiya CM, Rossi MI, Borojevic R. Adipose tissue of control and ex-obese patients exhibit differences in blood vessel content and resident mesenchymal stem cell population. *Obes Surg* 2009; **19**: 1304-1312 [PMID: 19562421 DOI: 10.1007/s11695-009-9899-2]

29 **Baptista LS**, Silva KR, Borojevic R. Obesity and weight loss could alter the properties of adipose stem cells? *World J Stem Cells* 2015; **7**: 165-173 [PMID: 25621116 DOI: 10.4252/wjsc.v7.i1.165]

30 **Bajek A**, Gurtowska N, Olkowska J, Kazmierski L, Maj M, Drewa T. Adipose-Derived Stem Cells as a Tool in Cell-Based Therapies. *Arch Immunol Ther Exp (Warsz)* 2016; **64**: 443-454 [PMID: 27178663 DOI: 10.1007/s00005-016-0394-x]

31 **Sági B**, Maraghechi P, Urbán VS, Hegyi B, Szigeti A, Fajka-Boja R, Kudlik G, Német K, Monostori E, Gócza E, Uher F. Positional identity of murine mesenchymal stem cells resident in different organs is determined in the postsegmentation mesoderm. *Stem Cells Dev* 2012; **21**: 814-828 [PMID: 22149974 DOI: 10.1089/scd.2011.0551]

32 **Ovsianikov A**, Khademhosseini A, Mironov V. The Synergy of Scaffold-Based and Scaffold-Free Tissue Engineering Strategies. *Trends Biotechnol* 2018; **36**: 348-357 [PMID: 29475621 DOI:

10.1016/j.tibtech.2018.01.005]
33 **Laschke MW**, Menger MD. Life is 3D: Boosting Spheroid Function for Tissue Engineering. *Trends Biotechnol* 2017; **35**: 133-144 [PMID: 27634310 DOI: 10.1016/j.tibtech.2016.08.004]
34 **Zhou Y**, Chen H, Li H, Wu Y. 3D culture increases pluripotent gene expression in mesenchymal stem cells through relaxation of cytoskeleton tension. *J Cell Mol Med* 2017; **21**: 1073-1084 [PMID: 28276635 DOI: 10.1111/jcmm.12946]
35 **Shahbazi MN**, Scialdone A, Skorupska N, Weberling A, Recher G, Zhu M, Jedrusik A, Devito LG, Noli L, Macaulay IC, Buecker C, Khalaf Y, Ilic D, Voet T, Marioni JC, Zernicka-Goetz M. Pluripotent state transitions coordinate morphogenesis in mouse and human embryos. *Nature* 2017; **552**: 239-243 [PMID: 29186120 DOI: 10.1038/nature24675]
36 **Jumabay M**, Boström KI. Dedifferentiated fat cells: A cell source for regenerative medicine. *World J Stem Cells* 2015; **7**: 1202-1214 [PMID: 26640620 DOI: 10.4252/wjsc.v7.i10.1202]
37 **Kuroda Y**, Kitada M, Wakao S, Nishikawa K, Tanimura Y, Makinoshima H, Goda M, Akashi H, Inutsuka A, Niwa A, Shigemoto T, Nabeshima Y, Nakahata T, Nabeshima Y, Fujiyoshi Y, Dezawa M. Unique multipotent cells in adult human mesenchymal cell populations. *Proc Natl Acad Sci USA* 2010; **107**: 8639-8643 [PMID: 20421459 DOI: 10.1073/pnas.0911647107]
38 **Labusca L**, Mashayekhi K. Human adult pluripotency: Facts and questions. *World J Stem Cells* 2019; **11**: 1-12 [PMID: 30705711 DOI: 10.4252/wjsc.v11.i1.1]
39 **Bogdanova-Jatniece A**, Berzins U, Kozlovska T. Growth Properties and Pluripotency Marker Expression of Spontaneously Formed Three-dimensional Aggregates of Human Adipose-derived Stem Cells. *Int J Stem Cells* 2014; **7**: 143-152 [PMID: 25473452 DOI: 10.15283/ijsc.2014.7.2.143]
40 **Ogura F**, Wakao S, Kuroda Y, Tsuchiyama K, Bagheri M, Heneidi S, Chazenbalk G, Aiba S, Dezawa M. Human adipose tissue possesses a unique population of pluripotent stem cells with nontumorigenic and low telomerase activities: potential implications in regenerative medicine. *Stem Cells Dev* 2014; **23**: 717-728 [PMID: 24256547 DOI: 10.1089/scd.2013.0473]
41 **Planat-Benard V**, Silvestre JS, Cousin B, André M, Nibbelink M, Tamarat R, Clergue M, Manneville C, Saillan-Barreau C, Duriez M, Tedgui A, Levy B, Pénicaud L, Casteilla L. Plasticity of human adipose lineage cells toward endothelial cells: physiological and therapeutic perspectives. *Circulation* 2004; **109**: 656-663 [PMID: 14734516 DOI: 10.1161/01.CIR.0000114522.38265.61]
42 **Matsumoto T**, Kano K, Kondo D, Fukuda N, Iribe Y, Tanaka N, Matsubara Y, Sakuma T, Satomi A, Otaki M, Ryu J, Mugishima H. Mature adipocyte-derived dedifferentiated fat cells exhibit multilineage potential. *J Cell Physiol* 2008; **215**: 210-222 [PMID: 18064604 DOI: 10.1002/jcp.21304]

World Journal of Stem Cells

Submit a Manuscript: https://www.f6publishing.com

World J Stem Cells 2020 January 26; 12(1): 8-24

DOI: 10.4252/wjsc.v12.i1.8

ISSN 1948-0210 (online)

REVIEW

Regeneration of the central nervous system-principles from brain regeneration in adult zebrafish

Alessandro Zambusi, Jovica Ninkovic

ORCID number: Alessandro Zambusi (0000-0003-4764-8448); Jovica Ninkovic (0000-0002-4381-0041).

Author contributions: All authors contributed equally to this paper in conception and design of the study; literature review and analysis; drafting, critical revision and editing; and approval of the final version.

Supported by the German Research foundation (DFG), No. SFB 870.

Conflict-of-interest statement: The authors declare no potential conflicts of interest.

Manuscript source: Invited Manuscript

Received: August 9, 2019
Peer-review started: August 9, 2019
First decision: August 30, 2019
Revised: November 25, 2019
Accepted: December 13, 2019
Article in press: December 13, 2019
Published online: January 26, 2020

Alessandro Zambusi, Jovica Ninkovic, Helmholtz Center Munich, Biomedical Center, Inst Stem Cell Res, Institute of Stem Cell Research, Department of Cell Biology and Anatomy, University of Munich, Planegg 82152, Germany

Corresponding author: Jovica Ninkovic, PhD, Professor, Helmholtz Center Munich, Biomedical Center, Inst Stem Cell Res, Institute of Stem Cell Research, University of Munich, Grosshadernerstrasse 9, Planegg 82152, Germany. ninkovic@helmholtz-muenchen.de

Abstract

Poor recovery of neuronal functions is one of the most common healthcare challenges for patients with different types of brain injuries and/or neurodegenerative diseases. Therapeutic interventions face two major challenges: (1) How to generate neurons *de novo* to replenish the neuronal loss caused by injuries or neurodegeneration (restorative neurogenesis) and (2) How to prevent or limit the secondary tissue damage caused by long-term accumulation of glial cells, including microglia, at injury site (glial scar). In contrast to mammals, zebrafish have extensive regenerative capacity in numerous vital organs, including the brain, thus making them a valuable model to improve the existing therapeutic approaches for human brain repair. In response to injuries to the central nervous system (CNS), zebrafish have developed specific mechanisms to promote the recovery of the lost tissue architecture and functionality of the damaged CNS. These mechanisms include the activation of a restorative neurogenic program in a specific set of glial cells (ependymoglia) and the resolution of both the glial scar and inflammation, thus enabling proper neuronal specification and survival. In this review, we discuss the cellular and molecular mechanisms underlying the regenerative ability in the adult zebrafish brain and conclude with the potential applicability of these mechanisms in repair of the mammalian CNS.

Key words: Zebrafish; Central nervous system; Brain injury; Glial scar; Regeneration; Restorative neurogenesis; Neural stem cells; Inflammation

Core tip: Poor recovery of neuronal functions is one of the most common healthcare challenges for patients with different types of brain injuries. In contrast to mammals, zebrafish have developed specific mechanisms to activate a restorative neurogenic program in a specific set of glial cells (ependymoglia) and to resolve both the glial scar and inflammation, thus enabling proper neuronal specification and survival. In this

P-Reviewer: Ding JX
S-Editor: Wang J
L-Editor: A
E-Editor: Xing YX

review, we discuss these mechanisms and their potential applicability for the repair of the mammalian central nervous system.

Citation: Zambusi A, Ninkovic J. Regeneration of the central nervous system-principles from brain regeneration in adult zebrafish. *World J Stem Cells* 2020; 12(1): 8-24
URL: https://www.wjgnet.com/1948-0210/full/v12/i1/8.htm
DOI: https://dx.doi.org/10.4252/wjsc.v12.i1.8

INTRODUCTION

In contrast to mammals, zebrafish can efficiently regenerate and recover lost tissue architecture and the function of vital organs including the spinal cord, retina, fin, heart and brain (Figure 1). Because traumatic brain injuries and neurodegenerative diseases pose a great burden to society, new therapeutic interventions must be developed. One possible approach is comparison between non-regenerative models (such as mammals, largely represented by mouse models) and regenerative models (often zebrafish or axolotl) to identify similarities and differences at the cellular and molecular levels that could be exploited to achieve regeneration in the human brain. One striking difference between these two models is the presence of numerous constitutively active neurogenic niches in the zebrafish adult central nervous system (CNS)[1-3]. This feature has long been speculated to be the driving force underlying the endogenous regeneration observed in the adult zebrafish brain[1,2,4]. However, neurogenic niches are also found in the mammalian CNS, albeit in lower numbers, thus suggesting the existence of additional cellular and molecular distinctions between mammals and zebrafish. To address these differences, endogenous regeneration in different areas of the zebrafish CNS has been extensively studied by using various injury paradigms[5-17]. Numerous programs actively involved in the activation of neuronal progenitors in response to injury and contributing to restorative neurogenesis have been identified[6,9,12-14,16,18]. Of note, these programs can be subdivided into specific categories: (1) Developmental programs that are reactivated in response to injury and that regenerate brain structures by mimicking developmental functions; (2) Injury-specific programs that are exclusively active in the context of regeneration and (3) Programs that are also active during development but have distinct functions in the context of regeneration[6,9,12-14,16,18]. In addition to different models activating the generation of new neurons, zebrafish can synchronize the addition of neurons with the resolution of both glial scar and inflammation, thereby achieving proper specification and long-term survival of new neurons[8,12-14]. These features have not been observed in mammals, in which neurons generated in response to injury do not survive, owing to the persistence of the glial scar. All these elements play a synergistic role in the endogenous regeneration of the adult zebrafish CNS. Therefore, we will focus on their comprehensive description after providing an introductory characterization of the cellular environment in different brain areas of the adult zebrafish brain under physiological conditions and the injury paradigms used to study regenerative responses in zebrafish.

Introduction and comparison of progenitor lineages in adult zebrafish and mouse brains

Similarly to the mammalian brain, the zebrafish brain contains several progenitor cell-types that generate distinct lineages. The most prominent feature of the adult zebrafish brain, in contrast to the mammalian brain, is the enrichment of neuronal progenitors within different neurogenic niches. These neuronal progenitors maintain a life-long capacity to produce new neurons[1-3,19-22], although this feature decreases with age[23], similarly to the mammalian adult neuronal progenitors[24]. Interestingly, glial progenitors are present in both zebrafish and mammalian brains with similar abundance and cellular characteristics[25-27]. These progenitors are scattered throughout the brain parenchyma and either self-renew or generate mature oligodendrocytes[25].

Neurogenic niches and neuronal progenitor cells

The adult zebrafish brain contains various niches with proliferating progenitors, many of which can generate new neurons (neurogenic progenitors)[1-3,19-22]. One of the best studied and characterized regions in the adult zebrafish brain is the telencephalon. This brain area contains a neurogenic niche lining in the ventricular

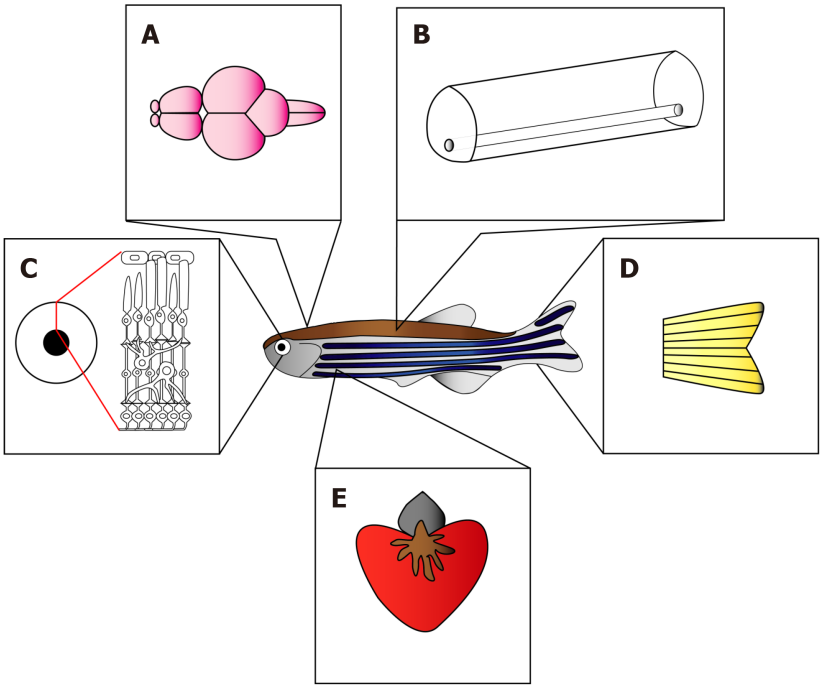

Figure 1 Regenerating organs in adult zebrafish. In contrast to mammals, adult zebrafish are able to efficiently regenerate the lost tissue architecture and retrieve the functions of brain (A), spinal cord (B), retina (C), fin (D) and heart (E).

zone (VZ), which is located at the outer brain surface, owing to the everted nature of this specific brain region (Figure 2A)[28]. New-born neurons are deposited immediately below the proliferative zone, in the so-called periventricular zone[19,20]. Progenitors residing in the VZ have a radial morphology similar to that of the mammalian neural stem cells (radial glia cells, RGCs) present during brain development. Their bodies are located at the ventricular surface, and their processes span throughout the parenchyma of the adult zebrafish telencephalon[29]. Moreover, these cells are the functional orthologs of mammalian ependymal cells; therefore, we will refer to them as ependymoglia. Importantly, only a proportion of these cells generate neurons under physiological conditions, whereas most remain quiescent, a common feature shared by classical ependymal cells[7,30,31]. However, numerous experimental manipulations such as changes in Notch signaling[30] or injuries induce cell-cycle re-entry in many ependymoglial cells and/or generation of new neurons[6-8,11-14,16,32,33]. Although almost all ependymoglial cells in the adult zebrafish telencephalon can generate neurons, there are at least two distinct neurogenic zones where ependymoglial cells are located: The dorsal and the medio-ventral neurogenic niches (Figure 2). These two zones differ in the proliferation rates of ependymoglial cells and their progenies, the size of the progenies that they produce and the type of newly generated neurons[19,20,29,34]. As previously mentioned, under physiological conditions, only a small proportion of ependymoglia in the dorsal neurogenic niche are actively proliferating, whereas the majority remain quiescent[7,30,31]. Ependymoglial cells express different markers including glial fibrillary acidic protein (Gfap), S100 calcium-binding protein B (S100β), Nestin, brain lipid-binding protein (Blbp) and SRY-box 2 (Sox2)[14,19,29,34-37], and can be further subdivided into non-dividing (type I) and dividing (type II) cells[34]. According to previously developed live-imaging techniques, not only the proliferative state of ependymoglia but also the mode of division differs[7,38]. Ependymoglial cells rarely divide symmetrically, thus giving rise to two new ependymoglial cells and thereby expanding the pool of adult neural stem cells (aNSCs). The largest fraction of activated ependymoglial cells divide asymmetrically, thus maintaining the stem cell pool and generating neuronal progeny[7,38]. Moreover, a substantial proportion of ependymoglia lose their aNSC hallmarks and upregulate the neuronal marker HuC/D, thus suggesting that direct conversion of ependymoglia into neurons substantially contributes to the constitutive neurogenesis at the expense of the stem cell pool[7]. Both direct conversion and generation of new neurons via intermediate progenitors in the dorsal neurogenic niche of the adult zebrafish telencephalon result in small neuronal clones (fewer than four cells)[7,31]. In contrast to the low proliferation rate and small neuronal output of ependymoglia in the dorsal neurogenic niche, medio-ventral ependymoglial cells proliferate at higher rates and

produce larger neuronal progenies[34]. Some progeny have migratory capacities and, similarly to those in the mammalian brain, migrate to the olfactory bulb through the rostral-migratory stream, whereas a proportion generate new neurons that are deposited periventricularly[19]. Because live-imaging and clonal analysis techniques in the medial-ventral neurogenic niche are lacking, it remains to be investigated whether the same cell has the capacity to generate neurons fated to populate both the olfactory bulb and the periventricular zone. Therefore, new genomic approaches must be used to identify the transcriptomes of single ependymoglial cells and address the existence of different sub-populations, identify specific markers to prospectively isolate these populations and subsequently decipher specific molecular pathways involved in region-specific generation of new neurons in the adult brain. The first steps toward the dissection of distinct molecular features of different progenitor cell types have enabled the identification of a population of Nestin-positive progenitor cells in the ventral nucleus of the ventral telencephalon, which weakly express canonical radial glial markers, display a typical neuroepithelial-like morphology and proliferate primarily with a short cell cycle duration (Figure 2B)[29,34,39]. Proliferating oligodendrocyte transcription factor 2-positive (Olig2$^+$) cells that are negative for typical oligodendrocyte markers, such as the SRY-related HMG-box 10 (Sox10) and myelin basic protein (Mbp), but are positive for polysialylated-neural cell adhesion molecule have also been found in the rostral migratory stream of the zebrafish telencephalon, together with a small population of Olig2-expressing cells positive for S100β and displaying a typical radial glia-like morphology[25]. However, the functions of these cells remain to be addressed.

Although the neurogenic niches and the mechanisms controlling neurogenesis in the adult zebrafish telencephalon are the most studied and best characterized, neurogenic niches are also present in other regions of the adult zebrafish brain, and they have specific features[1,2,20-22,40]. Hence, differences and similarities between neurogenic niches of different brain areas should be considered with regard to region-specific restorative neurogenesis. In the optic tectum and cerebellum, for instance, aNSCs do not express typical glial markers and display a neuroepithelial-like phenotype. Radial glia-like cells exist, but in lower numbers, and are quiescent[20,21,40-42]. In the junction between the mid- and hindbrain, hairy-related 5-positive cells exhibit some of the typical aNSC characteristics, including a slow cell cycle, self-renewal, and expression of Gfap, Blbp and Sox2, and they have the capacity to differentiate into neurons[22].

Glial cell composition of the zebrafish brain parenchyma

Proliferation does not occur only in the dorsal and medio-ventral neurogenic niches, because proliferating cells are also found throughout the parenchyma of the adult zebrafish telencephalon, where oligodendroglial and microglial cells reside (Figure 2)[25]. Cells belonging to the oligodendrocyte lineage express Olig2 and Sox10[43]. In the adult mammalian cerebral cortex, oligodendrocyte progenitors generate primarily neuron-glial antigen 2-positive glia, maintaining them in constant numbers throughout life[27], and to a lesser extent mature oligodendrocytes[26]. Olig2 and Sox10 lineage-marker positive-cells have also been identified in the parenchyma of the adult zebrafish telencephalon[25]. Additionally, a small proportion of these cells have been found to be positive for Mbp, a marker of mature oligodendrocytes[25]. Under physiological conditions, only a few oligodendroglial cells have been identified as actively proliferating oligodendroglial precursor cells, on the basis of co-staining with proliferating cell nuclear antigen and the incorporation of the DNA base analog bromodeoxyuridine[25]. Other studies in the adult zebrafish brain, and specifically in the cerebellum, have demonstrated the existence of a small proportion of Olig2-expressing cells positive for Sox10, which are located in the granule cell layer close to Purkinje cells, whereas most Olig2-expressing cells in this specific brain region display neuronal identity and are positive for the neuronal marker HuC/D[44]. Another important population that displays some grades of proliferation and is involved in the maintenance of homeostasis in the adult zebrafish brain consists of microglial cells, the resident phagocytes in the brain. Under normal conditions, microglial cells display a branched and elongated morphology[45]. However, under pathological conditions, microglial cells show a modified structure, acquiring an amoeboid-like morphology. In the mouse brain, "resting" microglia are not inactive and constantly use their processes to scan the CNS environment[46]. Numerous studies performed in both the mammalian and zebrafish CNS have demonstrated that in addition to their major task as CNS guardians, microglial cells play an important role in the regulation and pruning of synapses[47-50], apoptotic cell clearance[51,52] and CNS angiogenesis[53,54]. Interestingly, microglial cells located in the telencephalon, optic tectum and cerebellum of the adult zebrafish morphologically resemble those present in the mature mammalian CNS, and a large fraction of the microglial signature is also

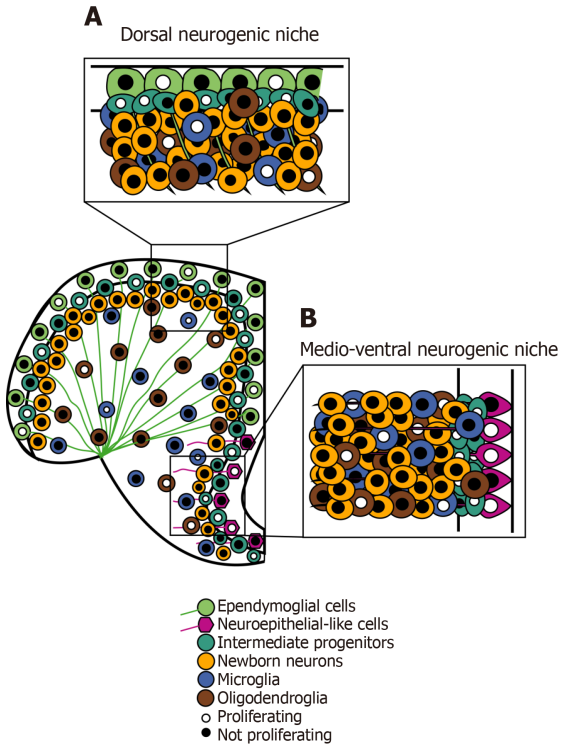

Figure 2 Schematic representation of the main cell types in the adult zebrafish telencephalon, with focus on two distinct neurogenic niches, the dorsal ventricular zone and the medio-ventricular zone. A: The dorsal ventricular zone hosts ependymoglial cells (light green), quiescent and slow-cycling adult neural stem cells, intermediate progenitor cells (light blue) and neurons (yellow); B: The medio-ventricular zone hosts neuroepithelial-like cells (magenta), characterized by faster cell cycle. Intermediate progenitor cells (light blue) are deposited in the subventricular layer and they can either differentiate into neurons (yellow) or migrate to the olfactoy bulb. Microglial (blue) and oligodendroglial (brown) cells can be found in the subventricular zone and in the parenchyma of the adult zebrafish telencephalon.

conserved in zebrafish[54,55]. Importantly, the adult zebrafish brain lacks the typical parenchymal, protoplasmic astrocytes, an abundant cell type that is present in the mammalian brain and has important functions under physiological conditions and after different types of injury or neurodegenerative diseases[56]. Moreover, questions remain regarding which cell type takes over the function of protoplasmic astrocytes and whether their absence offers any beneficial effect toward successful brain regeneration.

Paradigms to study neurodegeneration and regeneration in the adult zebrafish brain

Zebrafish are a suitable animal model to reproduce typical phenotypes of neurodegenerative diseases or injuries affecting the CNS in humans (Figure 3)[14,16,57-59]. However, these models very often replicate only a subset of phenotypes observed in degenerating or injured human brains, thus allowing useful but still restricted analysis of the regenerative responses. Therefore, understanding the limitations and specific features of each model system is crucial to allow proper cross-model comparison and to appreciate the applicability of these models to advance regenerative therapies in humans. Below, we summarize and compare most of the models used for brain regeneration studies in zebrafish.

To generate models for neurodegenerative diseases, methods have been largely based on alteration of specific gene expression, including transient downregulation by morpholinos[60], targeted gene disruption through use of zinc finger nucleases[61], transcription activator-like effector nucleases[62] or clustered regularly interspaced short palindromic repeats[63]. Most of the neurodegenerative models have been established in embryos or juvenile zebrafish. Indeed, these models have been valuable tools for understanding the etiology and the progression of specific diseases. Nonetheless, the programs activated at these stages are reminiscent of the endogenous programs active during development[64], a characteristic that has also been observed in the postnatal mammalian brain[65]. However, the mechanisms leading to endogenous regeneration in the adult zebrafish brain with signs of

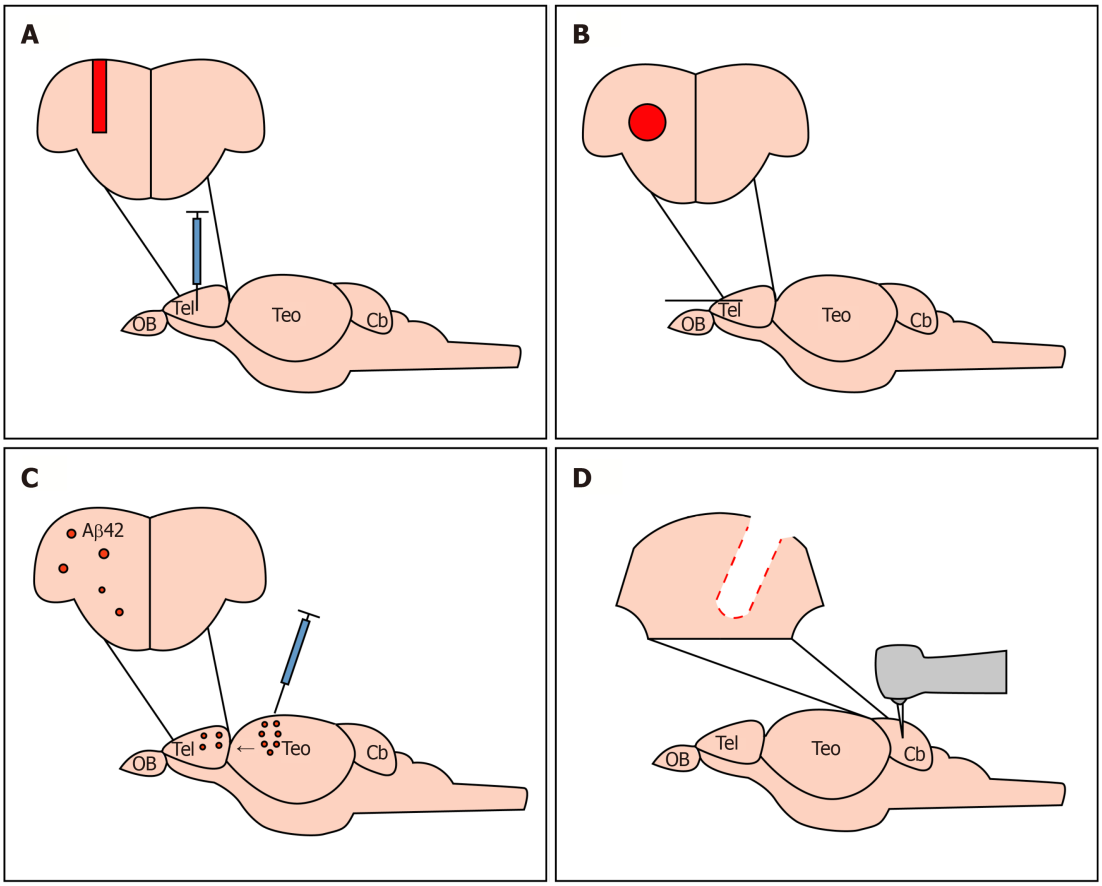

Figure 3 Established paradigms to study cellular and molecular mechanisms of regeneration in the telencephalon and cerebellum of adult zebrafish. A: Mechanical injury to lesion the adult zebrafish telencephalon, damaging the ventricular zone containing neural stem cells; B: Mechanical injury to lesion the adult zebrafish telencephalon, sparing the ventricular zone containing neural stem cells; C: Cerebroventricular microinjections of Aβ42 derivatives to study neurodegeneration in the adult zebrafish telencephalon; D: Mechanical injury of the adult zebrafish cerebellum.

neurodegenerative conditions such as Morbus Parkinson or Alzheimer's diseases still remain elusive. To address this question, a model for neurodegeneration in the adult zebrafish brain has been generated through cerebroventricular microinjection of Aβ42-derivates (Figure 3D)[57]. Injection of Aβ42-derivates in the adult zebrafish brain, causing Alzheimer's disease-like phenotypes (apoptosis, microgliosis and neuronal loss), promotes activation of ependymoglia and enhances neurogenesis, typical responses observed during zebrafish brain regeneration in models of mechanical injuries[6-8,11-14,16,32,33]. In this neurodegenerative model, the presence of Aβ42-derivates leads to interleukin 4 (IL4) upregulation in neurons and microglial cells. IL4 subsequently acts via signal transducer and activator of transcription 6 (Stat6) phosphorylation through the IL4 receptor present in aNSCs, thus leading to their activation[57].

In addition to the development of neurodegenerative models, first attempts to model chronic brain injuries, such as small brain vessel diseases, have been achieved[66]. To study the processes activated in response to rupture of microvessels and consequent microbleeds, a model of injury of blood vessel endothelial cells has been established by using a multi-photon laser[67]. This injury model may be promising if optimized for the adult zebrafish brain, because it has been shown to recapitulate both cerebral hemorrhage and microbleeds[67].

For traumatic brain injuries, numerous paradigms have been established to induce acute damage in different areas of the adult zebrafish CNS, to study the cellular and molecular mechanisms leading to endogenous regeneration[5-17]. In particular, these mechanisms have been extensively analyzed in the context of regeneration in the adult zebrafish telencephalon. A wide range of injury paradigms, damaging different telencephalic structures, have been established and characterized (Figure 3)[6-8,11-14,16,32,33]. In the current review, we refer to two different telencephalic injuries. In the first case, stab wound injury is performed through the skull into the medial region of the telencephalon. Owing to the everted structure of the adult zebrafish telencephalon, this injury damages the dorsal part of the VZ, containing

ependymoglial cells with stem cell properties, and the brain parenchyma, containing largely postmitotic neurons and glial progenitors (Figure 3A)[11,12,32,33]. In the second case, the stab wound injury is performed through the zebrafish nostrils. This injury exclusively damages the parenchyma of the telencephalon, leaving the ependimoglial layer intact (Figure 3B)[7,9,13,14,16]. The common features shared by these two different injury models are the activation of restorative programs in ependymoglial cells and the generation of new neurons. Therefore, the understanding of injury-mediated activation of cells with stem cell capacity in different injury models is also key to experimentally eliciting regeneration in species lacking endogenous restorative capacity. Moreover, because zebrafish have different cells with stem cell capacity spread throughout the adult brain[19-21,29,34,42], one additional approach may be the comparison of regeneration in different brain areas in response to mechanical injuries. Indeed, some of these brain regions, including the optic tectum and cerebellum, have been analyzed to different extents in the context of regeneration. The optic tectum contains ependymoglia, but in the intact brain they have only transient and limited neurogenic capacity[42,68]. However, in response to injury, ependymoglial cells enter cell cycle and generate new neurons engaged in regeneration[69,70].

Similarly, numerous studies have focused on the identification of relevant programs involved in cerebellar wound healing and regeneration, with a special focus on cross-talk among apoptosis, inflammation, immune response, the cell cycle and cell adhesion (Figure 3C)[15,17,71-73]. Interestingly, a recent study on regeneration in the adult zebrafish cerebellum has shed light on its limited restorative capacity to only specific cell lineages, in contrast to observations in the adult zebrafish telencephalon and optic tectum[15].

Moreover, cerebellar regeneration is mainly supported by neuroepithelial-like cells, whereas RGCs (possibly sharing some hallmarks with telencephalic ependymoglia) appear to play a minor role[15]. These results are in agreement with the observation that the RG cell pool is either quiescent or exhausted in the adult zebrafish cerebellum and that in response to injury, cell types derived from RGCs are not regenerated[15]. These findings highlight the importance of dedifferentiation and reactivation of glial cells in response to injury and their capacity to reacquire neuronal stem cell characteristics, a feature achieved in mammals only *in vitro*[74].

Beyond mechanical injuries, chemical compounds have been used to target specific or generic cell types in the adult zebrafish brain[75-78] and subsequently study the restorative responses. Quinolinic acid-induced neurotoxicity in the adult zebrafish telencephalon promotes ependymoglia proliferation and activates neurogenic programs, thus enabling the long-distance generation and integration of new-born neurons[77]. Paraquat intoxication results in altered redox levels and mitochondrial activity, thus partially mimicking the phenotypes of Parkinson's disease[76]. Administration of cadmium chloride can induce brain damage because of its cytotoxic activity on glial cells[75], and subchronic exposure to titanium (TiO2) nanoparticles can induce neurotoxicity[78]. Because these different injury models do not rely on mechanical injury and elicit rather limited inflammatory responses but still promote the activation of neurogenic programs, the analysis of these models may be relevant to identify core mechanisms of regeneration in the adult zebrafish CNS to experimentally activate them in the mammalian CNS.

Cellular and molecular mechanisms involved in regeneration and restorative neurogenesis in the adult zebrafish telencephalon

A fundamental feature of telencephalic injuries in the adult zebrafish is the capacity to restore the tissue architecture of the brain parenchyma, including the addition of new neurons. New neurons generated in response to injury (restorative neurogenesis) are positioned deep in the parenchyma (Figure 4D)[7,14], an area that does not accommodate new neurons under physiological conditions[19,20,31]. In fact, when neurons are generated in the intact telencephalon (constitutive neurogenesis), they are deposited in the layer underlying the VZ or in the olfactory bulb[19,20,31]. Importantly, ependymoglial cells can generate neurons that contribute to both constitutive and restorative neurogenesis but may possibly rely on different cellular and molecular mechanisms[4]. Importantly, endogenous neurogenesis supported by ependymoglial cells is not an absolute pre-requisite for successful regeneration. In fact, under physiological conditions, ependymoglia in the optic tectum are mostly quiescent. However, in response to injury, they become activated, generate new neurons and thus support the regeneration of this brain area. Specifically, the Wnt signaling pathway is activated in ependymoglial cells in response to injury and is a key regulator of ependymoglia proliferation and differentiation into neurons[69]. A follow-up study has identified additional molecular pathways important for optic tectum regeneration. Sonic hedgehog is increased in ependymoglia in response to injury, and its activation increases the number of proliferating ependymoglial cells, thereby

limiting their differentiation into neurons. Notch activity is also regulated, and its levels are decreased after injury, thus inducing the same phenotype in ependymoglial cells as that observed with Sonic hedgehog[70]. These results suggest that tight regulation of ependymoglia proliferation and differentiation is necessary to promote restorative neurogenesis in the adult zebrafish brain.

Although different injury paradigms vary in localization within the telencephalon and injury size, common cellular events in response to injury can be generalized (Figure 4). The first event occurring in response to traumatic brain injury is cell death, which is quickly followed by activation of an inflammatory response characterized by microglial cells' morphological modification and accumulation, together with leukocytes, at the injury site[9,13,14,45]. The mobilization of microglial cells toward the injury site is controlled by long-range Ca^{2+} waves activating ATP signaling-dependent chemotaxis, through the purinergic P2Y12 receptor (Figure 4B)[79,80]. Moreover, σ1 receptors are responsible for "switching off" activated microglia, thus allowing these cells to abandon the injury site[81]. Indeed, the inflammatory response is quickly resolved in the adult zebrafish telencephalon[9,13]. The immune cell response is followed by increased proliferation of different cell types, both at the injury site (largely glial, Olig2-positive progenitors) and at the VZ (largely neuronal progenitors and ependymoglia) (Figure 4C)[12-14,16]. Injuries in the adult zebrafish telencephalon not only increase proliferation of ependymoglia but also induce various injury-specific cellular behaviors. Continuous live-imaging of ependymoglial cells in the intact and injured zebrafish telencephalon has revealed symmetric non-gliogenic ependymoglial division in response to injury, a mode of division not previously observed in intact brains, which produces two intermediate neuronal progenitors and depletes the ependymoglial pool[7]. Interestingly, this specific cellular behavior is complemented by direct conversion of ependymoglia to neurons, thus enlarging the neuronal output in regenerating brains. Importantly, direct conversion as a mode of neurogenesis is also present in the intact telencephalon[7], thereby supporting the concept that successful regeneration in the adult zebrafish telencephalon depends both on mechanisms already present in uninjured conditions and on the activation of injury-specific pathways, including programs promoted by injury-induced inflammation[6,8,9,11,39,82,83]. The proper coordination of these programs is key for successful regeneration in the adult zebrafish brain. Indeed, the aryl hydrocarbon receptor (AhR) has been identified as a key synchronizing pathway linking the direct conversion of ependymoglia to neurons with the inflammatory state in the brain parenchyma[8]. AhR signaling is inactivated shortly after injury (period of high microglial activation) and subsequently promotes ependymoglial proliferation at the expense of neuronal differentiation (Figure 4E). This finding is also consistent with microglia-mediated activation of ependymoglia proliferation[9]. Neuronal differentiation of ependymoglia through direct conversion is possible only when AhR signaling returns to basal levels (7 days after injury), coinciding with decreased microglial activation. Interestingly, interference with temporal regulation of AhR signaling after injury leads to aberrant restorative neurogenesis, because newly formed neurons fail to survive[8]. In rodent models of stroke, ependymal cells have the potential to become activated and generate neuroblasts[84,85]. In this case, however, a large proportion of neuroblasts do not survive, and no mature neurons are formed[84,86]. These results lend strength to the concept that the activation of glial cells engaged in restorative neurogenesis by generating new neurons must be finely tuned and coordinated with the state of inflammation to enable proper neuronal survival and subsequent regeneration. After progenitor cells have been generated, they reuse developmental or constitutive neurogenic programs for neuronal differentiation. Prokineticin 2 (Prok2) and Sprouty-related EVH1 domain containing 2 (Spred2) are associated with migration and survival of neuronal progenitors to the injury site[11,16,33]. Ectopic Prok2 expression has been observed in the zebrafish telencephalon in proximity to the injury site, and Prok2 has been proposed to first act as a chemoattractant to direct migration and later act as a neurotrophic factor[16,33]. Similarly, young HuC/D-positive neurons use radial ependymoglial processes as a scaffold to migrate to their target sites in the injured brain[33], as they do during development along the radial glia processes[87]. These findings strengthen the hypothesis that the intrinsic capacity of regeneration in the adult zebrafish CNS may be supported by the ability to activate injury-specific programs and to enhance the restorative process by reactivating developmental programs and reinstructing the functions of genes normally present in the intact CNS. Therefore, we will further discuss the importance of these mechanisms in the context of regeneration.

Modifications of mechanisms present in the intact brain contributing to brain regeneration

The high correlation of restorative potential with the wide distribution of neurogenic

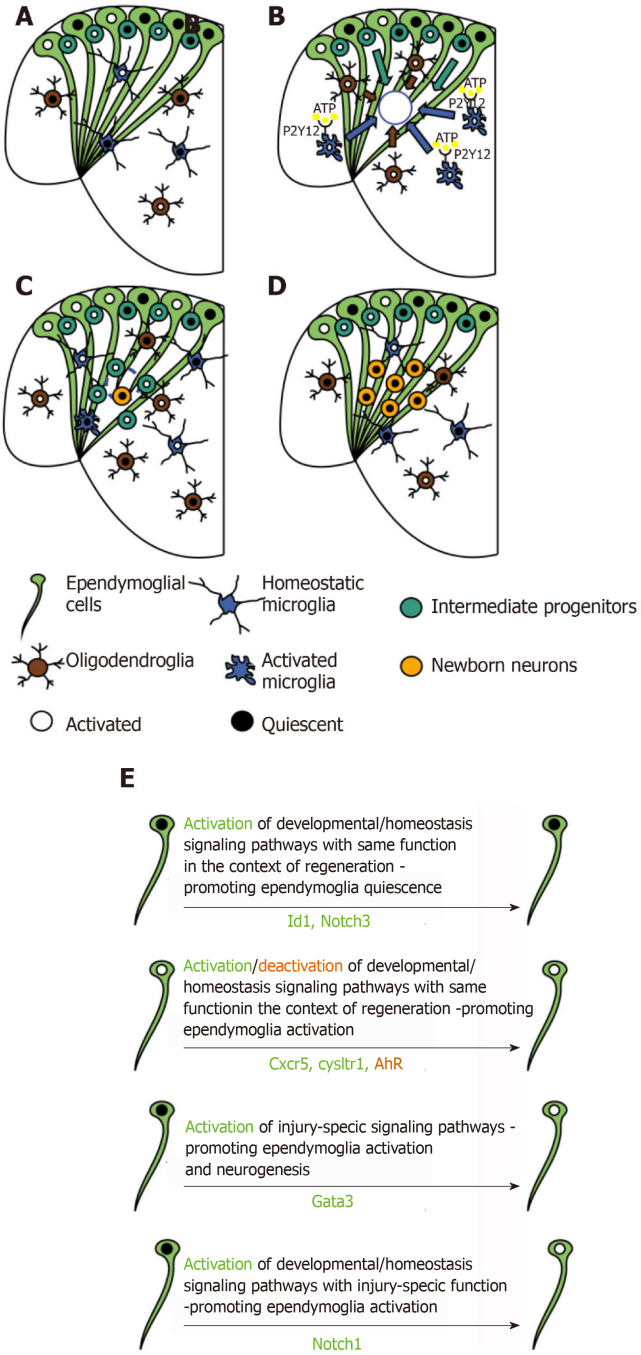

Figure 4 Glial cell reactivity and tissue restoration in the adult zebrafish telencephalon in response to stab wound injury. A: Representative scheme of cell composition in the intact telencephalon of adult zebrafish; B-D: Cellular response to mechanical injury in the adult zebrafish telencephalon; B: Injury-induced cell death stimulates the activation of inflammatory response. ATP is sensed by microglial cells (blue), through P2Y12 receptor, triggering their change in morphology and their migration, together with oligodendroglial precursor cells (OPCs, brown) at the injury site (blue circle); C: Microglial and oligodendroglial cell accumulation is resolved and intermediate progenitors (light blue), source of newly formed neurons (yellow), populate the injury site, where they start differentiating into neurons. Proliferation reaches its peak in the ventricular zone, where stem cells (ependymoglial cells, light green) reside. This cellular response seems to be required to increase the neuronal output and to re-populate the loss of progenitors in the subventricular zone, due to their migration to compensate the neuronal loss at the injury site; D: Regeneration is efficiently completed, stem cell activation returns to basal levels, surviving newborn neurons are found at the injury site and manage to survive, no signs of glial scar can be found; E: Scheme of genes specifically regulated in ependymoglial cells, relevant for their activation state and the promotion of restorative neurogenesis.

niches in the vertebrate brain supports the idea that at least some regulatory mechanisms that actively play a role in constitutive neurogenesis are re-used in the context of regeneration. Indeed, the Notch signaling regulates both constitutive and restorative neurogenesis. In the intact zebrafish brain, Notch signaling promotes ependymoglial quiescence[30,88]. Importantly, two Notch receptors, Notch1 and Notch3,

are upregulated in the adult zebrafish telencephalon in response to injury (Figure 4E)[6,11]. A correlation between Notch activation and neurogenesis has also been observed in the mouse brain[84,89]. Striatal stroke decreases Notch signaling in ependymal cells, and Notch reduction promotes their differentiation along the neuronal lineage, without entry into the cell cycle[84]. Forced activation of Notch1 in response to stroke prevents ependymal cell activation and the production of immature neurons. Moreover, Notch1 signaling is decreased in striatal astrocytes after stroke, thus promoting neurogenesis[89]. In contrast, Notch1 activation after injury in the adult zebrafish telencephalon is instrumental for restorative neurogenesis, and its inhibition prevents the injury-induced proliferation of ependymoglia[11]. These results suggest that Notch1 in zebrafish has an injury-specific function, promoting ependymoglial cell activation and proliferation, in contrast to its normal function under healthy conditions. Interestingly, blocking Notch3 upregulation after injury results in a significant increase in proliferating type II progenitors and a decrease in quiescent type I progenitors, thus suggesting that Notch3 signaling after injury has the same role as that observed in the intact brain: promoting ependymoglial cell quiescence[6,30,88]. Similarly, inhibitor of DNA binding 1 (Id1) has been unexpectedly found to be upregulated in the injured zebrafish telencephalon (Figure 4E). Id1 is predominantly associated with quiescent progenitors (type I) and is expressed by only a small proportion of proliferating progenitors (type II)[6,90]. The same pattern is maintained after injury, and increased numbers of Id1-positive cells as well as increased expression levels in individual cells promote their return to quiescence[6]. The opposite regulation of the ependymoglial state in response to injury by Notch1 on one side and Notch3 and Id1 signaling pathways on the other side suggests an important concept for long term maintenance of restorative capacity that relies on the development of mechanisms that tightly regulate ependymoglial activation. These mechanisms are required to prevent stem cell pool depletion, possibly even by using the same ligands, as in Notch1 and Notch3 signaling. These results support the hypothesis that zebrafish CNS regeneration relies not only on re-activation of developmental programs but also on their modification by injury-specific signals.

Positive contribution of inflammation-related programs to restorative neurogenesis and tissue restoration

Inflammation has long been considered detrimental for neurogenesis[91,92]. This concept has been challenged and revised to a model in which neurogenesis can be either promoted or impaired depending on the severity of the inflammatory stimulus and on the regenerative context[93-99]. Moreover, inflammation, if tightly regulated, is a key element for regeneration in the context of different organs including the fin, heart and spinal cord[100-106]. Indeed, the specific ablation of macrophages after adult zebrafish fin amputation affects wound healing, thus possibly impairing the proliferative capacity of the blastema[103]. The same outcome has been obtained by treating adult zebrafish with dexamethasone, a drug that acts as an immunosuppressor reducing the activation of the inflammatory response. Interestingly, the restorative outgrowth of the caudal fin is significantly lower in treated animals than controls[9]. These results confirm that inflammation is necessary to efficiently promote regeneration in many tissues, thus having a direct role in the regulation of numerous events, including cellular debris and fibrin clearance, angiogenesis and proliferation[105-107]. Immunosuppression and decreased neuroinflammation also negatively affect restorative neurogenesis by decreasing ependymoglial cell proliferation and the generation of new-born neurons[9,70]. In the adult zebrafish brain, various programs associated with inflammation and positive regulation of restorative neurogenesis have been identified. Among these, the chemokine receptor C-X-C chemokine receptor type 5 and cysteinyl leukotriene receptor 1 (Cysltr1) are upregulated in response to injury in the adult zebrafish telencephalon (Figure 4E)[9,83]. Their active role in promoting ependymoglial proliferation and generation of new-born neurons, enhancing restorative neurogenesis in response to injury, has been convincingly assessed[9,83]. Moreover, inflammation in the adult zebrafish regenerating brain not only regulates programs in the intact tissue but also promotes injury-specific programs, such as upregulation of GATA binding protein 3 (Gata3) (Figure 4E)[82]. The zinc-finger transcription factor Gata3 is not expressed in either the embryonic or the intact adult zebrafish telencephalon[82]. Gata3 upregulation in response to injury is required for neuronal regeneration, specifically promoting the proliferation of ependymoglia, neurogenesis and migration of new-born neurons[9,82]. Interestingly, Gata3 is upregulated in the regenerating heart and fin, and its inhibition is sufficient to decrease regeneration[82]. The effects of Gata3 on neurogenesis are strictly dependent on injury, because overexpression of Gata3 in uninjured conditions is not sufficient to increase neurogenesis[9,82]. Additionally, injection of inflammatory molecules such as zymosan

A and leukotriene C4, a ligand for the Cysltr1, are sufficient to induce Gata3 expression[82]. Together, these results suggest that tight temporal regulation of inflammation after injury is crucial for successful tissue restoration. This concept leads to key questions regarding the regulatory mechanisms defining the level of inflammation and the outcomes of restorative processes. In the zebrafish CNS, the initial acute inflammatory phase in response to injury is quickly resolved and is not followed by the prolonged activation typically observed in the mammalian brain[9,13,108]. Different kinetics of resolution of the inflammatory response between zebrafish and mammals may be a key factor promoting regeneration in the adult zebrafish CNS. In fact, inflammation can chronically accumulate over time in some diffuse insults to the mammalian CNS and become chronically detrimental to brain regeneration[109]. Moreover, zebrafish have also developed mechanisms to integrate neuroinflammation-induced programs with existing signaling governing neurogenesis in physiological conditions. For example, Gata3 expression after injury is dependent on the activity of the fibroblast growth factor (Fgf) signaling pathway, in both the regenerating brain and fin[82]. Under physiological conditions in the adult zebrafish cerebellum and telencephalon, Fgf signaling is required for proliferation and homeostasis of aNSCs[21,29]. In zebrafish larvae, similarly to the adult brain, the cerebellum can regenerate through repatterning of the anterior hindbrain, and this process is dependent on Fgf signaling[110]. Moreover, Fgf signaling is involved in the regeneration of other zebrafish organs, including the spinal cord, fin and heart, where it promotes the formation of glial bridges, the recruitment of epicardial cells at the regenerating tissue, blastema formation and restorative outgrowth[111-115]. These results convincingly show that regeneration relies not only on organ-specific programs but also on molecular mechanisms commonly activated in different tissues, thus strengthening the hypothesis that programs such as Fgf signaling, with important roles during development and adult brain homeostasis, may have a completely new function after they are integrated in the injury-induced context during regeneration. Interestingly, FGF is also increased in response to injury in the mouse brain[116]. When blocked, neural progenitor/stem cell proliferation is significantly decreased, thus indicating that FGF has a crucial role in response to injury[116]. However, despite FGF activation, the mouse CNS cannot regenerate, thereby highlighting the importance of synergistic activation of various programs, including the reactivation of developmental programs with distinct functions in the context of regeneration.

Similarly to models of traumatic brain injuries, a recent neurodegenerative model for Alzheimer's disease based on CMVI injection of Aβ42 derivates (see paragraph on experimental models) has enabled the discovery of another inflammation-induced pathway involved in aNSC plasticity and neurogenesis, IL4/Stat6 signaling[57]. The accumulation of Aβ42 in neurons leads to the activation of microglial cells/macrophages and the upregulation of IL4 in both neurons and microglial cells[57]. The IL4 receptor is present in aNSCs, where IL4 promotes proliferation and neurogenesis via Stat6 phosphorylation[57]. Interestingly, IL4 is not upregulated in response to mechanical injury, and Aβ42 microinjection does not promote Gata3 upregulation[57]. These results provide new insights into the association between aNSCs and immune cells and suggest that different mechanisms may be activated during regeneration in zebrafish, depending on the detrimental stimuli[57]. These examples demonstrate that inflammation, if properly tuned, promotes organ regeneration and, in the specific context of the adult zebrafish brain, positively affects ependymoglial proliferation and restorative neurogenesis, inducing the activation of different programs necessary to elicit efficient tissue restoration. Therefore, a deeper knowledge of injury-induced neuroinflammation and its integration with signaling pathways operating under physiological conditions, and the comparison of these mechanisms in the context of different injury paradigms, appears to be necessary to open new avenues for the discovery of effective therapeutic approaches for both traumatic brain injuries and neurodegenerative diseases.

CONCLUSION

Traumatic brain injuries and neurodegenerative diseases in humans are major burdens for society that affect a large number of patients. The most immediate problems are the massive loss of neurons that cannot be replaced and the subsequent loss of vital neurological functions[117,118]. Mouse models are indeed valuable tools to understand and characterize the cellular and molecular events following CNS injuries and diseases. However, similarly to humans, mouse models are characterized by poor regeneration and neuronal recovery in the CNS[108,119]. For this reason, cross-comparison of non-regenerative species (mouse and human) with regenerative

species (zebrafish and axolotl) is important and may ideally deepen knowledge of the core mechanisms promoting endogenous regeneration in the adult zebrafish CNS. These core mechanisms may be prime targets to enhance regeneration in the mammalian CNS.

Zebrafish models appear to be valuable tools to complement the existing knowledge gained from studies in mammals, thus improving understanding of the limitations to CNS repair. However, like all animal models, zebrafish have limitations that should be considered for translational purposes. As already mentioned, most neurodegenerative and chronic injury models in zebrafish often only partially recapitulate the phenotypes observed in the human brain and are generally characterized in embryos or juvenile animals. For this reason, knowledge of disease progression and of programs activated to support regeneration during adulthood remains elusive. Another limitation, which in some cases can be a key feature coinciding with the better regenerative capacity observed in the adult zebrafish CNS, is the different cellular composition of the brain. A clear example is astrocytes, a glial population with important functions under physiological conditions in the mammalian brain that is also associated with the formation of the glial scar in response to injury[120]. The glial scar is initially beneficial in limiting the injured tissue but is later detrimental, inducing a hostile environment for neuronal survival and integration[120]. Astrocytes have not yet been identified in the adult zebrafish brain, and whether other cell types take over their functions remains unknown. This example suggests that other intrinsic differences between the mouse and zebrafish CNS might exist and should be identified to better characterize the cellular and molecular differences and similarities in the context of regeneration between regenerative and non-regenerative species. Finally, owing to the extensive genomic duplication in zebrafish, compensatory mechanisms may actually mask the real function of numerous genes that may be relevant for the regeneration of mammalian CNS[121]. Nevertheless, gene duplication may also allow a higher degree of tuning of programs, thus promoting successful endogenous regeneration[122]. Therefore, these mechanisms would be particularly interesting to study in the context of regeneration.

Despite their limitations, zebrafish models offer excellent and unique possibilities for studying neurogenesis and regeneration in the brain. The existence of various neurogenic niches enables the study of neurogenesis under physiological conditions in different brain areas in the same model[3]. This comparison has enabled the identification of shared and unique cellular and molecular mechanisms promoting neurogenesis in different CNS areas that must be considered to better describe the role of restorative neurogenesis in CNS repair[1-3,19-22]. Complementarily, numerous traumatic injury paradigms targeting different regions of the adult zebrafish CNS have been carefully characterized. From these comparisons, regeneration has been observed to be carried out by different cell types and molecular programs in specific brain areas[5-17]. These results highlight the necessity to deeply understand the core mechanisms involved in the endogenous regeneration of the adult zebrafish brain, to target or introduce them in the mammalian CNS, with the aim of enhancing regeneration. Furthermore, because zebrafish do not display prolonged inflammation or persistence of glial scar at the injury site, they should be considered a valuable model for identifying key programs promoting the resolution of both inflammation and glial scar[9,13]. Indeed, studies in the adult zebrafish brain have led to revision of the long-standing concept that inflammation is detrimental to CNS regeneration. This concept has now been challenged and replaced by a working model in which inflammation can be detrimental, if it persists chronically, but also beneficial at early phases by promoting the activation of restorative neurogenesis programs[9]. Therefore, a detailed understanding of cellular and molecular processes in response to insult in the adult zebrafish brain may cause a paradigm shift in understanding regeneration in the CNS.

In this review, we have provided a detailed description of the main cell types in the adult zebrafish brain, a broad overview of relevant zebrafish models for neurodegeneration and traumatic brain injuries and basic principles unifying currently known mechanisms relevant for CNS repair. Thus, the stage is now set to better understand the cellular and molecular mechanisms that promote endogenous regeneration of several brain areas in the adult zebrafish CNS. These concepts provide further opportunities for deeper understanding of CNS repair in zebrafish and for integration of these findings with the data obtained from mammalian studies.

REFERENCES

1 **Chapouton P**, Jagasia R, Bally-Cuif L. Adult neurogenesis in non-mammalian vertebrates. *Bioessays*

2007; **29**: 745-757 [PMID: 17621643 DOI: 10.1002/bies.20615]
2 **Kaslin J**, Ganz J, Brand M. Proliferation, neurogenesis and regeneration in the non-mammalian vertebrate brain. *Philos Trans R Soc Lond B Biol Sci* 2008; **363**: 101-122 [PMID: 17282988 DOI: 10.1098/rstb.2006.2015]
3 **Diotel N**, Rodriguez Viales R, Armant O, März M, Ferg M, Rastegar S, Strähle U. Comprehensive expression map of transcription regulators in the adult zebrafish telencephalon reveals distinct neurogenic niches. *J Comp Neurol* 2015; **523**: 1202-1221 [PMID: 25556858 DOI: 10.1002/cne.23733]
4 **Barbosa JS**, Ninkovic J. Adult neural stem cell behavior underlying constitutive and restorative neurogenesis in zebrafish. *Neurogenesis (Austin)* 2016; **3**: e1148101 [PMID: 27606336 DOI: 10.1080/23262133.2016.1148101]
5 **Zupanc GK**, Kompass KS, Horschke I, Ott R, Schwarz H. Apoptosis after injuries in the cerebellum of adult teleost fish. *Exp Neurol* 1998; **152**: 221-230 [PMID: 9710521 DOI: 10.1006/exnr.1998.6853]
6 **Rodriguez Viales R**, Diotel N, Ferg M, Armant O, Eich J, Alunni A, März M, Bally-Cuif L, Rastegar S, Strähle U. The helix-loop-helix protein id1 controls stem cell proliferation during regenerative neurogenesis in the adult zebrafish telencephalon. *Stem Cells* 2015; **33**: 892-903 [PMID: 25376791 DOI: 10.1002/stem.1883]
7 **Barbosa JS**, Sanchez-Gonzalez R, Di Giaimo R, Baumgart EV, Theis FJ, Götz M, Ninkovic J. Neurodevelopment. Live imaging of adult neural stem cell behavior in the intact and injured zebrafish brain. *Science* 2015; **348**: 789-793 [PMID: 25977550 DOI: 10.1126/science.aaa2729]
8 **Di Giaimo R**, Durovic T, Barquin P, Kociaj A, Lepko T, Aschenbroich S, Breunig CT, Irmler M, Cernilogar FM, Schotta G, Barbosa JS, Trümbach D, Baumgart EV, Neuner AM, Beckers J, Wurst W, Stricker SH, Ninkovic J. The Aryl Hydrocarbon Receptor Pathway Defines the Time Frame for Restorative Neurogenesis. *Cell Rep* 2018; **25**: 3241-3251.e5 [PMID: 30566853 DOI: 10.1016/j.celrep.2018.11.055]
9 **Kyritsis N**, Kizil C, Zocher S, Kroehne V, Kaslin J, Freudenreich D, Iltzsche A, Brand M. Acute inflammation initiates the regenerative response in the adult zebrafish brain. *Science* 2012; **338**: 1353-1356 [PMID: 23138980 DOI: 10.1126/science.1228773]
10 **Zupanc GK**. Adult neurogenesis and neuronal regeneration in the central nervous system of teleost fish. *Brain Behav Evol* 2001; **58**: 250-275 [PMID: 11978945 DOI: 10.1159/000057569]
11 **Kishimoto N**, Shimizu K, Sawamoto K. Neuronal regeneration in a zebrafish model of adult brain injury. *Dis Model Mech* 2012; **5**: 200-209 [PMID: 22028327 DOI: 10.1242/dmm.007336]
12 **März M**, Schmidt R, Rastegar S, Strähle U. Regenerative response following stab injury in the adult zebrafish telencephalon. *Dev Dyn* 2011; **240**: 2221-2231 [PMID: 22016188 DOI: 10.1002/dvdy.22710]
13 **Baumgart EV**, Barbosa JS, Bally-Cuif L, Götz M, Ninkovic J. Stab wound injury of the zebrafish telencephalon: a model for comparative analysis of reactive gliosis. *Glia* 2012; **60**: 343-357 [PMID: 22105794 DOI: 10.1002/glia.22269]
14 **Kroehne V**, Freudenreich D, Hans S, Kaslin J, Brand M. Regeneration of the adult zebrafish brain from neurogenic radial glia-type progenitors. *Development* 2011; **138**: 4831-4841 [PMID: 22007133 DOI: 10.1242/dev.072587]
15 **Kaslin J**, Kroehne V, Ganz J, Hans S, Brand M. Distinct roles of neuroepithelial-like and radial glia-like progenitor cells in cerebellar regeneration. *Development* 2017; **144**: 1462-1471 [PMID: 28289134 DOI: 10.1242/dev.144907]
16 **Ayari B**, El Hachimi KH, Yanicostas C, Landoulsi A, Soussi-Yanicostas N. Prokineticin 2 expression is associated with neural repair of injured adult zebrafish telencephalon. *J Neurotrauma* 2010; **27**: 959-972 [PMID: 20102264 DOI: 10.1089/neu.2009.0972]
17 **Zupanc GK**. Adult neurogenesis and neuronal regeneration in the brain of teleost fish. *J Physiol Paris* 2008; **102**: 357-373 [PMID: 18984045 DOI: 10.1016/j.jphysparis.2008.10.007]
18 **Reimer MM**, Sörensen I, Kuscha V, Frank RE, Liu C, Becker CG, Becker T. Motor neuron regeneration in adult zebrafish. *J Neurosci* 2008; **28**: 8510-8516 [PMID: 18716209 DOI: 10.1523/JNEUROSCI.1189-08.2008]
19 **Adolf B**, Chapouton P, Lam CS, Topp S, Tannhäuser B, Strähle U, Götz M, Bally-Cuif L. Conserved and acquired features of adult neurogenesis in the zebrafish telencephalon. *Dev Biol* 2006; **295**: 278-293 [PMID: 16828638 DOI: 10.1016/j.ydbio.2006.03.023]
20 **Grandel H**, Kaslin J, Ganz J, Wenzel I, Brand M. Neural stem cells and neurogenesis in the adult zebrafish brain: origin, proliferation dynamics, migration and cell fate. *Dev Biol* 2006; **295**: 263-277 [PMID: 16682018 DOI: 10.1016/j.ydbio.2006.03.040]
21 **Kaslin J**, Ganz J, Geffarth M, Grandel H, Hans S, Brand M. Stem cells in the adult zebrafish cerebellum: initiation and maintenance of a novel stem cell niche. *J Neurosci* 2009; **29**: 6142-6153 [PMID: 19439592 DOI: 10.1523/JNEUROSCI.0072-09.2009]
22 **Chapouton P**, Adolf B, Leucht C, Tannhäuser B, Ryu S, Driever W, Bally-Cuif L. her5 expression reveals a pool of neural stem cells in the adult zebrafish midbrain. *Development* 2006; **133**: 4293-4303 [PMID: 17038515 DOI: 10.1242/dev.02573]
23 **Edelmann K**, Glashauser L, Sprungala S, Hesl B, Fritschle M, Ninkovic J, Godinho L, Chapouton P. Increased radial glia quiescence, decreased reactivation upon injury and unaltered neuroblast behavior underlie decreased neurogenesis in the aging zebrafish telencephalon. *J Comp Neurol* 2013; **521**: 3099-3115 [PMID: 23787922 DOI: 10.1002/cne.23347]
24 **Bast L**, Calzolari F, Strasser MK, Hasenauer J, Theis FJ, Ninkovic J, Marr C. Increasing Neural Stem Cell Division Asymmetry and Quiescence Are Predicted to Contribute to the Age-Related Decline in Neurogenesis. *Cell Rep* 2018; **25**: 3231-3240.e8 [PMID: 30566852 DOI: 10.1016/j.celrep.2018.11.088]
25 **März M**, Schmidt R, Rastegar S, Strähle U. Expression of the transcription factor Olig2 in proliferating cells in the adult zebrafish telencephalon. *Dev Dyn* 2010; **239**: 3336-3349 [PMID: 20981834 DOI: 10.1002/dvdy.22455]
26 **Dimou L**, Simon C, Kirchhoff F, Takebayashi H, Götz M. Progeny of Olig2-expressing progenitors in the gray and white matter of the adult mouse cerebral cortex. *J Neurosci* 2008; **28**: 10434-10442 [PMID: 18842903 DOI: 10.1523/JNEUROSCI.2831-08.2008]
27 **Simon C**, Götz M, Dimou L. Progenitors in the adult cerebral cortex: cell cycle properties and regulation by physiological stimuli and injury. *Glia* 2011; **59**: 869-881 [PMID: 21446038 DOI: 10.1002/glia.21156]
28 **Folgueira M**, Bayley P, Navratilova P, Becker TS, Wilson SW, Clarke JD. Morphogenesis underlying the development of the everted teleost telencephalon. *Neural Dev* 2012; **7**: 32 [PMID: 22989074 DOI: 10.1186/1749-8104-7-32]
29 **Ganz J**, Kaslin J, Hochmann S, Freudenreich D, Brand M. Heterogeneity and Fgf dependence of adult

neural progenitors in the zebrafish telencephalon. *Glia* 2010; **58**: 1345-1363 [PMID: 20607866 DOI: 10.1002/glia.21012]

30 **Chapouton P**, Skupien P, Hesl B, Coolen M, Moore JC, Madelaine R, Kremmer E, Faus-Kessler T, Blader P, Lawson ND, Bally-Cuif L. Notch activity levels control the balance between quiescence and recruitment of adult neural stem cells. *J Neurosci* 2010; **30**: 7961-7974 [PMID: 20534844 DOI: 10.1523/JNEUROSCI.6170-09.2010]

31 **Rothenaigner I**, Krecsmarik M, Hayes JA, Bahn B, Lepier A, Fortin G, Götz M, Jagasia R, Bally-Cuif L. Clonal analysis by distinct viral vectors identifies bona fide neural stem cells in the adult zebrafish telencephalon and characterizes their division properties and fate. *Development* 2011; **138**: 1459-1469 [PMID: 21367818 DOI: 10.1242/dev.058156]

32 **Diotel N**, Vaillant C, Gabbero C, Mironov S, Fostier A, Gueguen MM, Anglade I, Kah O, Pellegrini E. Effects of estradiol in adult neurogenesis and brain repair in zebrafish. *Horm Behav* 2013; **63**: 193-207 [PMID: 22521210 DOI: 10.1016/j.yhbeh.2012.04.003]

33 **Lim FT**, Ogawa S, Parhar IS. Spred-2 expression is associated with neural repair of injured adult zebrafish brain. *J Chem Neuroanat* 2016; **77**: 176-186 [PMID: 27427471 DOI: 10.1016/j.jchemneu.2016.07.005]

34 **März M**, Chapouton P, Diotel N, Vaillant C, Hesl B, Takamiya M, Lam CS, Kah O, Bally-Cuif L, Strähle U. Heterogeneity in progenitor cell subtypes in the ventricular zone of the zebrafish adult telencephalon. *Glia* 2010; **58**: 870-888 [PMID: 20155821 DOI: 10.1002/glia.20971]

35 **Pellegrini E**, Mouriec K, Anglade I, Menuet A, Le Page Y, Gueguen MM, Marmignon MH, Brion F, Pakdel F, Kah O. Identification of aromatase-positive radial glial cells as progenitor cells in the ventricular layer of the forebrain in zebrafish. *J Comp Neurol* 2007; **501**: 150-167 [PMID: 17206614 DOI: 10.1002/cne.21222]

36 **Lam CS**, März M, Strähle U. gfap and nestin reporter lines reveal characteristics of neural progenitors in the adult zebrafish brain. *Dev Dyn* 2009; **238**: 475-486 [PMID: 19161226 DOI: 10.1002/dvdy.21853]

37 **Lindsey BW**, Darabie A, Tropepe V. The cellular composition of neurogenic periventricular zones in the adult zebrafish forebrain. *J Comp Neurol* 2012; **520**: 2275-2316 [PMID: 22318736 DOI: 10.1002/cne.23065]

38 **Dray N**, Bedu S, Vuillemin N, Alunni A, Coolen M, Krecsmarik M, Supatto W, Beaurepaire E, Bally-Cuif L. Large-scale live imaging of adult neural stem cells in their endogenous niche. *Development* 2015; **142**: 3592-3600 [PMID: 26395477 DOI: 10.1242/dev.123018]

39 **Kizil C**, Kaslin J, Kroehne V, Brand M. Adult neurogenesis and brain regeneration in zebrafish. *Dev Neurobiol* 2012; **72**: 429-461 [PMID: 21595047 DOI: 10.1002/dneu.20918]

40 **Kaslin J**, Kroehne V, Benato F, Argenton F, Brand M. Development and specification of cerebellar stem and progenitor cells in zebrafish: from embryo to adult. *Neural Dev* 2013; **8**: 9 [PMID: 23641971 DOI: 10.1186/1749-8104-8-9]

41 **Grandel H**, Brand M. Comparative aspects of adult neural stem cell activity in vertebrates. *Dev Genes Evol* 2013; **223**: 131-147 [PMID: 23179636 DOI: 10.1007/s00427-012-0425-5]

42 **Ito Y**, Tanaka H, Okamoto H, Ohshima T. Characterization of neural stem cells and their progeny in the adult zebrafish optic tectum. *Dev Biol* 2010; **342**: 26-38 [PMID: 20346355 DOI: 10.1016/j.ydbio.2010.03.008]

43 **Zhou Q**, Wang S, Anderson DJ. Identification of a novel family of oligodendrocyte lineage-specific basic helix-loop-helix transcription factors. *Neuron* 2000; **25**: 331-343 [PMID: 10719889 DOI: 10.1016/S0896-6273(00)80898-3]

44 **Bae YK**, Kani S, Shimizu T, Tanabe K, Nojima H, Kimura Y, Higashijima S, Hibi M. Anatomy of zebrafish cerebellum and screen for mutations affecting its development. *Dev Biol* 2009; **330**: 406-426 [PMID: 19371731 DOI: 10.1016/j.ydbio.2009.04.013]

45 **Hanisch UK**, Kettenmann H. Microglia: active sensor and versatile effector cells in the normal and pathologic brain. *Nat Neurosci* 2007; **10**: 1387-1394 [PMID: 17965659 DOI: 10.1038/nn1997]

46 **Davalos D**, Grutzendler J, Yang G, Kim JV, Zuo Y, Jung S, Littman DR, Dustin ML, Gan WB. ATP mediates rapid microglial response to local brain injury in vivo. *Nat Neurosci* 2005; **8**: 752-758 [PMID: 15895084 DOI: 10.1038/nn1472]

47 **Stevens B**, Allen NJ, Vazquez LE, Howell GR, Christopherson KS, Nouri N, Micheva KD, Mehalow AK, Huberman AD, Stafford B, Sher A, Litke AM, Lambris JD, Smith SJ, John SW, Barres BA. The classical complement cascade mediates CNS synapse elimination. *Cell* 2007; **131**: 1164-1178 [PMID: 18083105 DOI: 10.1016/j.cell.2007.10.036]

48 **Kim HJ**, Cho MH, Shim WH, Kim JK, Jeon EY, Kim DH, Yoon SY. Deficient autophagy in microglia impairs synaptic pruning and causes social behavioral defects. *Mol Psychiatry* 2017; **22**: 1576-1584 [PMID: 27400854 DOI: 10.1038/mp.2016.103]

49 **Wake H**, Moorhouse AJ, Jinno S, Kohsaka S, Nabekura J. Resting microglia directly monitor the functional state of synapses in vivo and determine the fate of ischemic terminals. *J Neurosci* 2009; **29**: 3974-3980 [PMID: 19339593 DOI: 10.1523/JNEUROSCI.4363-08.2009]

50 **Paolicelli RC**, Bolasco G, Pagani F, Maggi L, Scianni M, Panzanelli P, Giustetto M, Ferreira TA, Guiducci E, Dumas L, Ragozzino D, Gross CT. Synaptic pruning by microglia is necessary for normal brain development. *Science* 2011; **333**: 1456-1458 [PMID: 21778362 DOI: 10.1126/science.1202529]

51 **Peri F**, Nüsslein-Volhard C. Live imaging of neuronal degradation by microglia reveals a role for v0-ATPase a1 in phagosomal fusion in vivo. *Cell* 2008; **133**: 916-927 [PMID: 18510934 DOI: 10.1016/j.cell.2008.04.037]

52 **Sierra A**, Encinas JM, Deudero JJ, Chancey JH, Enikolopov G, Overstreet-Wadiche LS, Tsirka SE, Maletic-Savatic M. Microglia shape adult hippocampal neurogenesis through apoptosis-coupled phagocytosis. *Cell Stem Cell* 2010; **7**: 483-495 [PMID: 20887954 DOI: 10.1016/j.stem.2010.08.014]

53 **Fantin A**, Vieira JM, Gestri G, Denti L, Schwarz Q, Prykhozhij S, Peri F, Wilson SW, Ruhrberg C. Tissue macrophages act as cellular chaperones for vascular anastomosis downstream of VEGF-mediated endothelial tip cell induction. *Blood* 2010; **116**: 829-840 [PMID: 20404134 DOI: 10.1182/blood-2009-12-257832]

54 **Svahn AJ**, Graeber MB, Ellett F, Lieschke GJ, Rinkwitz S, Bennett MR, Becker TS. Development of ramified microglia from early macrophages in the zebrafish optic tectum. *Dev Neurobiol* 2013; **73**: 60-71 [PMID: 22648905 DOI: 10.1002/dneu.22039]

55 **Oosterhof N**, Holtman IR, Kuil LE, van der Linde HC, Boddeke EW, Eggen BJ, van Ham TJ. Identification of a conserved and acute neurodegeneration-specific microglial transcriptome in the zebrafish. *Glia* 2017; **65**: 138-149 [PMID: 27757989 DOI: 10.1002/glia.23083]

56 **Mori T**, Buffo A, Götz M. The novel roles of glial cells revisited: the contribution of radial glia and

astrocytes to neurogenesis. *Curr Top Dev Biol* 2005; **69**: 67-99 [PMID: 16243597 DOI: 10.1016/S0070-2153(05)69004-7]

57 **Bhattarai P**, Thomas AK, Cosacak MI, Papadimitriou C, Mashkaryan V, Froc C, Reinhardt S, Kurth T, Dahl A, Zhang Y, Kizil C. IL4/STAT6 Signaling Activates Neural Stem Cell Proliferation and Neurogenesis upon Amyloid-β42 Aggregation in Adult Zebrafish Brain. *Cell Rep* 2016; **17**: 941-948 [PMID: 27760324 DOI: 10.1016/j.celrep.2016.09.075]

58 **Da Costa MM**, Allen CE, Higginbottom A, Ramesh T, Shaw PJ, McDermott CJ. A new zebrafish model produced by TILLING of SOD1-related amyotrophic lateral sclerosis replicates key features of the disease and represents a tool for in vivo therapeutic screening. *Dis Model Mech* 2014; **7**: 73-81 [PMID: 24092880 DOI: 10.1242/dmm.012013]

59 **Paquet D**, Bhat R, Sydow A, Mandelkow EM, Berg S, Hellberg S, Fälting J, Distel M, Köster RW, Schmid B, Haass C. A zebrafish model of tauopathy allows in vivo imaging of neuronal cell death and drug evaluation. *J Clin Invest* 2009; **119**: 1382-1395 [PMID: 19363289 DOI: 10.1172/JCI37537]

60 **Nasevicius A**, Ekker SC. Effective targeted gene 'knockdown' in zebrafish. *Nat Genet* 2000; **26**: 216-220 [PMID: 11017081 DOI: 10.1038/79951]

61 **Doyon Y**, McCammon JM, Miller JC, Faraji F, Ngo C, Katibah GE, Amora R, Hocking TD, Zhang L, Rebar EJ, Gregory PD, Urnov FD, Amacher SL. Heritable targeted gene disruption in zebrafish using designed zinc-finger nucleases. *Nat Biotechnol* 2008; **26**: 702-708 [PMID: 18500334 DOI: 10.1038/nbt1409]

62 **Huang P**, Xiao A, Zhou M, Zhu Z, Lin S, Zhang B. Heritable gene targeting in zebrafish using customized TALENs. *Nat Biotechnol* 2011; **29**: 699-700 [PMID: 21822242 DOI: 10.1038/nbt.1939]

63 **Hruscha A**, Krawitz P, Rechenberg A, Heinrich V, Hecht J, Haass C, Schmid B. Efficient CRISPR/Cas9 genome editing with low off-target effects in zebrafish. *Development* 2013; **140**: 4982-4987 [PMID: 24257628 DOI: 10.1242/dev.099085]

64 **Weber T**, Namikawa K, Winter B, Müller-Brown K, Kühn R, Wurst W, Köster RW. Caspase-mediated apoptosis induction in zebrafish cerebellar Purkinje neurons. *Development* 2016; **143**: 4279-4287 [PMID: 27729409 DOI: 10.1242/dev.122721]

65 **Donega V**, van Velthoven CT, Nijboer CH, Kavelaars A, Heijnen CJ. The endogenous regenerative capacity of the damaged newborn brain: boosting neurogenesis with mesenchymal stem cell treatment. *J Cereb Blood Flow Metab* 2013; **33**: 625-634 [PMID: 23403379 DOI: 10.1038/jcbfm.2013.3]

66 **Dichgans M**, Pulit SL, Rosand J. Stroke genetics: discovery, biology, and clinical applications. *Lancet Neurol* 2019; **18**: 587-599 [PMID: 30975520 DOI: 10.1016/S1474-4422(19)30043-2]

67 **Liu C**, Wu C, Yang Q, Gao J, Li L, Yang D, Luo L. Macrophages Mediate the Repair of Brain Vascular Rupture through Direct Physical Adhesion and Mechanical Traction. *Immunity* 2016; **44**: 1162-1176 [PMID: 27156384 DOI: 10.1016/j.immuni.2016.03.008]

68 **Galant S**, Furlan G, Coolen M, Dirian L, Foucher I, Bally-Cuif L. Embryonic origin and lineage hierarchies of the neural progenitor subtypes building the zebrafish adult midbrain. *Dev Biol* 2016; **420**: 120-135 [PMID: 27693369 DOI: 10.1016/j.ydbio.2016.09.022]

69 **Shimizu Y**, Ueda Y, Ohshima T. Wnt signaling regulates proliferation and differentiation of radial glia in regenerative processes after stab injury in the optic tectum of adult zebrafish. *Glia* 2018; **66**: 1382-1394 [PMID: 29411422 DOI: 10.1002/glia.23311]

70 **Ueda Y**, Shimizu Y, Shimizu N, Ishitani T, Ohshima T. Involvement of sonic hedgehog and notch signaling in regenerative neurogenesis in adult zebrafish optic tectum after stab injury. *J Comp Neurol* 2018; **526**: 2360-2372 [PMID: 30014463 DOI: 10.1002/cne.24489]

71 **Clint SC**, Zupanc GK. Neuronal regeneration in the cerebellum of adult teleost fish, Apteronotus leptorhynchus: guidance of migrating young cells by radial glia. *Brain Res Dev Brain Res* 2001; **130**: 15-23 [PMID: 11557090 DOI: 10.1016/S0165-3806(01)00193-6]

72 **Wu CC**, Tsai TH, Chang C, Lee TT, Lin C, Cheng IH, Sun MC, Chuang YJ, Chen BS. On the crucial cerebellar wound healing-related pathways and their cross-talks after traumatic brain injury in Danio rerio. *PLoS One* 2014; **9**: e97902 [PMID: 24926785 DOI: 10.1371/journal.pone.0097902]

73 **Liu Q**, Azodi E, Kerstetter AE, Wilson AL. Cadherin-2 and cadherin-4 in developing, adult and regenerating zebrafish cerebellum. *Brain Res Dev Brain Res* 2004; **150**: 63-71 [PMID: 15126039 DOI: 10.1016/j.devbrainres.2004.03.002]

74 **Sirko S**, Behrendt G, Johansson PA, Tripathi P, Costa M, Bek S, Heinrich C, Tiedt S, Colak D, Dichgans M, Fischer IR, Plesnila N, Staufenbiel M, Haass C, Snapyan M, Saghatelyan A, Tsai LH, Fischer A, Grobe K, Dimou L, Götz M. Reactive glia in the injured brain acquire stem cell properties in response to sonic hedgehog. [corrected]. *Cell Stem Cell* 2013; **12**: 426-439 [PMID: 23561443 DOI: 10.1016/j.stem.2013.01.019]

75 **Monaco A**, Grimaldi MC, Ferrandino I. Neuroglial alterations in the zebrafish brain exposed to cadmium chloride. *J Appl Toxicol* 2016; **36**: 1629-1638 [PMID: 27080906 DOI: 10.1002/jat.3328]

76 **Nunes ME**, Müller TE, Braga MM, Fontana BD, Quadros VA, Marins A, Rodrigues C, Menezes C, Rosemberg DB, Loro VL. Chronic Treatment with Paraquat Induces Brain Injury, Changes in Antioxidant Defenses System, and Modulates Behavioral Functions in Zebrafish. *Mol Neurobiol* 2017; **54**: 3925-3934 [PMID: 27229491 DOI: 10.1007/s12035-016-9919-x]

77 **Skaggs K**, Goldman D, Parent JM. Excitotoxic brain injury in adult zebrafish stimulates neurogenesis and long-distance neuronal integration. *Glia* 2014; **62**: 2061-2079 [PMID: 25043622 DOI: 10.1002/glia.22726]

78 **Sheng L**, Wang L, Su M, Zhao X, Hu R, Yu X, Hong J, Liu D, Xu B, Zhu Y, Wang H, Hong F. Mechanism of TiO2 nanoparticle-induced neurotoxicity in zebrafish (Danio rerio). *Environ Toxicol* 2016; **31**: 163-175 [PMID: 25059219 DOI: 10.1002/tox.22031]

79 **Sieger D**, Moritz C, Ziegenhals T, Prykhozhij S, Peri F. Long-range Ca2+ waves transmit brain-damage signals to microglia. *Dev Cell* 2012; **22**: 1138-1148 [PMID: 22632801 DOI: 10.1016/j.devcel.2012.04.012]

80 **Haynes SE**, Hollopeter G, Yang G, Kurpius D, Dailey ME, Gan WB, Julius D. The P2Y12 receptor regulates microglial activation by extracellular nucleotides. *Nat Neurosci* 2006; **9**: 1512-1519 [PMID: 17115040 DOI: 10.1038/nn1805]

81 **Moritz C**, Berardi F, Abate C, Peri F. Live imaging reveals a new role for the sigma-1 (σ1) receptor in allowing microglia to leave brain injuries. *Neurosci Lett* 2015; **591**: 13-18 [PMID: 25666889 DOI: 10.1016/j.neulet.2015.02.004]

82 **Kizil C**, Kyritsis N, Dudczig S, Kroehne V, Freudenreich D, Kaslin J, Brand M. Regenerative neurogenesis from neural progenitor cells requires injury-induced expression of Gata3. *Dev Cell* 2012; **23**: 1230-1237 [PMID: 23168169 DOI: 10.1016/j.devcel.2012.10.014]

83 **Kizil C**, Dudczig S, Kyritsis N, Machate A, Blaesche J, Kroehne V, Brand M. The chemokine receptor cxcr5 regulates the regenerative neurogenesis response in the adult zebrafish brain. *Neural Dev* 2012; **7**: 27 [PMID: 22824261 DOI: 10.1186/1749-8104-7-27]

84 **Carlén M**, Meletis K, Göritz C, Darsalia V, Evergren E, Tanigaki K, Amendola M, Barnabé-Heider F, Yeung MS, Naldini L, Honjo T, Kokaia Z, Shupliakov O, Cassidy RM, Lindvall O, Frisén J. Forebrain ependymal cells are Notch-dependent and generate neuroblasts and astrocytes after stroke. *Nat Neurosci* 2009; **12**: 259-267 [PMID: 19234458 DOI: 10.1038/nn.2268]

85 **Arvidsson A**, Collin T, Kirik D, Kokaia Z, Lindvall O. Neuronal replacement from endogenous precursors in the adult brain after stroke. *Nat Med* 2002; **8**: 963-970 [PMID: 12161747 DOI: 10.1038/nm747]

86 **Thored P**, Arvidsson A, Cacci E, Ahlenius H, Kallur T, Darsalia V, Ekdahl CT, Kokaia Z, Lindvall O. Persistent production of neurons from adult brain stem cells during recovery after stroke. *Stem Cells* 2006; **24**: 739-747 [PMID: 16210404 DOI: 10.1634/stemcells.2005-0281]

87 **Cooper JA**. Cell biology in neuroscience: mechanisms of cell migration in the nervous system. *J Cell Biol* 2013; **202**: 725-734 [PMID: 23999166 DOI: 10.1083/jcb.201305021]

88 **Alunni A**, Krecsmarik M, Bosco A, Galant S, Pan L, Moens CB, Bally-Cuif L. Notch3 signaling gates cell cycle entry and limits neural stem cell amplification in the adult pallium. *Development* 2013; **140**: 3335-3347 [PMID: 23863484 DOI: 10.1242/dev.095018]

89 **Magnusson JP**, Göritz C, Tatarishvili J, Dias DO, Smith EM, Lindvall O, Kokaia Z, Frisén J. A latent neurogenic program in astrocytes regulated by Notch signaling in the mouse. *Science* 2014; **346**: 237-241 [PMID: 25301628 DOI: 10.1126/science.346.6206.237]

90 **Diotel N**, Beil T, Strähle U, Rastegar S. Differential expression of id genes and their potential regulator znf238 in zebrafish adult neural progenitor cells and neurons suggests distinct functions in adult neurogenesis. *Gene Expr Patterns* 2015; **19**: 1-13 [PMID: 26107416 DOI: 10.1016/j.gep.2015.05.004]

91 **Leung JW**, Lau BW, Chan VS, Lau CS, So KF. Abnormal increase of neuronal precursor cells and exacerbated neuroinflammation in the corpus callosum in murine model of systemic lupus erythematosus. *Restor Neurol Neurosci* 2016; **34**: 443-453 [PMID: 27163251 DOI: 10.3233/RNN-160638]

92 **Ekdahl CT**, Claasen JH, Bonde S, Kokaia Z, Lindvall O. Inflammation is detrimental for neurogenesis in adult brain. *Proc Natl Acad Sci U S A* 2003; **100**: 13632-13637 [PMID: 14581618 DOI: 10.1073/pnas.2234031100]

93 **Whitney NP**, Eidem TM, Peng H, Huang Y, Zheng JC. Inflammation mediates varying effects in neurogenesis: relevance to the pathogenesis of brain injury and neurodegenerative disorders. *J Neurochem* 2009; **108**: 1343-1359 [PMID: 19154336 DOI: 10.1111/j.1471-4159.2009.05886.x]

94 **Kizil C**, Kyritsis N, Brand M. Effects of inflammation on stem cells: together they strive? *EMBO Rep* 2015; **16**: 416-426 [PMID: 25739812 DOI: 10.15252/embr.201439702]

95 **Kyritsis N**, Kizil C, Brand M. Neuroinflammation and central nervous system regeneration in vertebrates. *Trends Cell Biol* 2014; **24**: 128-135 [PMID: 24029244 DOI: 10.1016/j.tcb.2013.08.004]

96 **Tobin MK**, Bonds JA, Minshall RD, Pelligrino DA, Testai FD, Lazarov O. Neurogenesis and inflammation after ischemic stroke: what is known and where we go from here. *J Cereb Blood Flow Metab* 2014; **34**: 1573-1584 [PMID: 25074747 DOI: 10.1038/jcbfm.2014.130]

97 **Kohman RA**, Rhodes JS. Neurogenesis, inflammation and behavior. *Brain Behav Immun* 2013; **27**: 22-32 [PMID: 22985767 DOI: 10.1016/j.bbi.2012.09.003]

98 **Sierra A**, Beccari S, Diaz-Aparicio I, Encinas JM, Comeau S, Tremblay MÈ. Surveillance, phagocytosis, and inflammation: how never-resting microglia influence adult hippocampal neurogenesis. *Neural Plast* 2014; **2014**: 610343 [PMID: 24772353 DOI: 10.1155/2014/610343]

99 **Kulkarni A**, Ganesan P, O'Donnell LA. Interferon Gamma: Influence on Neural Stem Cell Function in Neurodegenerative and Neuroinflammatory Disease. *Clin Med Insights Pathol* 2016; **9**: 9-19 [PMID: 27774000 DOI: 10.4137/CPath.S40497]

100 **LeBert DC**, Huttenlocher A. Inflammation and wound repair. *Semin Immunol* 2014; **26**: 315-320 [PMID: 24853879 DOI: 10.1016/j.smim.2014.04.007]

101 **Caldwell LJ**, Davies NO, Cavone L, Mysiak KS, Semenova SA, Panula P, Armstrong JD, Becker CG, Becker T. Regeneration of Dopaminergic Neurons in Adult Zebrafish Depends on Immune System Activation and Differs for Distinct Populations. *J Neurosci* 2019; **39**: 4694-4713 [PMID: 30948475 DOI: 10.1523/JNEUROSCI.2706-18.2019]

102 **Li L**, Yan B, Shi YQ, Zhang WQ, Wen ZL. Live imaging reveals differing roles of macrophages and neutrophils during zebrafish tail fin regeneration. *J Biol Chem* 2012; **287**: 25353-25360 [PMID: 22573321 DOI: 10.1074/jbc.M112.349126]

103 **Petrie TA**, Strand NS, Yang CT, Rabinowitz JS, Moon RT. Macrophages modulate adult zebrafish tail fin regeneration. *Development* 2014; **141**: 2581-2591 [PMID: 24961798 DOI: 10.1242/dev.098459]

104 **Carrillo SA**, Anguita-Salinas C, Peña OA, Morales RA, Muñoz-Sánchez S, Muñoz-Montecinos C, Paredes-Zúñiga S, Tapia K, Allende ML. Macrophage Recruitment Contributes to Regeneration of Mechanosensory Hair Cells in the Zebrafish Lateral Line. *J Cell Biochem* 2016; **117**: 1880-1889 [PMID: 26755079 DOI: 10.1002/jcb.25487]

105 **de Preux Charles AS**, Bise T, Baier F, Sallin P, Jaźwińska A. Preconditioning boosts regenerative programmes in the adult zebrafish heart. *Open Biol* 2016; **6** [PMID: 27440423 DOI: 10.1098/rsob.160101]

106 **de Preux Charles AS**, Bise T, Baier F, Marro J, Jaźwińska A. Distinct effects of inflammation on preconditioning and regeneration of the adult zebrafish heart. *Open Biol* 2016; **6** [PMID: 27440424 DOI: 10.1098/rsob.160102]

107 **Huang WC**, Yang CC, Chen IH, Liu YM, Chang SJ, Chuang YJ. Treatment of Glucocorticoids Inhibited Early Immune Responses and Impaired Cardiac Repair in Adult Zebrafish. *PLoS One* 2013; **8**: e66613 [PMID: 23805247 DOI: 10.1371/journal.pone.0066613]

108 **Frik J**, Merl-Pham J, Plesnila N, Mattugini N, Kjell J, Kraska J, Gómez RM, Hauck SM, Sirko S, Götz M. Cross-talk between monocyte invasion and astrocyte proliferation regulates scarring in brain injury. *EMBO Rep* 2018; **19** [PMID: 29632244 DOI: 10.15252/embr.201745294]

109 **Burda JE**, Sofroniew MV. Reactive gliosis and the multicellular response to CNS damage and disease. *Neuron* 2014; **81**: 229-248 [PMID: 24462092 DOI: 10.1016/j.neuron.2013.12.034]

110 **Köster RW**, Fraser SE. FGF signaling mediates regeneration of the differentiating cerebellum through repatterning of the anterior hindbrain and reinitiation of neuronal migration. *J Neurosci* 2006; **26**: 7293-7304 [PMID: 16822987 DOI: 10.1523/jneurosci.0095-06.2006]

111 **Lepilina A**, Coon AN, Kikuchi K, Holdway JE, Roberts RW, Burns CG, Poss KD. A dynamic epicardial injury response supports progenitor cell activity during zebrafish heart regeneration. *Cell* 2006; **127**: 607-619 [PMID: 17081981 DOI: 10.1016/j.cell.2006.08.052]

112 **Shibata E**, Yokota Y, Horita N, Kudo A, Abe G, Kawakami K, Kawakami A. Fgf signalling controls diverse aspects of fin regeneration. *Development* 2016; **143**: 2920-2929 [PMID: 27402707 DOI: 10.1242/dev.140699]

113 **Goldshmit Y**, Sztal TE, Jusuf PR, Hall TE, Nguyen-Chi M, Currie PD. Fgf-dependent glial cell bridges facilitate spinal cord regeneration in zebrafish. *J Neurosci* 2012; **32**: 7477-7492 [PMID: 22649227 DOI: 10.1523/JNEUROSCI.0758-12.2012]

114 **Wills AA**, Kidd AR, Lepilina A, Poss KD. Fgfs control homeostatic regeneration in adult zebrafish fins. *Development* 2008; **135**: 3063-3070 [PMID: 18701543 DOI: 10.1242/dev.024588]

115 **Poss KD**, Shen J, Nechiporuk A, McMahon G, Thisse B, Thisse C, Keating MT. Roles for Fgf signaling during zebrafish fin regeneration. *Dev Biol* 2000; **222**: 347-358 [PMID: 10837124 DOI: 10.1006/dbio.2000.9722]

116 **Addington CP**, Roussas A, Dutta D, Stabenfeldt SE. Endogenous repair signaling after brain injury and complementary bioengineering approaches to enhance neural regeneration. *Biomark Insights* 2015; **10**: 43-60 [PMID: 25983552 DOI: 10.4137/BMI.S20062]

117 **Bramlett HM**, Dietrich WD. Long-Term Consequences of Traumatic Brain Injury: Current Status of Potential Mechanisms of Injury and Neurological Outcomes. *J Neurotrauma* 2015; **32**: 1834-1848 [PMID: 25158206 DOI: 10.1089/neu.2014.3352]

118 **Gitler AD**, Dhillon P, Shorter J. Neurodegenerative disease: models, mechanisms, and a new hope. *Dis Model Mech* 2017; **10**: 499-502 [PMID: 28468935 DOI: 10.1242/dmm.030205]

119 **Tanaka EM**, Ferretti P. Considering the evolution of regeneration in the central nervous system. *Nat Rev Neurosci* 2009; **10**: 713-723 [PMID: 19763104 DOI: 10.1038/nrn2707]

120 **Adams KL**, Gallo V. The diversity and disparity of the glial scar. *Nat Neurosci* 2018; **21**: 9-15 [PMID: 29269757 DOI: 10.1038/s41593-017-0033-9]

121 **Voldoire E**, Brunet F, Naville M, Volff JN, Galiana D. Expansion by whole genome duplication and evolution of the sox gene family in teleost fish. *PLoS One* 2017; **12**: e0180936 [PMID: 28738066 DOI: 10.1371/journal.pone.0180936]

122 **Grimholt U**. Whole genome duplications have provided teleosts with many roads to peptide loaded MHC class I molecules. *BMC Evol Biol* 2018; **18**: 25 [PMID: 29471808 DOI: 10.1186/s12862-018-1138-9]

World Journal of Stem Cells

Submit a Manuscript: https://www.f6publishing.com

World J Stem Cells 2020 January 26; 12(1): 25-34

DOI: 10.4252/wjsc.v12.i1.25

ISSN 1948-0210 (online)

REVIEW

Inducing human induced pluripotent stem cell differentiation through embryoid bodies: A practical and stable approach

Ning-Ning Guo, Li-Ping Liu, Yun-Wen Zheng, Yu-Mei Li

ORCID number: Ning-Ning Guo (0000-0002-9959-6435); Li-Ping Liu (0000-0003-4445-8403); Yun-Wen Zheng (0000-0001-9002-3190); Yu-Mei Li (0000-0002-9501-5314).

Author contributions: Guo NN conceived the study and drafted the manuscript; Liu LP, Zheng YW and Li YM contributed in discussions on the subject and reviewing the final manuscript text; all the authors approved the final version of the article; Guo NN and Liu LP contributed equally to this work; Li YM and Zheng YW are senior authors and co-correspondent to this work.

Supported by National Natural Science Foundation of China, No. 81770621, No. 81573053; Ministry of Education, Culture, Sports, Science, and Technology of Japan, KAKENHI, No. 16K15604, No. 18H02866; Natural Science Foundation of Jiangsu Province, No. BK20180281.

Conflict-of-interest statement: No potential conflict of interest.

Ning-Ning Guo, Li-Ping Liu, Yun-Wen Zheng, Yu-Mei Li, Institute of Regenerative Medicine, Affiliated Hospital of Jiangsu University, Jiangsu University, Zhenjiang 212001, Jiangsu Province, China

Yun-Wen Zheng, Department of Gastrointestinal and Hepato-Biliary-Pancreatic Surgery, University of Tsukuba Faculty of Medicine, Tsukuba, Ibaraki 305-8575, Japan

Yun-Wen Zheng, Yokohama City University School of Medicine, Yokohama, Kanagawa 234-0006, Japan

Yun-Wen Zheng, Division of Regenerative Medicine, Center for Stem Cell Biology and Regenerative Medicine, The Institute of Medical Science, the University of Tokyo, Tokyo 108-8639, Japan

Corresponding author: Yun-Wen Zheng, PhD, Associate Professor, Department of Gastrointestinal and Hepato-Biliary-Pancreatic Surgery, University of Tsukuba Faculty of Medicine,Tennodai 1-1-1, Tsukuba, Ibaraki 305-8575, Japan. ywzheng@md.tsukuba.ac.jp

Abstract

Human induced pluripotent stem cells (hiPSCs) are invaluable resources for producing high-quality differentiated cells in unlimited quantities for both basic research and clinical use. They are particularly useful for studying human disease mechanisms *in vitro* by making it possible to circumvent the ethical issues of human embryonic stem cell research. However, significant limitations exist when using conventional flat culturing methods especially concerning cell expansion, differentiation efficiency, stability maintenance and multicellular 3D structure establishment, differentiation prediction. Embryoid bodies (EBs), the multicellular aggregates spontaneously generated from iPSCs in the suspension system, might help to address these issues. Due to the unique microenvironment and cell communication in EB structure that a 2D culture system cannot achieve, EBs have been widely applied in hiPSC-derived differentiation and show significant advantages especially in scaling up culturing, differentiation efficiency enhancement, *ex vivo* simulation, and organoid establishment. EBs can potentially also be used in early prediction of iPSC differentiation capability. To improve the stability and feasibility of EB-mediated differentiation and generate high quality EBs, critical factors including iPSC pluripotency maintenance, generation of uniform morphology using micro-pattern 3D culture systems, proper cellular density inoculation, and EB size control are discussed on the basis of both published data and our own laboratory experiences. Collectively, the production of a large quantity of homogeneous EBs with high quality is important for the stability and feasibility of many PSCs related studies.

Manuscript source: Invited manuscript

Received: April 1, 2019
Peer-review started: April 3, 2019
First decision: August 23,2019
Revised: September 30, 2019
Accepted: December 13, 2019
Article in press: December 13, 2019
Published online: January 26, 2020

P-Reviewer: Stocco G
S-Editor: Dou Y
L-Editor: A
E-Editor: Xing YX

Key words: Induced pluripotent stem cells; Suspension culture; Embryoid body; Early prediction; Committed differentiation; Heterogeneity; Three-dimensional culture; Scaling-up; Quality control

Core tip: Embryoid body (EB) mediated induced pluripotent stem cell (iPSC) differentiation shows great advantages in culture scale-up, differentiation efficiency improvement, *ex vivo* simulation and organoid establishment. To improve the stability and feasibility of high quality EB generation, factors including iPSC pluripotency maintenance, generation of uniform morphology using micro-pattern 3D culture systems, proper cellular density inoculation and EB size control need to be considered.

Citation: Guo NN, Liu LP, Zheng YW, Li YM. Inducing human induced pluripotent stem cell differentiation through embryoid bodies: A practical and stable approach. *World J Stem Cells* 2020; 12(1): 25-34
URL: https://www.wjgnet.com/1948-0210/full/v12/i1/25.htm
DOI: https://dx.doi.org/10.4252/wjsc.v12.i1.25

INTRODUCTION

The emergence of human induced pluripotent stem cells (hiPSCs) has markedlypromoted the development of regenerative medicine. These cells are reprogrammed from differentiated human somatic cells by gene integration or non-integration methods and possess the properties ofself-proliferation and committed differentiation[1-4]. More importantly, compared to human embryonic stem cells (hESCs), the use of hiPSCs successfully avoids major immunoreactive and ethical issues[5]. As a result, hiPSCs have quickly become a critical resource for biomedical research and are expected to be used in clinical cellular transplantation, disease model establishment, and drug screening. Conventional methods, however, are usually established in flat culture systems, which impose significant limitations on cell expansion, differentiation efficiency, and multicellular 3D structure establishment. Embryoid bodies (EBs), which are cultured in a suspension system, might help to address these issues. Generally, EB is a multicellular aggregate spontaneously formed by pluripotent stem cells under suspension culture conditions, which has three germ layer structures and partially recapitulates the early embryonic development[6]. Such a multicellular 3D structure improves cell-cell contacts and intercellular communication and also enhances substance exchange[7]. Although the differentiation from iPSC to target cells is a relatively complex, time consuming, and unstable process[8], EBs have been widely used in iPSC differentiation and organoid construction because of their irreplaceable structural and functional advantages[9,10]. It has been demonstrated that a standardized EB formation procedure contributes to their high quality and improves differentiation[11,12]. Therefore, the key factors need to be carefully considered when EB-mediated differentiation is selected[9,13].

In order to understand the critical events of EB-mediated differentiation, explore better methods and solve the aforementioned problems, we recapitulated the current applications and advantages of using EBs in iPSC differentiation. Combining our own and previously published data related to EB formation and differentiation, we conducted a comparative and predictive analysis and aimed to provide a reference to create a more stable and practical way of high-quality EB generation.

APPLICATION AND ADVANTAGES OF EB USE IN IPSC DIFFERENTIATION

Scale-up of culture systems and differentiation efficiency

Clinical transplantation requires large quantities of functional target cells and most of the existing strategies are difficult to implement at a large scale or have a low differentiation efficiency, therefore posing barriers to further research. Compared to flat culture systems, EB-derived differentiation culture is kept in a relatively fixed position, which offers this method an obvious advantage in quantity and

differentiation efficiency[14-16]. A variety of cell lineages have been generated from hEBs such as brain, cornea, heart, liver, and blood (Table 1). In our study, we used a suspension EB-based system to generate iPSC-derived melanocytes and achieved a significantly higher differentiation efficiency compared to that in flat culture systems and these induced melanocytes showed long-term *in vivo* functionality after transplantation[17]. In short, differentiation from EB to specific cell lineages is an efficient method that is likely to yield large populations of functional cells.

Ex vivo simulation and organoids establishment

Recently, due to the features of their three germ layer structure[18], hEBs have become useful models for developing human ESC- and iPSC-derived organoids by stimulation with a cocktail of biological agents (Table 1). These EB-derived organoids not only contain some cell subtypes but also show distinct stratification which is similar to the *in vivo* structure of the tissues or organs developing[19,20]. For example, Jo *et al*[21] observed an identical organization structure in 3D cultured human midbrain-like organoids (hMLOs) compared with human postmortem midbrain tissue under the electron microscope. Furthermore, these EB-derived organoids are functional. Qian *et al*[22]found that EB-derived midbrain organoids not only expressed a wider range of characteristic markers common to normal midbrain tissue compared with direct differentiation from iPSCs, but also demonstrated firing action potentials in response to current injection which can be used to establish a disease model of microcephaly[22]. These EB-derived organoids could be used to understand unique features of specific human organs and to gain insights into different disorders.

Early prediction of differentiation potential

There is a remarkable difference in differentiation capability in distinct iPSC lineages, and it is urgently necessary to predict the differentiation potential in an early stage of the long differentiation period to avoid unnecessary resource losses. Because EBs can potentially develop into three germ layer tissues for multi-directional differentiation[23,24], it can be hypothesized that they may be suitable candidates for predicting iPSC differentiation potential. Kim *et al*[25]classified hESCs-derived EBs into several types including cystic, bright cavity and dark cavity according to their morphology. By detecting the expression of specific markers, they showed that most of the cells in cystic EBs are endoderm-lineage populations and both bright and dark cavity EBs own cells from all of the three germ layers. Besides the morphology, EB size can also be used determine the differentiation direction of iPSC. For example, the larger EBs (450 μm diameter) often contained cells of the cardiovascular system, while endothelial cells were usually generated in smaller EBs (150 μm diameter) and such differentiation potentials are mainly caused by the noncanonical WNT pathway[26]. Moreover, gene expression profiles of hPSCs and EBs recovered by high-throughput RNA sequencing can also be used for differentiation prediction, and the results is parallel to the germ layer development *in vivo*[27].

The novel methods described above have some limitations. Simple morphology or size-dependent prediction system is somewhat subjective, and it is also closely related to the viability of the cells inside EB[28,29], whereas high-throughput RNA sequencing is expensive and complicated. In our study, we developed a simple and practical system and identified a set of parameters combining EB formation, maintenance, and germ layer-specific gene expression in EB stage to predict the differentiation tendency of the various iPSC lines. The validity of this evaluation system was finally confirmed by differentiating these iPSC lines into melanocytes[24]. Recently, we summarized the current methods related to iPSC differentiation prediction and we also postulated that the use of EBs could be more efficient when combined with other modified detection methods such molecular probes[34].Thus, due to their special morphology and functionality, EBs have played an important role in the differentiation prediction related studies.

Multiple-cell environment and cell communication

The remarkable functionality and application prospects of EBs are a result of their unique 3D microstructure and cell communication. Frequent passage in the adherent culture system limits the cell–cell communication in both cell number and time. The suspension culture system for EBs provides extensive material exchange and increases both cell–cell interactions and cell–matrix communication in the aggregate, which is conducive to the transmission and action of cell signals[35,36]. In general, intercellular communication is increased both in space and time at the 3D level. Additionally, differentiation of EBs is an asynchronous process and 3D culture produces distinct layers of spheroids (EBs) as a result of concentration gradients in the culture medium[37]. The differentiation of the outer endoderm of EB caused by growth factors in the medium will further induce endoderm differentiation by producing signals[38].

Table 1 Updated summary of the formation of human embryoid bodies

Target cells or organoids	Culture vessels	Cell separation (cell suspension)	Culture period(d)	Media and supplements for EB formation	Ref.
Human brain organoids	Micropillar array plates	Accutase (single-)	11	KSR, Y27632, NEAA, GlutaMAX, bFGF	Zhu *et al*[65], 2017
Midbrain-like organoids	Low adhesion 96-well V-bottom multi-well plates	NA (single-)	4	mTeSR1, Y27632, Matrigel	Jo *et al*[21], 2016
Corneal epithelial cells	Static suspension culture	NA (non-single-)	14	E6 medium, Y27632, IWP-2, bFGF	Martínez García de la Torre*et al*[66], 2017
Osteoblast-like cells		Collagenase type IV, trypsin–EDTA (non-single-)	6	Human ES medium, thiazovivin	Ochiai-Shino*et al*[67], 2014
Cardiac cells		NA (non-single-)	6	DMEM/F-12, NEAA, GlutaMAX, FBS, DMSO	Hoque *et al*[68], 2018
Neurospheres		Accutase (single-)	5	KSR, Y27632, FGF-2, NEAA, L-Glutamine	Pauly *et al*[69], 2018;
Cardiomyocytes		Type IV collagenase (single-)	10	DMEM, FBS, NEAA, GlutaMAX	Chauveau *et al*[70], 2017;
Osteoprogenitors		Dispase (non-single-)	7	DMEM, FBS, Glutamax, ABAM	Roberts *et al*[71], 2017
Chondrocytes		NA (single-)	6	Aggrewell medium, TeSR-E8 medium	Nam *et al*[72], 2017
Hepatocytes		Trypsin and collagenase IV (non-single-)	5	Knockout DMEM, NEAA, L-glutamine, FBS	Tomotsune *et al*[17], 2016
Oligodendrocytes		Trypsin-EDTA (non-single-)	2	KnockOut-DMEM, KSR, NEAA, SB431542, glutamine, ITS, Dorsomorphin	Espinosa-Jeffrey*et al*[73], 2016
Hematopoietic stem cells		Dispase (non-single-)	7	KnockOut-DMEM, KSR, Y27632, GlutaMAX, NEAA	Phondeechareon *et al*[74], 2016
Neural precursor cells		EDTA (non-single-)	5	DMEM/F12, KSR, NEAA, SB431542, GlutaMAX, Recombinant Noggin	Plaisted *et al*[75], 2016
Mesenchymal stem cells (MSCs)		Collagenase type IV (non-single-)	10	DMEM/F12, KSR, MEF conditioned medium, NEAA, bFGF, glutamine	Tang *et al*[76], 2014
Chondrocyte-like cells	Non-adherent 96-well plate	Collagenase IV (non-single-)	7	DMEM F12, L-glutamine, FBS, KSR, NEAA	Suchorska *et al*[77], 2017
Chondrocyte-like cells	Low adhesion 96-well C-bottom multi-well plate	Trypsin-EDTA (single-)	1	DMEM/F12, Y27632, KSR, NEAA	Lach *et al*[78], 2018
Retinal tissue	96-well non-adherent U-bottom plate	Accutase (single-)	12	mTeSR1, Y27632	Hunt *et al*[79], 2017
Insulin-secreting cells	Agarose round-bottom microwell plate	Accutase (single-)	10	IMDM/F-12, FBS, insulin transferring selenium-A, monothioglycerol	Pettinato *et al*[52], 2014
Neural precursors	Static or dynamic suspension culture method (orbital shaker)	EDTA (non-single-)	6-9	mTeSR1, Y27632; special equipment: orbital shaker	Miranda *et al*[80], 2016
Macrophages	AggreWell™, 96-well round-bottomed multi-well plate	Collagenase-dispase mixture (single-)	4	DMEM/F12, Y27632, KSR, L-glutamine	Mukherjee *et al*[81], 2018
Primordial germ cell-likecells	AggreWell microwells	Accutase (single-)	1	KnockOut DMEM, Y27632, KSR, NEAA, bovine pancreas insulin, LIF, TGF-β, CHIR99021, PD0325901, BIRB796, SP600125	Mitsunaga *et al*[41], 2017
Forebrain cortical cells		Collagenase (non-single-)	4	DMEM/F12, KSR, glutamine, NEAA	Muratore *et al*[49], 2014

Melanocytes	24-well Elplasia™microwell plates (round bottom)	Accutase (single-)	7	mTeSR1, Y27632	Liu *et al*[82], 2019

"NA" means enzyme deficiency or mechanical dissection of the iPSC clones. E6 medium: Essential 6 medium; IMDM/F-12: Iscove's Modified Dulbecco's Medium/Nutrient Mixture F-12; DMEM/F-12: Dulbecco's Modified Eagle Medium/Nutrient Mixture F-12; mTeSR1: Standardized medium for the feeder-independent maintenance of hESCs and hiPSCs; TeSR-E8 medium: A feeder-free, animal component-free culture medium for hESCs and hiPSCs; MEF: Mouse embryonic fibroblast; FBS: Fetal bovine serum; LIF: Leukemia inhibitory factor; TGF-β: Transforming growth factor-beta; bFGF: Basic fibroblast growth factor; Y27632: Rho-associated kinas inhibitor; KSR: Knockout serum replacement; NEAA: Non-essential amino acids; DMSO: Dimethyl sulphoxide; IWP-2: Inhibitor of the WNT pathway; ITS: Insulin-Transferrin-Selenium; SB431542: Inhibitor of the activin type I receptor ALK4 and the nodal type I receptor ALK7; CHIR99021: Inhibitor of glycogen synthase kinase 3β (GSK3β); PD0325901: Inhibitor of the mitogen-activated protein kinase (MEK) pathway; BIRB796: Inhibitor of the mitogen-activated protein kinases (MAPK); SP600125: Inhibitor of c-Jun N-terminal kinase (JNK).

This unbalanced phenomenon also explains the heterogeneity throughout the differentiation process in EBs. Moreover, more intricate gene profiles could be expressed in a 3D culture system, reflecting original expression *in vivo* more accurately[16]. Jo *et al*[21] found that gene profiles detected by RNA sequencing analysis are analogously expressed between hMLOs and the human prenatal midbrain. However, there is a significant difference between the 2D dopamine neurons and normal tissue. The integrity of gene expression is a considerable advantage of the 3D culture system, providing a better foundation for future structural and functional studies. Meanwhile, for the hiPSC-based differentiation, the cadherin-β-catenin-Wnt pathway was found to be involved in the development of EBs by intercellular adhesion[39]. In addition, the activation or inhibition of relevant signaling pathways can yield a definitive lineage differentiation[22,40,41]. Therefore, controlling the dose and duration of cytokines regulates the differentiation of iPSCs by activating various pathways.

Compared with a flat culture, microgravity has been found to be a subsidiary factor that can regulate cell proliferation and survival in a 3D culture system[29-32]. Therefore, bioreactors and random positioning machines have been used to simulate states of microgravity and weightless condition for EB-derived differentiation[42,43].

In conclusion, EBs have shown great application potential in the generation of various functional cells and organoids at a large scale and also in the prediction of iPSC differentiation capability. These EB-derived cells and organoids highly resemble the *in vivo* status in both gene expression and function display as a result of the structure and microenvironment in the EB.

QUALITY CONTROL OF EB

Considering the wide range of applications of EBs in iPSC differentiation and their potential advantages, a comprehensive quality control of the EB formation process would help to improve the stability and feasibility of their application.

Pluripotency maintenancein iPSCs

To generate high quality EBs, the initial step is the pluripotency maintenance in iPSCs where the addition of various cytokines and inhibitors is essential. Two studies[15,44]demonstrated that basic fibroblast growth factor (bFGF) induced hES cell derived fibroblast-like cells produce insulin-like growth factor II and transforming growth factor β family of factors and indirectly establish a balanced stem cell niche of hESCs, contributing to maintain the undifferentiated state of hESCs. In addition, Y-27632 was confirmed to benefit the expression of POU class 5 homeobox 1 (OCT4) in EB formation[45-48]. Compared with the conventional methods, single cell culture system can reduce the complexity caused by feeder cells. However, it is more difficult to maintain undifferentiated status of iPSC when single-cell passage is used. Tsutsui *et al*[45]developed a unique combination of inhibition of Rho-associated kinase, glycogen synthase kinase and mitogen-activated protein kinase with bFGF for hES cells maintenance and they found these cells to present good pluripotency and genetic integrity in long-term maintenance (> 20 passages).

Formation and uniform morphology

In general, EBs can be spontaneously generated with hiPSC clusters[8,46] or single cells[41,49] in 3D culture systems using EB-specific medium. When conventional methods such as static suspension culture and the hanging drop method[50,51]are chosen, EB-derived differentiation seems unstable, which is in part associated with the heterogeneity of EBs[52,53]. Therefore, it is necessary to control the generation of uniform EBs for stable and reproducible differentiation. Recently, different types of micro-pattern plates have been developed and widely applied for the generation of

EBs with uniform size and morphology using single hiPSCs (Table 1) and on this basis, a variety of culture systems such as the micro-space system[50,51,54], spinner flasks[22], and the National Aeronautics and Space Administration developed rotary cell culture system (NASA rotary system)[55] have also been designed for scale-up.

Cellular density and EB size

Besides morphological uniformity, the efficiency and direction of differentiation are also affected by EB size[56-58] and which size is more appropriate depends on the specific cell lineages. It has been demonstrated that a larger amount of cardiomyocytes was found in hESC-derived differentiation using EBs with100 μm diameter when compared to larger ones (300 μm)[59]. However, we found that 300-400 μm might be a more suitable diameter for melanocytes differentiation compared to those bigger or smaller. Since the size and quality of EB during culture maintenance are affected by the number of inoculated cells, micro-pattern plates can be used to control EB size by adjusting cellular density. However, inoculated cell density also depends on the EB culture plate type and culture duration before differentiation. In a study of iPSC differentiation into cardiomyocytes, input of 1.5×10^4 to 4.0×10^4 cells per EB was determined to be the proper density to form homogenous and synchronized EBs. By contrast, we found that 5.0×10^2 to 1.0×10^3 cells were enough for each EB generation using an Elplasia™ micro-well plate and this density tended to yield stable and intact EBs (Figure 1) which could be maintained over a relatively long term for differentiation. Overly high cell density (2.0×10^3 cells/EB) will lead to breakage or fusion in a short time (Figure 1). In short, EBs within a certain size range are more conducive to differentiation which can be modified by cell density adjustment. However, size usually varies across different differentiation assays and needs to be optimized in accordance to the specific conditions.

FUTURE PERSPECTIVES AND CONCLUSION

EBs can effectively mimic the *in vivo* differentiation process and have shown excellent advantages in the field of iPSC-derived differentiation, especially in organoid establishment. However, a gap between these products and normal organs is still inevitable because the inclusion of a cocktail of factors and additives only provides a somewhat analogous survival environment rather than completely simulating the *in vivo* conditions and this difference generally leads to a temporal and spatial distinction[60,61]. To reduce these differences as much as possible, many studies have been carried out with the aim to optimize the culture system, including culture duration, plate type, dose of growth factors and small molecules, matrix proteins and even the order of the additives[35,36]based on research aims and differentiated cell types. In terms of iPSC-derived EB formation, the initial inoculation density is more critical than additives and centrifugation (forcing cell aggregation), and more of such insights can likely be obtained from tumor sphere related studies[62]. For example, magnetic levitation, a new method for spheroid formation, has been used to establish a levitation profile for distinct tumor cells[63]. Whether this novel technology can also be adopted for EB related differentiation and cell purification remains to be explored.

Overall, an EB mediated culture system is more amenable to improvement in differentiation efficiency and simulation of the human microenvironment compared to 2D differentiation. Cell proliferation, cell–cell interaction, and material metabolism partially undergo the influence of microgravity, achieving more intricate gene expression and epigenetic profiles. More importantly, most of the iPSC related studies require a relatively long observation time which inevitably leads to instability. EBs with good quality control could provide a stable and feasible system to better present the functional integrity of tissues and organs[64], underlining their potential in the exploration of promising drugs and precision medicine where classical 2D cell assays might fail.

Significantly, EBs are also expected to reveal the development of early human embryos, avoiding ethical issues. EB formation and lineage commitment have become the focus of research in terms of the structure and composition of differentiated cells. RNA sequencing of single EB cells will help to clarify the evolution or/and unknown event of early embryos and the fate development of individual cells. In conclusion, the production of a large quantity of homogeneous EBs with high quality is important for many PSCs related studies, including scaling up culturing, organoid formation, and differentiation potential prediction.

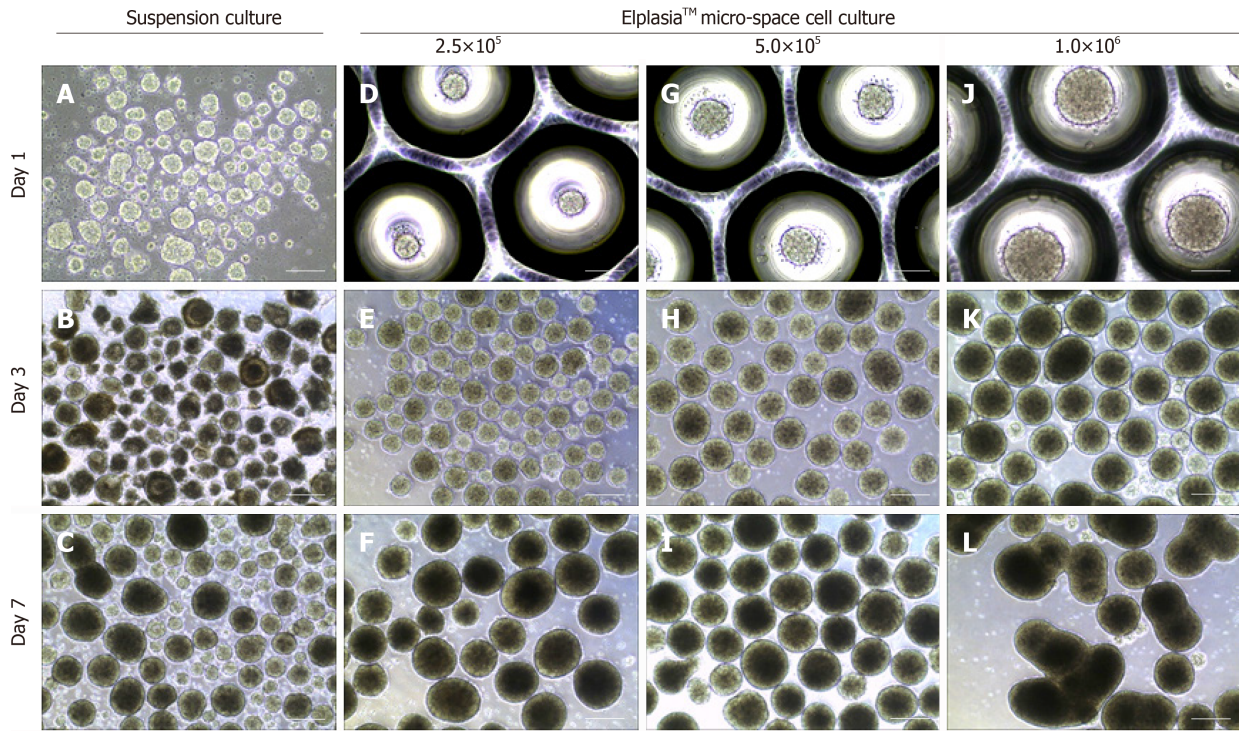

Figure 1 Static suspension culture and 24-well Elplasia™ micro-well culture with human induced pluripotent stem cells. A-C:Induced pluripotent stem cell (iPSC)-derived embryoid bodies (EBs) formed under a suspension system and cultured with mTeSR™, respectively, on day 1 (A), day 3 (B), and day 7 (C); D-L: iPSC-derived EBs formed with single hiPSCs in micro-space cell culture plates at different cell densities: D-F: 2.5 × 10^5 cells/mL; G–I: 5.0 × 10^5 cells/mL; and J–L: 1.0 × 10^6 cells/mL, respectively, on day 1 (D, G, and J), day 3 (E, H, and K), and day 7 (F, I, and L). Scale bars: A, D, G, and J 100 μm; resident graphs, 250 μm.

REFERENCES

1 **Zhao Y**, Zhao T, Guan J, Zhang X, Fu Y, Ye J, Zhu J, Meng G, Ge J, Yang S, Cheng L, Du Y, Zhao C, Wang T, Su L, Yang W, Deng H. A XEN-like State Bridges Somatic Cells to Pluripotency during Chemical Reprogramming. *Cell* 2015; **163**: 1678-1691 [PMID: 26686652 DOI: 10.1016/j.cell.2015.11.017]

2 **Warren L**, Manos PD, Ahfeldt T, Loh YH, Li H, Lau F, Ebina W, Mandal PK, Smith ZD, Meissner A, Daley GQ, Brack AS, Collins JJ, Cowan C, Schlaeger TM, Rossi DJ. Highly efficient reprogramming to pluripotency and directed differentiation of human cells with synthetic modified mRNA. *Cell Stem Cell* 2010; **7**: 618-630 [PMID: 20888316 DOI: 10.1016/j.stem.2010.08.012]

3 **Nakagawa M**, Koyanagi M, Tanabe K, Takahashi K, Ichisaka T, Aoi T, Okita K, Mochiduki Y, Takizawa N, Yamanaka S. Generation of induced pluripotent stem cells without Myc from mouse and human fibroblasts. *Nat Biotechnol* 2008; **26**: 101-106 [PMID: 18059259 DOI: 10.1038/nbt1374]

4 **Miyoshi N**, Ishii H, Nagano H, Haraguchi N, Dewi DL, Kano Y, Nishikawa S, Tanemura M, Mimori K, Tanaka F, Saito T, Nishimura J, Takemasa I, Mizushima T, Ikeda M, Yamamoto H, Sekimoto M, Doki Y, Mori M. Reprogramming of mouse and human cells to pluripotency using mature microRNAs. *Cell Stem Cell* 2011; **8**: 633-638 [PMID: 21620789 DOI: 10.1016/j.stem.2011.05.001]

5 **Menon S**, Shailendra S, Renda A, Longaker M, Quarto N. An Overview of Direct Somatic Reprogramming: The Ins and Outs of iPSCs. *Int J Mol Sci* 2016; 17 [PMID: 26805822 DOI: 10.3390/ijms17010141]

6 **Kurosawa H**. Methods for inducing embryoid body formation: in vitro differentiation system of embryonic stem cells. *J Biosci Bioeng* 2007; **103**: 389-398 [PMID: 17609152 DOI: 10.1263/jbb.103.389]

7 **Saltzman WM**, Kyriakides TR. Chapter 20 - Cell Interactions with Polymers. In: Principles of Tissue Engineering (Fourth Edition). Lanza R, Langer R, Vacanti J, Editors. 2014, Academic Press: Boston, 385-406. [DOI: 10.1016/B978-0-12-398358-9.00020-3]

8 **Chen KG**, Mallon BS, Johnson KR, Hamilton RS, McKay RD, Robey PG. Developmental insights from early mammalian embryos and core signaling pathways that influence human pluripotent cell growth and differentiation. *Stem Cell Res* 2014; **12**: 610-621 [PMID: 24603366 DOI: 10.1016/j.scr.2014.02.002]

9 **Lin RZ**, Chang HY. Recent advances in three-dimensional multicellular spheroid culture for biomedical research. *Biotechnol J* 2008; **3**: 1172-1184 [PMID: 18566957 DOI: 10.1002/biot.200700228]

10 **Breslin S**, O'Driscoll L. Three-dimensional cell culture: the missing link in drug discovery. *Drug Discov Today* 2013; **18**: 240-249 [PMID: 23073387 DOI: 10.1016/j.drudis.2012.10.003]

11 **Froehlich K**, Haeger JD, Heger J, Pastuschek J, Photini SM, Yan Y, Lupp A, Pfarrer C, Mrowka R, Schleußner E, Markert UR, Schmidt A. Generation of Multicellular Breast Cancer Tumor Spheroids: Comparison of Different Protocols. *J Mammary Gland Biol Neoplasia* 2016; **21**: 89-98 [PMID: 27518775 DOI: 10.1007/s10911-016-9359-2]

12 **Pyle AD**, Lock LF, Donovan PJ. Neurotrophins mediate human embryonic stem cell survival. *Nat Biotechnol* 2006; **24**: 344-350 [PMID: 16444268 DOI: 10.1038/nbt1189]

13 **Burridge PW**, Metzler SA, Nakayama KH, Abilez OJ, Simmons CS, Bruce MA, Matsuura Y, Kim P, Wu JC, Butte M, Huang NF, Yang PC. Multi-cellular interactions sustain long-term contractility of human

pluripotent stem cell-derived cardiomyocytes. *Am J Transl Res* 2014; **6**: 724-735 [PMID: 25628783]
14 **Alvarez-Pérez J**, Ballesteros P, Cerdán S. Microscopic images of intraspheroidal pH by 1H magnetic resonance chemical shift imaging of pH sensitive indicators. *MAGMA* 2005; **18**: 293-301 [PMID: 16328228 DOI: 10.1007/s10334-005-0013-z]
15 **Ungrin MD**, Joshi C, Nica A, Bauwens C, Zandstra PW. Reproducible, ultra high-throughput formation of multicellular organization from single cell suspension-derived human embryonic stem cell aggregates. *PLoS One* 2008; **3**: e1565 [PMID: 18270562 DOI: 10.1371/journal.pone.0001565]
16 **Hirschhaeuser F**, Menne H, Dittfeld C, West J, Mueller-Klieser W, Kunz-Schughart LA. Multicellular tumor spheroids: an underestimated tool is catching up again. *J Biotechnol* 2010; **148**: 3-15 [PMID: 20097238 DOI: 10.1016/j.jbiotec.2010.01.012]
17 **Tomotsune D**, Hirashima K, Fujii M, Yue F, Matsumoto K, Takizawa-Shirasawa S, Yokoyama T, Sasaki K. Enrichment of Pluripotent Stem Cell-Derived Hepatocyte-Like Cells by Ammonia Treatment. *PLoS One* 2016; **11**: e0162693 [PMID: 27632182 DOI: 10.1371/journal.pone.0162693]
18 **Brickman JM**, Serup P. Properties of embryoid bodies. *Wiley Interdiscip Rev Dev Biol* 2017; 6 [PMID: 27911036 DOI: 10.1002/wdev.259]
19 **Pavesi A**, Adriani G, Rasponi M, Zervantonakis IK, Fiore GB, Kamm RD. Controlled electromechanical cell stimulation on-a-chip. *Sci Rep* 2015; **5**: 11800 [PMID: 26135970 DOI: 10.1038/srep11800]
20 **Simmons CS**, Petzold BC, Pruitt BL. Microsystems for biomimetic stimulation of cardiac cells. *Lab Chip* 2012; **12**: 3235-3248 [PMID: 22782590 DOI: 10.1039/c2lc40308k]
21 **Jo J**, Xiao Y, Sun AX, Cukuroglu E, Tran HD, Göke J, Tan ZY, Saw TY, Tan CP, Lokman H, Lee Y, Kim D, Ko HS, Kim SO, Park JH, Cho NJ, Hyde TM, Kleinman JE, Shin JH, Weinberger DR, Tan EK, Je HS, Ng HH. Midbrain-like Organoids from Human Pluripotent Stem Cells Contain Functional Dopaminergic and Neuromelanin-Producing Neurons. *Cell Stem Cell* 2016; **19**: 248-257 [PMID: 27476966 DOI: 10.1016/j.stem.2016.07.005]
22 **Qian X**, Nguyen HN, Song MM, Hadiono C, Ogden SC, Hammack C, Yao B, Hamersky GR, Jacob F, Zhong C, Yoon KJ, Jeang W, Lin L, Li Y, Thakor J, Berg DA, Zhang C, Kang E, Chickering M, Nauen D, Ho CY, Wen Z, Christian KM, Shi PY, Maher BJ, Wu H, Jin P, Tang H, Song H, Ming GL. Brain-Region-Specific Organoids Using Mini-bioreactors for Modeling ZIKV Exposure. *Cell* 2016; **165**: 1238-1254 [PMID: 27118425 DOI: 10.1016/j.cell.2016.04.032]
23 **Itskovitz-Eldor J**, Schuldiner M, Karsenti D, Eden A, Yanuka O, Amit M, Soreq H, Benvenisty N. Differentiation of human embryonic stem cells into embryoid bodies compromising the three embryonic germ layers. *Mol Med* 2000; **6**: 88-95 [PMID: 10859025]
24 **Guo NN**, Liu LP, Zhang YX, Cai YT, Guo Y, Zheng YW, Li YM. Early prediction of the differentiation potential during the formation of human iPSC-derived embryoid bodies. *Biochem Biophys Res Commun* 2019; **516**: 673-679 [PMID: 31248595 DOI: 10.1016/j.bbrc.2019.06.081]
25 **Kim JM**, Moon SH, Lee SG, Cho YJ, Hong KS, Lee JH, Lee HJ, Chung HM. Assessment of differentiation aspects by the morphological classification of embryoid bodies derived from human embryonic stem cells. *Stem Cells Dev* 2011; **20**: 1925-1935 [PMID: 21388292 DOI: 10.1089/scd.2010.0476]
26 **Hwang YS**, Chung BG, Ortmann D, Hattori N, Moeller HC, Khademhosseini A. Microwell-mediated control of embryoid body size regulates embryonic stem cell fate via differential expression of WNT5a and WNT11. *Proc Natl Acad Sci U S A* 2009; **106**: 16978-16983 [PMID: 19805103 DOI: 10.1073/pnas.0905550106]
27 **Han X**, Chen H, Huang D, Chen H, Fei L, Cheng C, Huang H, Yuan GC, Guo G. Mapping human pluripotent stem cell differentiation pathways using high throughput single-cell RNA-sequencing. *Genome Biol* 2018; **19**: 47 [PMID: 29622030 DOI: 10.1186/s13059-018-1426-0]
28 **Cockburn K**, Rossant J. Making the blastocyst: lessons from the mouse. *J Clin Invest* 2010; **120**: 995-1003 [PMID: 20364097 DOI: 10.1172/JCI41229]
29 **Mueller-Klieser W**. Method for the determination of oxygen consumption rates and diffusion coefficients in multicellular spheroids. *Biophys J* 1984; **46**: 343-348 [PMID: 6487734 DOI: 10.1016/S0006-3495(84)84030-8]
30 **Jha R**, Wu Q, Singh M, Preininger MK, Han P, Ding G, Cho HC, Jo H, Maher KO, Wagner MB, Xu C. Simulated Microgravity and 3D Culture Enhance Induction, Viability, Proliferation and Differentiation of Cardiac Progenitors from Human Pluripotent Stem Cells. *Sci Rep* 2016; **6**: 30956 [PMID: 27492371 DOI: 10.1038/srep30956]
31 **Unsworth BR**, Lelkes PI. Growing tissues in microgravity. *Nat Med* 1998; **4**: 901-907 [PMID: 9701241]
32 **Zhang S**, Liu P, Chen L, Wang Y, Wang Z, Zhang B. The effects of spheroid formation of adipose-derived stem cells in a microgravity bioreactor on stemness properties and therapeutic potential. *Biomaterials* 2015; **41**: 15-25 [PMID: 25522961 DOI: 10.1016/j.biomaterials.2014.11.019]
33 **Pardo SJ**, Patel MJ, Sykes MC, Platt MO, Boyd NL, Sorescu GP, Xu M, van Loon JJ, Wang MD, Jo H. Simulated microgravity using the Random Positioning Machine inhibits differentiation and alters gene expression profiles of 2T3 preosteoblasts. *Am J Physiol Cell Physiol* 2005; **288**: C1211-C1221 [PMID: 15689415 DOI: 10.1152/ajpcell.00222.2004]
34 **Liu LP**, Zheng YW. Predicting differentiation potential of human pluripotent stem cells: Possibilities and challenges. *World J Stem Cells* 2019; **11**: 375-382 [PMID: 31396366 DOI: 10.4252/wjsc.v11.i7.375]
35 **Li Y**, Liu M, Yang ST. Dendritic cells derived from pluripotent stem cells: Potential of large scale production. *World J Stem Cells* 2014; **6**: 1-10 [PMID: 24567783 DOI: 10.4252/wjsc.v6.i1.1]
36 **Hodge AJ**, Zhong J, Lipke EA. Enhanced stem cell-derived cardiomyocyte differentiation in suspension culture by delivery of nitric oxide using S-nitrosocysteine. *Biotechnol Bioeng* 2016; **113**: 882-894 [PMID: 26444682 DOI: 10.1002/bit.25849]
37 **Bratt-Leal AM**, Carpenedo RL, McDevitt TC. Engineering the embryoid body microenvironment to direct embryonic stem cell differentiation. *Biotechnol Prog* 2009; **25**: 43-51 [PMID: 19198003 DOI: 10.1002/btpr.139]
38 **Burdsal CA**, Flannery ML, Pedersen RA. FGF-2 alters the fate of mouse epiblast from ectoderm to mesoderm in vitro. *Dev Biol* 1998; **198**: 231-244 [PMID: 9659929]
39 **Gumbiner BM**. Cell adhesion: the molecular basis of tissue architecture and morphogenesis. *Cell* 1996; **84**: 345-357 [PMID: 8608588 DOI: 10.1016/s0092-8674(00)81279-9]
40 **Mori S**, Sakakura E, Tsunekawa Y, Hagiwara M, Suzuki T, Eiraku M. Self-organized formation of developing appendages from murine pluripotent stem cells. *Nat Commun* 2019; **10**: 3802 [PMID: 31444329 DOI: 10.1038/s41467-019-11702-y]
41 **Mitsunaga S**, Odajima J, Yawata S, Shioda K, Owa C, Isselbacher KJ, Hanna JH, Shioda T. Relevance of

iPSC-derived human PGC-like cells at the surface of embryoid bodies to prechemotaxis migrating PGCs. *Proc Natl Acad Sci U S A* 2017; **114**: E9913-E9922 [PMID: 29087313 DOI: 10.1073/pnas.1707779114]

42 **England LS**, Gorzelak M, Trevors JT. Growth and membrane polarization in Pseudomonas aeruginosa UG2 grown in randomized microgravity in a high aspect ratio vessel. *BBA - General Subjects* 2003; **1624**: 76-80 [DOI: 10.1016/j.bbagen.2003.09.012]

43 **van Loon J**. Some history and use of the random positioning machine, RPM, in gravity related research. *Advances in Space Research* 2007; **39**: 1161-1165 [DOI: 10.1016/j.asr.2007.02.016]

44 **Takebe T**, Sekine K, Enomura M, Koike H, Kimura M, Ogaeri T, Zhang RR, Ueno Y, Zheng YW, Koike N, Aoyama S, Adachi Y, Taniguchi H. Vascularized and functional human liver from an iPSC-derived organ bud transplant. *Nature* 2013; **499**: 481-484 [PMID: 23823721 DOI: 10.1038/nature12271]

45 **Tsutsui H**, Valamehr B, Hindoyan A, Qiao R, Ding X, Guo S, Witte ON, Liu X, Ho CM, Wu H. An optimized small molecule inhibitor cocktail supports long-term maintenance of human embryonic stem cells. *Nat Commun* 2011; **2**: 167 [PMID: 21266967 DOI: 10.1038/ncomms1165]

46 **Watanabe K**, Ueno M, Kamiya D, Nishiyama A, Matsumura M, Wataya T, Takahashi JB, Nishikawa S, Nishikawa S, Muguruma K, Sasai Y. A ROCK inhibitor permits survival of dissociated human embryonic stem cells. *Nat Biotechnol* 2007; **25**: 681-686 [PMID: 17529971 DOI: 10.1038/nbt1310]

47 **Silva J**, Barrandon O, Nichols J, Kawaguchi J, Theunissen TW, Smith A. Promotion of reprogramming to ground state pluripotency by signal inhibition. *PLoS Biol* 2008; **6**: e253 [PMID: 18942890 DOI: 10.1371/journal.pbio.0060253]

48 **Khoo ML**, McQuade LR, Smith MS, Lees JG, Sidhu KS, Tuch BE. Growth and differentiation of embryoid bodies derived from human embryonic stem cells: effect of glucose and basic fibroblast growth factor. *Biol Reprod* 2005; **73**: 1147-1156 [PMID: 16079311 DOI: 10.1095/biolreprod.104.036673]

49 **Muratore CR**, Srikanth P, Callahan DG, Young-Pearse TL. Comparison and optimization of hiPSC forebrain cortical differentiation protocols. *PLoS One* 2014; **9**: e105807 [PMID: 25165848 DOI: 10.1371/journal.pone.0105807]

50 **Chandrasekaran A**, Avci HX, Ochalek A, Rösingh LN, Molnár K, László L, Bellák T, Téglási A, Pesti K, Mike A, Phanthong P, Bíró O, Hall V, Kitiyanant N, Krause KH, Kobolák J, Dinnyés A. Comparison of 2D and 3D neural induction methods for the generation of neural progenitor cells from human induced pluripotent stem cells. *Stem Cell Res* 2017; **25**: 139-151 [PMID: 29128818 DOI: 10.1016/j.scr.2017.10.010]

51 **Hemmi N**, Tohyama S, Nakajima K, Kanazawa H, Suzuki T, Hattori F, Seki T, Kishino Y, Hirano A, Okada M, Tabei R, Ohno R, Fujita C, Haruna T, Yuasa S, Sano M, Fujita J, Fukuda K. A massive suspension culture system with metabolic purification for human pluripotent stem cell-derived cardiomyocytes. *Stem Cells Transl Med* 2014; **3**: 1473-1483 [PMID: 25355733 DOI: 10.5966/sctm.2014-0072]

52 **Pettinato G**, Wen X, Zhang N. Formation of well-defined embryoid bodies from dissociated human induced pluripotent stem cells using microfabricated cell-repellent microwell arrays. *Sci Rep* 2014; **4**: 7402 [PMID: 25492588 DOI: 10.1038/srep07402]

53 **Messana JM**, Hwang NS, Coburn J, Elisseeff JH, Zhang Z. Size of the embryoid body influences chondrogenesis of mouse embryonic stem cells. *J Tissue Eng Regen Med* 2008; **2**: 499-506 [PMID: 18956411 DOI: 10.1002/term.125]

54 **Draper JS**, Moore HD, Ruban LN, Gokhale PJ, Andrews PW. Culture and characterization of human embryonic stem cells. *Stem Cells Dev* 2004; **13**: 325-336 [PMID: 15345125 DOI: 10.1089/scd.2004.13.325]

55 **Lei XH**, Ning LN, Cao YJ, Liu S, Zhang SB, Qiu ZF, Hu HM, Zhang HS, Liu S, Duan EK. NASA-approved rotary bioreactor enhances proliferation of human epidermal stem cells and supports formation of 3D epidermis-like structure. *PLoS One* 2011; **6**: e26603 [PMID: 22096490 DOI: 10.1371/journal.pone.0026603]

56 **Moon SH**, Ju J, Park SJ, Bae D, Chung HM, Lee SH. Optimizing human embryonic stem cells differentiation efficiency by screening size-tunable homogenous embryoid bodies. *Biomaterials* 2014; **35**: 5987-5997 [PMID: 24780170 DOI: 10.1016/j.biomaterials.2014.04.001]

57 **Koay EJ**, Hoben GM, Athanasiou KA. Tissue engineering with chondrogenically differentiated human embryonic stem cells. *Stem Cells* 2007; **25**: 2183-2190 [PMID: 17540854 DOI: 10.1634/stemcells.2007-0105]

58 **Murry CE**, Keller G. Differentiation of embryonic stem cells to clinically relevant populations: lessons from embryonic development. *Cell* 2008; **132**: 661-680 [PMID: 18295582 DOI: 10.1016/j.cell.2008.02.008]

59 **Mohr JC**, Zhang J, Azarin SM, Soerens AG, de Pablo JJ, Thomson JA, Lyons GE, Palecek SP, Kamp TJ. The microwell control of embryoid body size in order to regulate cardiac differentiation of human embryonic stem cells. *Biomaterials* 2010; **31**: 1885-1893 [PMID: 19945747 DOI: 10.1016/j.biomaterials.2009.11.033]

60 **Kempf H**, Olmer R, Kropp C, Rückert M, Jara-Avaca M, Robles-Diaz D, Franke A, Elliott DA, Wojciechowski D, Fischer M, Roa Lara A, Kensah G, Gruh I, Haverich A, Martin U, Zweigerdt R. Controlling expansion and cardiomyogenic differentiation of human pluripotent stem cells in scalable suspension culture. *Stem Cell Reports* 2014; **3**: 1132-1146 [PMID: 25454631 DOI: 10.1016/j.stemcr.2014.09.017]

61 **Otsuji TG**, Bin J, Yoshimura A, Tomura M, Tateyama D, Minami I, Yoshikawa Y, Aiba K, Heuser JE, Nishino T, Hasegawa K, Nakatsuji N. A 3D sphere culture system containing functional polymers for large-scale human pluripotent stem cell production. *Stem Cell Reports* 2014; **2**: 734-745 [PMID: 24936458 DOI: 10.1016/j.stemcr.2014.03.012]

62 **Chen YC**, Zhang Z, Fouladdel S, Deol Y, Ingram PN, McDermott SP, Azizi E, Wicha MS, Yoon E. Single cell dual adherent-suspension co-culture micro-environment for studying tumor-stromal interactions with functionally selected cancer stem-like cells. *Lab Chip* 2016; **16**: 2935-2945 [PMID: 27381658 DOI: 10.1039/c6lc00062b]

63 **Durmus NG**, Tekin HC, Guven S, Sridhar K, Arslan Yildiz A, Calibasi G, Ghiran I, Davis RW, Steinmetz LM, Demirci U. Magnetic levitation of single cells. *Proc Natl Acad Sci U S A* 2015; **112**: E3661-E3668 [PMID: 26124131 DOI: 10.1073/pnas.1509250112]

64 **Jeziorowska D**, Fontaine V, Jouve C, Villard E, Dussaud S, Akbar D, Letang V, Cervello P, Itier JM, Pruniaux MP, Hulot JS. Differential Sarcomere and Electrophysiological Maturation of Human iPSC-Derived Cardiac Myocytes in Monolayer vs. Aggregation-Based Differentiation Protocols. *Int J Mol Sci* 2017; 18 [PMID: 28587156 DOI: 10.3390/ijms18061173]

65 **Zhu Y**, Wang L, Yu H, Yin F, Wang Y, Liu H, Jiang L, Qin J. In situ generation of human brain organoids on a micropillar array. *Lab Chip* 2017; **17**: 2941-2950 [PMID: 28752164 DOI: 10.1039/c7lc00682a]

66 **Martínez García de la Torre RA**, Nieto-Nicolau N, Morales-Pastor A, Casaroli-Marano RP. Determination of the Culture Time Point to Induce Corneal Epithelial Differentiation in Induced Pluripotent Stem Cells. *Transplant Proc* 2017; **49**: 2292-2295 [PMID: 29198663 DOI: 10.1016/j.transproceed.2017.09.047]

67 **Ochiai-Shino H**, Kato H, Sawada T, Onodera S, Saito A, Takato T, Shibahara T, Muramatsu T, Azuma T. A novel strategy for enrichment and isolation of osteoprogenitor cells from induced pluripotent stem cells based on surface marker combination. *PLoS One* 2014; **9**: e99534 [PMID: 24911063 DOI: 10.1371/journal.pone.0099534]

68 **Hoque A**, Sivakumaran P, Bond ST, Ling NXY, Kong AM, Scott JW, Bandara N, Hernández D, Liu GS, Wong RCB, Ryan MT, Hausenloy DJ, Kemp BE, Oakhill JS, Drew BG, Pébay A, Lim SY. Mitochondrial fission protein Drp1 inhibition promotes cardiac mesodermal differentiation of human pluripotent stem cells. *Cell Death Discov* 2018; **4**: 39 [PMID: 29531836 DOI: 10.1038/s41420-018-0042-9]

69 **Pauly MG**, Krajka V, Stengel F, Seibler P, Klein C, Capetian P. Adherent vs. Free-Floating Neural Induction by Dual SMAD Inhibition for Neurosphere Cultures Derived from Human Induced Pluripotent Stem Cells. *Front Cell Dev Biol* 2018; **6**: 3 [PMID: 29468156 DOI: 10.3389/fcell.2018.00003]

70 **Chauveau S**, Anyukhovsky EP, Ben-Ari M, Naor S, Jiang YP, Danilo P, Rahim T, Burke S, Qiu X, Potapova IA, Doronin SV, Brink PR, Binah O, Cohen IS, Rosen MR. Induced Pluripotent Stem Cell-Derived Cardiomyocytes Provide In Vivo Biological Pacemaker Function. *Circ Arrhythm Electrophysiol* 2017; **10**: e004508 [PMID: 28500172 DOI: 10.1161/CIRCEP.116.004508]

71 **Roberts CL**, Chen SS, Murchison AC, Ogle RA, Francis MP, Ogle RC, Sachs PC. Preferential Lineage-Specific Differentiation of Osteoblast-Derived Induced Pluripotent Stem Cells into Osteoprogenitors. *Stem Cells Int* 2017; **2017**: 1513281 [PMID: 28250775 DOI: 10.1155/2017/1513281]

72 **Nam Y**, Rim YA, Jung SM, Ju JH. Cord blood cell-derived iPSCs as a new candidate for chondrogenic differentiation and cartilage regeneration. *Stem Cell Res Ther* 2017; **8**: 16 [PMID: 28129782 DOI: 10.1186/s13287-017-0477-6]

73 **Espinosa-Jeffrey A**, Blanchi B, Biancotti JC, Kumar S, Hirose M, Mandefro B, Talavera-Adame D, Benvenisty N, de Vellis J. Efficient Generation of Viral and Integration-Free Human Induced Pluripotent Stem Cell-Derived Oligodendrocytes. *Curr Protoc Stem Cell Biol* 2016; **38**: 2D.18.1-2D.18.27 [PMID: 27532816 DOI: 10.1002/cpsc.11]

74 **Phondeechareon T**, Wattanapanitch M, U-Pratya Y, Damkham C, Klincumhom N, Lorthongpanich C, Kheolamai P, Laowtammathron C, Issaragrisil S. Generation of induced pluripotent stem cells as a potential source of hematopoietic stem cells for transplant in PNH patients. *Ann Hematol* 2016; **95**: 1617-1625 [PMID: 27465155 DOI: 10.1007/s00277-016-2756-1]

75 **Plaisted WC**, Zavala A, Hingco E, Tran H, Coleman R, Lane TE, Loring JF, Walsh CM. Remyelination Is Correlated with Regulatory T Cell Induction Following Human Embryoid Body-Derived Neural Precursor Cell Transplantation in a Viral Model of Multiple Sclerosis. *PLoS One* 2016; **11**: e0157620 [PMID: 27310015 DOI: 10.1371/journal.pone.0157620]

76 **Tang M**, Chen W, Liu J, Weir MD, Cheng L, Xu HH. Human induced pluripotent stem cell-derived mesenchymal stem cell seeding on calcium phosphate scaffold for bone regeneration. *Tissue Eng Part A* 2014; **20**: 1295-1305 [PMID: 24279868 DOI: 10.1089/ten.TEA.2013.0211]

77 **Suchorska WM**, Augustyniak E, Richter M, Trzeciak T. Comparison of Four Protocols to Generate Chondrocyte-Like Cells from Human Induced Pluripotent Stem Cells (hiPSCs). *Stem Cell Rev Rep* 2017; **13**: 299-308 [PMID: 27987073 DOI: 10.1007/s12015-016-9708-y]

78 **Lach MS**, Kulcenty K, Jankowska K, Trzeciak T, Richter M, Suchorska WM. Effect of cellular mass on chondrogenic differentiation during embryoid body formation. *Mol Med Rep* 2018; **18**: 2705-2714 [PMID: 30015965 DOI: 10.3892/mmr.2018.9272]

79 **Hunt NC**, Hallam D, Karimi A, Mellough CB, Chen J, Steel DHW, Lako M. 3D culture of human pluripotent stem cells in RGD-alginate hydrogel improves retinal tissue development. *Acta Biomater* 2017; **49**: 329-343 [PMID: 27826002 DOI: 10.1016/j.actbio.2016.11.016]

80 **Miranda CC**, Fernandes TG, Diogo MM, Cabral JM. Scaling up a chemically-defined aggregate-based suspension culture system for neural commitment of human pluripotent stem cells. *Biotechnol J* 2016; **11**: 1628-1638 [PMID: 27754603 DOI: 10.1002/biot.201600446]

81 **Mukherjee C**, Hale C, Mukhopadhyay S. A Simple Multistep Protocol for Differentiating Human Induced Pluripotent Stem Cells into Functional Macrophages. *Methods Mol Biol* 2018; **1784**: 13-28 [PMID: 29761384 DOI: 10.1007/978-1-4939-7837-3_2]

82 **Liu LP**, Li YM, Guo NN, Li S, Ma X, Zhang YX, Gao Y, Huang JL, Zheng DX, Wang LY, Xu H, Hui L, Zheng YW. Therapeutic Potential of Patient iPSC-Derived iMelanocytes in Autologous Transplantation. *Cell Rep* 2019; **27**: 455-466.e5 [PMID: 30970249 DOI: 10.1016/j.celrep.2019.03.046]

World Journal of Stem Cells

Submit a Manuscript: https://www.f6publishing.com

World J Stem Cells 2020 January 26; 12(1): 35-54

DOI: 10.4252/wjsc.v12.i1.35

ISSN 1948-0210 (online)

ORIGINAL ARTICLE

Basic Study

Sphere-forming corneal cells repopulate dystrophic keratoconic stroma: Implications for potential therapy

Himanshu Wadhwa, Salim Ismail, Jennifer J McGhee, Bert Van der Werf, Trevor Sherwin

ORCID number: Himanshu Wadhwa (0000-0002-3287-4453); Salim Ismail (0000-0002-6644-9615); Jennifer J McGhee (0000-0001-7488-9250); Bert Van der Werf (0000-0003-3072-5937); Trevor Sherwin (0000-0002-9090-1034).

Author contributions: Wadhwa H and Ismail S participated in the experimental design, data acquisition analysis and manuscript writing; McGhee JJ participated in experimental design and cell and tissue preparation; Van der Werf B participated in data analysis and manuscript writing; Sherwin T participated in study design, experimental design and manuscript writing; All authors read, edited and approved the final manuscript.

Supported by Save Sight Society of New Zealand, No. 37116543; New Zealand Wound Care Society, No. 3713325; New Zealand Wound Care Society, No. 3713325; John Hamel MacGregor Trust.

Institutional review board statement: This study was conducted under ethical approval by the Northern X Regional Ethics Committee and since reviewed by the Northern A Health and Disability Ethics Committee (New Zealand). Ethics reference: NTX/07/08/080/AM06

Conflict-of-interest statement: Prof. Sherwin reports grants from Save Sight Society of New Zealand, grants from Auckland Medical Research Foundation, grants from New Zealand Wound Care Society, and grants from John Hamel

Himanshu Wadhwa, Salim Ismail, Jennifer J McGhee, Trevor Sherwin, Department of Ophthalmology, Faculty of Medical and Health Sciences, The University of Auckland, Auckland 1023, New Zealand

Bert Van der Werf, Department of Epidemiology and Biostatistics, School of Population Health, Faculty of Medical and Health Sciences, The University of Auckland, Auckland 1023, New Zealand

Corresponding author: Trevor Sherwin, PhD, Professor, Department of Ophthalmology, Faculty of Medical and Health Sciences, The University of Auckland, Private Bag 92019, Auckland 1023, New Zealand. t.sherwin@auckland.ac.nz

Abstract

BACKGROUND

Keratoconus is a degenerative corneal disease characterised by aberrant cell behaviour and loss of matrix that can result in vision loss. Cells extracted from peripheral corneas can form stem cell-enriched spheres, which have shown the potential to repopulate the normal peripheral corneal stroma *in vitro* upon sphere implantation but have not been previously studied in keratoconic tissue.

AIM

To investigate the therapeutic potential of stem cell-enriched spheres formed from extracted peripheral human corneal cells when introduced to keratoconic tissue.

METHODS

Stem cell-enriched spheres were formed from extracts of normal cadaveric human peripheral corneal cells. These spheres were implanted into incisions created in full thickness and onto the surface of 10 μm thin sections of keratoconic and normal stromal tissues *in vitro*. Tissue sections were used to maximise use of limited keratoconic tissue available for research. Living cells were stained with Calcein-AM and visualised with stereo and fluorescence microscopy to assess survival and behaviours between the time of implantation day 0 and 14 d (D14) from implantation. Sphere cells in implanted tissues were characterised for stem cell and differentiation markers using immunohistochemistry and droplet digital PCR to assess the potential implications of these characteristics in the use of spheres in keratoconus treatment.

RESULTS

Spheres were successfully implanted into full-thickness central corneal tissue and

MacGregor Trust during the conduct of the study.

Data sharing statement: The datasets used and/or analysed during the current study are available from the corresponding author on reasonable request.

Manuscript source: Unsolicited manuscript

Received: June 25, 2019
Peer-review started: June 29, 2019
First decision: July 31, 2019
Revised: September 11, 2019
Accepted: November 13, 2019
Article in press: November 13, 2019
Published online: January 26, 2020

P-Reviewer: Exbrayat JM, Grawish M, Sorio C, Liu X, Li SC
S-Editor: Zhang L
L-Editor: Filipodia
E-Editor: Xing YX

onto the surface of 10 μm thin *en face* tissue sections. No observable differences were seen in sphere migration, proliferation or differentiation in keratoconic tissue compared to normal between day 0 and D14. Spheres stained positively with Calcein-AM up to D14. Cell migration increased from day 0 to D14, occurring radially in three dimensions from the sphere and in alignment with tissue edges. Cell proliferation marker, EdU, was detected at day 10. Implanted spheres stained positively for putative stem cell markers ΔNp63α and ABCB5, while ABCG2, ABCB5, ΔNp63 and p63α were detectable by droplet digital PCR up to D14. Double immunolabelling revealed absence of ABCB5 staining in migrated cells but positive staining of alpha smooth muscle actin (myofibroblast marker) in some migrated cells. Droplet digital PCR showed similar expression patterns of differentiation markers but a reduction in stem cell markers between normal and keratoconic tissue with an increase in stromal cell markers and a reduction in epithelial cell markers, indicating an appropriate response to repopulating diseased tissue.

CONCLUSION
Cells from implanted stem cell-enriched spheres can repopulate a keratoconic corneal stromal surface in a directed manner and exhibit migratory stromal cell phenotypes.

Key words: Keratoconus; Cell culture; Immunohistochemistry; Quantitative PCR; Digital PCR; Spheroid; Holoclone; Neurosphere; Regeneration

Core tip: Keratoconus is a degenerative corneal disease characterised by aberrant cell behaviour and loss of matrix that can result in vision loss. Cells extracted from peripheral corneas can form stem cell-enriched spheres, which we introduced into normal and keratoconic corneal stroma. This study shows for the first time that implanted stem cell-enriched spheres are capable of repopulating the dystrophic corneal stromal surface in a directed manner. Spheres may therefore be used to replace or supplement diseased cells in keratoconic patients, thereby serving as an adjunct to current treatments.

Citation: Wadhwa H, Ismail S, McGhee JJ, Werf BVD, Sherwin T. Sphere-forming corneal cells repopulate dystrophic keratoconic stroma: Implications for potential therapy. *World J Stem Cells* 2020; 12(1): 35-54
URL: https://www.wjgnet.com/1948-0210/full/v12/i1/35.htm
DOI: https://dx.doi.org/10.4252/wjsc.v12.i1.35

INTRODUCTION

Keratoconus is a degenerative ocular disease in which corneas of affected individuals become thin and protrude, resulting in the typical cone-shaped corneal distortion[1]. In keratoconus, the normal architecture and cell milieu of the anterior cornea is disrupted. Pathological changes include altered cell morphology, altered cell alignment and organisation, loss of resident keratocyte cell density from the corneal stroma, loss of cell matrix and eventually increased areas of fibrosis and scarring[2-6]. Both the epithelial and stromal layers of the cornea are affected but due to the complexity of this disease, it is still not definitively known in which layer/s the pathology originates[7]. Despite this, therapies like corneal collagen cross-linking[8,9], corneal transplantation (penetrating keratoplasty) and deep anterior lamellar keratoplasty that target the corneal stroma for treatment are efficacious.

Both corneal transplantation and corneal collagen cross-linking strengthen the central corneal stroma, and yet rates of disease recurrence are significantly less in transplanted patients despite having more advanced disease. Kelly *et al*[10] conducted a large cohort study in which they found 89% of grafts for keratoconus remained viable at 10 years, and only 4% of all regrafts were performed for recurrence. While some may argue that these cases of recurrence represent undiagnosed keratoconus in the

donor tissue[11], the rates of recurrence are significantly low even if these are a true recurrence in grafted tissues. After a cross-linking procedure, on the other hand, measures that may indicate disease recurrence, like simulated maximum keratometry values, increase as early as 18 mo after the procedure[12]. We hypothesise that decreased rates of recurrence in corneal transplant patients are due to the introduction of normal cells along with their normal matrix rather than simply removing the native aberrant cells in the central cornea. On a cellular level, both treatments remove the host's central epithelial cells and central keratocytes, the latter from either ultraviolet radiation-induced cell death during cross-linking and the former by removal entirely during transplantation. The host's limbal cells are preserved with both treatment modalities, which likely mount a wound healing response to repopulate the decellularised tissues. Within 6 mo, native keratocytes eventually repopulate the cross-linked native keratoconic stroma[13] and likely the transplanted corneal stroma also. Following this line of thinking, it may further be postulated that introducing healthy cells, as a supplement to collagen cross linking, into a keratoconic cornea could perhaps impact the host cells and shift the balance from a degenerative state to a healthy state.

Stem cells are increasingly being studied for their potential use in regeneration and repair of tissues in many specialties and could be a promising potential method of introducing a sustainable source of normal cells into the keratoconic environment. Humans have an endogenous population of oligopotent adult stem cells that are involved in the maintenance of the structure and function of the cornea. The epithelial and stromal cell populations are maintained by corneal epithelial and stromal stem cells, respectively. These stem cells reside in the corneal limbus, the area between the white sclera and transparent cornea, which make them relatively easily accessible to harvest. Corneal limbal stem cells can be extracted and isolated using the established neurosphere assay[14-16]. Corneal stem cell spheres are of mesenchymal origin. Numerous studies have demonstrated the ability of mesenchymal stem cells to enhance endogenous tissue repair by reducing inflammation and immune response, inducing angiogenesis, reducing apoptosis and oxidative stress and stimulating recruitment, retention, proliferation and differentiation of tissue-residing stem cells[17,18] and possibly through mitochondrial transfer[19]. Many of these reparative processes are impaired in keratoconus[20-25], which strengthens the case to evaluate the therapeutic potential of corneal stromal stem cell-containing spheres for keratoconus. Damaged rat corneas treated with mesenchymal stem cells have been shown to be able to restore visual function, probably by reducing levels of inflammatory markers interleukin-2, matrix metalloproteinase-2 and common leukocyte antigen and without differentiating into epithelial cells[26]. Looking at mesenchymal stem cells from the limbus in particular, human (and rabbit) limbal mesenchymal stem cells cocultured with immune cells from mismatched donors *in vitro* have suppressed T cell proliferation by up to 75%[27], mediated by secretion of transforming growth factor beta-1[14]. The inherent immunosuppressant effect is important to note because keratoconus affects both eyes albeit asymmetrically. Therefore, autologous stem cells from the less affected eye are still likely to be affected by the dystrophic process.

Our laboratory and others have previously characterised stem cell-enriched spheres, which contain cells from a spectrum of less to more differentiated cells: Stem cells, transient amplifying cells and differentiated cells from a combination of epithelial and stromal origins[16,28]. We have also shown that spheres are dynamic entities that can maintain themselves for up to 4 mo[16], are capable of eliciting wound healing responses[29] and are capable of repopulating the normal stromal ocular surface[30]. To date, *in situ* stem cell sphere behaviours in response to diseased human corneal tissues have not been investigated. In this paper, we present our novel findings of the *in situ* behaviours of corneal stem cell spheres in response to dystrophic keratoconic stromal matrix.

MATERIALS AND METHODS

Human tissue

Fresh or frozen human central cornea, peripheral corneo-scleral tissue or whole corneo-scleral tissue from living or cadaveric donors were used with consent and handled in accordance with procedures approved by the Northern X Regional Ethics Committee and since reviewed by the Northern A Regional Ethics Committee (Ethics reference: NTX/07/08/080/AM06).

Sphere formation and culture

Corneo-limbal stromal tissues from cadaveric human donors were enzymatically

digested, the extracted cells mechanically filtered and then cultured in non-adherent conditions using Supplemented Neurobasal-A medium (standard culture medium) using the previously published method[16,30]. Cells congregated together and formed self-renewing, stem cell-enriched spheres. All spheres were maintained in culture for at least 21 d prior to use in implantation experiments. Medium changes (50% of the volume) were performed twice a week.

Preparation of tissue for sphere implantation

Four keratoconic central corneas from patients who were recipients of full-thickness penetrating keratoplasties (keratoconic button) and four central corneas from cadaveric donor corneas (non-keratoconic button) used for Descemet stripping automated endothelial keratoplasty (n = 2), Descemet's layer endothelial keratoplasty (n = 1) or decompensated cornea (tissue that failed New Zealand Eye Bank's endothelial count criteria for use as a graft, n = 1) were used for sphere implantation. Corneas from six donors were used for full thickness implants and corneas from four donors were used for creating tissue sections for implantation; corneas from two of these donors were used for both purposes.

Central corneal buttons: Corneal buttons were first decellularised by subjecting the tissue to three "freeze-thaw cycles," which has previously been shown to completely remove live cells[30]. Corneal buttons were then prepared for implantation as described in detail previously[31]. Briefly, the epithelium is scraped and rinsed away, v-shaped wedge incisions in the anterior two-thirds of the corneal buttons are created and then spheres are implanted within the incisions. Because de-epithelialized anterior stroma was used from each of keratoconic and non-keratoconic corneal buttons, tissues were deemed equivalent and comparable.

Implanted spheres were incubated at 37 °C for 10 min to encourage adherence to the tissue prior to addition of 2-3 mL of standard culture medium. The point at which spheres were able to be visualised *in situ* after culture medium had been added was defined as time equals day 0. Sphere-implanted tissues were inverted so that the epithelial side apposed the bottom of the Petri dish during culture and incubated at 37 °C for up to 10 d.

***En face* stromal sections:** Due to the limited availability of keratoconic tissue for research, it was pertinent to develop a method to maximise the use of available tissue. To facilitate this, we developed a technique for the placement of spheres onto e*n face* (coronal) 10 μm sections of central corneal tissue. Decellularised tissues were frozen at -20 °C in Tissue-Tek® OCT™ compound (OCT) (4583, Sakura) and cryosectioned to yield 10 μm thin tissue sections, which were washed thrice with sterile PBS for 10 min each to remove surrounding OCT prior to use. *En face* tissue sections were stored in PBS at 4 °C until required. One sphere was carefully seeded onto the surface of each 10 μm tissue section under a Leica DM IL inverted contrasting microscope, allowed to adhere and overlaid with culture medium as described above. Tissue sections from two keratoconic and two normal corneal "tissue donors" were seeded with a combination of spheres derived from six human donors (sphere donors).

Sphere-implanted tissues were cultured for up to 14 d and 50% medium changes were completed biweekly. At day 0, 1 and 3 or 4 post-seeding, sections were fixed for immunohistochemistry as described below. The rationale for these time points was based primarily on observations with spheres placed on collagen-coated surfaces, which indicated that these times were the critical points where an increase in cell migration and proliferation occurred. Experiments were concluded at day 14 due to the observation of complete tissue matrix repopulation.

Visualising live cells and proliferating cells

Live cells both within spheres and migrating outward were visualised using the LIVE/DEAD® Viability/Cytotoxicity Kit (L3224, Life Technologies), whereby samples were incubated in 2 μM Calcein-AM and 4 μM Ethidium homodimer-1 for 40 min at 37 °C. Staining solutions were then carefully aspirated, discarded and replaced with fresh culture medium.

Cell proliferation was detected using Click-iT® EdU Alexa Fluor® 594 Imaging Kit (C10339, ThermoFisher) by supplementing standard culture medium with 5-ethynyl-2′-deoxyuridine, a nucleoside analogue of thymidine, at a concentration of 10 μM.

Phase contrast, bright-field and fluorescence microscopy images were assessed and captured using the following microscopes: Leica DM-RA upright fluorescence microscope (Leica)–images analysed using NIS-Elements Basic Research Microscope Imaging Software version 4.30.00, Nikon TE2000 Inverted Fluorescence Microscope (Nikon)–images analysed using NIS-Elements Advanced Research Microscope Imaging Software version 4.50.00. and FLoid Cell Imaging station (Life Technologies).

Images were analysed using its fully integrated image capture and analysis system.

Immunohistochemistry

Immunohistochemistry was performed essentially as described previously[30]. Samples were fixed using 4% paraformaldehyde (Sigma) unless specified otherwise, permeabilised with ice cold methanol for 20 min to expose antigens, blocked with a solution of 100 mM glycine, 0.1% Triton X-100 and 10% normal goat serum (NGS) to reduce non-specific binding of subsequent antibody treatments, incubated with primary antibodies overnight at 4 °C, secondary antibodies for 3 h and the nuclear stain DAPI (D9542, Sigma). Samples were immersed in Citifluor anti-fade reagent and sealed with a coverslip for viewing with fluorescence microscopy.

Primary antibodies used in this work were as follows: Anti-ATP binding cassette subfamily B member 5 (anti-ABCB5) antibody produced in rabbit at 1:125 (HPA026975, Sigma), anti-tumour protein p63 alpha chain, N-terminal isoform (anti-ΔNp63α) antibody produced in rabbit at 1:160 (private order, PickCell Laboratories) and anti-smooth muscle actin (anti-αSMA) antibody produced in mouse at 1:80 (A2547; Sigma Aldrich). Secondary antibodies were used at 1:350 goat anti-mouse Alexa488 (A11029, ThermoFisher) to detect anti-αSMA, goat anti-rabbit Alexa488 (A11034, ThermoFisher) to detect anti-ΔNp63α and goat anti-rabbit Alexa568 (A11011, ThermoFisher) to detect anti-ABCB5 primary antibodies.

Based on previously established methodologies[16,30], an adapted protocol was used for cross-sections of implanted full-thickness tissues. Sphere-implanted corneal buttons were frozen at -20 °C in Tissue-Tek® OCT compound (Sakura) before being cryosectioned to obtain 20 μm "cross-sections," which were mounted onto glass microscope slides. These cross-sections were washed in PBS for 10 min three times. Sections were fixed with 2.5% paraformaldehyde in PBS for 10 min (except those for detecting ΔNp63α, which were not fixed) and rinsed in PBS for 15 min three times. Sections were treated with 2 mg/mL bovine testicular hyaluronidase in PBS for 1 hour at 37 °C in a humidity chamber, permeabilised in methanol at -20°C for 20 min and washed in PBS for 15 min three times. This was followed by treatment with 20 mM glycine in PBS for 30 min at room temperature and washed in 0.1% NGS in PBS three times for 15 min. Sections were subsequently treated with a 2% NGS with 0.1% Triton X-100 in PBS solution for 30 min at room temperature. Primary and secondary antibodies were prepared in 0.1% NGS to desired concentrations as described earlier and sections incubated overnight in primary antibody prior to washing with 0.1% NGS and incubation in secondary antibody for 2 h at ambient temperature. Counterstaining was completed with 0.1 μg/mL DAPI for 10 min prior to mounting in Citifluor antifade using a glass coverslip, which was sealed with nail varnish. The microscopes and imaging software used were: The Leica DM-RA upright fluorescence microscope described earlier and the Olympus FV 1000 Confocal laser scanning microscope (Olympus) with the FV10-ASW ver.0.4.00 image capture and analysis software.

Gene expression quantification

Sphere implanted tissue sections were carefully removed from the glass slide and transferred to an RNase-free tube. RNA extraction and genomic DNA removal was subsequently performed using the $_{RNA}$Gem™ Tissue Plus Kit (RTP0200, ZyGem) as per manufacturer's protocol. Samples were tested for presence of PCR inhibitors using the SPUD assay[32]. Inhibitory samples were further purified using the PureLink® RNA Mini Kit (12183018A, ThermoFisher) as per manufacturer guidelines as required. Complementary DNA (cDNA) was synthesised using the SuperScript® VILO™ cDNA Synthesis Kit (11754-050, ThermoFisher) according to manufacturer guidelines using 10 μL of the DNase I treated total RNA extracts.

Successful cDNA synthesis was confirmed by performing a β-actin polymerase chain reaction on all cDNA preparations and resolving PCR products by agarose gel electrophoresis to confirm successful amplification. The following primers were used: AACTCCATCATGAAGTGTGACG (forward) and GATCCACATCTGCTGGAAG (reverse) which yield a 224 bp amplicon. cDNA samples were subsequently diluted 1:5 and then analysed using droplet digital PCR (ddPCR). The primers and probes used are listed in Table 1. All primers were commercial PrimeTime qPCR assays that utilise the 56-FAM fluorophore and both the ZEN and 3IABkFQ quenchers. Detailed sequences of the primer set and probe sequences can be obtained from the manufacturer.

For each ddPCR assay, one positive control and one "no template" control was included in addition to samples. Purified PCR product used at a concentration of 1.2 × 10^4 copies/μL were used for the positive controls.

PCR reactions were set up containing final concentrations of 1 × PrimeTime qPCR assay, 1 × ddPCR supermix for probes (no dUTP) and 2 μL of diluted cDNA in 24 μL

Table 1 PrimeTime quantitative polymerase chain reaction assays used for droplet digital polymerase chain reaction

Product of interest: Gene	Reference gene or gene of interest	Assay identification	Size of complimentary DNA amplicon, base pairs
Actin, beta	Reference	Hs.PT.39a.22214847	109
Beta-2-microglobulin	Reference	Hs.PT.58v.18759587	142
Glucuronidase beta	Reference	Hs.PT.58v.27737538	127
Glycreraldehyde-3-phosphate dehydrogenase	Reference	Hs.PT.39a.22214836	142
Hypoxanthine phosphoribosyltransferase 1	Reference	Hs.PT.58v.45621572	148
Peptidylprolyl isomerase A	Reference	Hs.PT.58v.38887593. g	101
Actin, alpha 2, smooth muscle, aorta	Gene of interest	Hs.PT.56a.2542642	131
ATP binding cassette subfamily B member 5	Gene of interest	Hs.PT.58.38502346	106
ATP-binding cassette, sub-family G member 2	Gene of interest	Hs.PT.58.20889058	114
Collagen type I, alpha 1 chain	Gene of interest	Hs.PT.58.15517795	130
Collagen type I, alpha 2 chain	Gene of interest	Hs.PT.58.26714160	108
Integrin, subunit beta 1	Gene of interest	Hs.PT.58.39883300	141
Keratin 3	Gene of interest	Hs.PT.58.25330614	126
Keratocan	Gene of interest	Hs.PT.58.45594658	130
Laminin, subunit alpha 1	Gene of interest	Hs.PT.58.3170022	129
Notch1	Gene of interest	Hs.PT.58.23074795	112
Proliferating cell nuclear antigen	Gene of interest	Hs.PT.58.4761611	94
Tumour protein p63, transcript variant 1, C-terminal isoform α	Gene of interest	Hs.PT.58.39019253	108
Tumour protein p63, transcript variant 1, N-terminal isoform	Gene of interest	Hs.PT.58.19710922	104
Vimentin	Gene of interest	Hs.PT.58.38906895	141

reactions. Where samples did not yield an expression quantity due to low target abundance, increasing amounts of diluted cDNA from 2 μL, 4 μL, 6 μL up to a maximum of 10 μL were used in repeat reactions. For droplet generation, 20 μL of each PCR reaction was loaded into the appropriate wells of DG8 droplet generation cartridges along with 70 μL of droplet generation oil, covered with a DG8 gasket and placed into the droplet generator to generate droplets. Droplets (40 μL) were transferred to a semi-skirted PCR plate, sealed and amplified in a C1000 Touch thermal cycler (Bio-Rad). The thermal-cycling conditions used were: 95 °C for 10 min for initialisation followed by 40 cycles of denaturation at 94 °C for 30 s and annealing at 60 °C for 60 s. After cycle 40, samples were heated to 98 °C for 10 min and cooled to 12 °C for temporary storage. After amplification, fluorescent and non-fluorescent droplets were analysed using the Bio-Rad QX200 droplet reader (Bio-Rad). The resulting ddPCR data was analysed with QuantaSoft analysis software (version 1.7.4). A threshold line was manually placed above the negative level determined from the no template control and below the positive level determined from the positive control.

Results were normalised to the geometric mean of six reference genes (listed in Table 1). Expression difference in spheres implanted on *en face* keratoconic tissue sections and cultured over 14 d were compared to freshly implanted spheres at day 0 (calibrator sample).

Biostatistics

Statistical analysis on normalised gene expression values generated by ddPCR was conducted with a linear mixed model having donor and day within donor as random terms. Fixed model terms were gene, diseased matrix and day. Data values were natural log transformed to meet the assumptions of the analysis. Calculations were done using the lme4 package[33] in R version 3.5.0[34]. The resulting estimates with their covariances were used to create the values in Table 2, Table 3 and Figure 1. The statistical methods of this study were reviewed by Bert Van der Werf, Biostatistician from The University of Auckland.

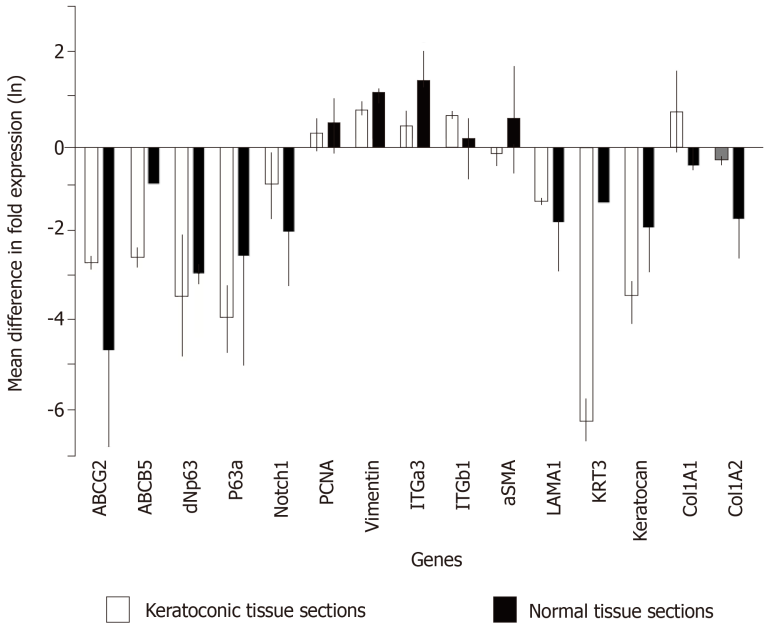

Figure 1 Estimated fold differences in expression of proliferation, stem cell and epithelial and stromal cell markers in sphere-seeded tissue sections at day 14. Expression of stem cell markers: ATP-binding cassette, sub-family G member 2, ATP binding cassette subfamily B member 5, tumour protein p63, transcript variant 1, N-terminal isoform, tumour protein p63, transcript variant 1, C-terminal isoform α, limbal niche marker Notch1, proliferation marker proliferating cell nuclear antigen, mesenchymal cell marker vimentin, adhesion molecules integrin subunit α3 and β1, myofibroblast marker alpha smooth muscle actin, epithelial markers laminin α1 and keratin 3, keratocyte marker keratocan, collagen type I, alpha 1 chain and collagen type I, alpha 2 chain genes in sphere-seeded normal (black squares) and keratoconic (white squares) 10 μm *en face* decellularised central corneal stromal tissue sections. Spheres were derived from two human donors and expression data at days 0 and 14, normalised to reference genes β-actin, glycreraldehyde-3-phosphate dehydrogenase, glucuronidase beta, hypoxanthine phosphoribosyltransferase 1, peptidylprolyl isomerase A and β2-microglobulin. Data is expressed as estimated fold difference between day 14 and day 0 based on raw data and plotted as the natural logarithm mean differences in fold expression ± standard deviation.

RESULTS

Repopulation of keratoconic tissue surface

Spheres were seeded on to a total of 28 thin 10 μm tissue sections and assessed for viability. Cells were deemed non-viable based on complete absence of LIVE staining of cells across the entire implanted tissue section. Of these 28 tissue sections, 17 were keratoconic tissue sections and 11 were normal tissue sections. The keratoconic and normal tissue sections were each sourced from two different human tissue donors. Cells were viable in 28 out of 28 (100%) tissue sections assessed at day 1 post-seeding. Two tissue sections were fixed for immunohistochemistry. The remaining 26 tissue sections (16 keratoconic and 10 normal) were assessed at day 3, of which 20 (77%) were viable. Six tissue sections, two keratoconic and four normal, were non-viable, and two tissue sections were fixed for immunohistochemistry. At day 7, 18 tissue sections were assessed with the viability stain, of which 16 (89%) were viable. Spheres and cells remained viable at day 14 in at least two keratoconic tissue sections. All of the tissue sections that became non-viable were implanted with spheres from the same donor. However, two other keratoconic and two other normal tissue sections implanted with spheres derived from this sphere donor remained viable to day 7 (Table 4).

Viable cells increased in number and migrated over observed time periods between 0 and 14 d. Cells were seen to have migrated radially in all directions from the centre of spheres as early as day 1. Similar processes were observed in keratoconic and normal tissues. Sphere-derived cells completely repopulated the surfaces of keratoconic tissue sections (Figure 2A) (n = 2) at day 14 (Figure 2B). Cells at tissue edges at various time points were observed to align with the edge (example in Figure 3A, white arrows). Migrated cells were not seen on the culture dish surface in any samples where tissue sections had not been completely repopulated. Two tissue sections, both keratoconic, were observed to be repopulated to complete confluency. Periodic examination of these two samples with a light microscope revealed that at

Table 2 Statistical analysis of difference in gene expression in sphere-seeded tissue sections as measured by droplet digital polymerase chain reaction, effect of time: day 0 *vs* day 14

	Day 0	Day 14	Day 14 - Day 0	
Target	Estimate[1] (lower.95, upper.95)	Estimate[1] (lower.95, upper.95)	*P*	
ABCB5	0.02 (0.01, 0.08)	0 (0, 0.01)	0.003	S
ABCG2	0.71 (0.25, 1.99)	0.02 (0.01, 0.05)	0.000	S
aSMA	0.21 (0.07, 0.58)	0.23 (0.09, 0.62)	0.871	NS
Col1A1	4.66 (1.65, 13.12)	4.97 (1.84, 13.44)	0.929	NS
Col1A2	11.33 (4.02, 31.92)	3.89 (1.44, 10.52)	0.145	NS
dNp63	0.03 (0.01, 0.09)	0 (0, 0)	0.000	S
ITGa3	0.12 (0.04, 0.33)	0.28 (0.10, 0.75)	0.244	NS
ITGb1	5.81 (2.06, 16.36)	7.99 (2.96, 21.59)	0.663	NS
Keratocan	0.14 (0.05, 0.39)	0.01 (0, 0.03)	0.000	S
KRT3	0.28 (0.08, 0.96)	0 (0, 0.01)	0.000	S
LAMA1	0.33 (0.12, 0.94)	0.07 (0.03, 0.19)	0.032	S
Notch1	0.43 (0.15, 1.21)	0.10 (0.04, 0.26)	0.043	S
P63a	0.05 (0.02, 0.15)	0 (0, 0.01)	0.000	S
PCNA	0.52 (0.19, 1.48)	0.71 (0.26, 1.92)	0.681	NS
Vimentin	16.96 (6.02, 47.77)	42.18 (15.61, 113.96)	0.214	NS

[1]Values are the back-transformed estimates from the multivariate regression; NS: Not significant; S: Significant ($P \leq 0.05$); ABCB5: ATP binding cassette subfamily B member 5; ABCG2: ATP-binding cassette, sub-family G member 2; αSMA: Smooth muscle, actin; COL1A1: Collagen type I, alpha 1 chain; COL1A2: Collagen type I, alpha 2 chain; TP63: Tumour protein p63; ΔNP63: Transcript variant 1, ΔNP63: N-terminal isoform, ITGa3: Integrin, subunit alpha 3; ITGB1: Integrin, subunit beta 1; KRT3: Keratin 3; LAMA1: Laminin, subunit alpha 1; TP63: Tumour protein p63; PCNA: Proliferating cell nuclear antigen.

approximately day 11, cells appeared to migrate initially as cell columns when leaving the tissue edge (although not invariably), and then cells would migrate to fill the space between the columns. Cells at the leading edge of these migratory columns had fine cell processes connecting the cells to neighbouring cells (Figure 3B, orange arrows).

Immunohistochemistry of sphere-seeded tissue sections

Spheres seeded onto keratoconic tissue sections stained positively for the putative stem cell marker ABCB5 and the myofibroblast marker αSMA at day 0, day 1 and day 4. At all three time points, labelling of ABCB5 appeared to be concentrated within spheres and not outside (Figure 4A-C, red), indicating presence of stem cells within spheres alone. Appearance of positive αSMA staining in small numbers of cells within spheres (Figure 4A-C, green) indicated some differentiation to myofibroblast cells (highly likely from daughter cells), and indeed some of these αSMA-positive cells were seen outside spheres at day 1 (Figure 4D) but also at day 4. Positive staining was above the fluorescence signal of the secondary antibody only control (Figure 4E).

Gene expression analysis

Analysis of variance revealed a significant effect of day (day 0 *vs* day 14; $P \leq 0.016$) and diseased matrix (keratoconic *vs* normal; $P \leq 0.006$). At day 14 post sphere seeding, there was an overall significant reduction in expression of putative stem cell makers (ABCB5, ATP-binding cassette, sub-family G member 2 (ABCG2), ΔNp63, tumour protein p63 C-terminal isoform α (p63α)), limbal (notch1), epithelial (keratin 3), keratocyte (keratocan) and extracellular matrix (laminin α1 (LAMA1)) markers tested using ddPCR (Table 2; Figure 1). In both keratoconic and normal tissue sections, expression of the putative stem cell markers and the limbal niche marker notch1 decreased over time as did the epithelial and extracellular matrix markers keratin 3, collagenA2, laminin and the stromal cell marker keratocan. While proliferating cell nuclear antigen (PCNA), vimentin and the adhesion molecules integrin alpha 3 and integrin beta 1 all increased at day 14 in both keratoconic and normal tissue matrices (Figure 1).

When comparing tissue matrices (keratoconic *vs* normal sections), there were no significant differences in gene expression between spheres seeded on keratoconic

Table 3 Statistical analysis of difference in gene expression in sphere-seeded tissue sections as measured by droplet digital polymerase chain reaction, effect of matrix, keratoconic *vs* normal

	Keratoconic	Normal	Keratoconic-normal	
Target	Estimate[1] (lower.95, upper.95)	Estimate[1] (lower.95, upper.95)	*P*	
ABCB5	0 (0, 0.01)	0.01 (0, 0.03)	0.351	NS
ABCG2	0.03 (0.01, 0.09)	0.37 (0.14, 0.99)	0.001	S
aSMA	0.24 (0.09, 0.64)	0.20 (0.07, 0.54)	0.800	NS
Col1A1	6.40 (2.37, 17.25)	3.62 (1.34, 9.77)	0.418	NS
Col1A2	9.30 (3.45, 25.08)	4.74 (1.76, 12.79)	0.337	NS
dNp63	0 (0, 0.01)	0.02 (0.01, 0.05)	0.004	S
ITGa3	0.16 (0.06, 0.43)	0.21 (0.08, 0.56)	0.695	NS
ITGb1	7.63 (2.83, 20.57)	6.09 (2.26, 16.42)	0.748	NS
Keratocan	0.03 (0.01, 0.08)	0.04 (0.02, 0.12)	0.588	NS
KRT3	0.01 (0.01, 0.04)	0.04 (0.01, 0.12)	0.211	NS
LAMA1	0.17 (0.06, 0.46)	0.13 (0.05, 0.36)	0.726	NS
Notch1	0.07 (0.03, 0.20)	0.58 (0.21, 1.56)	0.003	S
P63a	0.01 (0, 0.01)	0.02 (0.01, 0.06)	0.053	NS
PCNA	0.51 (0.19, 1.38)	0.73 (0.27, 1.97)	0.612	NS
Vimentin	24.29 (9.01, 65.52)	29.45 (10.92, 79.43)	0.784	NS
ABCB5	0 (0, 0.01)	0.01 (0, 0.03)	0.351	NS

[1]Values are the back-transformed estimates from the multivariate regression; NS: Not significant; S: Significant ($P \leq 0.05$); ABCB5: ATP binding cassette subfamily B member 5; ABCG2: ATP-binding cassette, sub-family G member 2; αSMA: Smooth muscle, actin; COL1A1: Collagen type I, alpha 1 chain; COL1A2: Collagen type I, alpha 2 chain; TP63: Tumour protein p63; ΔNP63: Transcript variant 1, ΔNP63: N-terminal isoform, ITGa3: Integrin, subunit alpha 3; ITGB1: Integrin, subunit beta 1; KRT3: Keratin 3; LAMA1: Laminin, subunit alpha 1; TP63: Tumour protein p63; PCNA: Proliferating cell nuclear antigen.

tissue sections and spheres seeded on normal tissue sections for cell proliferation (PCNA), epithelial (keratin 3), keratocyte (keratocan), extracellular matrix (LAMA1), collagen I α1 (Col1A1), collagen I α2 (Col1A2)), adhesion (integrin α3, integrin β1), myofibroblast (αSMA) or mesenchymal cell (vimentin) markers tested using ddPCR (Table 3; Figure 1). Only limbal and stem cell markers (notch1, ABCG2, ΔNp63) showed a significant reduction in gene expression on keratoconic sections, while p63α reduced to a level that did not reach significance ($P = 0.053$). The putative stem cell marker ABCB5 was also observed to have reduced expression on keratoconic matrix but not significantly so (Table 3; Figure 1).

Only the repair cell marker αSMA showed an overall increase in normal tissue sections and a decrease in keratoconic tissue sections, while conversely collagenA1 showed a decrease in normal tissue sections and an increase in keratoconic tissue sections (Figure 1). However, this difference in expression pattern on normal *versus* diseased tissue matrix was not statistically significant, which may be due to sphere donor variation for both αSMA and collagenA1.

Sphere implantation into full thickness tissue

Sphere behaviours once implanted into full thickness keratoconic tissue were similar to those observed on thin tissue sections and to those observed in full thickness non-keratoconic tissue controls. Six decellularised full-thickness central corneal tissues (corneal buttons) from post-keratoplasty keratoconic patients ($n = 3$) and from non-keratoconic cadaveric donor corneas with normal anterior corneas ($n = 3$) were successfully implanted with a total of 16 spheres using our wedge-shaped incision technique. The spheres were derived from three different human donors: Eight implanted in keratoconic tissue and eight implanted in non-keratoconic tissue. All spheres successfully survived the implantation procedure (confirmed by positive staining with Calcein-AM), tissue handling and new culture conditions for at least three days from the time of implantation (day 3) as seen in Figure 5A-B. In implanted keratoconic buttons, six of eight spheres and their derivative cells were viable at day 7. In comparison, five of eight spheres and their derivative cells were viable at day 7 in non-keratoconic buttons.

Cell migration was monitored to day 7 post-implantation in all implanted buttons

Table 4 Viability of spheres cultured on keratoconic and normal tissue sections

Day post implantation	Keratoconic tissue sections		Normal tissue sections	
	Number of sphere-implanted tissue sections cultured to time point	Number of sphere-implanted tissue sections viable at time point	Number of sphere-implanted tissue sections cultured to time point	Number of sphere-implanted tissue sections viable at time point
0	17		11	
1	17	17	11	11
3	16	14	10	6
7	13	11	5	5
14	2	2		

with two buttons extended out to day 10 (Figure 5C-D). All implanted spheres exhibited radial cell migration from the centre of the sphere up to day 3, however the extent of cell migration from each sphere varied not only in replicate tissue samples but also within the same tissue. The extent of cell migration from the centre of spheres increased from day 3 to day 7 in 11/16 implanted spheres. Of the five spheres that did not increase cell migration from day 3 to day 7, two were implanted in keratoconic tissue and three in non-keratoconic tissue. An example of this is shown in Figure 5D where the sphere marked by a yellow arrow shows reduced cell migration at day 10 compared with day 3 (Figure 5B).

Cell morphology and cell orientation was variable in different areas of the implanted tissue. However, morphological patterns and cell orientation patterns in the keratoconic and non-keratoconic corneal buttons were similar. Cells close to the sphere (Figure 5E) were long and thin in appearance with their long axes appearing to radiate away from the centre of the sphere. The cells distant from the sphere appeared plumper (Figure 5F). The long axes of cells at the edge of the tissue appeared parallel to the edge, whereas the long axes of those distant from both the tissue edge and centre of spheres seemed to have no obvious pattern of alignment (Figure 5G). Cells that migrated from two spheres implanted close to one another seemed to align to form what appeared to be "cellular bridges" between the spheres (Figure 5C, white arrows).

The incisions made for implantation into the full-thickness tissue do not appear to significantly affect cell migration. Sphere-derived cells migrate to an incision, align with the incised tissue edge and over time the incision lines cannot be clearly demarcated and migrated cells can be seen on both sides of the incision. The left-most sphere in the implanted normal button in Figure 5B and 5D illustrates this.

Cross-sectional immunohistochemistry

Cross sections through implanted non-keratoconic and keratoconic corneal buttons were analysed by immunohistochemistry to further characterise the phenotypes of these cells. Cells within implanted spheres stained positively for the putative stem cell marker ΔNp63α while migrated cells did not (Figure 6A-B). Cells within implanted spheres as well as cells adjacent to but outside of the sphere (Figure 6C-D) stained positively for proliferation marker EdU at day 10.

DISCUSSION

Spheres derived from normal peripheral cornea behave normally on keratoconic matrix

Spheres and sphere-derived cells implanted in or on keratoconic tissue elicited similar viability, adherence, migration, division and differentiation responses to non-keratoconic tissue (normal anterior corneas). Spheres have previously been shown to be able to remain viable when implanted into normal peripheral corneal tissue matrix[30]. This study shows that spheres can also remain viable in central corneal tissue matrix. Notably for the first time, we have also shown that spheres can remain viable in diseased tissue matrix. Moreover, the spheres themselves maintained their morphological structure in most cases. The same implantation technique that we have previously employed for normal peripheral cornea was used for keratoconic central corneas. This shows that the implantation technique can be used with more friable and weaker tissues as are apparent in severe keratoconus.

No observable difference was seen in viability between spheres implanted on keratoconic tissue and non-keratoconic tissue. Implanted tissues were cultured for up

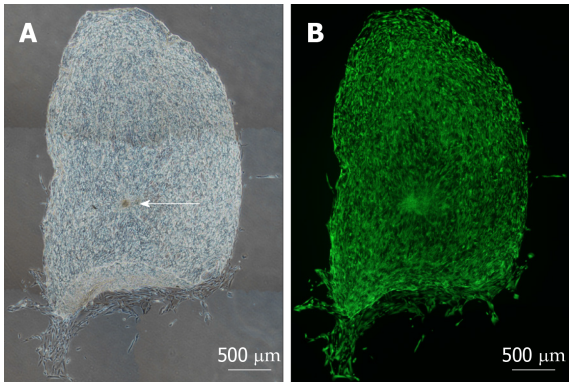

Figure 2 Cellular repopulation of the surface of *en face* keratoconic tissue sections. A: A stem cell-enriched sphere (arrow) was seeded onto a keratoconic decellularised central corneal stromal section (phase contrast image); B: Assessed for viability with Calcein-AM (green) at day 14 (fluorescence image). Montage imaging of the entire tissue section shows cells have repopulated the tissue section to complete confluence by day 14. Scale bar = 500 μm.

to 14 d, and spheres demonstrated the potential to remain viable for the entire duration. However, some spheres lost viability prematurely in some keratoconic and normal tissues even with biweekly medium changes. Speculative causes include intersphere variability or focal features of matrix that were not conducive to sphere growth (even in normal implants). The loss of sphere viability is unlikely to be attributable to matrix type (normal or diseased) as there was no consistency in terms of which matrix spheres prematurely lost viability. The initial implantation procedure, tissue handling or change in culture conditions are also unlikely causes as all spheres survived at least the first day. In our experience, spheres are discrete entities. The relative proportions of stem, progenitor, epithelial and stromal cells that comprise each sphere can vary. This intersphere variability may have been responsible for some spheres losing viability over time as the environment they were seeded/implanted into may not have supported the propagation of the majority cell populations present within these spheres.

There was no qualitative difference observed in the ability of spheres and their derivative cells to adhere to keratoconic tissue compared with normal tissue. Although the levels of relevant adhesion molecules in keratoconus used by nonimmunological migrating corneal cells are not known, decreased levels of collagen XII[35], integrin beta 4[36] and interfibrillar and interlamellar cohesive forces[37] have been observed in keratoconic stroma. However, these are unlikely to be applicable to the adhesion of spheres to stroma. The patterns of expression of integrin α3 and β1 chains, which dimerise to form the adhesion molecule integrin α3β1 found in basal epithelium and stromal cells, showed an increase at day 14 post-seeding of spheres, although this was not-significant ($P \leq 0.7$). Thus there was no clear pattern of expression differentiating normal *vs* keratoconic matrices in our ddPCR results.

Both the extent and pattern of cell migration observed in keratoconic tissues were similar to those observed in normal tissues. Cells tended to migrate from the sphere radially in all directions and this increased over time, as has been observed previously in peripheral corneo-scleral rims[30]. This is expected, given that there is no limbal or scleral region to polarise cell migration in a particular direction as is the case in peripheral cornea. Cells in keratoconic tissue appeared to respond to other nearby spheres as seen previously in normal tissue[16]. They also appeared to respond to the tissue edge, reflected by the apparent alignment of cells observed when implanted spheres were close to one another coupled with a consistent change in orientation when cells approached the tissue edge. These observations suggest that sphere-derived cells recognise tissue boundaries. In full thickness tissue, the tissue edge may have provided a physical barrier. However, in tissue sections cells migrated beyond the tissue section boundaries and onto the dish surface eventually but not prior to complete repopulation of the stromal section. This is despite the dish being a tissue culture treated surface designed to promote cellular attachment and outgrowth. This confirms that the corneal collagen matrix is the preferred substrate for sphere-derived cells. Although our results show cell migration primarily on the surface of full thickness tissues, previous results with induced pluripotent cells have shown cells can also migrate deeply within tissue[38].

Our results assessing active cell division confirmed the presence of EdU within sphere cells and amongst migrating cells as well as continued expression of PCNA

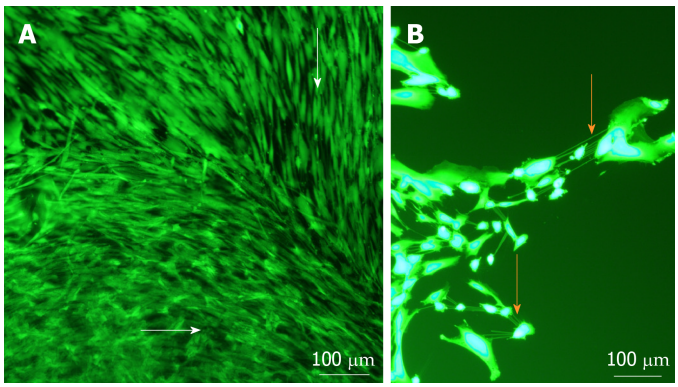

Figure 3 Cell morphology and migration patterns on the surface of sphere-seeded *en face* keratoconic tissue sections. A: Representative images of migrated cells over the surface of keratoconic tissue sections show cells from the centre of the sphere aligned radially while cells close to the tissue edge align parallel with the tissue edge (white arrows show cell orientations); B: When cells at one of the migrating edges are magnified and overexposed, fine cell projections can be seen connecting cells to neighbouring ones (orange arrows). Scale bar = 100 μm.

over time. PCNA expression showed variability between sphere donors suggesting the proliferative response was not temporally the same between donors. By 14 d, PCNA expression had increased from day 0 in all samples, which corresponds to the observation of complete tissue section repopulation at this time point.

Collectively, these results show that the abnormal structure of the diseased tissue was not a deterrent to sphere attachment, migration and division. However, there was no observable increase in any of these measures in response to diseased tissue compared to normal tissue either.

Functionality of the repopulated cells

Spheres, although stem cell enriched, do not exclusively contain undifferentiated cells[16,30]. Our findings were consistent with these cited observations. In addition, our findings also showed that spheres may maintain their stemness to some extent for at least 14 d after implantation in both keratoconic and normal implants. This was evidenced by their ability to maintain their definitive sphere structure *in situ*, detection of gene expression of putative stem cell markers over time and positive immunostaining of some of these markers (ΔNp63α and ABCB5). However, this retention of stemness was significantly reduced on keratoconic tissue sections (Table 3).

The reasons for this significant reduction in expression of stem cell markers on keratoconic matrix is unclear. It may be a tissue effect in that there is less signal coming from keratoconic tissue to maintain stem cells. Alternatively, it may be a cell effect in that stem cells within spheres change their response to diseased tissue more towards a pattern of differentiation rather than maintaining stemness. This may indicate that a greater number of spheres will be required to repair dystrophic tissue. Additionally, diseased tissue may be too far outside of the required stem cell niche to perpetuate maintenance of the stem cells to the same level as that of normal tissue. In our laboratory's previous results[30], we also observed a reduction in expression levels of putative stem cell markers to undetectable levels over time by qPCR. Presumably, this was due to the sheer numbers of migrated and differentiated cells over time diluting out the relatively few stem cells being maintained within a sphere. ddPCR is considered more sensitive than qPCR for detecting low abundance targets. Our ddPCR data in this study correlated well with previous qPCR data. ABCG2 expression decreased at similar rates in keratoconic implants and normal implants over 14 d. Similarly, stem cell markers ABCB5, ΔNp63 and p63α and limbal niche marker notch1 were detectable at low levels by ddPCR and also decreased by day 14. Our current findings reinforce our previous thoughts that message from differentiated cells was saturating any stem cell messages present from the few stem cells contributing to any given cDNA sample.

The evidence for cells differentiating as they leave the sphere lies in the absence of purported stem cell markers in migrated cells, cell morphologies of migrated cells and the presence of differentiation markers. Culture in serum-containing medium is known to stimulate differentiation, so this result is not surprising. Most cells that migrated from spheres at any time point between day 1 and 14 had a fusiform morphology. There was a noticeable effect at days 7 and 14 on the cell migration patterns of spheres placed on to keratoconic stromal sections that appeared to have a

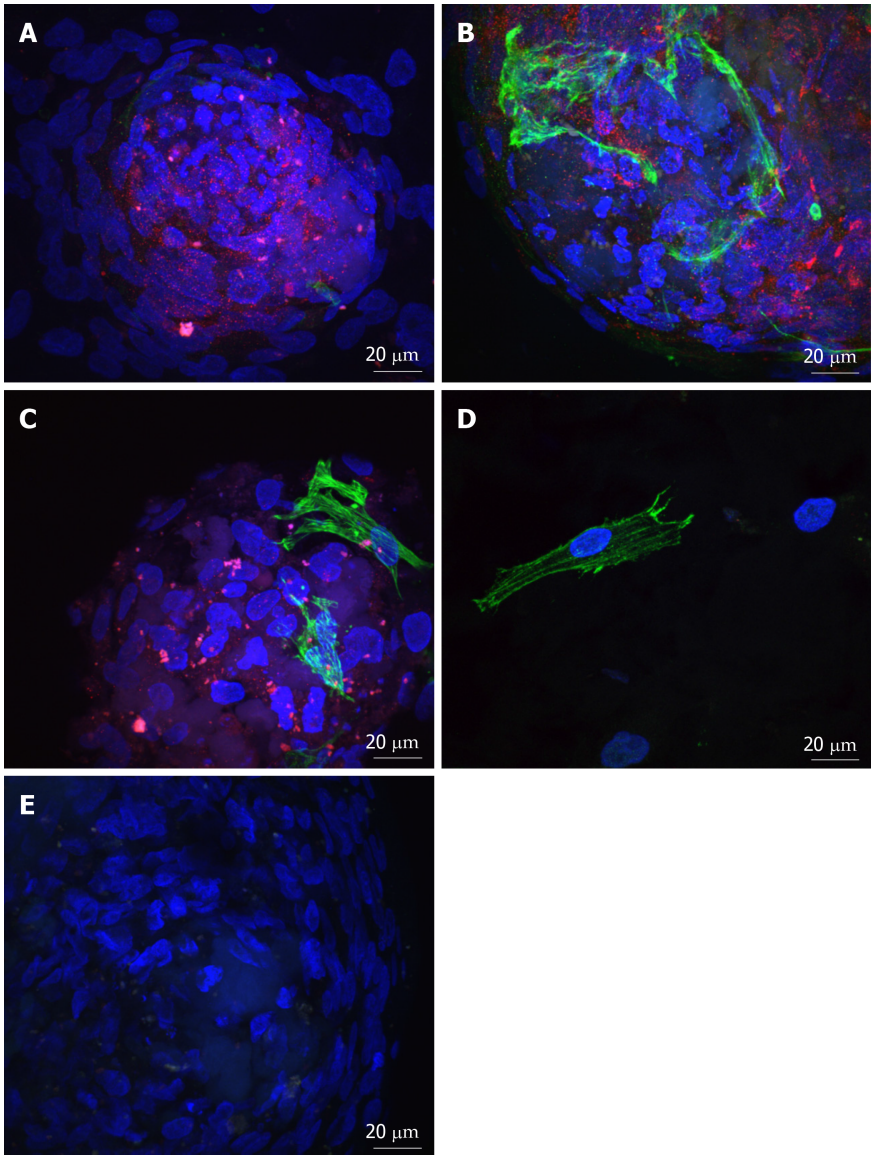

Figure 4 Adenosine triphosphate binding cassette subfamily B member 5 and α-smooth muscle actin expression in spheres and migrated cells seeded onto keratoconic tissue sections. A, B, C: Spheres seeded onto keratoconic tissue sections were fixed at day 0, 1 and 4 post-implantation and double primary antibody immunolabelled with putative stem cell marker ATP binding cassette subfamily B member 5 (ABCB5) (red) and myofibroblast marker alpha smooth muscle actin (αSMA) (green). Cell nuclei were counterstained with DAPI (blue). Confocal projection images of z stacks were taken. Spheres labelled positively with ABCB5 and αSMA at days 0 (A), 1 (B) and 4 (C); D: Migrated cells at days 1 and 4 appeared similar, a representative image at day 1 is shown; E: Spheres labelled with secondary antibody had no detectable red and green fluorescence when imaged at the same levels as A-C. Scale bar = 20 μm.

much looser arrangement of collagen fibrils. In these sections, cell orientation took on a less organized and a more random orientation pattern that was not observed in normal stromal sections. Coupled with an observed increase in expression of mesenchymal marker vimentin over time when compared to day 0, there is a good chance that these cells were stromal fibroblasts, which may or may not have been activated fibroblasts.

From as early as the time of adherence (day 0), some cells in the sphere labelled positively for the myofibroblast marker, αSMA. The majority of migrated cells were negative for this marker over the course of four days in immunocytochemistry sections. This coincides with ddPCR data, which showed decreased expression of αSMA below the level at day 0 in keratoconic sections over 14 d in culture. There was increased expression of αSMA in samples from one sphere donor seeded onto normal tissue relative to day 0 that resulted in a high level of donor-donor variation on normal tissue for αSMA expression. Perhaps the spheres from this donor on day 0 had an unusually low expression of αSMA. Therefore, even small increases in αSMA expression in other samples appeared magnified relative to day 0, or possibly these

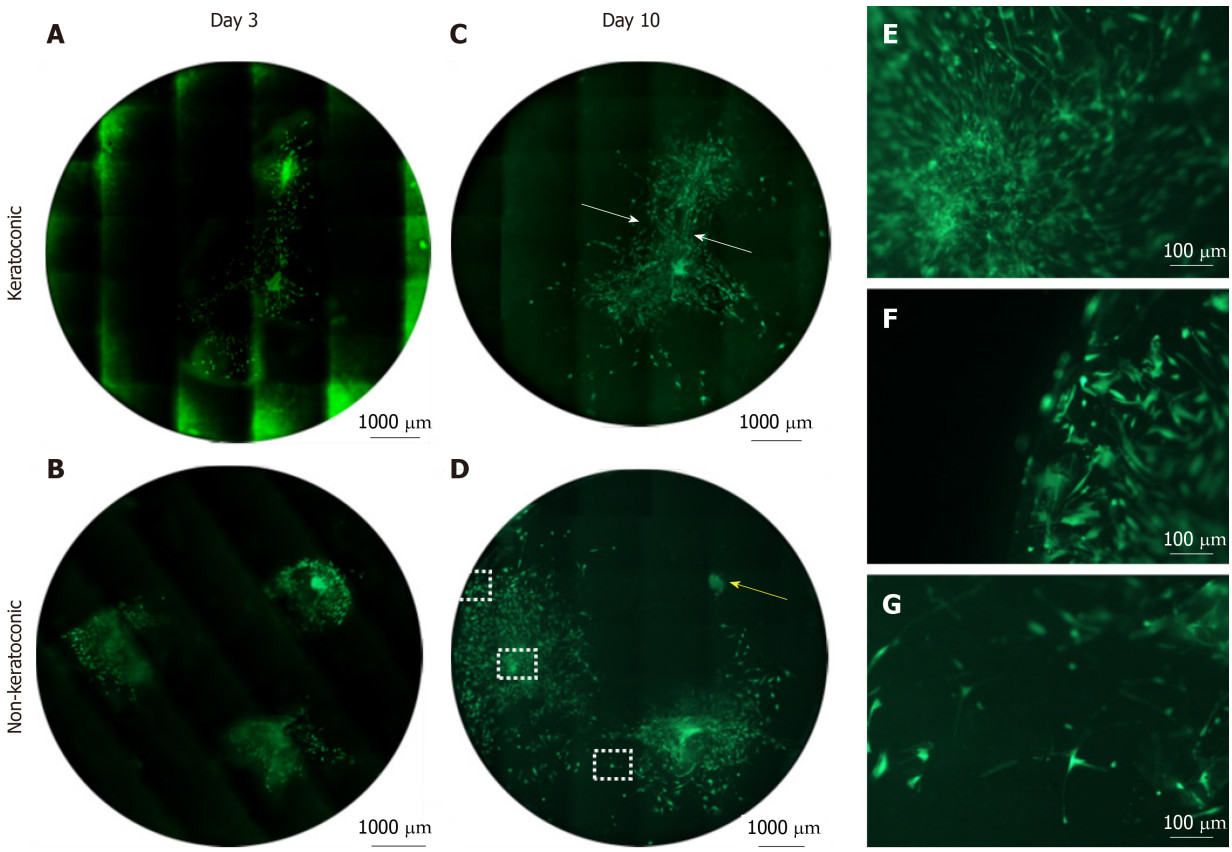

Figure 5 Cell viability of spheres and sphere-derived cells within implanted full-thickness corneal tissue. A-D: Decellularised full-thickness central corneal stromal tissues (corneal buttons) implanted with three spheres each and assessed for cell viability with Calcein-AM (green) were imaged at 50 × magnification with a fluorescence microscope and montaged to maintain detail of individual cells throughout the entire corneal button. Each circle represents the corneal button edge. Three days after implantation (day 3), spheres in keratoconic (A) and non-keratoconic (decompensated: normal anterior cornea with failed endothelium) (B) matrices are viable and have viable cells radiating from the sphere. At day 10, spheres in keratoconic (C) and non-keratoconic (D) matrices remain viable, and the viable cells have migrated further outward from the centre of the sphere. An exception to this was one sphere within non-keratoconic tissue, which showed reduced cell migration at day 10 compared with day 3 (yellow arrow, D); E-G: Panels E-G are magnified areas from D indicated by dotted squares (E = central square, F = top square, G = lower square). When spheres are implanted close to each other, cells align between them as if forming "cellular bridges" (white arrows, C). Cells near the centre of the sphere orientate radially from the centre of the sphere (E) while cells near the tissue edge are aligned parallel with the edge (F). Cells distant from both the nearest sphere and the tissue edge appear to lose their alignment (G). Scale bar = 1000 μm for A-D and 100 μm for E-G. Bright green fluorescence at left edge of tiles in montage (A) is artefactual.

spheres mounted a more aggressive wound healing response. Sphere-derived cell migration may represent an early phase of wound healing or may be a response similar to the migration of neural crest cells seen embryologically, which are also vimentin-positive from studies of mammalian and avian embryogenesis[39].

Expression of epithelial cell marker, keratin 3, was detected at very low levels in the majority of samples, and its expression significantly decreased over time in both tissue types. There was also significantly decreased temporal expression of laminin α1, which is associated with epithelial cells. Taken together, these findings suggest that the migrated cells were eliciting a stromal cell response on what was largely a stromal matrix.

Cells of varying morphology were occasionally seen in long-term tissue-seeded or implanted cultures, including what appeared to be cells with keratocyte-like morphology. However, detection of the keratocyte marker keratocan by ddPCR was significantly reduced over time and did not appear to support the differentiation of sphere cells into functioning keratocytes. It is likely that the 14-d duration of our repopulation experiments was too short for true keratocyte differentiation to be initiated. Similarly, we did not observe any consistent increase in collagen I production (neither α1 nor α2 chains), although there was an observed nonsignificant increase in expression of the alpha chain variant in keratoconic tissue but again with high donor-donor variation. The fact that we observed similar levels of collagen expression in keratoconic and normal tissue may indicate the beginnings of these cells laying down new matrix. Whether this would result in repair of the abnormal collagen matrix in keratoconic stroma remains to be seen. Longer term experiments may help in elucidating this.

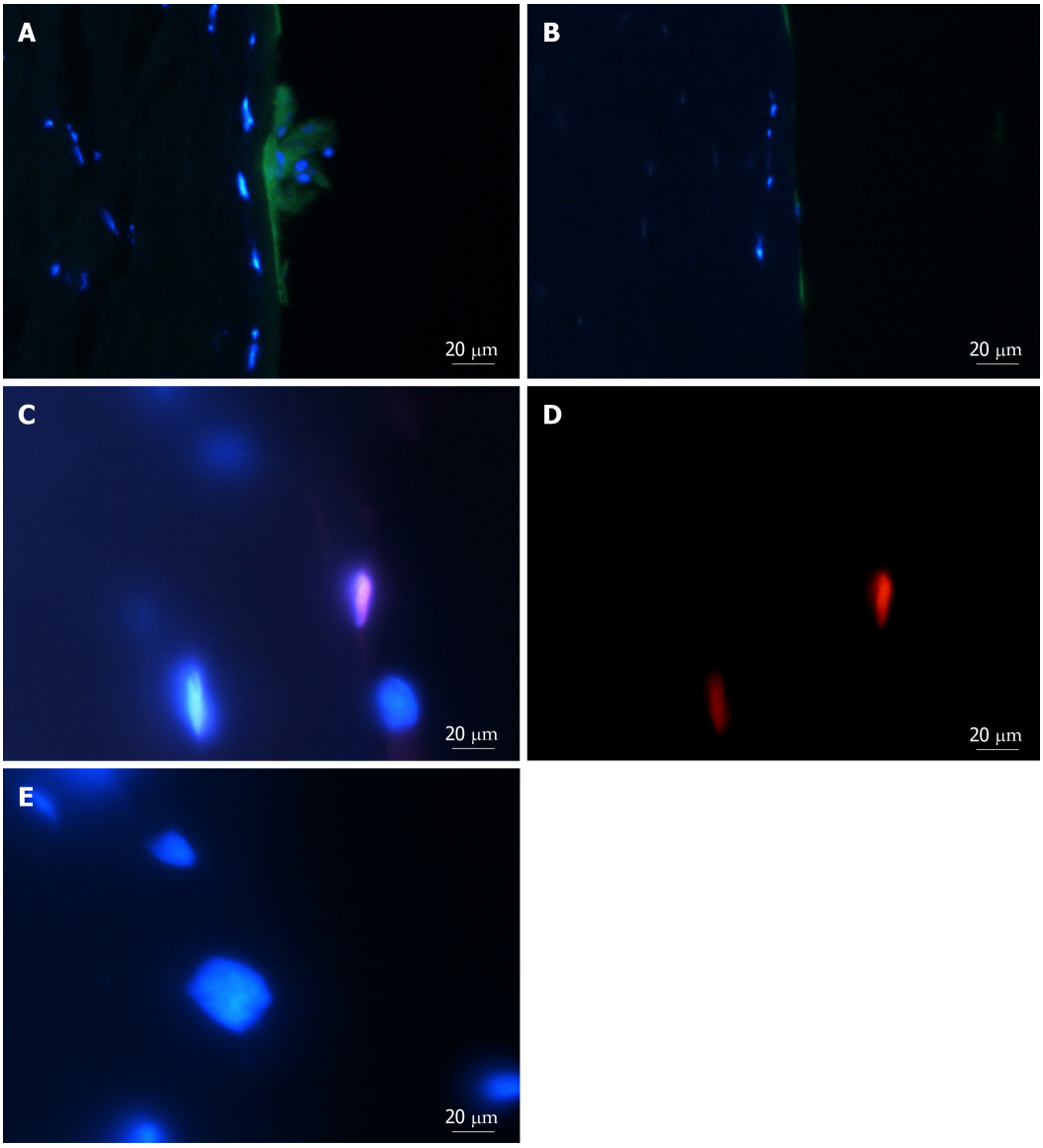

Figure 6 Putative stem-cell marker tumour protein p63, transcript variant 1, N-terminal isoform and cell-proliferation marker 5-ethynyl-2'-deoxyuridine in cells within sphere-implanted-full-thickness tissue at day 10. A: Representative images of cross sections with spheres and cells derived from spheres implanted into full-thickness keratoconic and non-keratoconic central corneal buttons at day 10 show positive staining within the sphere for the putative stem cell marker tumour protein p63, transcript variant 1, N-terminal isoform (ΔNp63α) (green); B: Cells stained without primary antibody (secondary antibody only control) show low green fluorescence. Cell nuclei are stained with DAPI (blue); C, D: Some, but not all cells show evidence of cell division (detected with ClickiT 5-ethynyl-2'-deoxyuridine (EdU) (red), a cell proliferation marker), as shown by pink cell nuclei in superimposed images of DAPI and EdU staining (C) and its equivalent image with red signal only (D); E: A negative control (EdU incubation without processing with its reaction solution) imaged at the same signal intensity as D is shown superimposed on DAPI for comparison. Scale bar = 20 μm.

Taken together, these results suggest that when spheres are implanted into or onto corneal stromal matrix, sphere-derived cells migrate and differentiate down a lineage appropriate to the matrix they are exposed to. Although there is evidence they can maintain a level of stemness after implantation, this ability appears to be impaired on keratoconic tissue. It may be that we are below the stem cell threshold required within keratoconic tissue to retain stemness to a similar level to that of normal tissue that may indicate the need for implantation of more spheres in keratoconic corneas. Culture conditions would also play a role, in particular culture medium components such as growth factors would dictate whether cells take a certain path towards differentiation or not. Cells could be directed as to which trajectory to take: adult wound healing or foetal wound healing (for example by addition of cytokines like transforming growth factor β1 or β2 for the former or transforming growth factor β3 for the latter)[40].

In this study, we have relied upon the inherent properties of the spheres to detect the matrix onto which they are placed and react accordingly by producing cells of the correct lineage for that particular surface. In our observations, spheres react to the

matrix in which they are placed, and this appears to stimulate differentiation of sphere-derived cells. As the identification of signalling molecules that drive differentiation of sphere cells placed onto corneal matrices was beyond the scope of this study, we currently do not have data on the specific signalling molecules that drive this differentiation in a specific direction and thus are relying more on the environmental cues that sphere cells receive. Although the use of signalling molecules to direct sphere cell differentiation along a specific path may be beneficial, the molecular interactions are highly complex and unlikely to be completely reproduced by a single or even a mixture of signalling molecules.

A migratory, rather than differentiation, response of spheres is consistently observed when spheres are cultured with serum-containing medium despite different types of collagen substrates[16,30]. Our results show that when cell signals are controlled, and normal cells are exposed to keratoconic matrix, cells do not change their behavioural response to the diseased matrix. This suggests that diseased matrix in itself may not perpetuate the pathogenic process of keratoconus. The combination of scar-promoting cell signalling, inept wound healing capability of keratoconic stromal cells and abnormal matrix are likely to feed each other in the cycle of its pathogenesis. It is likely that a treatment that utilises both normal cells and normal cell signals may be able to alter the trajectory of the healing process towards normal. There are already some promising results of scarless regeneration of ablated stroma in corneal mouse wounds[41].

Spheres are a suitable delivery system of stem cells

Spheres have previously been shown as a delivery system for stem cells into normal tissue matrix but not in diseased tissue, which differs morphologically[30]. There are a number of advantages of using spheres as the mode of stem cell delivery. Firstly, spheres contain a heterogeneous population of cells of both epithelial and stromal origin in a 3D format, which better simulates the *in vivo* niche. This may be useful to treat keratoconus, which has features of both epithelial and stromal cell dysfunction. Secondly, sphere-forming assays are commonly used retrospectively to identify stem cells[42], so spheres can be confidently used knowing undifferentiated cells are present. Thirdly, spheres are dynamic entities shown to be capable of reacting to their environment whilst maintaining themselves for up to 4 mo[16]. Finally, spheres can be transplanted as defined entities and have shown capability to repopulate the normal stromal ocular surface[30].

Although we did not look at immune rejection markers in our study because our host tissues were decellularised, this is an important consideration for further research in this field. An alternative to sphere-based stem cell delivery is transplantation of stem cells in the form of corneal limbal explants. Limbal explants have been successful in treating patients with limbal stem cell deficiency; these have their own limitations, however. Autografts are more successful than allografts owing to the lower likelihood of immune rejection, but keratoconus is a bilateral disease and even in patients who appear to have a non-affected eye, they are likely to develop bilateral disease long-term[43]. Also, the genotype of the autograft will still remain keratoconic. Allografts, on the other hand, have a high risk of rejection. This has been shown in mice[44] and even in human leukocyte-antigen matched grafts. One study found that one-third of matched limbal grafts had failed at 5 years[45].

Sphere-based stem cell delivery also has some limitations that need to be considered. Firstly, the neurosphere assay, or any technique utilising culture with high concentrations of mitogens to expand stem cells, is unlikely to detect quiescent stem cells[42]. While this means that the stem cells in spheres are possibly not representative of the entire *in vivo* stem cell populations, this does not necessarily limit therapeutic application in tissue repair. Also, the quiescent stem cells may not be able to be rapidly expanded *in vitro* with mitogens, which is not ideal for therapeutic use. Secondly, spheres are not clones, so intersphere variations are an inherent limitation and even without factoring patient response, therapeutic efficacy of each sphere will be different. However, given that stem cell enriched peripheral corneal spheres formed by sphere forming assay represent a way to apply a well-defined, known cell population, they may provide an improved method for treating corneal dystrophies like keratoconus.

Integrating stem cell implantation with current treatments

For spheres to be used for tissue repair with good functional outcomes, several factors need to be considered and compared to keratoplasty, the current definitive treatment. Safety factors such as tumorigenic potential and immune compatibility, practicality factors such as method of delivery and tissue availability, and therapeutic factors such as efficacy and sustainability of treatment need to be considered.

We have demonstrated the ability of spheres to perceive the environment they are

exposed to and respond to it accordingly. This has been evidenced by spheres respecting artefactual gaps in tissue sections, their alignment with tissue section edges as well as differentiation into cells appropriate to the matrix they are implanted on. Previous studies have also shown that spheres implanted into limbal matrix preferentially migrate onto cornea over sclera. Moreover, unlike oncogenic cells, spheres respond to signals given to them. Unrestricted cell growth from spheres therefore seems unlikely.

Owing to the relatively immunoprivileged status of the cornea and reduced rejection rates from avoiding breach of the corneal endothelium[1], introduction of spheres into the corneal stroma is likely to have a low risk of immune rejection. As with any allogenic transplant, human leukocyte antigen matching may help to further mitigate risk of immune rejection.

Spheres are transplantable; they can successfully be surgically implanted into full-thickness corneas and adhere relatively reliably within 30 min. While direct implantation could be one possible method of sphere delivery, alternative routes could be explored. Spheres and sphere-derived cells have demonstrated preference for collagen over plastic, so sphere-coated contact lenses may be an alternative. Amniotic membrane could also potentially be used, as it has been successfully used as a mode of delivery for limbal explants.

Compared to keratoplasty, spheres have the advantage of being able to utilise limited resource donor tissue to potentially treat more people as many spheres can be generated from a single donor corneo-scleral rim.

Cells can migrate up to 5 mm away from the central sphere in 14 d and contain actively dividing cells. These features mean that spheres can potentially be implanted at a single or a few points and not necessarily in most severely affected areas. Cells could migrate to the areas needed and multiple implants may not be needed as spheres possess the ability to divide and maintain themselves.

While spheres can repopulate a corneal tissue surface, studies into the potential interaction with native corneal cells and matrix production are necessary before their full therapeutic efficacy can be assessed. If decellularisation is necessary, spheres could potentially be introduced after corneal collagen cross-linking treatments.

We hypothesised that the improved outcome from keratoplasty compared to collagen cross-linking is likely due to the introduction of normal cells and matrix to the diseased cornea. We extrapolate this idea to propose that the introduction of normal cells alone would rehabilitate the keratoconic cornea, and the introduction of normal cells to a post collagen cross-linked cornea may also prove of benefit. We have shown that stem cell enriched spheres cultured in the laboratory from limbal cell extracts can be successfully seeded onto keratoconic *en face* tissue sections and implanted into full thickness central corneal tissue. We have confirmed the ability of these spheres to respond to diseased tissue in a similar way to their response to normal tissue and that the cells showed the correct markers and morphological tendencies for the tissue structures they were placed in. Spheres were able to repopulate the diseased tissue surface either partially or entirely with the number of spheres implanted appearing to be the only limitation to complete surface repopulation. Over 14 d, the cells remained in a largely migratory state but the cells showed the beginning of differentiation into the appropriate cell types. Longer term experiments coupled with the addition of appropriate cell signalling molecules may direct them towards a more regenerative state. Our findings indicate that the presence of diseased matrix does not appear to direct normal cells to behave abnormally and thus conversely normal cells implanted into diseased matrix may drive the repair of the matrix into a normal phenotype. These results are an important initial step towards the development of an enhanced treatment or perhaps even cure for keratoconus in the future.

ARTICLE HIGHLIGHTS

Research background

Keratoconus is a disease in which the front part of the eye, the cornea, becomes cone-shaped resulting in impaired vision. It is not clear why this disease occurs and why it progresses, although current treatments can help to improve vision. Reports in the literature of cross link treatments that removed some of the native cells and strengthened the matrix, only halted or slowed the disease process for relatively short periods. On the contrary, transplanting healthy tissue containing healthy cells and matrix reduced recurrence rates. From this, we hypothesised that introducing healthy cells may be able to stop progression of the disease process. Stem cells possess many reparative and regenerative characteristics. Stem cell-enriched spheres cultured from healthy human corneal donors have been shown to be able to elicit healing responses and also can be implanted into normal corneal tissue to repopulate it. However, this regenerative ability of spheres has not previously been studied in diseased corneal tissue.

Research motivation
This study aimed to analyse how stem cell spheres behave in keratoconic tissue. It was not known whether stem cell spheres could survive or how they would behave when implanted into diseased corneal tissue. The eventual goal is to be able to use stem cell spheres for implantation and direct them to regenerate or repair diseased cornea with minimal invasiveness to donors and recipients.

Research objectives
Our research objectives were to implant stem cell spheres into keratoconic tissue and observe cell survival, proliferation, migration and differentiation. This data will inform the use of stem cell spheres for implantation into diseased tissue as a therapeutic tool.

Research methods
Spheres were implanted into full-thickness keratoconic tissues and also onto 10 μm thin slices of keratoconic stromal tissues. Similar implants were done in non-keratoconic tissues for comparison. Spheres were stained with the live cell stain Calcein-AM and imaged between days 0 and 14. Sphere implanted tissues were also analysed using indirect immunohistochemistry and droplet digital PCR.

Research results
Our results showed that spheres were able to survive to 14 d after being implanted into keratoconic and non-keratoconic tissues, both into full-thickness tissues as well as onto 10 μm tissue slices. There were no significant differences observed between how spheres migrated on keratoconic tissue compared to non-keratoconic tissue. Cells migrated from spheres radially and aligned with tissue edges. Cells were observed to increase in number with time by direct observation and by detection of cell proliferation markers. Putative stem cell markers were still detected 14 d post implantation but with lower levels of expression in the spheres implanted on keratoconic tissue compared to those implanted on normal tissue. Stromal cell markers increased while epithelial cell markers reduced indicating that spheres exhibit a response appropriate to the stimulus of stromal tissue. Future work will determine whether the cells will ultimately differentiate into keratocytes or how sphere-derived cells would progress *in vivo*.

Research conclusions
This study provided a novel insight into the implantation of healthy cells aimed at reducing disease progression in degenerative diseases like keratoconus. It has shown early insights into how spheres behave when implanted into diseased keratoconic corneal tissues. If healthy cells derived from implanted stem cell spheres can influence the diseased milieu into a healthier scenario, stem cell sphere implantation could be used to supplement corneal cross-linking procedures and delay the deterioration of vision for patients with keratoconus.

Research perspectives
This study informs the use of stem cell-enriched spheres as therapeutic agents in ocular tissue matrices. Future research would aim to study these interactions and how best to progress towards being able to use stem cells as a therapeutic adjunct to current treatments.

ACKNOWLEDGEMENTS

The authors want to thank both the people who donated their tissues and their families for their selfless contribution to this research. They would also like to acknowledge Judy Loh, Jeremy Mathan, Jacqui Ross, Wayne McCollough and Professor Charles McGhee from University of Auckland for advice and assistance with laboratory, technical, imaging, practical and translational aspects of this work, respectively.

REFERENCES

1 **Romero-Jiménez M**, Santodomingo-Rubido J, Wolffsohn JS. Keratoconus: a review. *Cont Lens Anterior Eye* 2010; **33**: 157-66; quiz 205 [PMID: 20537579 DOI: 10.1016/j.clae.2010.04.006]
2 **Sherwin T**, Brookes NH. Morphological changes in keratoconus: pathology or pathogenesis. *Clin Exp Ophthalmol* 2004; **32**: 211-217 [PMID: 15068441 DOI: 10.1111/j.1442-9071.2004.00805.x]
3 **Somodi S**, Hahnel C, Slowik C, Richter A, Weiss DG, Guthoff R. Confocal in vivo microscopy and confocal laser-scanning fluorescence microscopy in keratoconus. *Ger J Ophthalmol* 1996; **5**: 518-525 [PMID: 9479549]
4 **Sherwin T**, Brookes NH, Loh IP, Poole CA, Clover GM. Cellular incursion into Bowman's membrane in the peripheral cone of the keratoconic cornea. *Exp Eye Res* 2002; **74**: 473-482 [PMID: 12076091 DOI: 10.1006/exer.2001.1157]
5 **Kenney MC**, Nesburn AB, Burgeson RE, Butkowski RJ, Ljubimov AV. Abnormalities of the extracellular matrix in keratoconus corneas. *Cornea* 1997; **16**: 345-351 [PMID: 9143810 DOI: 10.1097/00003226-199705000-00016]
6 **Erie JC**, Patel SV, McLaren JW, Nau CB, Hodge DO, Bourne WM. Keratocyte density in keratoconus. A confocal microscopy study(a). *Am J Ophthalmol* 2002; **134**: 689-695 [PMID: 12429244 DOI:

10.1016/s0002-9394(02)01698-7]
7 **Davidson AE**, Hayes S, Hardcastle AJ, Tuft SJ. The pathogenesis of keratoconus. *Eye (Lond)* 2014; **28**: 189-195 [PMID: 24357835 DOI: 10.1038/eye.2013.278]
8 **Wollensak G**. Crosslinking treatment of progressive keratoconus: new hope. *Curr Opin Ophthalmol* 2006; **17**: 356-360 [PMID: 16900027 DOI: 10.1097/01.icu.0000233954.86723.25]
9 **Raiskup-Wolf F**, Hoyer A, Spoerl E, Pillunat LE. Collagen crosslinking with riboflavin and ultraviolet-A light in keratoconus: long-term results. *J Cataract Refract Surg* 2008; **34**: 796-801 [PMID: 18471635 DOI: 10.1016/j.jcrs.2007.12.039]
10 **Kelly TL**, Williams KA, Coster DJ; Australian Corneal Graft Registry. Corneal transplantation for keratoconus: a registry study. *Arch Ophthalmol* 2011; **129**: 691-697 [PMID: 21320951 DOI: 10.1001/archophthalmol.2011.7]
11 **Bourges JL**, Savoldelli M, Dighiero P, Assouline M, Pouliquen Y, BenEzra D, Renard G, Behar-Cohen F. Recurrence of keratoconus characteristics: a clinical and histologic follow-up analysis of donor grafts. *Ophthalmology* 2003; **110**: 1920-1925 [PMID: 14522765 DOI: 10.1016/S0161-6420(03)00617-1]
12 **Chunyu T**, Xiujun P, Zhengjun F, Xia Z, Feihu Z. Corneal collagen cross-linking in keratoconus: a systematic review and meta-analysis. *Sci Rep* 2014; **4**: 5652 [DOI: 10.1038/srep05652]
13 **Mazzotta C**, Balestrazzi A, Traversi C, Baiocchi S, Caporossi T, Tommasi C, Caporossi A. Treatment of progressive keratoconus by riboflavin-UVA-induced cross-linking of corneal collagen: ultrastructural analysis by Heidelberg Retinal Tomograph II in vivo confocal microscopy in humans. *Cornea* 2007; **26**: 390-397 [PMID: 17457184 DOI: 10.1097/ICO.0b013e318030df5a]
14 **Garfias Y**, Nieves-Hernandez J, Garcia-Mejia M, Estrada-Reyes C, Jimenez-Martinez MC. Stem cells isolated from the human stromal limbus possess immunosuppressant properties. *Mol Vis* 2012; **18**: 2087-2095 [PMID: 22876135]
15 **Chen SY**, Hayashida Y, Chen MY, Xie HT, Tseng SC. A new isolation method of human limbal progenitor cells by maintaining close association with their niche cells. *Tissue Eng Part C Methods* 2011; **17**: 537-548 [PMID: 21175372 DOI: 10.1089/ten.TEC.2010.0609]
16 **Yoon JJ**, Wang EF, Ismail S, McGhee JJ, Sherwin T. Sphere-forming cells from peripheral cornea demonstrate polarity and directed cell migration. *Cell Biol Int* 2013; **37**: 949-960 [PMID: 23619932 DOI: 10.1002/cbin.10119]
17 **Joyce N**, Annett G, Wirthlin L, Olson S, Bauer G, Nolta JA. Mesenchymal stem cells for the treatment of neurodegenerative disease. *Regen Med* 2010; **5**: 933-946 [PMID: 21082892 DOI: 10.2217/rme.10.72]
18 **Phinney DG**, Prockop DJ. Concise review: mesenchymal stem/multipotent stromal cells: the state of transdifferentiation and modes of tissue repair--current views. *Stem Cells* 2007; **25**: 2896-2902 [PMID: 17901396 DOI: 10.1634/stemcells.2007-0637]
19 **Spees JL**, Olson SD, Whitney MJ, Prockop DJ. Mitochondrial transfer between cells can rescue aerobic respiration. *Proc Natl Acad Sci U S A* 2006; **103**: 1283-1288 [PMID: 16432190 DOI: 10.1073/pnas.0510511103]
20 **Wilson SE**, Liu JJ, Mohan RR. Stromal-epithelial interactions in the cornea. *Prog Retin Eye Res* 1999; **18**: 293-309 [DOI: 10.1016/S1350-9462(98)00017-2]
21 **Wilson SE**, He YG, Weng J, Li Q, McDowall AW, Vital M, Chwang EL. Epithelial injury induces keratocyte apoptosis: hypothesized role for the interleukin-1 system in the modulation of corneal tissue organization and wound healing. *Exp Eye Res* 1996; **62**: 325-327 [PMID: 8795451 DOI: 10.1006/exer.1996.0038]
22 **Arnal E**, Peris-Martínez C, Menezo JL, Johnsen-Soriano S, Romero FJ. Oxidative stress in keratoconus? *Invest Ophthalmol Vis Sci* 2011; **52**: 8592-8597 [PMID: 21969298 DOI: 10.1167/iovs.11-7732]
23 **Buddi R**, Lin B, Atilano SR, Zorapapel NC, Kenney MC, Brown DJ. Evidence of oxidative stress in human corneal diseases. *J Histochem Cytochem* 2002; **50**: 341-351 [PMID: 11850437 DOI: 10.1177/002215540205000306]
24 **Mackiewicz Z**, Määttä M, Stenman M, Konttinen L, Tervo T, Konttinen YT. Collagenolytic proteinases in keratoconus. *Cornea* 2006; **25**: 603-610 [PMID: 16783151 DOI: 10.1097/01.ico.0000208820.32614.00]
25 **Cheung IM, McGhee CNj, Sherwin T**. Deficient repair regulatory response to injury in keratoconic stromal cells. *Clin Exp Optom* 2014; **97**: 234-239 [PMID: 24147544 DOI: 10.1111/cxo.12118]
26 **Ma Y**, Xu Y, Xiao Z, Yang W, Zhang C, Song E, Du Y, Li L. Reconstruction of chemically burned rat corneal surface by bone marrow-derived human mesenchymal stem cells. *Stem Cells* 2006; **24**: 315-321 [PMID: 16109757 DOI: 10.1634/stemcells.2005-0046]
27 **Bray LJ**, Heazlewood CF, Munster DJ, Hutmacher DW, Atkinson K, Harkin DG. Immunosuppressive properties of mesenchymal stromal cell cultures derived from the limbus of human and rabbit corneas. *Cytotherapy* 2014; **16**: 64-73 [PMID: 24094499 DOI: 10.1016/j.jcyt.2013.07.006]
28 **Zhu WZ**, Van Biber B, Laflamme MA. Methods for the derivation and use of cardiomyocytes from human pluripotent stem cells. *Methods Mol Biol* 2011; **767**: 419-431 [PMID: 21822893 DOI: 10.1007/978-1-61779-201-4_31]
29 **Huang SU**, Yoon JJ, Ismail S, McGhee JJ, Sherwin T. Sphere-forming cells from peripheral cornea demonstrate a wound-healing response to injury. *Cell Biol Int* 2015; **39**: 1274-1287 [PMID: 26094955 DOI: 10.1002/cbin.10501]
30 **Mathan JJ**, Ismail S, McGhee JJ, McGhee CN, Sherwin T. Sphere-forming cells from peripheral cornea demonstrate the ability to repopulate the ocular surface. *Stem Cell Res Ther* 2016; **7**: 81 [PMID: 27250558 DOI: 10.1186/s13287-016-0339-7]
31 **Mathan JJ**, Ismail S, McGhee JJ, McGhee CN, Sherwin T. Sphere-forming cells from peripheral cornea demonstrate the ability to repopulate the ocular surface. *Stem Cell Res Ther* 2016; **7**: 81 [PMID: 27250558 DOI: 10.1186/s13287-016-0339-7]
32 **Nolan T**, Hands RE, Ogunkolade W, Bustin SA. SPUD: a quantitative PCR assay for the detection of inhibitors in nucleic acid preparations. *Anal Biochem* 2006; **351**: 308-310 [PMID: 16524557 DOI: 10.1016/j.ab.2006.01.051]
33 **Bates D**, Mächler M, Bolker B, Walker S. Fitting Linear Mixed-Effects Models Using lme4. *J Stat Softw* 2015; **67**: 1-48 [DOI: 10.18637/jss. v067. i01]
34 **The R Core Team**. R: A Language and Environment for Statistical Computing; Version 3.6.1, 2019. Available from: URL: https://www.R-project.org
35 **Cheng EL**, Maruyama I, SundarRaj N, Sugar J, Feder RS, Yue BY. Expression of type XII collagen and hemidesmosome-associated proteins in keratoconus corneas. *Curr Eye Res* 2001; **22**: 333-340 [PMID: 11600933 DOI: 10.1076/ceyr.22.5.333.5491]
36 **Tuori AJ**, Virtanen I, Aine E, Kalluri R, Miner JH, Uusitalo HM. The immunohistochemical composition

of corneal basement membrane in keratoconus. *Curr Eye Res* 1997; **16**: 792-801 [PMID: 9255508 DOI: 10.1076/ceyr.16.8.792.8989]

37 **Meek KM**, Tuft SJ, Huang Y, Gill PS, Hayes S, Newton RH, Bron AJ. Changes in collagen orientation and distribution in keratoconus corneas. *Invest Ophthalmol Vis Sci* 2005; **46**: 1948-1956 [PMID: 15914608 DOI: 10.1167/iovs.04-1253]

38 **Naylor RW**, McGhee CN, Cowan CA, Davidson AJ, Holm TM, Sherwin T. Derivation of Corneal Keratocyte-Like Cells from Human Induced Pluripotent Stem Cells. *PLoS One* 2016; **11**: e0165464 [PMID: 27792791 DOI: 10.1371/journal.pone.0165464]

39 **Bronner-Fraser M**, Stern CD, Fraser S. Analysis of neural crest cell lineage and migration. *J Craniofac Genet Dev Biol* 1991; **11**: 214-222 [PMID: 1725870]

40 **Karamichos D**, Zareian R, Guo X, Hutcheon AE, Ruberti JW, Zieske JD. Novel in Vitro Model for Keratoconus Disease. *J Funct Biomater* 2012; **3**: 760-775 [PMID: 23888249 DOI: 10.3390/jfb3040760]

41 **Basu S**, Hertsenberg AJ, Funderburgh ML, Burrow MK, Mann MM, Du Y, Lathrop KL, Syed-Picard FN, Adams SM, Birk DE, Funderburgh JL. Human limbal biopsy-derived stromal stem cells prevent corneal scarring. *Sci Transl Med* 2014; **6**: 266ra172 [PMID: 25504883 DOI: 10.1126/scitranslmed.3009644]

42 **Pastrana E**, Silva-Vargas V, Doetsch F. Eyes wide open: a critical review of sphere-formation as an assay for stem cells. *Cell Stem Cell* 2011; **8**: 486-498 [PMID: 21549325 DOI: 10.1016/j.stem.2011.04.007]

43 **Rabinowitz YS**, Yang H, Rasheed K, Li X. Longitudinal Analysis of the Fellow Eyes in Unilateral Keratoconus. *Invest Ophthalmol Vis Sci* 2003; **44**: 1311-1315

44 **Mills RA**, Coster DJ, Williams KA. Effect of immunosuppression on outcome measures in a model of rat limbal transplantation. *Invest Ophthalmol Vis Sci* 2002; **43**: 647-655 [PMID: 11867579]

45 **Reinhard T**, Spelsberg H, Henke L, Kontopoulos T, Enczmann J, Wernet P, Berschick P, Sundmacher R, Böhringer D. Long-term results of allogeneic penetrating limbo-keratoplasty in total limbal stem cell deficiency. *Ophthalmology* 2004; **111**: 775-782 [PMID: 15051212 DOI: 10.1016/j.ophtha.2003.07.013]

World Journal of Stem Cells

Submit a Manuscript: https://www.f6publishing.com

World J Stem Cells 2020 January 26; 12(1): 55-69

DOI: 10.4252/wjsc.v12.i1.55

ISSN 1948-0210 (online)

ORIGINAL ARTICLE

Basic Study

Early therapeutic effect of platelet-rich fibrin combined with allogeneic bone marrow-derived stem cells on rats' critical-sized mandibular defects

Muhammad A Awadeen, Fouad A Al-Belasy, Laila E Ameen, Mohamad E Helal, Mohammed E Grawish

ORCID number: Muhammad A Awadeen (0000-0001-5413-4491); Fouad A Al-Belasy (0000-0001-9857-6873); Laila E Amin (0000-0002-2357-0810); Mohamad E Helal (0000-0002-0434-1529); Mohammed E Grawish (0000-0003-4732-8022).

Author contributions: Awadeen MA generated the figures, tables and wrote the manuscript; Al-Belasy FA, Grawish ME, Ameen LE and Helal ME provided an intellectual contribution to the content, contributed to writing of the manuscript, and made all critical revisions; all authors read, reviewed and approved the final version of the manuscript.

Institutional animal care and use committee statement: All experimental procedures were performed under a protocol approved by the Ethics Committee of the Faculty of Dentistry, Mansoura University, Egypt. The rats were cared for and housed in standard cages by the guidelines of the Faculty of Medicine, Medical Research Centre, Mansoura University, Egypt.

Conflict-of-interest statement: Authors declare no conflict of interests for this article.

Data sharing statement: The datasets supporting the conclusions of this article are included in the article.

ARRIVE guidelines statement: The authors have read the ARRIVE

Muhammad A Awadeen, Mohammed E Grawish, Department of Oral Biology, Faculty of Oral and Dental Medicine, Delta University for Science and Technology, Mansoura 11152, Egypt

Fouad A Al-Belasy, Department of Oral Surgery and Anesthesia, Faculty of Oral and Dental Medicine, Delta University for Science and Technology, Mansoura 11152, Egypt

Laila E Ameen, Mohamad E Helal, Mohammed E Grawish, Department of Oral Biology, Faculty of Dentistry, Mansoura University, Mansoura 35516, Egypt

Corresponding author: Mohammed E Grawish, BDS, MSc, PhD, Professor, Department of Oral Biology, Faculty of Dentistry, Mansoura University, Dakahlia Governorate, Mansoura 35516, Egypt. grawish2005@yahoo.com

Abstract

BACKGROUND

Critically sized bone defects represent a significant challenge to orthopaedic surgeons worldwide. These defects generally result from severe trauma or resection of a whole large tumour. Autologous bone grafts are the current gold standard for the reconstruction of such defects. However, due to increased patient morbidity and the need for a second operative site, other lines of treatment should be introduced. To find alternative unconventional therapies to manage such defects, bone tissue engineering using a combination of suitable bioactive factors, cells, and biocompatible scaffolds offers a promising new approach for bone regeneration.

AIM

To evaluate the healing capacity of platelet-rich fibrin (PRF) membranes seeded with allogeneic mesenchymal bone marrow-derived stem cells (BMSCs) on critically sized mandibular defects in a rat model.

METHODS

Sixty-three Sprague Dawley rats were subjected to bilateral bone defects of critical size in the mandibles created by a 5-mm diameter trephine bur. Rats were allocated to three equal groups of 21 rats each. Group I bone defects were irrigated with normal saline and designed as negative controls. Defects of group II were grafted with PRF membranes and served as positive controls, while defects of group III were grafted with PRF membranes seeded with allogeneic BMSCs. Seven rats from each group were killed at 1, 2 and 4 wk. The mandibles

were dissected and prepared for routine haematoxylin and eosin (HE) staining, Masson's trichrome staining and CD68 immunohistochemical staining.

RESULTS

Four weeks postoperatively, the percentage area of newly formed bone was significantly higher in group III (0.88 ± 0.02) than in groups I (0.02 ± 0.00) and II (0.60 ± 0.02). The amount of granulation tissue formation was lower in group III (0.12 ± 0.02) than in groups I (0.20 ± 0.02) and II (0.40 ± 0.02). The number of inflammatory cells was lower in group III (0.29 ± 0.03) than in groups I (4.82 ± 0.08) and II (3.09 ± 0.07).

CONCLUSION

Bone regenerative quality of critically sized mandibular bone defects in rats was better promoted by PRF membranes seeded with BMSCs than with PRF membranes alone.

Key words: Platelet-rich fibrin membrane; Bone marrow-derived stem cells; Critical-sized mandibular defects; Rats; Histological and immunohistochemical staining

Core tip: Our findings are derived from a rat model for treating critical-sized mandibular bone defects. Defects were grafted with platelet-rich fibrin (PRF) membranes seeded with allogeneic bone marrow-derived stem cells (BMSCs). Our findings confirm the *in vivo* anti-inflammatory effects of allogenic BMSCs. In addition, BMSCs seeded on the PRF membranes exhibited beneficial syngeneic effects in promoting and accelerating the healing of critically sized mandibular defects. Routine and specific histological and immunohistochemical staining demonstrated for the first time that experimentally treated critically sized mandibular defects with PRF membrane and BMSC combined therapy increased the amount and the rate of the newly formed bone and decreased the amount of granulation tissue with a reduction in the number of inflammatory cell infiltrates.

Citation: Awadeen MA, Al-Belasy FA, Ameen LE, Helal ME, Grawish ME. Early therapeutic effect of platelet-rich fibrin combined with allogeneic bone marrow-derived stem cells on rats' critical-sized mandibular defects. *World J Stem Cells* 2020; 12(1): 55-69
URL: https://www.wjgnet.com/1948-0210/full/v12/i1/55.htm
DOI: https://dx.doi.org/10.4252/wjsc.v12.i1.55

guidelines, and the manuscript was prepared and revised according to the ARRIVE guidelines.

Manuscript source: Invited Manuscript.

Received: March 7, 2019
Peer-review started: March 8, 2019
First decision: April 16, 2019
Revised: May 13, 2019
Accepted: November 29, 2019
Article in press: November 29, 2019
Published online: January 26, 2020

P-Reviewer: Goebel WS, Jun VM, Miloso M, Li SC
S-Editor: Ma YJ
L-Editor: A
E-Editor: Ma YJ

INTRODUCTION

Animal models are often considered appropriate analogues to clinical conditions. Such models have been appropriately used to check the reliability of a particular hypothesis to recognize the pathogenesis of new toxicity before clinical settings[1]. Rodents share many features with humans, and they are suitable for answering many research questions. They have biological, genetic, and behavioural characteristics closely resembling those of humans, and many symptoms of human disorders can be replicated in rats[2]. One of the major surgical challenges in regenerative medicine is the reconstruction of critically sized bone defects in the craniofacial complex. The treatment of such defects remains debated, particularly defects that are of a critical size caused by removal of a tumour, trauma or congenital malformations and abnormalities. Current treatments depend on the use of autologous bone grafts as a gold standard and consequently have many disadvantages, such as an insufficient amount of bone for prosthetic rehabilitation and donor site morbidity[3].

The advent of a new era of tissue engineering-based strategies has led to promising techniques for the reconstruction of cranio-maxillofacial defects that are of critical size[4]. Significant progress has been made in craniofacial surgery with the usage of tissue engineering-based therapies that employ biomaterial scaffolds covered with adult osteogenic cells and/or osteoinductive factors[5]. Adult mesenchymal stem cells and biomaterials/scaffold-based bone substitutes are a favourable alternative to natural bone grafts[6]. Tissue-engineered bone alternates are fundamentally intended to reproduce bone autograft performance with the least injury and morbidity to the

patient while achieving the mechanical properties that are mandatory for bone regeneration and reconstruction. Several techniques have been developed that integrate combinations of osteoinductive signals, osteogenic cells and osteoconductive scaffolds or matrices[7].

Platelet concentrates are used to enhance osseous tissue healing in oral and craniofacial surgery[8]. They can stimulate bone regeneration with minimum inflammatory response and unwanted complications. The usage of these concentrates was derived from the high content of growth factors that can be liberated from platelets at the time of tissue damage; these growth factors are essential for hard and soft tissue repair mechanisms. Among the advantages of platelet concentrates, their safety as an autologous source helps enhance early stability of grafts[9]. In recent years, platelet-rich fibrin (PRF) has gained wide attention for its utilization as a biocompatible regenerative material not only in the dental field but also in medical fields[10].

Mesenchymal stem cells (MSCs) are multipotent, can be isolated from multiple distinctive tissues, and have the ability to differentiate into several cell types of cells, such as osteoblasts and pre-osteogenic chondroblasts[11]. The use of MSCs in tissue engineering is highly recommended because they have a high osteogenic differentiation capacity[12]. The integration of MSCs into bone tissue-engineered biomaterials is a widely studied technique for enhancing bone osteointegration and formation in the repair of bony defects. These cells can migrate to sites of injury, they are capable of suppressing the local immune response, and they are available in large quantities from the patients themselves[13]. Cumulative evidence has proven that bone marrow-derived stem cells (BMSCs) play an efficient role in bone regeneration in a variety of orthopaedic diseases; however, some restrictions still hinder their use in clinical settings. A major obstacle lies in their very low yield, and accordingly, an adequate number of MSCs for successful bone regeneration may be transplanted into defect sites[14].

Previous studies have reported the use of combined therapy of MSCs with PRF concentrate for the treatment of articular cartilage defects[15-18], mandibular reconstruction and regeneration[19,20], alveolar bone defects and clefts[21,22], tibial bone defects[23] and bone remodelling[24]. However, none of these studies performed experiments on a critically sized defect model. We hypothesized that combination therapy of PRF membranes and BMSCs may enable the reconstruction of critically sized mandibular defects in rats. The main purpose of the present study was to assess the possible regenerative capacity of PRF membranes with/without allogeneic BMSCs on critically sized defects in rat mandibles. Our null hypothesis was that PRF membranes, in combination with BMSCs, have no effect on the regenerative capacity of critically sized mandibular defects in rats. The ARRIVE Checklist (https://www.nc3rs.org.uk/arrive-guidelines) and the guidelines of the Animal Research: Reporting *In Vivo* Experiments were followed in performing this study.

MATERIALS AND METHODS

Animal selection and ethical approval

G* Power 3.1.9.2 software was used to statistically compute the sample size of this animal study. An *a priori* analysis was performed to compute the required sample size, and ANOVA was then performed to test for fixed effects, special effects, main effects, and interactions. The input parameters were an α error probability of 0.05, an effect size f of 0.40, a power of 0.95 and 3 degrees of freedom, as the predictor variables included 3 examination time points and 3 groups. The estimated sample size was 121. Five additional rats were included to allow division of the total number by 3 without a remainder, and consequently, the sample size was 126 (42 rats/group). The mandibular surgical defects were performed bilaterally (21 rats/group); thus, the sample size was 63 rats.

Sixty-three adult, male, pathogen-free Sprague Dawley rats were selected, housed and cared for in standard cages in accordance with the guiding principles of the Faculty of Medicine, Medical Research Centre, Mansoura University, Egypt. The rats were housed at a temperature under 22 °C and at 65%-70% relative humidity. All rats were maintained in a 12-h light and 12-h dark cycle and were fed a regular diet with water. The Research Randomizer software package (https://www.randomizer.org/) was used to randomly assign the rats into 3 equal groups (I, II, and III) of 21 animals each. All experimental steps and protocols were approved by the Ethical Committee of Research Center at Faculty of Dentistry, Mansoura University, Egypt.

PRF preparation technique

Blood samples were collected from the orbital sinus of ten rats under anaesthesia (xylazine + ketamine) through a punctured tube devoid of anticoagulant into 10-mL test tubes, which were rapidly centrifuged (Centrifuge Z 206 A HERMLE Labortechnik GmbH, Germany) for 10 min at 3000 rpm. After centrifugation, three layers formed in the test tube: red blood cells collected at the bottom, a PRF clot formed in the middle and cellular plasma collected at the surface. The PRF clot was easily separated from the tube and then squeezed between two hard objects to transform it into a thin PRF membrane (Figure 1A).

Source of allogeneic BMSCs

Second passage rat allogeneic BMSCs were purchased and obtained through a cryopreserved sub-cultured primary cell line of 10^6 cell density from Nile Center for Experimental Researches, Mansoura, Egypt (Figure 1B). After six months of cryopreservation, cells were thawed under a proper aseptic technique, and work was performed in a laminar flow hood. The lower half of the cryovial containing the frozen cells was rapidly thawed for 60 s in a 37 °C water bath. The cryovial was decontaminated by spraying and wiping the exterior of the vial with 70% ethanol. In a biosafety hood, cells were gently resuspended and transferred to a sterile 15-mL conical tube containing 5 mL DMEM with 10% foetal calf serum (FCS), pre-warmed at 37 °C, using a sterile transfer pipette. The BMSCs were centrifuged for 3 min at 200× g, and the supernatant was aspirated without disturbing the cell pellet. The cell pellet was resuspended in fresh, pre-warmed DMEM and transferred to a T25 flask. The flask was gently rocked and incubated in a humidified incubator specified for tissue culture at 37 °C with 5% CO_2.

Assessment of cell viability

The cell viability was determined by adding 10 μL trypan blue to 10 μL cell suspensions and mixing. Finally, 10 μL of the mixture was placed in a haemocytometer chamber (Cambridge Instruments, Buffalo, NY, United States), and the cell number was determined.

Characterization

Four million BMSCs were trypsinized and harvested. They were washed and then resuspended in phosphate-buffered saline (PBS) enriched with 3% foetal bovine serum that contained a saturating concentration (1:100) of the six subsequent fluorescein isothiocyanate-conjugated monoclonal antibodies anti-CD14, anti-CD19, anti-CD44, anti-CD45, anti-CD105 and anti-CD90 and one phycoerythrin-conjugated monoclonal antibody, anti-CD34. The cells were incubated against isotype controls in the dark for 30 min at room temperature. Normal rat IgG peridinin chlorophyll protein complex was used as an isotype control to differentiate nonspecific background signals from specific antibody signals. Then, the cells were washed using 2 mL PBS and centrifuged for 5 min at 1500 rpm, and the resulting supernatant was discarded. The cells were suspended in 0.2 mL of 0.5% paraformaldehyde in PBS. Fluorescein activated cell sorting [(FACS) Canto, BD, United States)] was used for acquisition and analysis of CD34 and CD45, and the data were analysed with BD CellQuestTM Pro version 6.0 software (dot plot). A BD Accuri C6 flow cytometer was used for the analysis of CD14, CD19, CD44, CD105 and CD90, and the data were analysed with BD Accuri C6 program software (histogram plot). All these steps were carried out at the Genetic Department, Children's Hospital, Mansoura University.

Osteogenic differentiation assay

The *in vitro* differentiation of BMSCs toward an osteogenic lineage was induced using an alizarin red assay with an ELISA reader on the 14th day. The osteogenic differentiation potential of BMSCs was assessed using a protocol described by Saeed *et al*[25].

Seeding of BMSCs on PRF membranes

Using 48-well plates, BMSCs of passage 3 were seeded on PRF pieces at a density of 5 × 10^3 cells/well. The cells were cultured on the PRF membrane pieces in 200 μL of DMEM with 5% CO_2 at 37 °C in a humidified atmosphere for 3 d. The cultures were microscopically observed at this stage.

Surgical procedures

Critical-sized bone defects were created in accordance with the method reported by Zhang *et al*[26]. Briefly, all rats were anaesthetized by an intraperitoneal injection of 75 mg/kg body weight ketamine and 25 mg/kg body weight xylazine. The operative areas of all animals were shaved, and the skin covering these regions was scrubbed

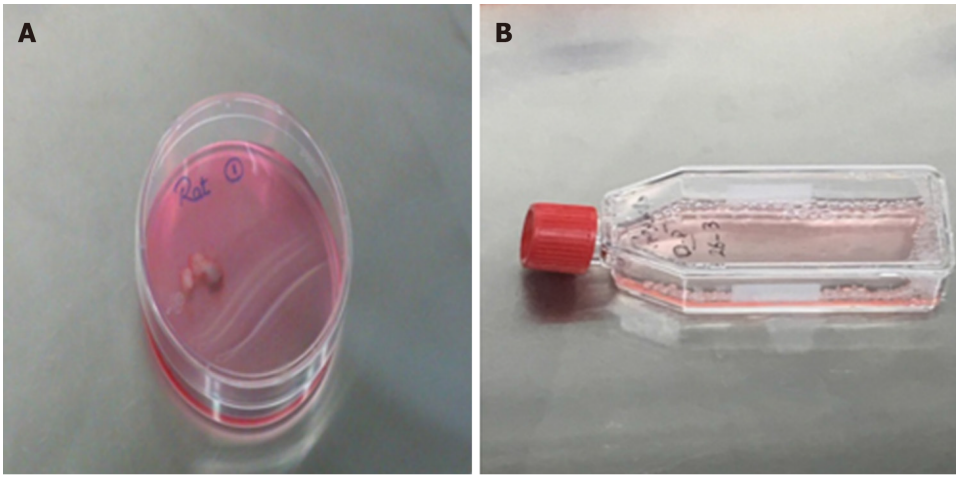

Figure 1 PRF and BMSCs in nutritional media. A: Photographs showing platelet-rich fibrin membrane in nutritional media ready for incubation; B: Photographs showing a T25 flask containing 1 × 10^6 of bone marrow-derived stem cells in nutritional media.

thoroughly with povidone-iodine (Betadine). A 1-cm incision above and parallel with the mandible was made using Bard-Parker No. 15 blade. The lower boundary of the mandible was exposed by blunt dissection. A bone defect of critical size with a depth of 2 mm was produced using a 5 mm diameter trephine bur, contiguous with the inferior border of the mandible and posterior to the incisor (Figure 2A).

Experimental design

In group I, defects were irrigated with saline solution and left empty to serve as controls. Group II defects were grafted with PRF membrane by which the incubated PRF membrane was sliced into 5 mm pieces and then carefully placed into the defects using sterilized scissors. Group III defects were grafted with PRF membrane seeded with BMSCs. The previously isolated and cultured BMSCs were seeded on PRF membrane that was sliced into 5 mm segments and placed into the defects. The surgical area was washed with normal saline, and the two edges of the skin were sutured using 3/0 silk mounted on a 3/8 half-circle needle. Seven rats from each group were euthanized at time points of 1, 2 and 4 wk.

Histological analysis

The mandibles were removed, fixed in buffered formalin for 4 h, decalcified in ethylenediaminetetraacetic acid solution and embedded in paraffin. Serial sections were cut at 4 μm thickness. Sections of specimens were processed for routine haematoxylin and eosin (HE) staining, Masson's trichrome staining (for revealing collagen fibres and newly formed bone), and CD68 immunohistochemical staining to detect the number of inflammatory cell infiltrates.

Histomorphometric analysis

Slides stained with Masson's trichrome were investigated using an Olympus microscope with a 1/2 photo adaptor. Digital images were captured by a ToupView digital camera with an objective lens for a magnification of ×4. Seven images with 300 dpi resolution from each group at each time point were digitally analysed with Fiji Image processing software (https://fiji.sc/). The parameters assessed were the total tissue area, including unmineralized bone or osteoid area (OA), and granulation tissue (GT)[27]. To count the number of inflammatory cell infiltrates, VideoTest Morphology® software (Russia) on an Intel® Core I3® based computer was used for staining quantification and area measurements of the resultant immunostained images.

Statistical analysis

Statistical Package for the Social Sciences, version 21.0 (SPSS, IBM Corp., Armonk, NY, United States) was used for statistical evaluation of the tabulated raw data. Normality of the distribution was evaluated using the Shapiro–Wilk statistical test, and homogeneity of variance was tested using Levene's test. OA, GT, and the number of inflammatory cell infiltrates were calculated as descriptive values. Two-way ANOVA was used to determine significant differences between the different groups, followed by Tukey's post hoc statistical test. Student's *t*-test was used to determine significant differences between the two groups. Mean differences were considered

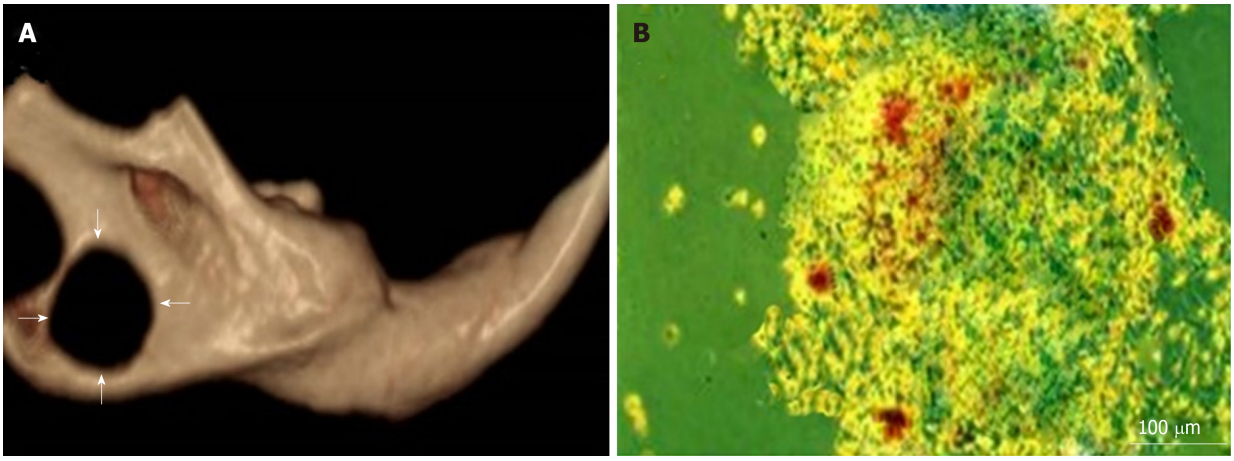

Figure 2 CBCT and inverted microscopic imaging. A: CBCT images of critical-sized defects (arrows) in rats' mandibles; B: An inverted light microscopic image of bone marrow-derived stem cells differentiated in osteogenic medium with mineralized deposits identified by alizarin red staining on the 7th day.

statistically significant at $P < 0.05$.

RESULTS

Clinical results

Rats generally recovered quickly within 2 d after surgery and returned to their routine activities, such as grooming, eating and drinking. The rats showed normal chewing efficiency without any weight loss or postoperative complications at the three experimental time points.

Osteodifferentiation results

Mineralized nodules were formed and stained with alizarin red within all wells (Figure 2B).

Flow cytometric analysis for characterization of BMSCs

The results of flow cytometric analysis revealed that surface markers of the BMSCs were strongly negative for CD34 (6.8%), CD45 (6.8%) and CD19 (2.7%) and moderately negative for CD14 (48.4%), while their surface markers were positive for CD44 (59.1%), CD105 (61.4%) and CD90 (74%) (Figure 3), confirming the immunophenotypic profile of the BMSCs and the adequate collection and isolation of these cells from bone marrow samples.

HE staining results

One week postoperatively, group I empty bone defects that were irrigated only with normal saline showed loose connective tissue containing many inflammatory cells and debris of bone spicules. At 2 wk postoperatively, fibroblast-like cells were increased in number, and the connective tissue became more organized concomitant with a decrease in the number of inflammatory cells. Four weeks postoperatively, the majority of the area of the bone defects remained free of bone and was filled only with dense connective tissue that contained fewer cells and more collagen fibres with a very minute amount of newly formed bone limited to the borders of the defects. After the first postoperative week, the bone defects of group II were filled with connective tissue of high vascularity consisting of proliferating fibroblasts, newly formed capillaries and a residual of inflammatory cells. In addition, thin layers of osteoid were formed at the edges of the defects. At the second postoperative week, newly formed thin projections of interconnected trabecular bone were formed and extended from the lateral walls to the central regions of the defects. The GT at the edges of the defects was markedly decreased. At the fourth postoperative week, the defects showed thin osteoid bone trabeculae oriented perpendicular to the old bone and radiated to the centre of the defects with wide bone marrow spaces. In group III, the bone defects after the first postoperative week showed newly formed thin bone trabeculae lined by osteoblasts at the borders of the defects and osteoid tissue formation intermingled with GT with inflammatory cell infiltration in the central area. At 2 wk postoperatively, there was an increased number of more organized bone trabeculae with narrow bone marrow spaces. At 4 wk postoperatively, the borders of

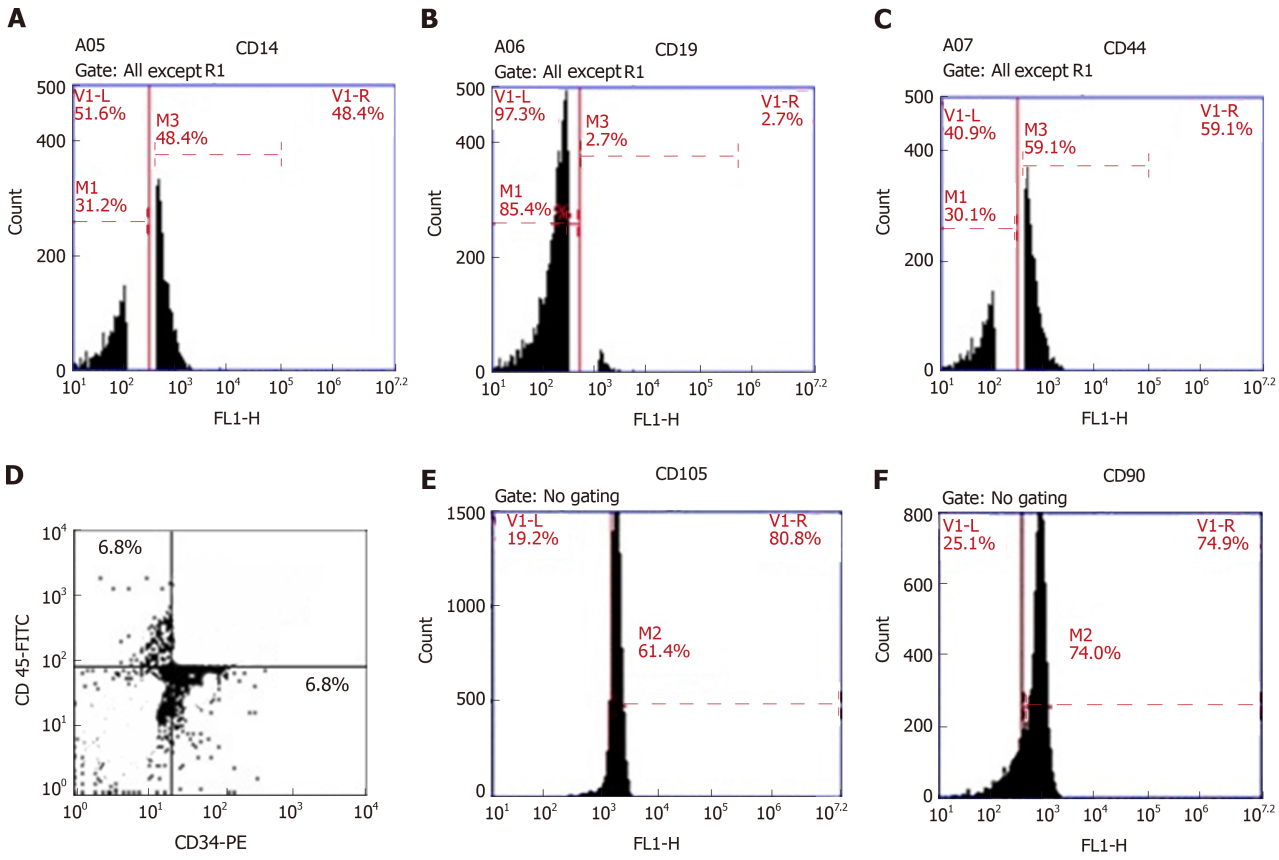

Figure 3 Plots of the flow cytometric analysis of bone marrow-derived stem cells. A: anti-CD14; B: anti-CD19; C: anti-CD44; D: anti-CD34 (FL1-H) and anti-CD45 (FL2-H); E: anti-CD105; F: anti-CD90. A, B, C, E, and F are histograms of the relative fluorescence height (FL1-H) of surface markers against cell count, while D is a dot plot of the relative fluorescence height of the surface marker CD34-PE (FL1-H) against the relative fluorescence height of the surface marker CD45-FITC (FL2-H).

the bone defects became indistinct and were difficult to differentiate from the original surrounding bone (Figure 4).

Masson's trichrome staining results

With Masson's trichrome staining, the cytoplasm and osteoids are coloured red, collagen and mineralized bone are coloured blue, and nuclei are stained black to dark brown. Four weeks postoperatively, the group I bone defects showed a small amount of loose irregular connective tissue without new bone formation throughout the whole defect (Figure 5A-C). Engrafting the defects with PRF membranes in the defects of group II encouraged the formation of bony projections that enlarged to form thin bone tissue strips in the central area of the bony defect. These centrally located bony islands were enclosed by dense connective tissue of blue colour. The bone defects revealed intimate integration of newly formed osteoid tissue with the old mature lamellar bone, characterized by more red-stained newly formed osteoid tissue and deep blue-stained mineralized areas (Figure 5D-F). A marked increase in the amount of new bone formation was observed after the fourth postoperative week in group III, which was treated with both PRF membrane and BMSCs. The development of high-quality lamellar mature bone was clearly observed at 4 wk postoperatively, and the defect was ultimately occupied with bone (Figure 5G-I).

Two-way ANOVA of the mean values of OA (Figure 6) and the amount of GT (Figure 6) revealed significant differences between different time points ($P < 0.05$) and different groups ($P < 0.05$) and a significant interaction of time and group ($P < 0.05$). After weeks 1, 2, and 4, group III exhibited the highest mean values of OA (0.18 ± 0.04, 0.40 ± 0.02 and 0.88 ± 0.02, respectively), whereas group I exhibited the lowest mean values at the same time points (0.01 ± 0.00, 0.02 ± 0.00 and 0.02 ± 0.00, respectively). The mean values of OA in group II after weeks 1, 2, and 4 were 0.10 ± 0.02, 0.22 ± 0.04 and 0.60 ± 0.02, respectively (Table 1). After weeks 1, 2 and 4, the mean values of the amount of GT in group III were 0.88 ± 0.02, 0.60 ± 0.03 and 0.12 ± 0.02, respectively, whereas mean values of GT in group I after the same time points were 0.03 ± 0.00, 0.05 ± 0.00 and 0.20 ± 0.02, respectively. The mean values of GT after weeks 1, 2 and 4 in group II were 0.90 ± 0.03 and 0. 88 ± 0.03 and 0.40 ± 0.02, respectively (Table 2).

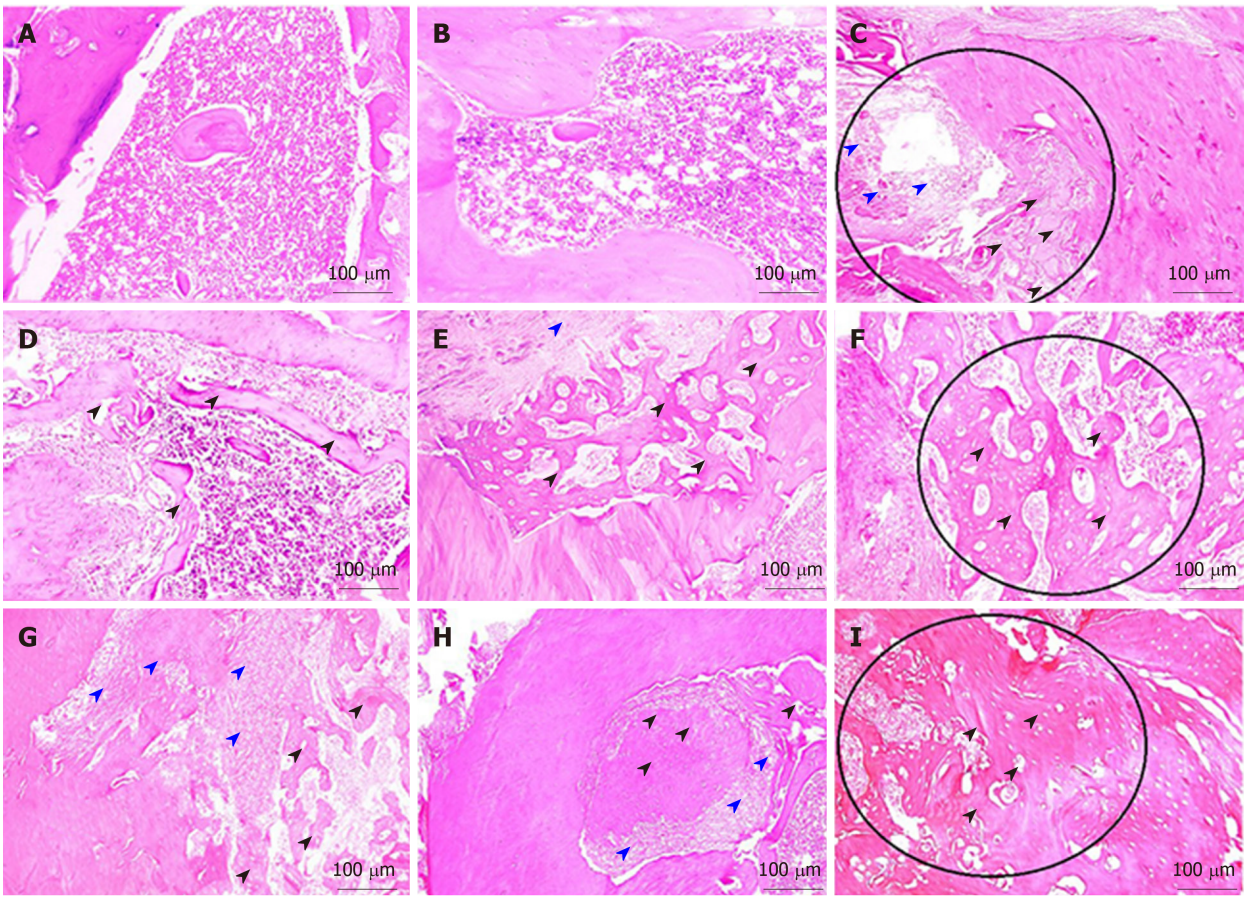

Figure 4 Hematoxylin and eosin staining. A-C: Decalcified 4-μm thick sections showing the empty bone defect area of group I at 1, 2 and 4 wk; D-F: the bone defect area of group II grafted with rich fibrin membrane at 1, 2 and 4 wk; G-I: the bone defect area of group III grafted with platelet-rich fibrin membrane and seeded with bone marrow-derived stem cells at 1, 2 and 4 wk. Black arrowheads (osteoid bone); red arrowheads (granulation tissue).

Tukey's post hoc test revealed significant differences in OA between groups I and II, groups I and III and groups II and III at each examination time point. The statistical test revealed significant differences in the amount of GT between groups I and II, groups I and III and groups II and III at 2 and 4 wk. At the 1-wk examination, no significant difference was found between groups II and III, whereas significant differences were found between groups I and II and groups I and III. Student's t-test revealed significant differences in the mean OA between 1 and 2 wk, 1 and 4 wk and 2 and 4 wk for group II and group III but no significant differences between these time points for group I. Significant differences were found in the amount of GT between 1 and 4 wk and 2 and 4 wk for groups I, II and III. No significant differences were found between 1 and 2 wk for groups I and II, while a significant difference was found for group III (Tables 1 and 2).

Immunohistochemical results

According to CD68 immunostaining, the bone defects of group I at the 4th week showed intense positive immune reactivity to CD68. The GT of group II at the 4th week showed moderate immune reactivity to the CD68 antibody. The bone defects of group III at the 4th week showed negativity for the immune reaction after the formation of large bone trabeculae. Two-way ANOVA of the number of inflammatory cell infiltrates (Figure 6) revealed a significant difference between different time points ($P < 0.05$) and groups ($P < 0.05$) and a significant interaction of time and group ($P < 0.05$). The highest mean values of CD68-immunostained inflammatory cells were found in group I, which corresponded to 29.22 ± 2.53, 15.62 ± 1.09 and 4.82 ± 0.08 at weeks 1, 2, and 4, respectively. The lowest mean values of CD68-immunostained inflammatory cells were found in group III, which were 19.04 ± 0.95, 8.13 ± 0.13, and 0.29 ±0.03 at weeks 1, 2, and 4, respectively. The mean values in group II were 23.57 ± 1.08, 9.92 ± 1.07 and 3.09 ± 0.07 at weeks 1, 2, and 4, respectively (Table 3, Figure 7). Tukey's *post hoc* test revealed significant differences in CD68-immunostained inflammatory cells between groups I and II, groups I and III and groups II and III at each examination time point. Student's *t*-test for the mean values of CD68

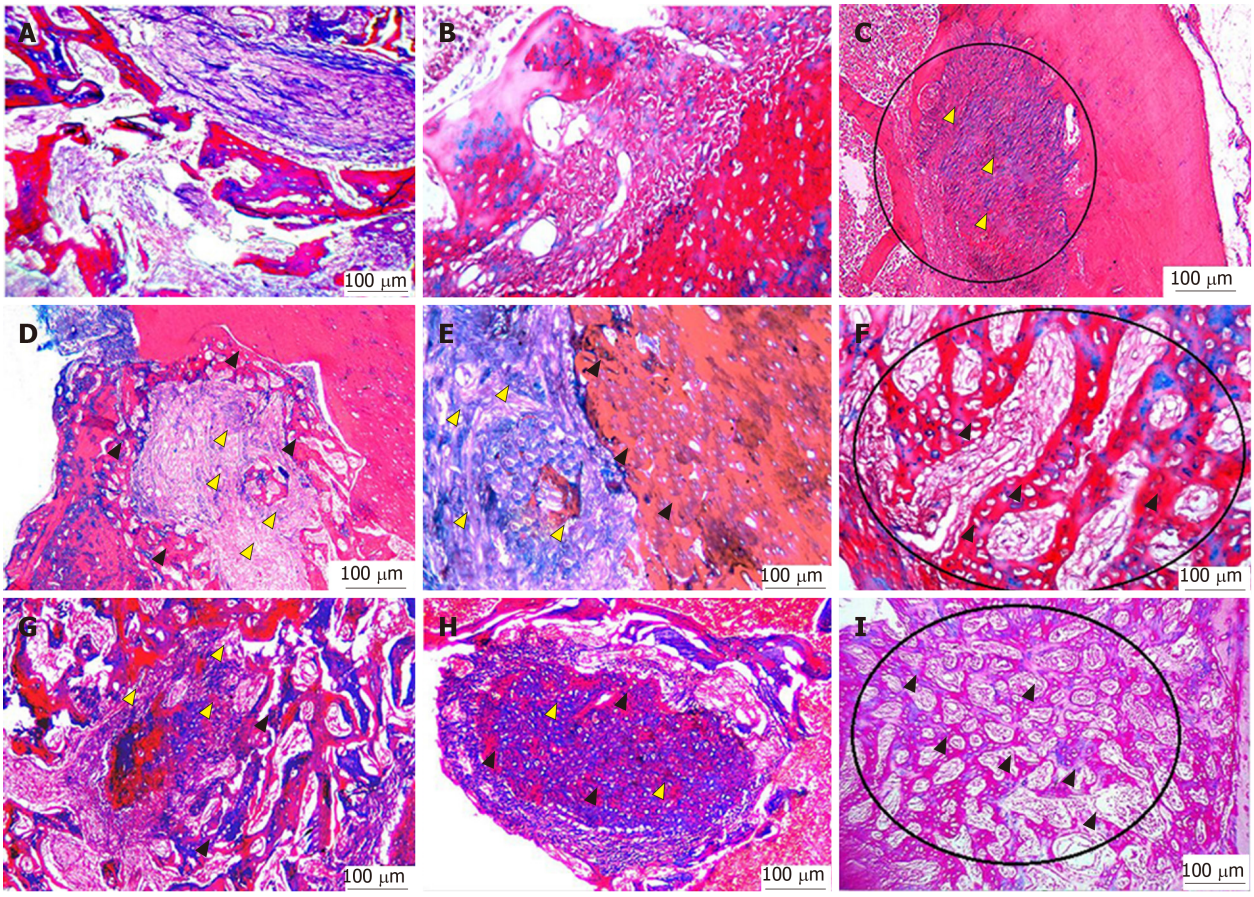

Figure 5 Masson's trichrome staining. A-C: Decalcified 4-μm thick sections showing the empty bone defect area of group I at 1, 2 and 4 wk; D-F: the bone defect area of group II grafted with rich fibrin membrane at 1, 2 and 4 wk; G-I: the bone defect area of group III grafted with platelet-rich fibrin membrane and seeded with bone marrow-derived stem cells at 1, 2 and 4 wk. Green arrowheads (osteoid bone); yellow arrowheads (granulation tissue).

immunostained inflammatory cells revealed significant differences between 1 and 2 wk, 1 and 4 wk and 2 and 4 wk for each group (Table 3).

DISCUSSION

Bone healing depends on the coordinated action of several cell types and a cascade of biological events. Bone healing is an extremely complex process and has been considered a major medical concern[28]. The current study evaluated the efficacy of BMSCs seeded on PRF membrane in comparison with PRF membrane alone for the treatment of critically sized mandibular defects in a rat model. The HE staining results revealed that the bone defects of group II grafted with PRF membranes exhibited faster GT formation and more newly formed osteoid tissue than the bone defects of group I that were irrigated with normal saline. These results are in accordance with those of He *et al*[29], who reported that PRF membranes released autologous and multiple growth factors that gradually induced a more durable and stronger effect on the differentiation and proliferation of rat osteoblasts. Usage of the PRF membrane appears to be a highly favourable approach for improving bone healing in a manageable and reasonably long-term effect.

The slow and natural polymerization that occurs during centrifugation of PRF leads to the development of a fibrin network with a consistent 3-dimensional pattern. Massive platelet activation occurs as a consequence of the absence of anticoagulant in the test tube. The structural configuration of PRF with progressive polymerization significantly increases the incorporation of circulating intrinsic cytokines into the fibrin meshes. This configuration implies an increase in the lifespan for these cytokines, as they will be released and used only at the time of initial cicatricial remodelling[30].

The present study reports that group III, which was treated with a combination of BMSCs and PRF membrane, exhibited faster healing of bone defects than group II, and thus, this combination could be used to repair alveolar bone defects without the

Table 1 Two-way ANOVA for the amount of osteoid area (%) and the significance of comparisons

Groups	mean ± SD			Student *t*-test (*P* value)			Two-way ANOVA (*P* value)
	Week 1	Week 2	Week 4	1 × 2	1 × 4	2 × 4	
I	0.01 ± 0.00	0.02 ± 0.00	0.02 ± 0.00	$P > 0.05$	$P > 0.05$	$P > 0.05$	$P < 0.05$
II	0.10 ± 0.02	0.22 ± 0.04	0.60 ± 0.02	$P < 0.05$	$P < 0.05$	$P < 0.05$	
III	0.18 ± 0.04	0.40 ± 0.02	0.88 ± 0.02	$P < 0.05$	$P < 0.05$	$P < 0.05$	
Tukey's test (*P* value)							
I × II	$P < 0.05$	$P < 0.05$	$P < 0.05$				
I × III	$P < 0.05$	$P < 0.05$	$P < 0.05$				
II ×III	$P < 0.05$	$P < 0.05$	$P < 0.05$				

need for exogenous scaffolds or additional growth factors. These results are in accordance with those of Chen *et al*[31], who reported that PRF membrane stimulates the proliferation of BMSCs and improves osteogenic capacity *in vivo* and *in vitro* more than PRF membrane alone. In addition, Gassling *et al*[32] evaluated the use of PRF membranes as scaffolds for periosteal tissue engineering and compared the *in vitro* biocompatibility and effects of both PRF membranes and collagen membranes on the proliferation of periosteal stem cells. They found that the PRF membrane is preferable to collagen as a scaffold material for human periosteal cell proliferation and is a suitable candidate for the *in vitro* cultivation of periosteal cells for engineering bony tissues.

The seeding of BMSCs on PRF membranes for topical engraftments in bone defects was performed in accordance with the report of Knapen *et al*[33], who found that the PRF membrane has no limited effect on the quantity, quality and kinetics of bone regeneration. This result could be attributed to the early engraftment of the PRF membrane at the time of surgery, when neither osteoblast precursors nor connective-vascularized tissue are yet available on site. In addition, the use of autologous PRF membranes seeded with BMSCs in alveolar bone defects is beneficial for organizing formative cells (especially osteoblasts) and promoting neovascularization with more rapid and faster apposition of bone matrix[34].

These results were supported by the increase in the amount of trabecular bone with more extended trabecular width and cortical width and the greater number of osteoblasts, osteocytes and blood vessels in the bone defects in group III than in group I and group II. These results were in accordance with Simonpieri *et al*[35], who explained that the PRF membrane can integrate with the fibrin network and facilitate cellular migration and angiogenesis.

The statistical analysis of the histomorphometric results, namely, the amount of GT and osteoid tissue formation, revealed that the use of PRF membranes seeded with BMSCs not only enhanced new bone formation but also decreased the amount of GT formation. These results are in accordance with those of Yuanzheng *et al*[22], who used a combination of PRF membranes and BMSCs to enhance osteointegration of autologous iliac bone grafts in dogs and reported that complete healing was achieved according to histologic and histomorphometric analysis of the specimens.

In the current work, the statistical results of the immunohistochemical analysis of the presence of macrophages in bony defects suggested that the bone defects of group I showed the highest degree of early macrophage presence in the first week, compared with the other two groups. The obvious presence of macrophages in group III decreased markedly by the end of the 4th week, while the other groups showed higher levels of macrophages. Our results were in accordance with those of Andrew *et al*[36], who reported that macrophages present in wound sites increase during the early differentiation of osteoblasts and decrease during bone formation. Macrophages are important angiogenic effector cells that produce a number of growth inhibitors, stimulators and proteolytic enzymes that have the capacity to modulate new vessel formation[37].

Compared with the results of a study performed by Alge *et al*[38], flow cytometric analysis of the surface markers used in the present study showed a higher profile in the negativity of CD34 and CD45 and a lower profile in the positivity of CD14, CD19, CD44, CD105, and CD90. These features may be attributed to the differences in medium composition, cell seeding density, and oxygen partial pressure, as these conditions influence cell phenotype.

Within the limitations of the current animal model and the present findings, we reject the null hypothesis and conclude that bone regenerative quality was better

Table 2 Two-way ANOVA for the amount of granulation tissue (%) and the significance of comparisons

Groups	mean ± SD			Student *t*-test (*P* value)			Two-way ANOVA (*P* value)
	Week 1	Week 2	Week 4	1 × 2	1 × 4	2 × 4	
I	0.03 ± 0.00	0.05 ± 0.00	0.20 ± 0.02	$P > 0.05$	$P < 0.05$	$P < 0.05$	$P < 0.05$
II	0.90 ± 0.03	0. 88 ± 0.03	0.40 ± 0.02	$P > 0.05$	$P < 0.05$	$P < 0.05$	
III	0.88 ± 0.02	0.60 ± 0.03	0.12 ± 0.02	$P < 0.05$	$P < 0.05$	$P < 0.05$	
Tukey's test (*P* value)							
I × II	$P < 0.05$	$P < 0.05$	$P < 0.05$				
I × III	$P < 0.05$	$P < 0.05$	$P < 0.05$				
II x× III	$P > 0.05$	$P < 0.05$	$P < 0.05$				

promoted with the use of PRF membranes seeded with BMSCs than with PRF membranes alone in critically sized bone defects in rats. However, further long-term and large-scale *in vivo* studies are necessary to verify our results in terms of determining the most suitable method for PRF membrane application and the adequate number of BMSCs for treating critical-sized mandibular defects. Moreover, more in-depth studies are needed to identify how the presence of BMSCs contributes to more effective bone regeneration in the presence of PRF and whether BMSCs improve growth factor release from the PRF membrane or excrete other factors that synergistically promote bone regeneration.

Table 3 Two-way ANOVA for the number of CD68 positively stained cells and the significance of comparisons

Groups	mean ± SD			Student *t*-test (*P* value)			Two-way ANOVA (*P* value)
	Week 1	Week 2	Week 4	1 × 2	1 × 4	2 × 4	
I	29.22 ± 2.53	15.62 ± 1.09	4.82 ± 0.08	$P < 0.05$	$P < 0.05$	$P < 0.05$	$P < 0.05$
II	23.57 ± 1.08	9.92 ± 1.07	3.09 ± 0.07	$P < 0.05$	$P < 0.05$	$P < 0.05$	
III	19.04 ± 0.95	8.13 ± 0.13	0.29 ±0.03	$P < 0.05$	$P < 0.05$	$P < 0.05$	
Tukey's test (*P* value)							
I × II	$P < 0.05$	$P < 0.05$	$P < 0.05$				
I × III	$P < 0.05$	$P < 0.05$	$P < 0.05$				
II × III	$P < 0.05$	$P < 0.05$	$P < 0.05$				

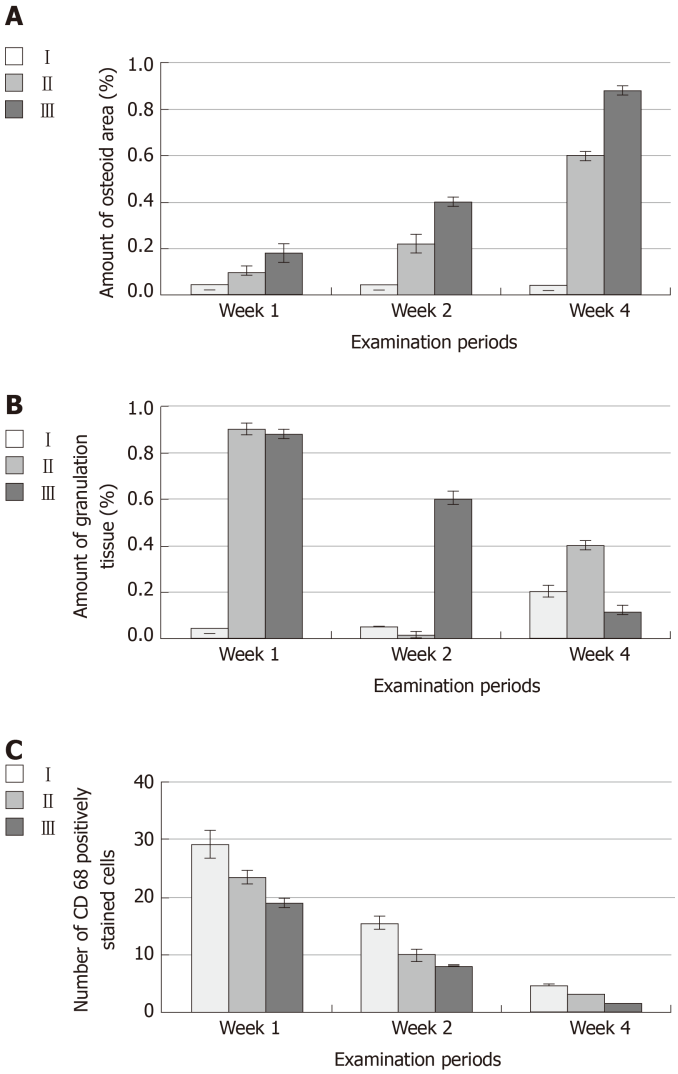

Figure 6 Mean values of osteoid area, granulation tissue and CD68 positively stained cells. A: Bar charts of the mean values and standard deviations of osteoid bone; B: Amount of granulation tissue; C: Number of CD68 positively stained cells.

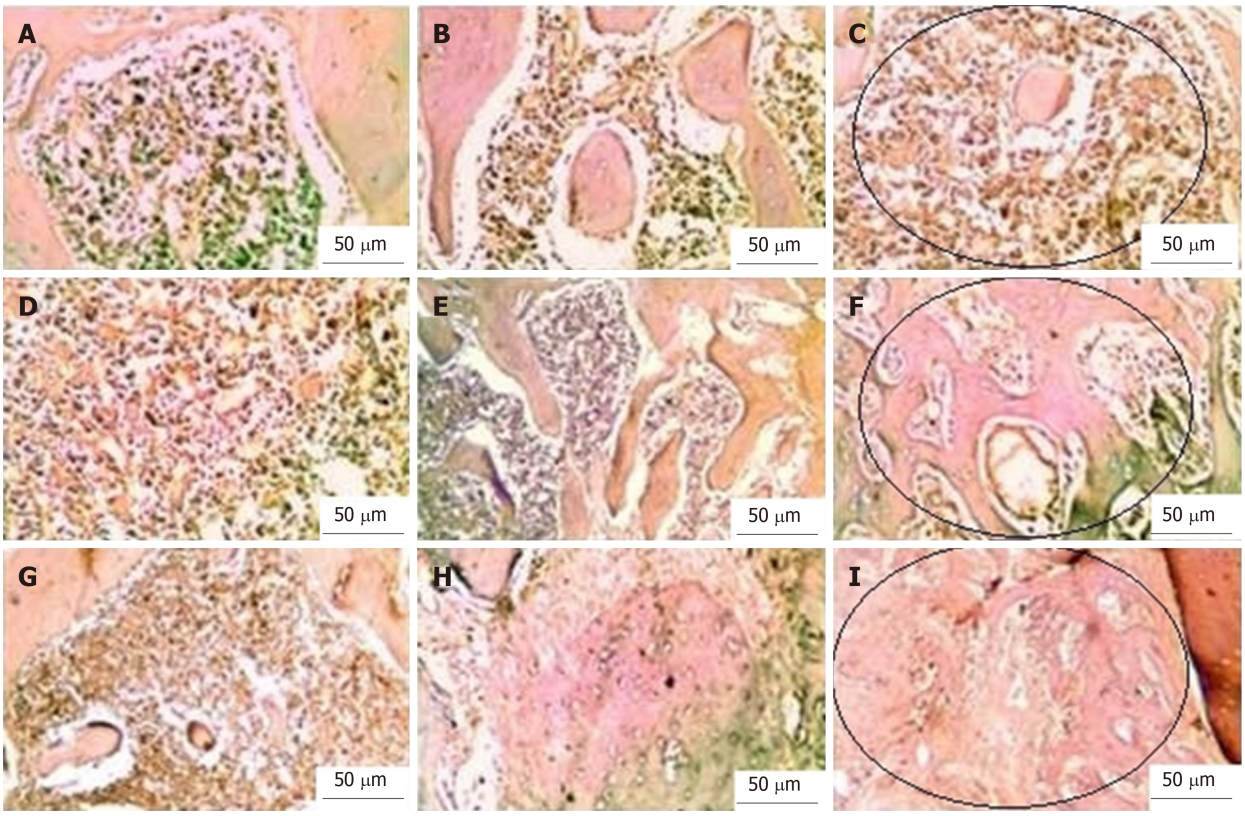

Figure 7 Photomicrograph of bone cavities of different groups at 1, 2 and 4 wk showing different immune reactivity to CD68 antibody. A-C: Group I; D-F: Group II; G-I: Group III.

ARTICLE HIGHLIGHTS

Research background

Regeneration of critical-sized bone defects remains a major clinical problem in the field of orthopaedic surgery, and therefore, novel treatment methods must be developed. Currently, the management of such defects mainly depends on the use of autologous bone grafts. However, complications such as donor site morbidity drive us to find other lines of treatments.

Research motivation

To investigate whether allogenic bone marrow-derived stem cells (BMSCs) seeded on platelet-rich fibrin (PRF) membranes have the ability to regenerate critical-sized mandibular defects in rats and, therefore, whether this combination therapy is a suitable approach for developing a new line of treatment for such bony defects.

Research objectives

The objectives of the present study were to create critical-sized mandibular defects, to seed BMSCs on PRF membranes, to fill these defects with the combination therapy, and finally, to assess the possible regenerative effect of PRF membranes with or without allogeneic BMSCs on such bony defects in rat models.

Research methods

We induced critically sized defects and treated these defects with a combined therapy, followed by performing histological and immunohistochemical analyses. The data of the histomorphometric analysis were statistically analysed.

Research results

The percentage area of newly formed bone was significantly higher in the defects treated with the combined therapy than in the defects treated with the PRF membrane alone and untreated defects. However, the amount of granulation tissue formation and the number of inflammatory cells were lower in the defects treated with the combined therapy than in the defects treated with the PRF membrane alone.

Research conclusions

The combined therapy of BMSCs and PRF membrane showed a regenerative effect in critically sized bone defects and may represent a potential therapeutic alternative for bone regeneration.

Research perspectives

Based on our results, we believe that BMSCs seeded on platelet-rich plasma could be clinically applied for treating critically sized bone defects and promoting wound regeneration in the future.

REFERENCES

1 **Morgan SJ**, Elangbam CS, Berens S, Janovitz E, Vitsky A, Zabka T, Conour L. Use of animal models of human disease for the nonclinical safety assessment of novel pharmaceuticals. *Toxicol Pathol* 2013; **41**: 508-518 [PMID: 22968286 DOI: 10.1177/0192623312457273]

2 **Vandamme TF**. Use of rodents as models of human diseases. *J Pharm Bioallied Sci* 2014; **6**: 2-9 [PMID: 24459397 DOI: 10.4103/0975-7406.124301]

3 **Shah SR**, Young S, Goldman JL, Jansen JA, Wong ME, Mikos AG. A composite critical-size rabbit mandibular defect for evaluation of craniofacial tissue regeneration. *Nat Protoc* 2016; **11**: 1989-2009 [PMID: 27658014 DOI: 10.1038/nprot.2016.122]

4 **Petrovic V**, Zivkovic P, Petrovic D, Stefanovic V. Craniofacial bone tissue engineering. *Oral Surg Oral Med Oral Pathol Oral Radiol* 2012; **114**: e1-e9 [PMID: 22862985 DOI: 10.1016/j.oooo.2012.02.030]

5 **Khaled EG**, Saleh M, Hindocha S, Griffin M, Khan WS. Tissue engineering for bone production- stem cells, gene therapy, and scaffolds. *Open Orthop J* 2011; **5** Suppl 2: 289-295 [PMID: 21886695 DOI: 10.2174/1874325001105010289]

6 **Wang X**, Xing H, Zhang G, Wu X, Zou X, Feng L, Wang D, Li M, Zhao J, Du J, Lv Y, E L, Liu H. Restoration of a Critical Mandibular Bone Defect Using Human Alveolar Bone-Derived Stem Cells and Porous Nano-HA/Collagen/PLA Scaffold. *Stem Cells Int* 2016; **2016**: 8741641 [PMID: 27118977 DOI: 10.1155/2016/8741641]

7 **Lee SH**, Shin H. Matrices and scaffolds for delivery of bioactive molecules in bone and cartilage tissue engineering. *Adv Drug Deliv Rev* 2007; **59**: 339-359 [PMID: 17499384 DOI: 10.1016/j.addr.2007.03.016]

8 **Daif ET**. Effect of autologous platelet-rich plasma on bone regeneration in mandibular fractures. *Dent Traumatol* 2013; **29**: 399-403 [PMID: 23164343 DOI: 10.1111/edt.12021]

9 **Lee HR**, Park KM, Joung YK, Park KD, Do SH. Platelet-rich plasma loaded hydrogel scaffold enhances chondrogenic differentiation and maturation with up-regulation of CB1 and CB2. *J Control Release* 2012; **159**: 332-337 [PMID: 22366523 DOI: 10.1016/j.jconrel.2012.02.008]

10 **Verma UP**, Yadav RK, Dixit M, Gupta A. Platelet-rich Fibrin: A Paradigm in Periodontal Therapy - A Systematic Review. *J Int Soc Prev Community Dent* 2017; **7**: 227-233 [PMID: 29026693 DOI: 10.4103/jispcd.JISPCD_429_16]

11 **Oryan A**, Kamali A, Moshiri A, Baghaban Eslaminejad M. Role of Mesenchymal Stem Cells in Bone Regenerative Medicine: What Is the Evidence? *Cells Tissues Organs* 2017; **204**: 59-83 [PMID: 28647733 DOI: 10.1159/000469704]

12 **Chen JP**, Chang YS. Preparation and characterization of composite nanofibers of polycaprolactone and nanohydroxyapatite for osteogenic differentiation of mesenchymal stem cells. *Colloids Surf B Biointerfaces* 2011; **86**: 169-175 [PMID: 21514800 DOI: 10.1016/j.colsurfb.2011.03.038]

13 **De Witte TM**, Fratila-Apachitei LE, Zadpoor AA, Peppas NA. Bone tissue engineering via growth factor delivery: from scaffolds to complex matrices. *Regen Biomater* 2018; **5**: 197-211 [PMID: 30094059 DOI: 10.1093/rb/rby013]

14 **Jin YZ**, Lee JH. Mesenchymal Stem Cell Therapy for Bone Regeneration. *Clin Orthop Surg* 2018; **10**: 271-278 [PMID: 30174801 DOI: 10.4055/cios.2018.10.3.271]

15 **Haleem AM**, Singergy AA, Sabry D, Atta HM, Rashed LA, Chu CR, El Shewy MT, Azzam A, Abdel Aziz MT. The Clinical Use of Human Culture-Expanded Autologous Bone Marrow Mesenchymal Stem Cells Transplanted on Platelet-Rich Fibrin Glue in the Treatment of Articular Cartilage Defects: A Pilot Study and Preliminary Results. *Cartilage* 2010; **1**: 253-261 [PMID: 21170288 DOI: 10.1177/1947603510366027]

16 **Kazemi D**, Shams Asenjan K, Dehdilani N, Parsa H. Canine articular cartilage regeneration using mesenchymal stem cells seeded on platelet rich fibrin: Macroscopic and histological assessments. *Bone Joint Res* 2017; **6**: 98-107 [PMID: 28235767 DOI: 10.1302/2046-3758.62.BJR-2016-0188.R1]

17 **Hsu YK**, Sheu SY, Wang CY, Chuang MH, Chung PC, Luo YS, Huang JJ, Ohashi F, Akiyoshi H, Kuo TF. The effect of adipose-derived mesenchymal stem cells and chondrocytes with platelet-rich fibrin releasates augmentation by intra-articular injection on acute osteochondral defects in a rabbit model. *Knee* 2018; **25**: 1181-1191 [PMID: 30420268 DOI: 10.1016/j.knee.2018.10.005]

18 **Xu F**, Yang Y, Yang T, Dai T, Shao X, Xu H, An R, Liu Y, Liu B. The use of allogenic adipose-derived stem cells in combination with platelet-rich fibrin for the treatment of cartilage defects in rabbit ear. *Am J Transl Res* 2018; **10**: 1900-1907 [PMID: 30018729]

19 **Liao HT**, Chen CT, Chen CH, Chen JP, Tsai JC. Combination of guided osteogenesis with autologous platelet-rich fibrin glue and mesenchymal stem cell for mandibular reconstruction. *J Trauma* 2011; **70**: 228-237 [PMID: 20664370 DOI: 10.1097/TA.0b013e3181e12b56]

20 **Maĭborodin IV**, Matveeva VA, Kolesnikov IS, Drovosekov MN, Toder MS, Shevela AI. [Regeneration of the damaged mandibular bone in rat after the injection of autologous mesenchymal stem cells of bone marrow origin adsorbed on the fibrin clot]. *Morfologiia* 2011; **140**: 79-85 [PMID: 22506358]

21 **Zhou C**, Li S, Wenqiguli N, Yu L, Zhao L, Wu P, Nijiati T. [The expressions of the Notch and Wnt signaling pathways and their significance in the repair process of alveolar bone defects in rabbits with bone marrow stem cells compounded with platelet-rich fibrin]. *Hua Xi Kou Qiang Yi Xue Za Zhi* 2016; **34**: 130-135 [PMID: 27443002]

22 **Yuanzheng C**, Yan G, Ting L, Yanjie F, Peng W, Nan B. Enhancement of the repair of dog alveolar cleft by an autologous iliac bone, bone marrow-derived mesenchymal stem cell, and platelet-rich fibrin mixture. *Plast Reconstr Surg* 2015; **135**: 1405-1412 [PMID: 25835246 DOI: 10.1097/PRS.0000000000001166]

23 **Rady D**, Mubarak R, Abdel Moneim RA. Healing capacity of bone marrow mesenchymal stem cells versus platelet-rich fibrin in tibial bone defects of albino rats: an *in vivo* study. *F1000Res* 2018; **7**: 1573 [PMID: 30345033 DOI: 10.12688/f1000research.15985.1]

24 **Nugraha AP**, Narmada IB, Ernawati DS, Dinaryanti A, Hendrianto E, Riawan W, Rantam FA. Bone alkaline phosphatase and osteocalcin expression of rat's Gingival mesenchymal stem cells cultured in

platelet-rich fibrin for bone remodeling (*in vitro* study). *Eur J Dent* 2018; **12**: 566-573 [PMID: 30369804 DOI: 10.4103/ejd.ejd_261_18]

25 **Saeed MA**, El-Rahman MA, Helal ME, Zaher AR, Grawish ME. Efficacy of Human Platelet Rich Fibrin Exudate vs Fetal Bovine Serum on Proliferation and Differentiation of Dental Pulp Stem Cells. *Int J Stem Cells* 2017; **10**: 38-47 [PMID: 28215057 DOI: 10.15283/ijsc16067]

26 **Zhang J**, Feng Z, Wei J, Yu Y, Luo J, Zhou J, Li Y, Zheng X, Tang W, Liu L, Long J, Li X, Jing W. Repair of Critical-Sized Mandible Defects in Aged Rat Using Hypoxia Preconditioned BMSCs with Up-regulation of Hif-1α. *Int J Biol Sci* 2018; **14**: 449-460 [PMID: 29725266 DOI: 10.7150/ijbs.24158]

27 **Egan KP**, Brennan TA, Pignolo RJ. Bone histomorphometry using free and commonly available software. *Histopathology* 2012; **61**: 1168-1173 [PMID: 22882309 DOI: 10.1111/j.1365-2559.2012.04333.x]

28 **Pountos I**, Georgouli T, Blokhuis TJ, Pape HC, Giannoudis PV. Pharmacological agents and impairment of fracture healing: what is the evidence? *Injury* 2008; **39**: 384-394 [PMID: 18316083 DOI: 10.1016/j.injury.2007.10.035]

29 **He L**, Lin Y, Hu X, Zhang Y, Wu H. A comparative study of platelet-rich fibrin (PRF) and platelet-rich plasma (PRP) on the effect of proliferation and differentiation of rat osteoblasts in vitro. *Oral Surg Oral Med Oral Pathol Oral Radiol Endod* 2009; **108**: 707-713 [PMID: 19836723 DOI: 10.1016/j.tripleo.2009.06.044]

30 **Dohan DM**, Choukroun J, Diss A, Dohan SL, Dohan AJ, Mouhyi J, Gogly B. Platelet-rich fibrin (PRF): a second-generation platelet concentrate. Part II: platelet-related biologic features. *Oral Surg Oral Med Oral Pathol Oral Radiol Endod* 2006; **101**: e45-e50 [PMID: 16504850 DOI: 10.1016/j.tripleo.2005.07.009]

31 **Chen B**, Sun HH, Wang HG, Kong H, Chen FM, Yu Q. The effects of human platelet lysate on dental pulp stem cells derived from impacted human third molars. *Biomaterials* 2012; **33**: 5023-5035 [PMID: 22516606 DOI: 10.1016/j.biomaterials.2012.03.057]

32 **Gassling V**, Douglas T, Warnke PH, Açil Y, Wiltfang J, Becker ST. Platelet-rich fibrin membranes as scaffolds for periosteal tissue engineering. *Clin Oral Implants Res* 2010; **21**: 543-549 [PMID: 20443805 DOI: 10.1111/j.1600-0501.2009.01900.x]

33 **Knapen M**, Gheldof D, Drion P, Layrolle P, Rompen E, Lambert F. Effect of leukocyte- and platelet-rich fibrin (L-PRF) on bone regeneration: a study in rabbits. *Clin Implant Dent Relat Res* 2015; **17** Suppl 1: e143-e152 [PMID: 24004245 DOI: 10.1111/cid.12146]

34 **Stübinger S**, Dard M. The rabbit as experimental model for research in implant dentistry and related tissue regeneration. *J Invest Surg* 2013; **26**: 266-282 [PMID: 23617292 DOI: 10.3109/08941939.2013.778922]

35 **Simonpieri A**, Del Corso M, Sammartino G, Dohan Ehrenfest DM. The relevance of Choukroun's platelet-rich fibrin and metronidazole during complex maxillary rehabilitations using bone allograft. Part I: a new grafting protocol. *Implant Dent* 2009; **18**: 102-111 [PMID: 19359860 DOI: 10.1097/ID.0b013e318198cf00]

36 **Andrew JG**, Andrew SM, Freemont AJ, Marsh DR. Inflammatory cells in normal human fracture healing. *Acta Orthop Scand* 1994; **65**: 462-466 [PMID: 7976298 DOI: 10.3109/17453679408995493]

37 **Polverini PJ**. Role of the macrophage in angiogenesis-dependent diseases. *EXS* 1997; **79**: 11-28 [PMID: 9002218 DOI: 10.1007/978-3-0348-9006-9_2]

38 **Alge DL**, Zhou D, Adams LL, Wyss BK, Shadday MD, Woods EJ, Gabriel Chu TM, Goebel WS. Donor-matched comparison of dental pulp stem cells and bone marrow-derived mesenchymal stem cells in a rat model. *J Tissue Eng Regen Med* 2010; **4**: 73-81 [PMID: 19842108 DOI: 10.1002/term.220]

World Journal of Stem Cells

Submit a Manuscript: https://www.f6publishing.com

World J Stem Cells 2020 January 26; 12(1): 70-86

DOI: 10.4252/wjsc.v12.i1.70

ISSN 1948-0210 (online)

ORIGINAL ARTICLE

Basic Study

Generation of induced secretome from adipose-derived stem cells specialized for disease-specific treatment: An experimental mouse model

Ok-Hee Kim, Ha-Eun Hong, Haeyeon Seo, Bong Jun Kwak, Ho Joong Choi, Kee-Hwan Kim, Joseph Ahn, Sang Chul Lee, Say-June Kim

ORCID number: Ok-Hee Kim (0000-0002-9204-2587); Ha-Eun Hong (0000-0002-4361-4809); Bong Jun Kwak (0000-0003-2409-9386); Ho Joong Choi (0000-0002-0862-098X); Kee-Hwan Kim (0000-0001-6219-6027); Joseph Ahn (0000-0001-8528-4919); Sang Chul Lee (0000-0002-8681-7059); Say-June Kim (0000-0001-5171-4837); Haeyeon Seo (0000-0003-2992-8112).

Author contributions: All authors contributed to manuscript preparation; Kim SJ designed the research and analyzed data; Kim OH wrote the paper, performed *in vitro* experiment, and analyzed data; Hong HE and Seo H performed *in vitro* experiments; Kwak BJ, Choi HJ, Kim KH, Ahn J, and Lee SC performed *in vivo* experiments and analyzed data.

Supported by National Research Foundation of Korea, No. NRF-2015R1C1A1A02036931

Institutional animal care and use committee statement: Approved by the Animal Care Committee of the Catholic University of Korea, No. CMCDJ-AP-2016-001.

Conflict-of-interest statement: The authors have declared no potential conflicts of interest.

Data sharing statement: Requests for access to data should be addressed to the corresponding author.

ARRIVE guidelines statement: The

Ok-Hee Kim, Ha-Eun Hong, Haeyeon Seo, Kee-Hwan Kim, Sang Chul Lee, Say-June Kim, Catholic Central Laboratory of Surgery, Institute of Biomedical Industry, College of Medicine, the Catholic University of Korea, Seoul 06591, South Korea

Ok-Hee Kim, Ha-Eun Hong, Haeyeon Seo, Bong Jun Kwak, Ho Joong Choi, Joseph Ahn, Say-June Kim, Department of Surgery, Division of Hepato-biliary Pancreatic Surgery, Seoul St. Mary's Hospital, College of Medicine, the Catholic University of Korea, Seoul 06591, South Korea

Kee-Hwan Kim, Department of Surgery, Uijeongbu St. Mary's Hospital, College of Medicine, the Catholic University of Korea, Seoul 11765, South Korea

Sang Chul Lee, Department of Surgery, Daejeon St. Mary's Hospital, College of Medicine, The Catholic University of Korea, Seoul 34943, South Korea

Corresponding author: Say-June Kim, MD, PhD, Professor, Department of Surgery, Division of Hepato-biliary Pancreatic Surgery, Seoul St. Mary's Hospital, College of Medicine, the Catholic University of Korea, 222, Banpo-daero, Seocho-gu, Seoul 06591, South Korea. sayjunekim@gmail.com

Abstract

BACKGROUND

Recently, the exclusive use of mesenchymal stem cell (MSC)-secreted molecules, named as the secretome, have been evaluated for overcoming the limitations of cell-based therapy while maintaining its advantages.

AIM

To improve cell-free therapy by adding disease-specificity through stimulation of MSCs using disease-causing materials.

METHODS

We collected the secretory materials (named as inducers) released from AML12 hepatocytes that had been pretreated with thioacetamide (TAA) and generated the TAA-induced secretome (TAA-isecretome) after stimulating adipose-derived stem cells with the inducers. The TAA-isecretome was intravenously administered to mice with TAA-induced hepatic failure and those with partial hepatectomy.

RESULTS

authors have read the ARRIVE guidelines, and the manuscript was prepared and revised according to the ARRIVE guidelines.

Manuscript source: Unsolicited manuscript

Received: April 12, 2019
Peer-review started: April 14, 2019
First decision: May 16, 2019
Revised: August 16, 2019
Accepted: September 26, 2019
Article in press: September 26, 2019
Published online: January 26, 2020

P-Reviewer: Akiyama Y, Sundararajan V
S-Editor: Ma YJ
L-Editor: Filipodia
E-Editor: Liu MY

TAA-isecretome infusion showed higher therapeutic potential in terms of (1) restoring disorganized hepatic tissue to normal tissue; (2) inhibiting proinflammatory cytokines (interleukin-6 and tumor necrosis factor-α); and (3) reducing abnormally elevated liver enzymes (aspartate aminotransferase and alanine aminotransferase) compared to the naïve secretome infusion in mice with TAA-induced hepatic failure. However, the TAA-isecretome showed inferior therapeutic potential for restoring hepatic function in partially hepatectomized mice. Proteomic analysis of TAA-isecretome identified that antioxidant processes were the most predominant enriched biological networks of the proteins exclusively identified in the TAA-isecretome. In addition, peroxiredoxin-1, a potent antioxidant protein, was found to be one of representative components of TAA-isecretome and played a central role in the protection of TAA-induced hepatic injury.

CONCLUSION
Appropriate stimulation of adipose-derived stem cells with TAA led to the production of a secretome enriched with proteins, especially peroxiredoxin-1, with higher antioxidant activity. Our results suggest that appropriate stimulation of MSCs with pathogenic agents can lead to the production of a secretome specialized for protecting against the pathogen. This approach is expected to open a new way of developing various specific therapeutics based on the high plasticity and responsiveness of MSCs.

Key words: Adipose-derived stem cells; Disease-specificity; Mesenchymal stem cells; Secretome; Peroxiredoxin-1; Thioacetamide; Toxic hepatic failure

Core tip: Appropriate stimulation of adipose-derived stem cells with thioacetamide (TAA) led to the production of a secretome enriched with proteins, especially peroxiredoxin-1, with higher antioxidant activity. Free radicals are principal pathogenic agents in the pathogenesis of TAA-induced hepatic injury. The TAA-induced secretome was superior to the naïve secretome in restoring hepatic function while minimizing inflammatory processes in mice with TAA-induced hepatic failure. However, it was less effective in the mice with partial hepatectomy, suggestive of disease-specificity. Our results suggest that appropriate stimulation of adipose-derived stem cells with pathogenic agents can lead to the production of a secretome specialized for protecting against the pathogen.

Citation: Kim OH, Hong HE, Seo H, Kwak BJ, Choi HJ, Kim KH, Ahn J, Lee SC, Kim SJ. Generation of induced secretome from adipose-derived stem cells specialized for disease-specific treatment: An experimental mouse model. *World J Stem Cells* 2020; 12(1): 70-86
URL: https://www.wjgnet.com/1948-0210/full/v12/i1/70.htm
DOI: https://dx.doi.org/10.4252/wjsc.v12.i1.70

INTROCUCTION

For several decades, numerous efforts have been made to harness the potential of mesenchymal stem cells (MSCs) for biotherapeutic applications. MSCs have a variety of advantages, including high availability, ease of isolation and expansion, functional plasticity, and low immunogenicity[1-3]. Although application of MSCs has shown promising preclinical and clinical outcomes, their clinical applications remain challenging, possibly because of their genetic instability during *in vitro* expansion, poor growth kinetics, early senescence, and particularly the potential for malignant transformation[4-9].

Recently, the exclusive use of MSC-secreted molecules rather than the cells alone has gained attention for overcoming the limitations of cell-based therapy while maintaining its advantages. The total set of molecules secreted or surface-shed by cells is generally referred to as the secretome. The secretome includes bioactive peptides, such as cytokines, chemokines, and growth factors[10,11]. Accumulating evidence

supports that the principal action mechanism of MSCs is secretome-mediated[10,12-14]. These soluble factors are released from MSCs either alone or in extracellular vesicles (EVs). Therefore, using these cell-free products may indeed represent an alternative to therapies based on cell transplantation.

The composition of the secretome is influenced by various external factors, including the cell source, type of culture media, culturing period, and preconditioning treatment. Therefore, one can use a secretome therapeutically either without manipulation or by manipulating MSCs to release specific secretome components. The latter includes (1) adjustments to the physicochemical environment during secretome preparations; and (2) development of genetically-engineered MSCs. We previously validated the amplified therapeutic potential of adipose-derived stem cell (ASC)-secretome by physicochemically controlling the secretome-obtaining process, such as hypoxic preconditioning[15,16] or using an endotoxin (lipopolysaccharide)[17].

Interestingly, proteomic analysis of EVs obtained from hepatocytes exposed to liver toxins revealed that they contained higher levels of vital liver-specific proteins, such as carbamoyl phosphate synthetase 1, *S*-adenosyl methionine synthetase 1, and catechol-*O*-methyltransferase[18,19]. This suggests that MSCs can be induced to generate a specialized secretome customized to a specific disease. We herein defined induced secretome (isecretome) as the secretome released from MSCs that had been stimulated by disease-causing materials to treat the specific disease. Thioacetamide (TAA) is a well-known hepatotoxin. In this study, we attempted to validate the higher therapeutic effects of the secretome induced by TAA (TAA-isecretome) compared to the naïve secretome, specifically in mice with TAA-induced hepatic failure. If the superiority of an isecretome over a naïve secretome is demonstrated, it could provide a foundation for producing a disease-specific isecretome applicable to specific diseases.

MATERIALS AND METHODS

Cell culture

The AML12 mouse hepatocyte cell line was obtained from American Type Culture Collection (ATCC; Manassas, VA, United States). AML12 cells were maintained in DMEM/F12 (Dulbecco's Modified Eagle Medium/Ham's F-12; Thermo, Carlsbad, CA, United States). The medium was supplemented with 10% FBS (fetal bovine serum; GibcoBRL, Carlsbad, CA, United States), 1% antibiotics (Thermo), 1x ITS supplement (Insulin-Transferrin-Selenium-G supplement; Invitrogen, Carlsbad, CA, United States), and 40 ng/ml dexamethasone (Sigma-Aldrich, St. Louis, MO, United States) at 37 °C. Human ASCs were kindly donated by Hurim BioCell Co. (Seoul, South Korea). ASCs were cultured in MesenPRO RS basal medium (GibcoBRL) supplemented with antibiotics (Penicillin-streptomycin; GibcoBRL) at 37 °C.

Preparation of the secretome released from ASCs

After reaching 70%–80% confluence, ASCs were refed with serum free DMEM low-glucose medium (Thermo Fisher Scientific, Waltham, MA, United States) at 37 °C under 5% CO_2. The conditioned media (CM) obtained from each set of ASCs were concentrated by 25-fold using ultrafiltration units (Amicon Ultra-PL 3; Millipore, Bedford, MA, United States) with a 3-kDa cutoff. The concentrated CM, which had been attained from TAA-untreated, TAA-treated, and pcDNA-HBx[20] transfected culturing conditions, was named as CM (or control secretome), TAA-induced CM (TAA-iCM, representing the TAA-isecretome), and HBx-induced CM (HBx-iCM), respectively.

Cell proliferation assay

Cell proliferation was evaluated with 2-(4-iodophenyl)-3-(4-nitrophenyl)-5-(2,4-disulfophenyl)-2H-tetrazolium (water soluble tetrazolium salt, WST-1) assay using EZ-Cytox Cell Proliferation Assay kit (Itsbio, Seoul, South Korea) according to the manufacturer's instruction. Absorbance was measured at 450 nm using the microplate reader (model 680; Bio-Rad, Hercules, CA, United States)[16].

Western blot analysis

AML12 cells and liver specimens obtained from mice were lysed using the EzRIPA Lysis kit (ATTO Corporation; Tokyo, Japan) and quantified by Bradford reagent (Bio-Rad). Proteins were visualized by western analysis using the following primary antibodies (1:1000 dilution) at 4 °C overnight and then with horseradish (HRP)-conjugated secondary antibodies (1:2000 dilution) for 1 h at 25 °C[16]. From Cell Signaling Technology (Beverly, MA, United States), we obtained primary antibodies against BAX (Bcl-2-like protein 4), BIM (Bcl-2-like protein 11), GPx (glutathione

peroxidase), HGF (hepatocyte growth factor), Mcl-1 (myeloid cell leukemia 1), PARP (poly ADP-ribose polymerase), PCNA (proliferating cell nuclear antigen), p-ERK (phosphorylated extracellular signal-regulated kinase), p-STAT3, SOD (superoxide dismutase), STAT3 (signal transducer and activator of transcription 3), VEGF (vascular endothelial growth factor), c-caspase-3 (cleaved caspase 3), fibronectin, F4/80, p-ERK, β-actin, and HRP-conjugated secondary antibody. Specific immune complexes were detected using the Western Blotting Plus Chemiluminescence Reagent (Millipore, Bedford, MA, United States).

Animals and study design

Eight-week-old male BALB/c mice (Damool Science, Daejeon, South Korea) were used in this study. Animal studies were carried out in compliance with the guidelines of the Institute for Laboratory Animal Research, Korea (IRB No: CMCDJ-AP-2016-001). We compared the effects of the TAA-isecretome in an *in vivo* model of TAA-induced hepatic failure. The *in vivo* model was generated by subcutaneous injection of TAA (300 mg/kg, 24 h intervals for 2 d) into experimental mice. Subsequently, control mice and TAA-treated mice were intravenously (using tail vein) infused with normal saline (n = 15), CM (n = 15), and TAA-iCM (n = 15). An *in vivo* model of 70% partial hepatectomy was performed (n = 12)[21].

Serology test and enzyme-linked immunosorbent assay

Blood samples were collected from each mouse, centrifuged for 10 min at 9500 g, and serum was collected. We measured the concentrations of markers for liver injury and kidney injury, such as aspartate transaminase, alanine transaminase, and creatine, using an IDEXX VetTest Chemistry Analyzer (IDEXX Laboratories, Inc., Westbrook, ME, United States). The concentrations of mouse IL-6 and tumor necrosis factor (TNF)-α were measured by sandwich enzyme-linked immunosorbent (ELISA) assay (Abcam, Cambridge, United Kingdom) according to the manufacturer's instructions.

Histological assessment of mouse specimens

Mouse livers and kidneys from each group were fixed in 10% buffered formalin, embedded in paraffin, and sectioned at 4 μm thickness. Tissue sections were stained with hematoxylin and eosin. The scores for the severity of liver and kidney injury were as follows: 1 (normal); 2 (mild injury); 3 (moderate injury); and 4 (severe injury). Three liver sections were examined per mouse, and three randomly selected high-power fields (40x) were analyzed for each liver section. The mean score for each animal was determined by summing all scores.

Immunohistochemistry staining

For immunohistochemical analysis, formalin-fixed, paraffin-embedded tissue sections were deparaffinized, rehydrated in an ethanol series, and subjected to epitope retrieval using standard procedures. Antibodies against CD68, PECAM (platelet endothelial cell adhesion molecule), and albumin (Cell Signaling Technology, Danvers, MA, United States) were used for immunochemical staining. The samples were then examined under a laser-scanning microscope (Eclipse TE300; Nikon, Tokyo, Japan) to analyze the expression of CD68, PECAM, and albumin.

Liquid chromatography–mass spectrometry/mass spectrometry on the Q-Exactive Plus mass spectrometry

All digested peptides were separated and identified using online nano liquid chromatography and analyzed by electrospray tandem mass spectrometry. For peptide identification, MS/MS spectra were searched by MASCOT (Matrix science, version 2.41)[22]. The genome sequence of the Uniprot_Human was used as the database for protein identification. To predict affected pathways among the differentially expressed genes, gene ontology (GO) enrichment analysis were performed using DAVID (http://david.abcc.ncifcrf.gov/).

Statistical analysis

Statistical analyses were performed with SPSS 11.0 software (SPSS Inc., Chicago, IL, United States) and SigmaPlot® ver. 12.0 (Systat Software Inc., Chicago, IL, United States). The data are presented as mean ± SD. Statistical comparison among groups was determined using Kruskal–Wallis test followed by Dunnett's test as the post hoc analysis. Probability values of $P < 0.05$ were regarded as statistically significant.

RESULTS

Generation of an isecretome specialized for recovering TAA-induced toxic hepatic failure

Figure 1A shows the concept of generating the TAA-isecretome for treating TAA-induced hepatic failure. We first determined the TAA concentration required to produce the TAA-isecretome. To achieve this, we investigated AML12 cell proliferation and the expression of proliferation intermediates (PCNA, p-STAT3, and STAT3) in AML12 cells at different TAA concentrations (Figure 1B and 1C). We found that 0.25 mmol/L TAA was appropriate because it moderately increased proliferation intermediates without significantly decreasing cell viability. We named the secretory materials released from TAA-treated AML12 cells as "inducer."

Next, we examined the dilution rate of inducers that maximizes the expression of the proliferation markers (PCNA, p-ERK, p-STAT, and HGF) in ASCs. Of the tested dilution rates (1:100, 1:500, and 1:1000), 1:1000 maximally induced the expression of these markers (Figure 1D).

Determination of in vitro effects of TAA-isecretome

Next, we evaluated the effects of the TAA-isecretome in an *in vitro* model of TAA-induced hepatic failure. We found that 50 mM TAA was effective for generating the *in vitro* model of TAA-induced hepatic failure based on the results of cell viability assay and western blot analyses (Figure 2A and 2B). Briefly, we named the secretome obtained from 48 h of incubation of ASCs as CM (normal conditioned media) and that used to generate the TAA-isecretome as iCM (induced conditioned media). We then treated normal and TAA-treated hepatocytes with CM and iCM, respectively. Cell viability tests showed that iCM-treated hepatocytes had the highest cell viability in both normal and TAA-treated hepatocytes (Figure 2C). Additionally, iCM-treated hepatocytes showed the highest expression of markers reflecting liver regeneration (HGF, VEGF, PCNA, and p-ERK) and lowest expression of markers reflecting apoptosis and inflammation (PARP, BIM, BAX, and F4/80) by western blot analysis (Figure 2D).

Determination of in vivo effects of isecretome and comparison of systemic markers after each treatment

We then compared the effects of the TAA-isecretome in an *in vivo* model of TAA-induced hepatic failure. The *in vivo* model was generated by subcutaneous injection of TAA (300 mg/kg, 24-h intervals for 2 d) into experimental mice. Subsequently, control mice and TAA-treated mice were intravenously (using tail vein) infused with normal saline, CM, and iCM (Figure 3A). At 48 h after treatment, the mice were euthanized, and the specimens were investigated. Serologic tests showed that among these groups, iCM administration showed the greatest effects in lowering the serum levels of aspartate transaminase, alanine transaminase, and creatinine in TAA-treated mice (Figure 3B). Similarly, ELISA showed that iCM administration decreased the serum levels of IL-6 and TNF-α in TAA-treated mice more than in the other groups (Figure 3C).

Comparison of markers reflecting liver regeneration and inflammation in liver specimens of each group

We performed western blot analysis to compare the expression of various markers reflecting liver regeneration and inflammation in the liver specimens of each group. iCM infusion caused the highest expression of PCNA, p-ERK, p-STAT, and fibronectin in both control livers and those of TAA-treated mice (Figure 4A). Additional western blot analysis showed that iCM infusion most significantly increased the expression of antioxidant enzymes (SOD, catalase, and GPx), and an antiapoptotic protein (Bcl-xL) and most significantly decreased the expression of proapoptotic proteins (c-caspase-3 and Bax) (Figure 4B and 4C).

iCM infusion most significantly decreased both liver-damage and kidney-damage scores that had been calculated based on hematoxylin and eosin staining (Figure 5A). Further, immunohistochemical staining showed that iCM infusion most significantly decreased the expression of inflammatory markers (CD68 and PECAM) and most significantly increased the expression of albumin (Figure 5B).

Validation of disease-specificity of isecretome and analysis of their contents

To validate disease-specific effectiveness of the TAA-isecretome, we intravenously infused the TAA-isecretome into another model of liver injury, a mouse model of 70% partial hepatectomy. At 2 d after infusion, the mice were euthanized, and the specimens were investigated. Western blot analysis revealed that CM infusion, rather

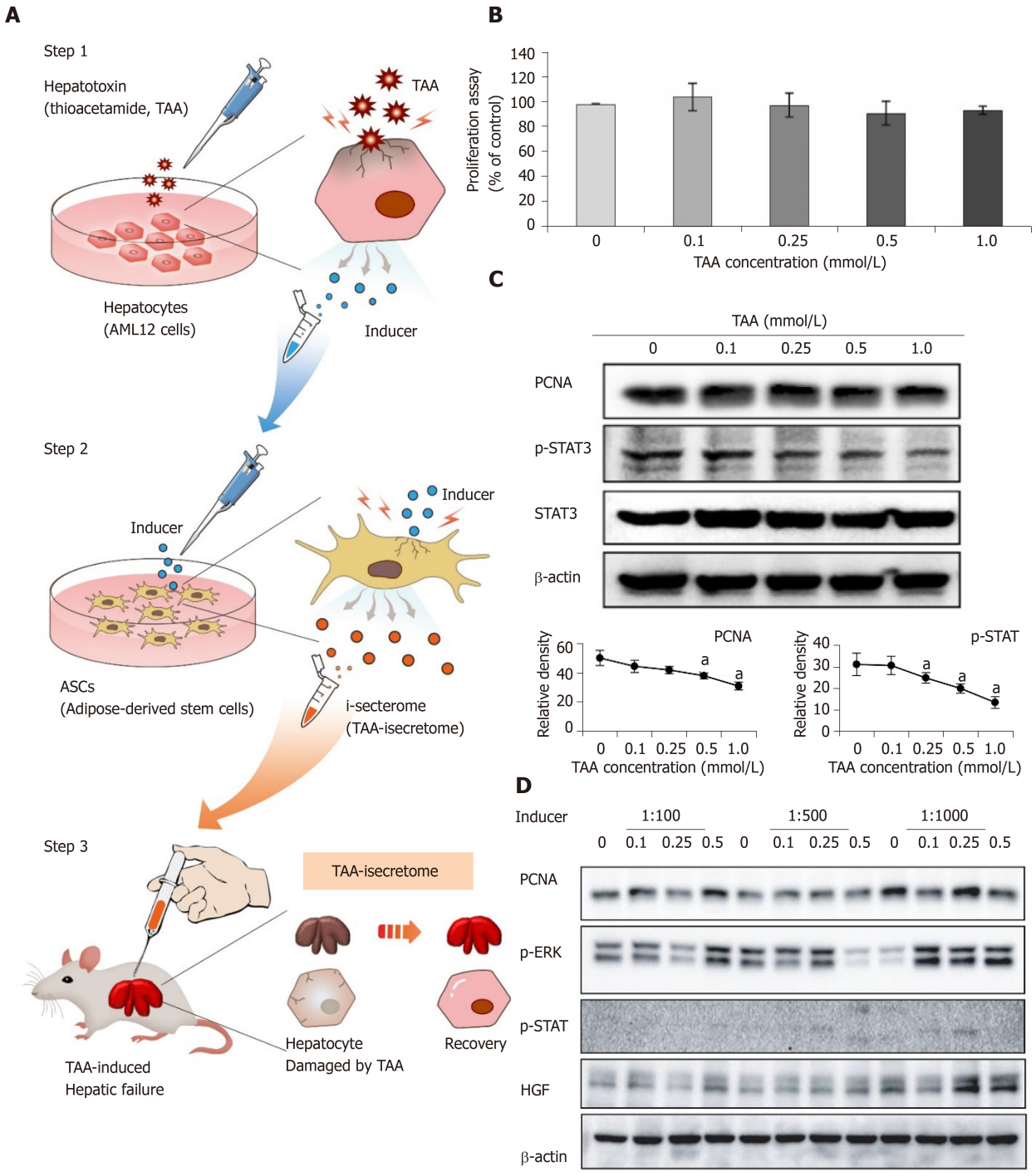

Figure 1 Generation of thioacetamide-induced secretome specialized for thioacetamide-induced toxic hepatic failure. A: Basic concept of induced secretome (isecretome) conditioned media-based therapy. Induced secretome conditioned media therapy utilizes the mesenchymal stem cell ability to generate disease-protecting materials for specific pathogens. After identifying disease-causing materials (TAA), mouse hepatocytes were treated with TAA, and then secretary proteins (inducers) were collected. The inducers were utilized to induce adipose-derived stem cells to release the TAA-induced secretome; B: AML12 cell proliferation assay according to TAA concentrations. No significant changes in the range of tested concentrations were found; C: Western blotting showing the expression of proliferation markers in AML12 cells according to TAA concentrations. We determined that 0.25 mmol/L TAA was an "inducer" of adipose-derived stem cells because it moderately increased proliferation marker expression without reducing proliferation; D: Western blotting to determine dilution rate of inducers that maximized the expression of markers related to liver regeneration in adipose-derived stem cells. A dilution rate of 1000-fold maximally induced marker expression. Values are presented as mean ± SD of three independent experiments. $^{a}P < 0.05$. PCNA: Proliferating cell nuclear antigen; p-ERK: Phosphorylated extracellular signal-regulated kinases; p-STAT3: Phosphorylated signal transducer and activator of transcription 3; TAA: Thioacetamide; ASCs: Adipose-derived stem cells.

than TAA-iCM infusion, induced higher expression of proliferation markers (p-ERK and PCNA) and an antiapoptotic marker (Mcl-1) as well as lower expression of a proapoptotic marker (Bax). (Figure 6A). Taken altogether, the TAA-isecretome had the best proliferative and anti-inflammatory effects, particularly in TAA-induced hepatic failure, indicating the potential for disease-specific treatment.

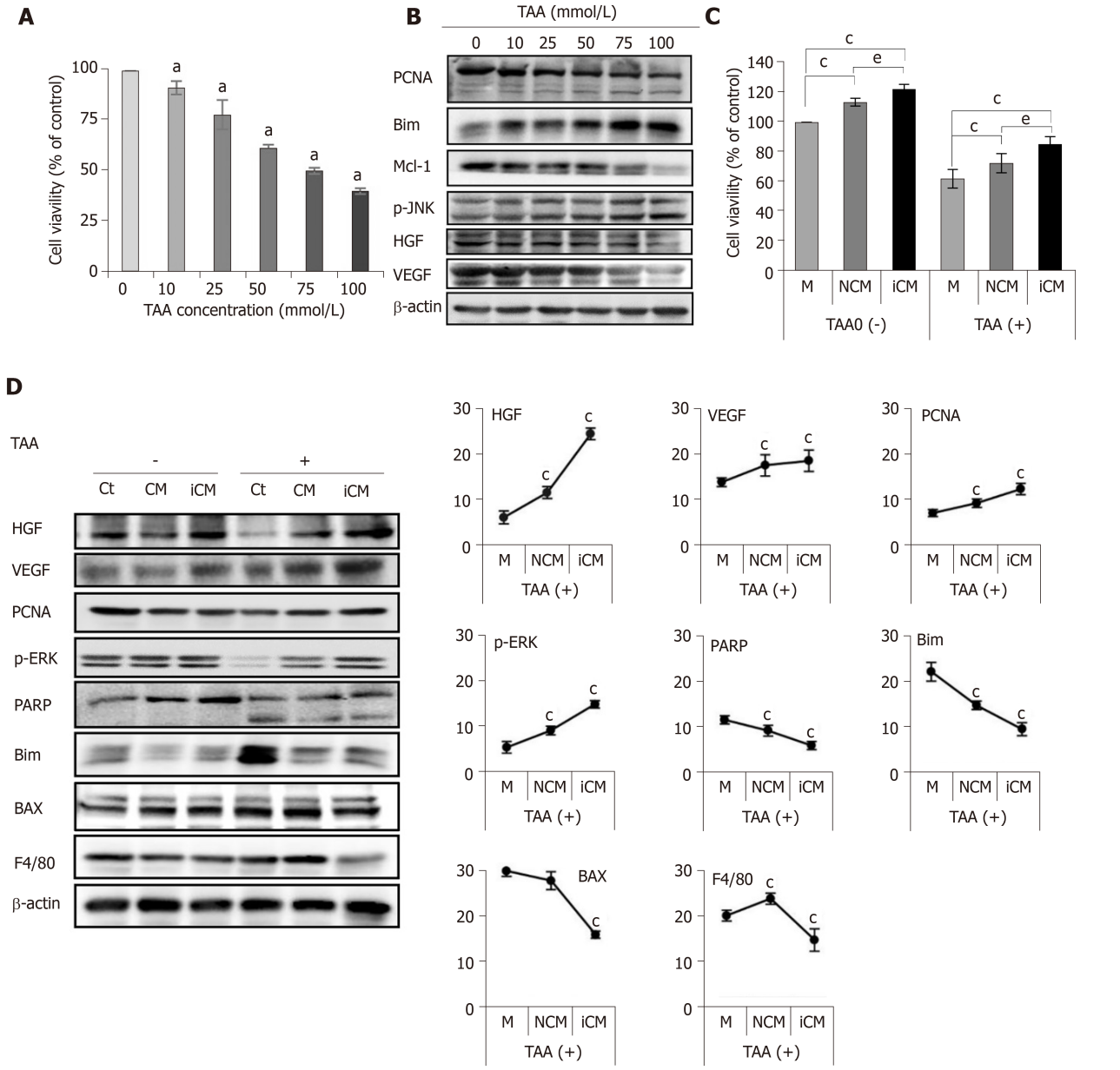

Figure 2 Determination of *in vitro* effects of thioacetamide-induced secretome. A, B: Cell proliferation test (A) and western blotting (B) of AML12 cells to determine TAA concentration for generating an *in vitro* model of TAA-induced hepatic failure. A TAA concentration of 50 mM was used for TAA-induced hepatocytes; C, D: Effects of the TAA-induced secretome on the *in vitro* model of TAA-induced hepatic failure. Cell proliferation test (C) demonstrated that induced conditioned media-treated hepatocytes showed the highest cell proliferation in both normal and TAA-treated hepatocytes. In western blot analysis (D), induced conditioned media-treated hepatocytes showed the highest expression of liver regeneration markers and lowest expression of apoptosis and inflammation markers. Values are presented as mean ± SD of three independent experiments. $^{a}P < 0.05$; $^{c}P < 0.05$ *vs* media; $^{e}P < 0.05$ between conditioned media and induced conditioned media. Bax: Bcl-2-like protein 4; BIM: Bcl-2-like protein 11; Ct: Control; iCM: Induced secretome group of which components were the TAA-induced secretome; HGF: Hepatocyte growth factor; M: Media group of which components were commercialized conditioned media; Mcl-1: Myeloid cell leukemia 1; CM: Normal conditioned media group of which components were the naïve secretome; PARP: Poly adenosine diphosphate-ribose polymerase; PCNA: Proliferating cell nuclear antigen; p-ERK: Phosphorylated extracellular signal-regulated kinases; p-JNK: Phosphorylated Jun N-terminal kinase; TAA: Thioacetamide; VEGF: Vascular endothelial growth factor.

Various sets of isecretome specialized for individual diseases can be produced using corresponding disease-causing materials. We additionally generated an HBx-isecretome (HBx-iCM) using hepatitis X antigens as inducer and compared the components of the CM, TAA-iCM, and HBx-iCM using liquid chromatography–mass spectrometry (LC/MS). Of the total proteins identified in the CM, TAA-iCM, and HBx-iCM, 32 secretory proteins were quite different according to each secretome (Figure 6B). Of them, we further investigated ten proteins that had been identified in TAA-iCM, but not in the CM. To predict affected pathways among the differentially expressed genes of the ten proteins, GO enrichment analysis were performed using DAVID (http://david.abcc.ncifcrf.gov/). GO enrichment analysis identified 19 enriched biological networks of the 10 proteins that had been exclusively identified in TAA-isecretome. Of the 19 enriched biological networks, the two most prominent

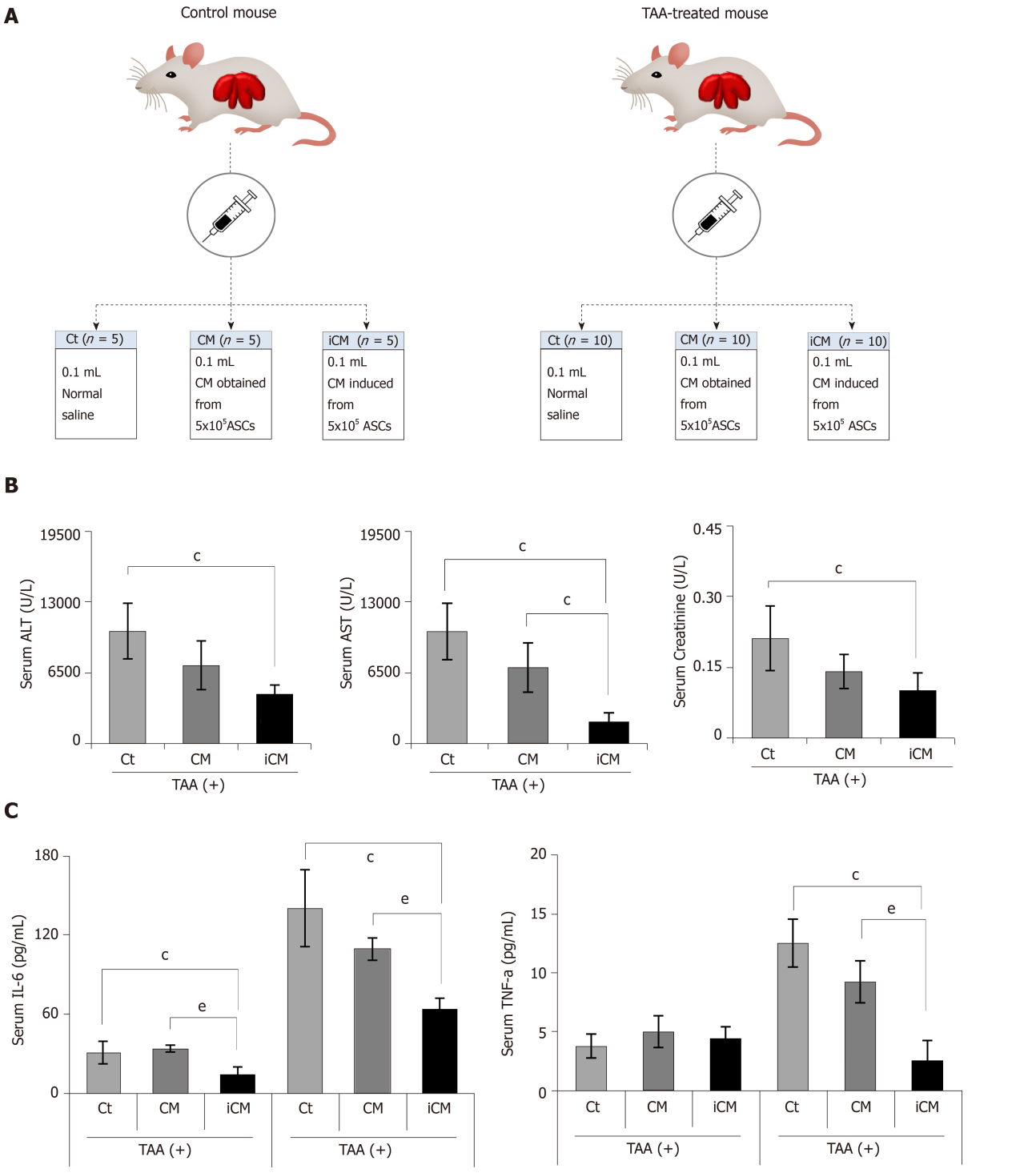

Figure 3 Animal study design and comparison of systemic effects in each group. A: Animal study design. Control mice and TAA-treated mice were intravenously (using tail vein) infused with normal saline, conditioned media (CM), and induced CM (iCM); B: Serology tests of aspartate transaminase, alanine transaminase, and creatinine in TAA-treated mice. iCM infusion decreased the serum levels of aspartate transaminase, alanine transaminase, and creatinine to the greatest extent; C: Results of ELISA showing serum levels of inflammatory markers (IL-6 and TNF-α) in each group. iCM administration lowered the serum levels of IL-6 and TNF-α the most in TAA-treated mice. Values are presented as mean ± SD of three independent experiments. $^{c}P < 0.05$ *vs* control (saline); $^{e}P < 0.05$ between CM and iCM. ALT: Alanine transaminase; AST: Aspartate transaminase; iCM: Isecretome group of which components were the TAA-induced secretome; NCM: Normal conditioned media group of which components were the naïve secretome; PECAM: Platelet endothelial cell adhesion molecule; TAA: Thioacetamide.

biological processes were the response to reactive oxygen species and cell redox homeostasis, all of which were related with antioxidant activity. Of the ten proteins, peroxiredoxin-1 (Prdx-1) attracted our attention because it is known to have potent antioxidant activity (Figure 6C).

Prdx-1 exerts its antioxidant activity by catalyzing the reduction of H_2O_2 and alkyl hydroperoxide and thus protects cells from the attack of free radicals. Prdx-1 belongs to the toll-like receptor 4 (TLR4) ligand[23]. We thus compared the expression of a

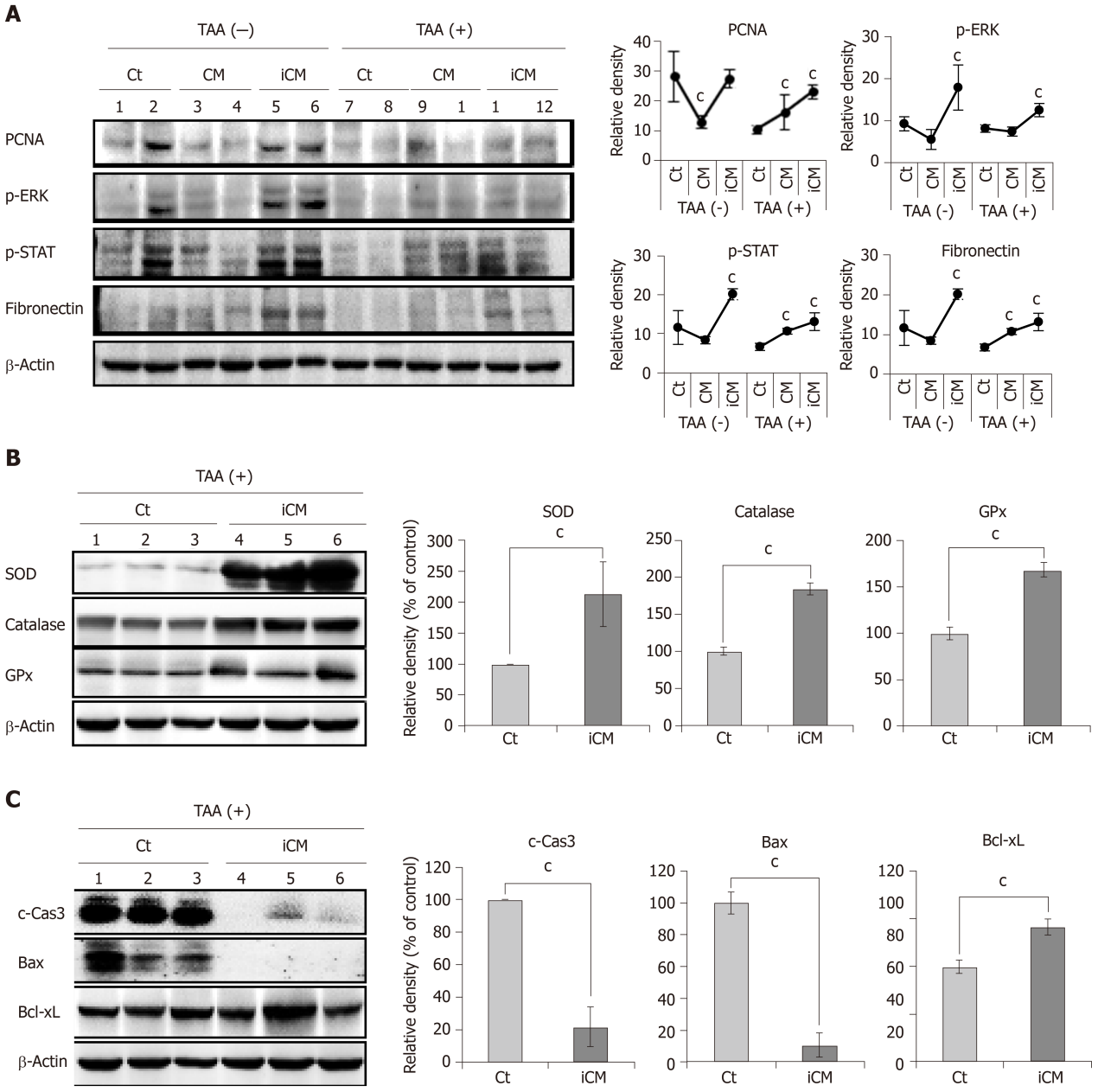

Figure 4 Molecular studies validating effects of thioacetamide-induced secretome in the mouse model of thioacetamide-induced hepatic failure. A: Pro-proliferative actions of the TAA-induced secretome in the mouse model of TAA-induced hepatic failure. Western blot analysis comparing the expression of various markers reflecting liver regeneration and inflammation in liver specimens of each group. TAA-induced conditioned media infusion induced the highest expression of PCNA, p-ERK, p-STAT, and fibronectin in both control livers and those of TAA-treated mice; B: Antioxidant actions of TAA-induced secretome in the mouse model of TAA-induced hepatic failure. Western blot analysis was performed to compare the expression of antioxidant enzymes (SOD, catalase, and GPx) in liver specimens from each group. The TAA-induced conditioned media infusion group showed the higher expression of antioxidant enzymes in the livers of TAA-treated mice compared to in the control group; C: Anti-apoptotic actions of the TAA-induced secretome in the mouse model of TAA-induced hepatic failure. TAA-iCM infusion group showed lower expression of proapoptotic proteins (c-Caspase-3 and Bax) and higher expression of an anti-apoptotic protein (Bcl-xL) in the livers of TAA-treated mice compared to in the control group. Values are presented as mean ± SD of three independent experiments. $^{c}P < 0.05$ *vs* control (saline). Bax: Bcl-2-like protein 4; Bcl-xL: B-cell lymphoma-extra large; c-Cas3: Cleaved caspase-3; GPx: Glutathione peroxidase; iCM: Induced secretome group of which components were the TAA-induced secretome; CM: Normal conditioned media group of which components were the naïve secretome; PCNA: Proliferating cell nuclear antigen; p-ERK: Phosphorylated extracellular signal-regulated kinases; p-STAT3: Phosphorylated signal transducer and activator of transcription 3; SOD: Superoxide dismutase; TAA: Thioacetamide.

hepatoproliferative marker (p-ERK) according to the expression of Prdx-1 (Figure 6D). After treatment with the TAA-iCM, AML2 hepatocytes showed the higher expression of p-ERK as well as Prdx-1 compared with AML2 cells treated with the CM ($P < 0.05$). Subsequently, we compared the efficacy of the TAA-iCM after pre-treatment of TAK242, a TLR4 inhibitor. Pre-treatment of TAK242 did not only inhibit the expression of Prdx-1 but also inhibited the expression of p-ERK, the hepato-proliferative marker. Taken altogether, our results suggest that Prdx-1 is one of the essential components in TAA-iCM and plays a central role in the protection of TAA-

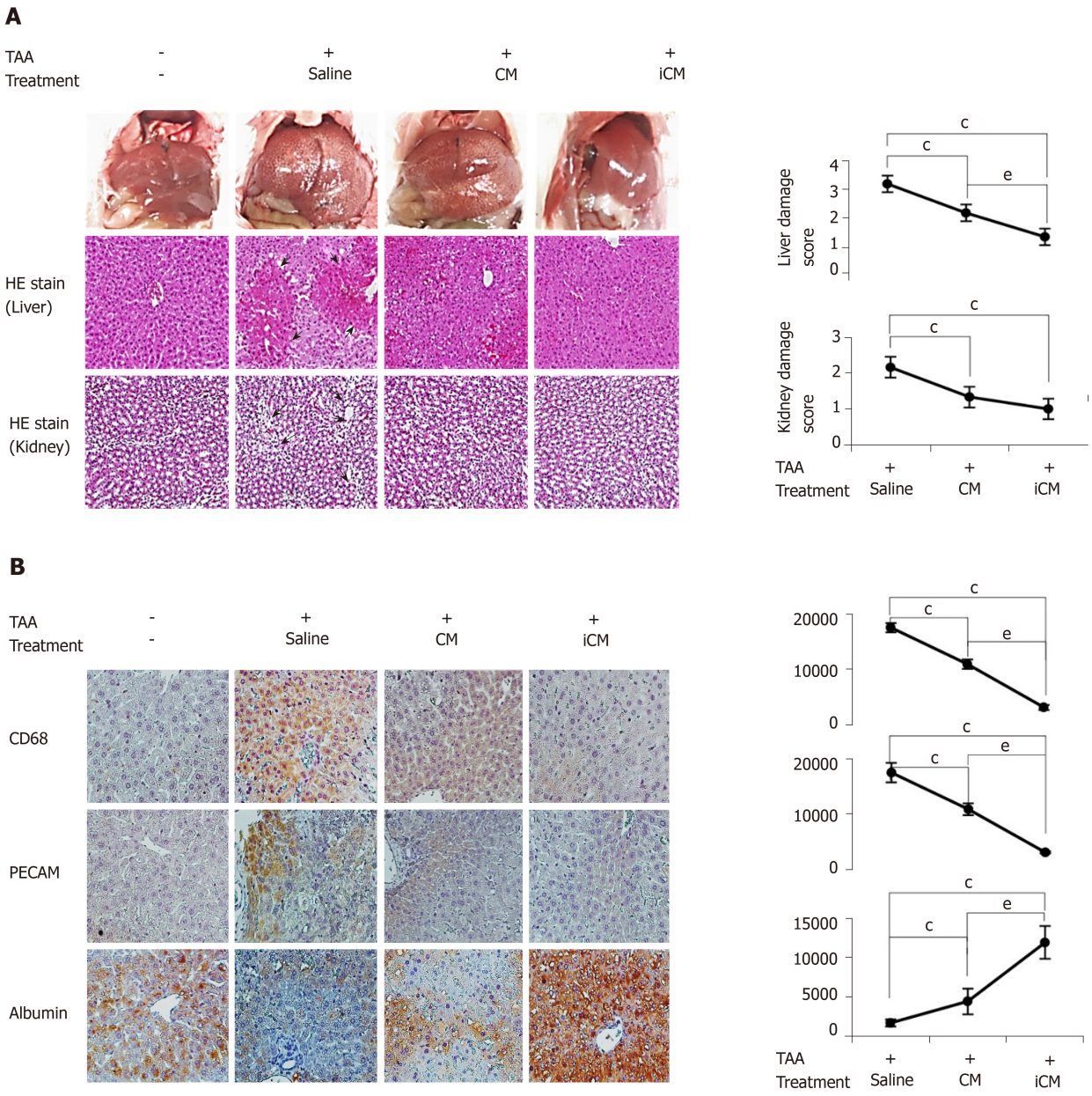

Figure 5 Various stains validating effects of thioacetamide-induced secretome in the mouse model of thioacetamide-induced hepatic failure. A: TAA-induced conditioned media infusion significantly decreased both liver damage and kidney damage scores calculated based on hematoxylin and eosin staining; B: Immunohistochemical staining of liver specimens. Immunohistochemical stains showed that TAA-induced conditioned media infusion significantly decreased the expression of inflammatory markers (CD68 and PECAM) and significantly increased the expression of albumin. Values are presented as mean ± SD of three independent experiments. $^{c}P < 0.05$ *vs* control (saline); $^{e}P < 0.05$ between conditioned media and induced conditioned media. iCM: Induced secretome group of which components were the TAA-induced secretome; CM: Normal conditioned media group of which components were the naïve secretome; TAA: Thioacetamide.

induced hepatic injury.

DISCUSSION

In this study, we showed that the TAA-isecretome was superior to the naïve secretome in restoring hepatic function while minimizing inflammatory processes in mice with TAA-induced hepatic failure. Specifically, isecretome infusion showed higher therapeutic potential in terms of (1) Restoring disorganized hepatic tissue to normal tissue; (2) inhibiting proinflammatory cytokines; and (3) reducing abnormally elevated liver enzymes compared to naïve secretome infusion. The plasticity of MSCs in response to specific toxins may have led to the generation and secretion of protective agents (isecretome) against them. Our proteomic analysis indicated that the secretome components exhibited considerable differences according to the "inducing materials." We expect that clinical application of this concept would be useful for

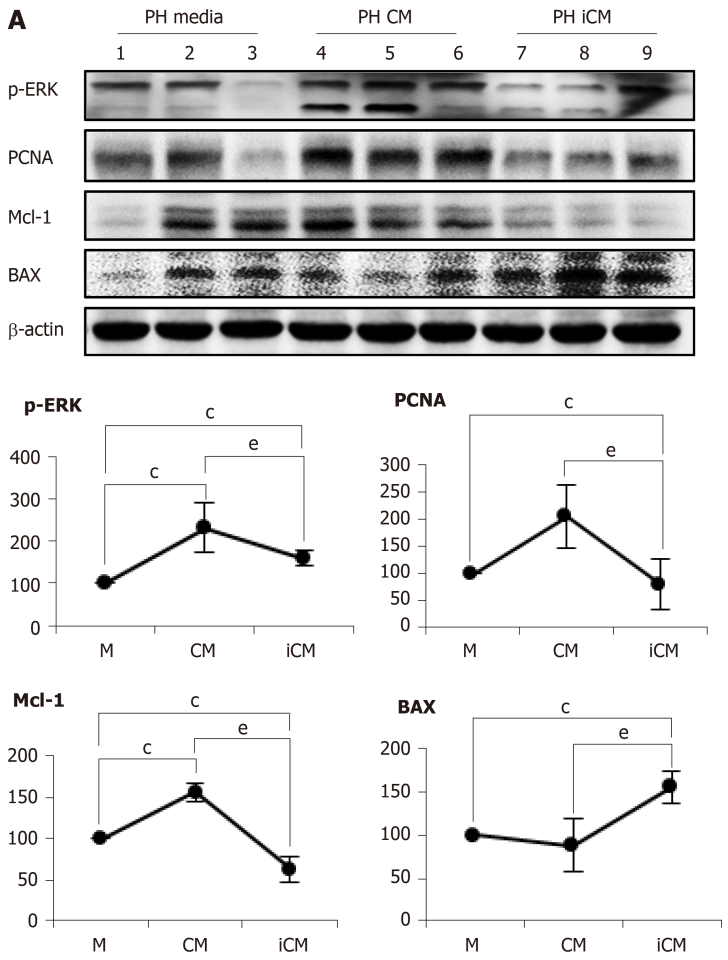
A
PH media
PH CM
PH iCM
1 2 3 4 5 6 7 8 9
p-ERK
PCNA
Mcl-1
BAX
β-actin
p-ERK
PCNA
Mcl-1
BAX
M
CM
iCM
c
e

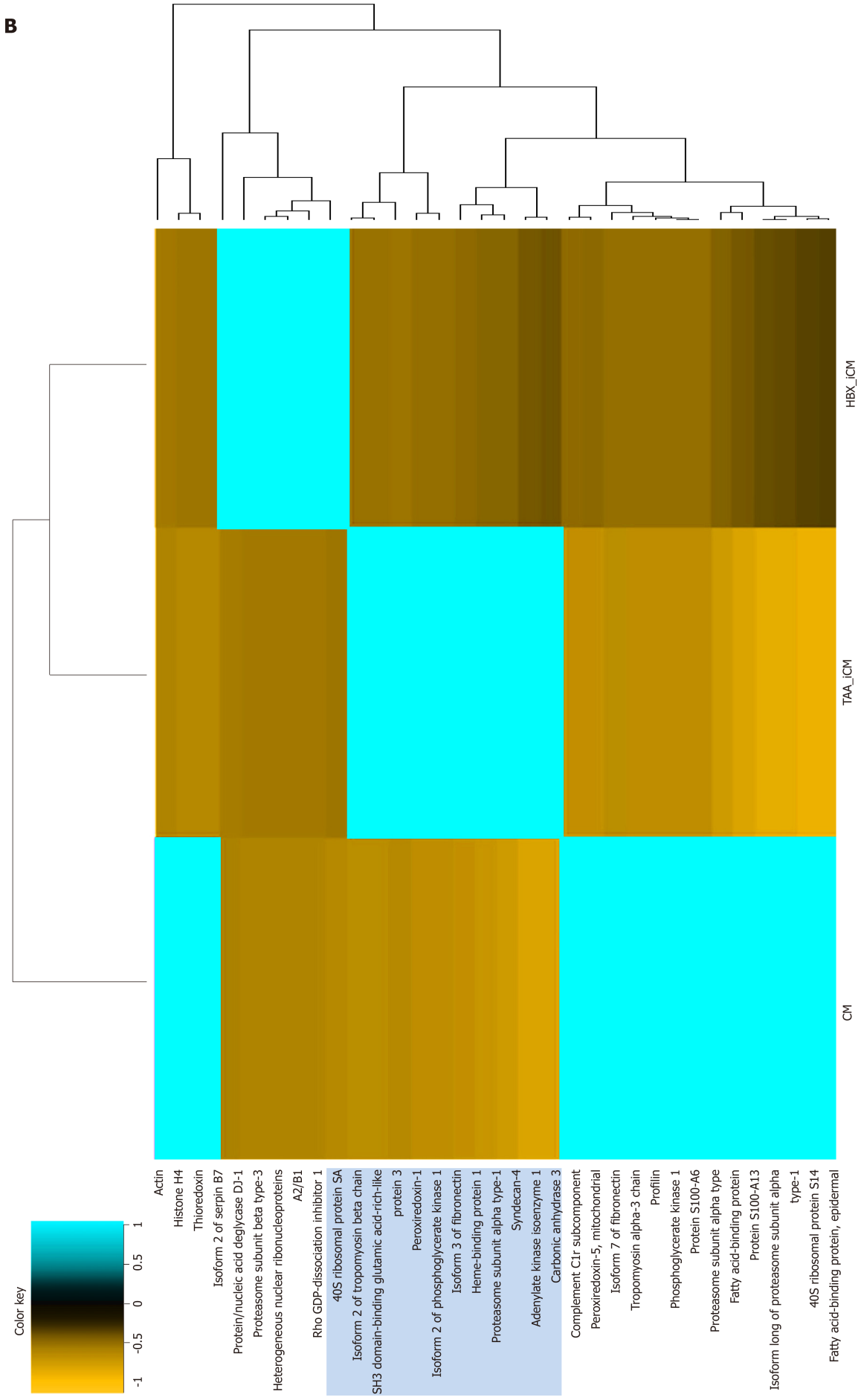
B
HBX_iCM
TAA_iCM
CM
Actin
Histone H4
Thioredoxin
Isoform 2 of serpin B7
Protein/nucleic acid deglycase DJ-1
Proteasome subunit beta type-3
Heterogeneous nuclear ribonucleoproteins A2/B1
Rho GDP-dissociation inhibitor 1
40S ribosomal protein SA
Isoform 2 of tropomyosin beta chain
SH3 domain-binding glutamic acid-rich-like protein 3
Peroxiredoxin-1
Isoform 2 of phosphoglycerate kinase 1
Isoform 3 of fibronectin
Heme-binding protein 1
Proteasome subunit alpha type-1
Syndecan-4
Adenylate kinase isoenzyme 1
Carbonic anhydrase 3
Complement C1r subcomponent
Peroxiredoxin-5, mitochondrial
Isoform 7 of fibronectin
Tropomyosin alpha-3 chain
Profilin
Phosphoglycerate kinase 1
Protein S100-A6
Proteasome subunit alpha type
Fatty acid-binding protein
Protein S100-A13
Isoform long of proteasome subunit alpha type-1
40S ribosomal protein S14
Fatty acid-binding protein, epidermal
Color key
-1
-0.5
0
0.5
1

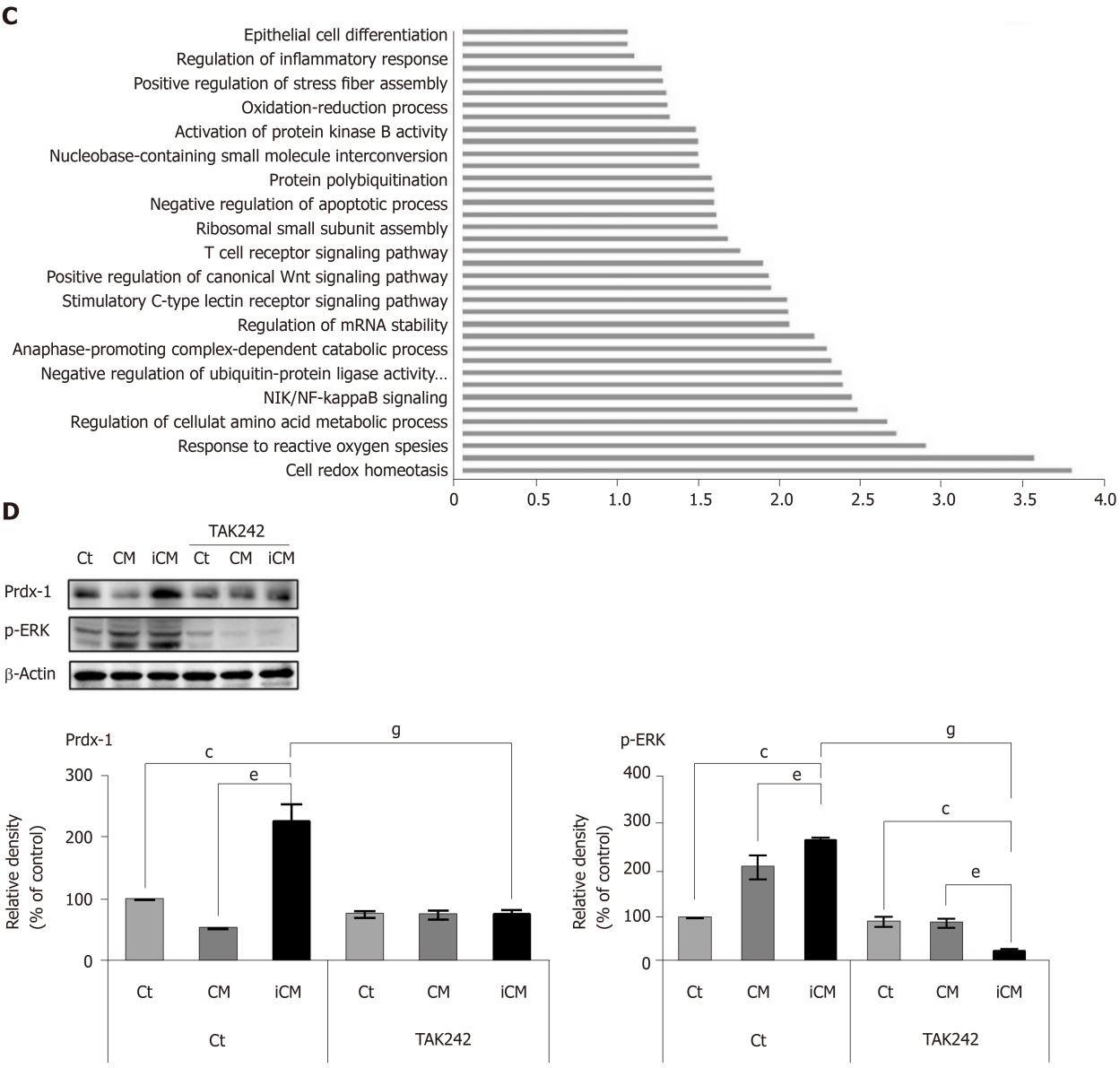

Figure 6 Validation of disease specificity and analysis of secretome components. A: Western blot analysis showing effectiveness of the TAA-induced secretome (isecretome) in partially hepatectomized mice. TAA-induced conditioned media (iCM) infusion was inferior to CM infusion in partially hepatectomized mice, considering the lower expression of proliferation markers (p-ERK and PCNA), and an anti-apoptotic marker (Mcl-1) and higher expression of a proapoptotic marker (Bax) following TAA-iCM infusion; B: Heat map generated from label-free liquid chromatography–mass spectrometry for quantitative proteomics reflecting protein expression values of the secretome, TAA-isecretome, and HBx-isecretome. Samples are arranged in columns and proteins in rows. Red shades indicate increased expression in samples compared to in control samples; green shades indicate reduced expression; black indicates median expression. Each sample for liquid chromatography–mass spectrometry was pooled from three samples of the secretome. The components and concentration of various essential proteins varied widely between iCM and HBx-iCM, validating their specificity. Values are presented as mean ± SD of three independent experiments; C: Gene ontology enrichment analysis of the ten proteins that had been exclusively identified in the TAA-isecretome. Gene ontology enrichment analysis identified the 19 enriched biological networks of the 10 proteins. Of the 19 enriched biological networks, two of the most prominent biological processes were the response to reactive oxygen species and cell redox homeostasis, all of which were related to antioxidant activity; D: Peroxiredoxin-1 (Prdx-1) inhibition test. Prdx-1 is one of the potent antioxidant proteins and was found to be one of ten proteins that had been exclusively identified in the TAA-isecretome. We performed Prdx-1 inhibition test for the determination of the role of Prdx-1 in the hepatic reparative process. Herein, liver regenerative capacity was estimated by the expression of a hepatoproliferative marker (p-ERK). When treated with the TAA-iCM, AML2 hepatocytes showed increased expression of p-ERK as well as Prdx-1 compared with AML2 cells treated with the control CM ($P < 0.05$). Subsequently, we compared the efficacy of the TAA-iCM after pre-treatment of TAK242, a TLR4 inhibitor. Pre-treatment of TAK242 did not only inhibit the expression of Prdx-1 but also inhibited the expression of p-ERK, the hepatoproliferative marker, suggesting the hepatoprotective role of Prdx-1 in the liver. $^{c}P < 0.05$ *vs* control (saline); $^{e}P < 0.05$ between CM and iCM; $^{g}P < 0.05$ between iCMs with or without TAK242. BIM: Bcl-2-like protein 11; iCM: Isecretome group of which components were the TAA-induced secretome; HBx-iCM: Isecretome group of which components were the HBx-induced secretome; Mcl-1: Myeloid cell leukemia 1; CM: Normal conditioned media group of which components were the naïve secretome; PCNA: Proliferating cell nuclear antigen; Prdx-1: Peroxiredoxin-1.

overcoming a variety of diseases for which therapeutics have not been discovered.

Generally, cells have the propensity to protect themselves after exposure to detrimental stimuli or toxins. Because MSCs are unspecialized cells, they have higher plasticity and responsiveness than other cell types, *i.e.* they can either differentiate into specialized cells or release responsive materials more proficiently than

differentiated cells depending on the external stimuli. Rodríguez-Suárez *et al*[18] investigated the proteome of EVs secreted by primary hepatocytes after exposure to well-known liver toxins (galactosamine and *Escherichia coli*-derived lipopolysaccharide). EVs exposed to liver toxins contained higher levels of vital liver-specific proteins, such as carbamoyl phosphate synthetase 1, *S*-adenosyl methionine synthetase 1, and catechol-*O*-methyltransferase compared to control EVs. The secretome composition is influenced by a variety of external factors, including the cell source, type of culture media, culturing period, and physicochemical environment. Vizoso *et al*[24] classified the external stimuli into four major categories: (1) Hypoxic preconditioning; (2) Pro-inflammatory stimuli, such as TNF-α, lipopolysaccharide, toll-like receptor agonists; (3) Three-dimensional growth, such as spheroid culture, which stimulates trophic factor secretion; and (4) Microparticle engineering, by which the release of a secretome is manipulated. Using the higher plasticity and responsiveness of MSCs, we induced a specific secretome specialized for treating a specific disease.

Whereas the secretome was obtained by nonspecific stimulation, the isecretome was obtained by using stimuli specific for individual diseases, allowing for disease-specific therapy. The isecretome for a specific disease is obtained by stimulating MSCs with specific pathogens involved in the pathogenesis of the disease. This concept is based on the superior responsiveness and plasticity of MSCs compared to host cells, which were exploited in several previous studies[25,26]. Prado *et al*[27] reported the successful prevention of allergic reaction by intranasal administration of EVs in a murine model of Ole e 1 (the main allergen of olive tree pollen)-allergic sensitization. The EVs were first obtained from bronchoalveolar lavage fluid in mice that had been exposed to Ole e 1. Their favorable results were based on the plasticity of mature respiratory cells. In contrast, our experiment is based on the plasticity of MSCs that are far higher than that of mature cells and demonstrated the increased therapeutic potential.

A prerequisite to obtaining a disease-specific secretome is to determine optimized conditions under which pathogenic materials appropriately induce MSCs to produce protective materials. Too strong or too weak stimulation of MSCs is undesirable because this can lead to either MSC damage or insufficient generation of the isecretome, respectively. To obtain the TAA-isecretome, we first collected the secretory materials from hepatocytes after treating the cells with a TAA, which were named as inducers. We then harnessed ASCs to release the isecretome by treating ASCs with inducers. For this, we determined (1) the concentration of TAA that both maximally stimulated and minimally damaged hepatocytes; and (2) the optimal dilution rate of inducers for harnessing ASCs to release the isecretome with maximal therapeutic potential. We validated this process by western blot analyses of markers reflecting the proliferation and apoptosis of cells.

The hepatotoxic effect of TAA is attributed to its metabolic intermediate, thioacetamide-S-oxide[28]. It is a free radical that binds to hepatic macromolecules, subsequently leading to necrosis of hepatocytes. Silymarin is one of the best known hepatoprotective drugs (the mechanism of action is largely dependent on its antioxidant and free radical scavenging activities)[29]. Throughout LC/MS analysis, we recognized ten proteins that had been exclusively identified in the TAA-iCM but not in the CM. GO enrichment analysis of these proteins found that antioxidant processes were the most predominant enriched biological networks. Of the ten proteins, Prdx-1 attracted our attention because it is known to have potent antioxidant activity.

Prdx-1 is an antioxidant enzyme belonging to the peroxiredoxin family of proteins. It has excellent antioxidant activity by catalyzing the reduction of H_2O_2 and alkyl hydroperoxide and thus protects cells from the attack of free radicals. In an experiment, Prdx-1 knockdown significantly increased the cellular levels of free radicals, while Prdx-1 overexpression reversed them[30]. Binding of Prdx-1 to TLR4 induced the release of numerous cytokines and growth factors, such as IL-6, TNF-α, and VEGF[23,31]. Moreover, we found that the inhibition of TLR4 by TAK242 (a TLR4 inhibitor) led to significant reduction in the expression of p-ERK (a proliferative marker) as well as Prdx-1. Taken altogether, our results suggest that Prdx-1 is one of the representative components released from ASCs that had been induced by TAA and plays a central role in the protection of TAA-induced hepatic injury.

The principle of generating the isecretome is similar to how antibodies against specific antigens are obtained in serotherapy. In serotherapy, introduction of attenuated antigens into the host induces the generation of antibodies against these antigens, which are collected to treat patients suffering from antigen-related disease. Similarly, in isecretome-based therapy, presensitization of MSCs with pathogens induced the generation of the secretome including protective agents against pathogens, which were collected to treat pathogen-causing disease. Because isecretome therapy provides a disease-specific approach, specific therapeutics can be

developed based on high plasticity and responsiveness of MSCs. Further studies on the isecretome are expected to identify therapeutic materials by reproducing the pathogenesis of a certain disease within MSCs. There are numerous diseases for which therapeutics have not been developed or are ineffective. We presumed that MSCs can reproduce the repair materials against certain incurable illnesses when encountered during pathogenesis. There are two main clinical applications of the isecretome:1) direct utilization as therapeutic materials and 2) identification of more specific ingredients as therapeutic materials. The latter is accomplished by proteomic studies of isecretome components. Using isecretome-based technology, we could build "biological drug factories" based on the plasticity of MSCs that produce therapeutic materials from MSCs.

In conclusion, we showed that the TAA-isecretome was superior to the naïve secretome in restoring hepatic function while minimizing inflammatory processes in mice with TAA-induced hepatic failure. However, such superiority was not observed in the mouse model of partial hepatectomy. This suggests that the specific pathogen induces MSCs to release the secretome specialized for the pathogen. Free radicals are principal pathogenic agents in the pathogenesis of TAA-induced hepatic injury. LC/MS analysis and subsequent GO enrichment analysis of TAA-isecretome identified that antioxidant processes were the most predominantly enriched biological networks of the proteins exclusively identified in the TAA-isecretome. In addition, Prdx-1, a potent antioxidant protein, was found to be one of the representative components of the TAA-isecretome and played a central role in the protection of TAA-induced hepatic injury.

ARTICLE HIGHLIGHTS

Research background

The exclusive use of mesenchymal stem cell (MSC)-secreted molecules, named as the secretome, rather than stem cells have been evaluated for overcoming the limitations of cell-based therapy while maintaining its advantages. As recent studies have shown that this secretome has therapeutic effects similar to stem cells, the secretome has become the basis of cell-free therapy.

Research motivation

The composition of the secretome is influenced by various external factors, including the cell source, type of culture media, culturing period, and preconditioning treatment. Previous studies suggest that MSCs can be induced to generate a specialized secretome customized to a specific disease. We herein defined induced secretome (isecretome) as the secretome released from MSCs that had been stimulated by disease-causing materials to treat the specific disease.

Research objectives

Thioacetamide (TAA) is a well-known hepatotoxin. We thus attempted to validate the higher therapeutic effects of the secretome induced by TAA (TAA-isecretome) compared to the naïve secretome, specifically in mice with TAA-induced hepatic failure. If the superiority of the isecretome over the naïve secretome is demonstrated, it could provide a foundation for producing a disease-specific isecretome applicable to specific diseases.

Research methods

We collected the secretory materials (named as inducers) released from AML12 hepatocytes that had been pretreated with TAA and generated the TAA-isecretome after stimulating ASCs with the inducers. The TAA-isecretome was intravenously administered to mice with TAA-induced hepatic failure and those with partial hepatectomy. In addition, we generated an HBx-isecretome using hepatitis X antigens as inducers and compared the components of the naïve secretome, TAA-isecretome, and HBx-isecretome using liquid chromatography–mass spectrometry.

Research results

Compared to the naïve secretome infusion, TAA-isecretome infusion showed higher therapeutic potential in terms of (1) restoring disorganized hepatic tissue to normal tissue; (2) Inhibiting proinflammatory cytokines (interleukin-6 and tumor necrosis factor-α); and (3) Reducing abnormally elevated liver enzymes (aspartate aminotransferase and alanine aminotransferase) in mice with TAA-induced hepatic failure. However, the TAA-isecretome showed inferior therapeutic potential for restoring hepatic function in partially hepatectomized mice. Proteomic analysis of the TAA-isecretome identified that antioxidant processes were the most predominant enriched biological networks of the proteins exclusively identified in the TAA-isecretome. In addition, peroxiredoxin-1, a potent antioxidant protein, was found to be one of the representative components of the TAA-isecretome.

Research conclusions

We showed that the TAA-isecretome was superior to the naïve secretome in restoring hepatic function while minimizing inflammatory processes in mice with TAA-induced hepatic failure. However, such superiority was not observed in the mouse model of partial hepatectomy, suggesting disease-specificity of the TAA-isecretome. Free radicals are principal pathogenic

agents in the pathogenesis of TAA-induced hepatic injury. Proteomic analysis of TAA-isecretome identified that antioxidant processes were the most predominantly enriched biological networks of the proteins exclusively identified in the TAA-isecretome. In addition, Prdx-1, a potent antioxidant protein, was found to be one of the representative components of the TAA-isecretome.

Research perspectives

Our results suggest that appropriate stimulation of MSCs with pathogenic agents can lead to the production of a secretome specialized for protecting against the pathogen. This approach is expected to open a new way of developing various specific therapeutics based on the high plasticity and responsiveness of MSCs.

ACKNOWLEDGEMENTS

We would like to thank Drug and Disease Target Team (Ochang), Korea Basic Science Institute for supporting funds for this experiment. We would like to thank Hye-Jung Kim for photoshop work that improved the figure quality. We would like to thank Francis Sahngun Nahm (a professional statistician) for his devoted assistance of statistical analysis. Finally, we would like to thank Hye-Jeong Kim and Ji-Hye Park for data processing and photoshop work.

REFERENCES

1 **Lee SK**, Lee SC, Kim SJ. A novel cell-free strategy for promoting mouse liver regeneration: utilization of a conditioned medium from adipose-derived stem cells. *Hepatol Int* 2015; **9**: 310-320 [PMID: 25788187 DOI: 10.1007/s12072-014-9599-4]
2 **Guglielmi A**, Ruzzenente A, Conci S, Valdegamberi A, Iacono C. How much remnant is enough in liver resection? *Dig Surg* 2012; **29**: 6-17 [PMID: 22441614 DOI: 10.1159/000335713]
3 **An SY**, Jang YJ, Lim HJ, Han J, Lee J, Lee G, Park JY, Park SY, Kim JH, Do BR, Han C, Park HK, Kim OH, Song MJ, Kim SJ, Kim JH. Milk Fat Globule-EGF Factor 8, Secreted by Mesenchymal Stem Cells, Protects Against Liver Fibrosis in Mice. *Gastroenterology* 2017; **152**: 1174-1186 [PMID: 27956229 DOI: 10.1053/j.gastro.2016.12.003]
4 **Miura M**, Miura Y, Padilla-Nash HM, Molinolo AA, Fu B, Patel V, Seo BM, Sonoyama W, Zheng JJ, Baker CC, Chen W, Ried T, Shi S. Accumulated chromosomal instability in murine bone marrow mesenchymal stem cells leads to malignant transformation. *Stem Cells* 2006; **24**: 1095-1103 [PMID: 16282438 DOI: 10.1634/stemcells.2005-0403]
5 **Lapidot T**, Sirard C, Vormoor J, Murdoch B, Hoang T, Caceres-Cortes J, Minden M, Paterson B, Caligiuri MA, Dick JE. A cell initiating human acute myeloid leukaemia after transplantation into SCID mice. *Nature* 1994; **367**: 645-648 [PMID: 7509044 DOI: 10.1038/367645a0]
6 **Tolar J**, Nauta AJ, Osborn MJ, Panoskaltsis Mortari A, McElmurry RT, Bell S, Xia L, Zhou N, Riddle M, Schroeder TM, Westendorf JJ, McIvor RS, Hogendoorn PC, Szuhai K, Oseth L, Hirsch B, Yant SR, Kay MA, Peister A, Prockop DJ, Fibbe WE, Blazar BR. Sarcoma derived from cultured mesenchymal stem cells. *Stem Cells* 2007; **25**: 371-379 [PMID: 17038675 DOI: 10.1634/stemcells.2005-0620]
7 **Thomson BM**, Bennett J, Dean V, Triffitt J, Meikle MC, Loveridge N. Preliminary characterization of porcine bone marrow stromal cells: skeletogenic potential, colony-forming activity, and response to dexamethasone, transforming growth factor beta, and basic fibroblast growth factor. *J Bone Miner Res* 1993; **8**: 1173-1183 [PMID: 8256654 DOI: 10.1002/jbmr.5650081004]
8 **Wang Y**, Huso DL, Harrington J, Kellner J, Jeong DK, Turney J, McNiece IK. Outgrowth of a transformed cell population derived from normal human BM mesenchymal stem cell culture. *Cytotherapy* 2005; **7**: 509-519 [PMID: 16306013 DOI: 10.1080/14653240500363216]
9 **Le Blanc K**, Rasmusson I, Sundberg B, Götherström C, Hassan M, Uzunel M, Ringdén O. Treatment of severe acute graft-versus-host disease with third party haploidentical mesenchymal stem cells. *Lancet* 2004; **363**: 1439-1441 [PMID: 15121408 DOI: 10.1016/S0140-6736(04)16104-7]
10 **Baglio SR**, Pegtel DM, Baldini N. Mesenchymal stem cell secreted vesicles provide novel opportunities in (stem) cell-free therapy. *Front Physiol* 2012; **3**: 359 [PMID: 22973239 DOI: 10.3389/fphys.2012.00359]
11 **Ranganath SH**, Levy O, Inamdar MS, Karp JM. Harnessing the mesenchymal stem cell secretome for the treatment of cardiovascular disease. *Cell Stem Cell* 2012; **10**: 244-258 [PMID: 22385653 DOI: 10.1016/j.stem.2012.02.005]
12 **Gnecchi M**, Zhang Z, Ni A, Dzau VJ. Paracrine mechanisms in adult stem cell signaling and therapy. *Circ Res* 2008; **103**: 1204-1219 [PMID: 19028920 DOI: 10.1161/Circresaha.108.176826]
13 **Hoch AI**, Binder BY, Genetos DC, Leach JK. Differentiation-dependent secretion of proangiogenic factors by mesenchymal stem cells. *PLoS One* 2012; **7**: e35579 [PMID: 22536411 DOI: 10.1371/journal.pone.0035579]
14 **Yang Z**, Di Santo S, Kalka C. Current developments in the use of stem cell for therapeutic neovascularisation: is the future therapy "cell-free"? *Swiss Med Wkly* 2010; **140**: w13130 [PMID: 21170763 DOI: 10.4414/smw.2010.13130]
15 **Lee SC**, Jeong HJ, Lee SK, Kim SJ. Hypoxic Conditioned Medium From Human Adipose-Derived Stem Cells Promotes Mouse Liver Regeneration Through JAK/STAT3 Signaling. *Stem Cells Transl Med* 2016; **5**: 816-825 [PMID: 27102647 DOI: 10.5966/sctm.2015-0191]
16 **Lee SC**, Kim KH, Kim OH, Lee SK, Hong HE, Won SS, Jeon SJ, Choi BJ, Jeong W, Kim SJ. Determination of optimized oxygen partial pressure to maximize the liver regenerative potential of the secretome obtained from adipose-derived stem cells. *Stem Cell Res Ther* 2017; **8**: 181 [PMID: 28774345 DOI: 10.1186/s13287-017-0635-x]
17 **Lee SC**, Jeong HJ, Lee SK, Kim SJ. Lipopolysaccharide preconditioning of adipose-derived stem cells improves liver-regenerating activity of the secretome. *Stem Cell Res Ther* 2015; **6**: 75 [PMID: 25890074

DOI: 10.1186/s13287-015-0072-7]
18 **Rodríguez-Suárez E**, Gonzalez E, Hughes C, Conde-Vancells J, Rudella A, Royo F, Palomo L, Elortza F, Lu SC, Mato JM, Vissers JP, Falcón-Pérez JM. Quantitative proteomic analysis of hepatocyte-secreted extracellular vesicles reveals candidate markers for liver toxicity. *J Proteomics* 2014; **103**: 227-240 [PMID: 24747303 DOI: 10.1016/j.jprot.2014.04.008]
19 **Keppler D**, Lesch R, Reutter W, Decker K. Experimental hepatitis induced by D-galactosamine. *Exp Mol Pathol* 1968; **9**: 279-290 [PMID: 4952077 DOI: 10.1016/0014-4800(68)90042-7]
20 **Chen S**, Liu C, Wang X, Li X, Chen Y, Tang N. 15-Deoxy-Δ(12,14)-prostaglandin J2 (15d-PGJ2) promotes apoptosis of HBx-positive liver cells. *Chem Biol Interact* 2014; **214**: 26-32 [PMID: 24582817 DOI: 10.1016/j.cbi.2014.02.009]
21 **Galanos C**, Lüderitz O, Rietschel ET, Westphal O, Brade H, Brade L, Freudenberg M, Schade U, Imoto M, Yoshimura H. Synthetic and natural Escherichia coli free lipid A express identical endotoxic activities. *Eur J Biochem* 1985; **148**: 1-5 [PMID: 2579812 DOI: 10.1111/j.1432-1033.1985.tb08798.x]
22 **Choi CW**, Park EC, Yun SH, Lee SY, Lee YG, Hong Y, Park KR, Kim SH, Kim GH, Kim SI. Proteomic characterization of the outer membrane vesicle of Pseudomonas putida KT2440. *J Proteome Res* 2014; **13**: 4298-4309 [PMID: 25198519 DOI: 10.1021/pr500411d]
23 **Riddell JR**, Wang XY, Minderman H, Gollnick SO. Peroxiredoxin 1 stimulates secretion of proinflammatory cytokines by binding to TLR4. *J Immunol* 2010; **184**: 1022-1030 [PMID: 20018613 DOI: 10.4049/jimmunol.0901945]
24 **Vizoso FJ**, Eiro N, Cid S, Schneider J, Perez-Fernandez R. Mesenchymal Stem Cell Secretome: Toward Cell-Free Therapeutic Strategies in Regenerative Medicine. *Int J Mol Sci* 2017; **18**: E1852 [PMID: 28841158 DOI: 10.3390/ijms18091852]
25 **Zipori D**. Mesenchymal stem cells: harnessing cell plasticity to tissue and organ repair. *Blood Cells Mol Dis* 2004; **33**: 211-215 [PMID: 15528133 DOI: 10.1016/j.bcmd.2004.08.019]
26 **Jiang Y**, Vaessen B, Lenvik T, Blackstad M, Reyes M, Verfaillie CM. Multipotent progenitor cells can be isolated from postnatal murine bone marrow, muscle, and brain. *Exp Hematol* 2002; **30**: 896-904 [PMID: 12160841 DOI: 10.1016/s0301-472x(02)00869-x]
27 **Prado N**, Marazuela EG, Segura E, Fernández-García H, Villalba M, Théry C, Rodríguez R, Batanero E. Exosomes from bronchoalveolar fluid of tolerized mice prevent allergic reaction. *J Immunol* 2008; **181**: 1519-1525 [PMID: 18606707 DOI: 10.1016/j.ceb.2004.02.003]
28 **Staňková P**, Kučera O, Lotková H, Roušar T, Endlicher R, Cervinková Z. The toxic effect of thioacetamide on rat liver in vitro. *Toxicol In Vitro* 2010; **24**: 2097-2103 [PMID: 20600801 DOI: 10.1016/j.tiv.2010.06.011]
29 **Ghosh S**, Sarkar A, Bhattacharyya S, Sil PC. Silymarin Protects Mouse Liver and Kidney from Thioacetamide Induced Toxicity by Scavenging Reactive Oxygen Species and Activating PI3K-Akt Pathway. *Front Pharmacol* 2016; **7**: 481 [PMID: 28018219 DOI: 10.3389/fphar.2016.00481]
30 **Chae S**, Lee HK, Kim YK, Jung Sim H, Ji Y, Kim C, Ismail T, Park JW, Kwon OS, Kang BS, Lee DS, Bae JS, Kim SH, Min KJ, Kyu Kwon T, Park MJ, Han JK, Kwon T, Park TJ, Lee HS. Peroxiredoxin1, a novel regulator of pronephros development, influences retinoic acid and Wnt signaling by controlling ROS levels. *Sci Rep* 2017; **7**: 8874 [PMID: 28827763 DOI: 10.1038/s41598-017-09262-6]
31 **Riddell JR**, Bshara W, Moser MT, Spernyak JA, Foster BA, Gollnick SO. Peroxiredoxin 1 controls prostate cancer growth through Toll-like receptor 4-dependent regulation of tumor vasculature. *Cancer Res* 2011; **71**: 1637-1646 [PMID: 21343392 DOI: 10.1158/0008-5472.Can-10-3674]

World Journal of Stem Cells

Submit a Manuscript: https://www.f6publishing.com

World J Stem Cells 2020 January 26; 12(1): 87-99

DOI: 10.4252/wjsc.v12.i1.87

ISSN 1948-0210 (online)

ORIGINAL ARTICLE

Basic Study

HIF-2α regulates CD44 to promote cancer stem cell activation in triple-negative breast cancer *via* PI3K/AKT/mTOR signaling

Jie Bai, Wei-Bin Chen, Xiao-Yu Zhang, Xiao-Ning Kang, Li-Jun Jin, Hui Zhang, Zun-Yi Wang

ORCID number: Jie Bai (0000-0002-9825-5030); Wei-Bin Chen (0000-0001-5858-2435); Xiao-Yu Zhang (0000-0002-6363-0435); Xiao-Ning Kang (0000-0002-9480-8929); Li-Jun Jin (0000-0002-9818-3815); Hui Zhang (0000-0001-7352-3566); Zun-Yi Wang (0000-0002-4318-0813).

Author contributions: Bai J and Wang ZY conceived and designed the study; Bai J, Chen WB, and Zhang XY performed the experiments; Zhang XY and Kang XN acquired the patients' data; Bai J, Kang XN, Jin LJ, and Zhang H analyzed the data and drafted the report; Wang ZY supervised the study; all authors reviewed and revised the manuscript critically and approved the final version to be published.

Institutional review board statement: The study was approved by the Ethics Committee of Cangzhou Central Hospital.

Conflict-of-interest statement: The authors report no conflicts of interest in this work.

Jie Bai, Xiao-Yu Zhang, Li-Jun Jin, Zun-Yi Wang, Thyroid and Breast Deptartment III, Cangzhou Central Hospital, Cangzhou 061001, Hebei Province, China

Wei-Bin Chen, Department of Radiology, North China University of Science and Technology Affiliated Hospital, Tangshan 063000, Hebei Province, China

Xiao-Ning Kang, Department of Second Ultrasound, Cangzhou Central Hospital, Cangzhou 061001, Hebei Province, China

Corresponding author: Zun-Yi Wang, MD, Doctor, Department of Third Surgical Oncology, Cangzhou Central Hospital, No. 16, West Xinhua Road, Cangzhou 061001, Hebei Province, China. czwzy99@163.com

Abstract

BACKGROUND

Breast cancer is a common malignant tumor that seriously threatens women's health. Breast cancer stem cell (CSC)-like cell population may be the main factor for breast cancer metastasis. Therefore, targeted therapy for CSCs has great potential significance. Hypoxia-inducible factor is a transcription factor widely expressed in tumors. Studies have shown that down-regulation of the hypoxia signaling pathway inhibits tumor stem cell self-renewal and increases the sensitivity of stem cells to radiotherapy and chemotherapy mediated by hypoxia-inducible factor-2α (HIF-2α). However, the specific mechanism remains unclear and further research is necessary.

AIM

To investigate the effect of HIF-2α down-regulation on stem cell markers, microsphere formation, and apoptosis in breast cancer cell line MDA-MB-231 under hypoxia and its possible mechanism.

METHODS

Immunohistochemistry was used to detect the expression of HIF-2α and CD44 in triple-negative breast cancer (TNBC) and non-TNBC tissues. Double-labeling immunofluorescence was applied to detect the co-expression of HIF-2α and CD44 in MDA-MB-231 cells and MCF-7 cells. HIF-2α was silenced by RNA interference, and the expression of CD44 and transfection efficiency were detected by real-time fluorescent quantitative PCR. Further, flow cytometry, TdT-mediated X-dUTP nick end labeling, and mammosphere formation assays were used to evaluate the effect of HIF-2α on CSCs and apoptosis. The possible mechanisms were analyzed by Western blot.

Manuscript source: Unsolicited manuscript

Received: June 15, 2019
Peer-review started: June 18, 2019
First decision: July 31, 2019
Revised: August 12, 2019
Accepted: October 14, 2019
Article in press: October 14, 2019
Published online: January 26, 2020

P-Reviewer: Kruis W, Reich K, Manuel CF
S-Editor: Zhang L
L-Editor: Wang TQ
E-Editor: Xing YX

RESULTS

The results of immunohistochemistry showed that HIF-2α was highly expressed in both TNBC and non-TNBC, while the expression of CD44 in different molecular types of breast cancer cells was different. In *in vitro* experiments, it was found that HIF-2α and CD44 were expressed almost in the same cell. Compared with hypoxia + negative-sequence control, HIF-2α small interfering ribonucleic acid transfection can lower the expression of HIF-2α and CD44 mRNA($P < 0.05$), increase the percentage of apoptotic cells ($P < 0.05$), and resulted in a reduction of $CD44^+/CD24^-$ population ($P < 0.05$) and mammosphere formation ($P < 0.05$) in hypoxic MDA-MB-231 cells. Western blot analysis revealed that phosphorylated protein-serine-threonine kinase (p-AKT) and phosphorylated mammalian target of rapamycin (p-mTOR) levels in MDA-MB-231 decreased significantly after HIF-2α silencing ($P < 0.05$).

CONCLUSION

Down-regulation of HIF-2α expression can inhibit the stemness of human breast cancer MDA-MB-231 cells and promote apoptosis, and its mechanism may be related to the CD44/phosphoinosmde-3-kinase/AKT/mTOR signaling pathway.

Key words: Breast cancer; Hypoxia-inducible factor-2α; Cancer stem cells; CD44

Core tip: Cancer stem cells (CSCs) play an important role in tumor formation, growth, invasion, metastasis, and recurrence. Hypoxia can promote the differentiation of various tumor cells, enable cells to acquire stem cell characteristics, and enhance tumor cell invasion and tumorigenicity. In the long-term exposure of tumors to hypoxia, the major regulatory factor is hypoxia-inducible factor-2α (HIF-2α), which can promote the malignant biological behavior of tumors by activating its downstream target genes. Studies have shown that the effect of HIF-2α on tumor cells may be related to CD44, a marker for breast CSCs. In this study, breast cancer cell line MCF-7 and basal breast cancer cell line MDA-MB-231 were utilized to investigate the relationship between HIF-2α and CD44 gene expression and the regulatory effect of HIF-2α on CD44.

Citation: Bai J, Chen WB, Zhang XY, Kang XN, Jin LJ, Zhang H, Wang ZY. HIF-2α regulates CD44 to promote cancer stem cell activation in triple-negative breast cancer *via* PI3K/AKT/mTOR signaling. *World J Stem Cells* 2020; 12(1): 87-99
URL: https://www.wjgnet.com/1948-0210/full/v12/i1/87.htm
DOI: https://dx.doi.org/10.4252/wjsc.v12.i1.87

INTRODUCTION

Breast cancer is one of the most common malignant tumors. Its incidence rate is the highest in females and has a rising trend[1-3]. Although advanced medical technology has significantly improved the 5-year survival rate of many types of breast cancer, there are still 20% to 30% of patients who will have recurrence, serious complications, and even death after treatment[4-6]. According to the report by Dent *et al*[7], the 5-year survival rate of patients with recurrent breast cancer is only about 60%. Distant metastasis is one of the most important reasons. In particular, attention needs to be paid to patients with triple-negative breast cancer (TNBC), which is highly invasive and more prone to recurrence and metastasis than other forms of breast cancer[8-10]. Therefore, studies on TNBC are popular in clinical research. In recent years, researchers have found a small number of highly tumorigenic cell populations in breast tumors that express stem cell-like properties and are capable of self-renewal and differentiation, which are considered to be the source of tumor recurrence[11-13]. Some latest studies have suggested that deaths caused by TNBC are mainly associated with persistent cancer stem cells (CSCs)[14-16]. An *in vitro* experiment with CSCs from Lu *et al*[17] also showed that chemotherapy can enrich CSCs in TNBC and induce recurrence. Hence, targeted therapy for inhibiting CSC population has great clinical value. In the study of Samanta *et al*[18], hypoxia can promote the ability of tumor cells

to obtain the features of stem cells and enhance the resistance of breast cancer cells to chemotherapy. Carroll *et al*[19] revealed the role of gene expression of hypoxia-inducible factor-1α (HIF-1α) and hypoxia-inducible factor-2α (HIF-2α) in breast cancer cell proliferation. It is worth noting that HIF-2α is more important in regulating the state of CSCs. Studies have confirmed that HIF-2α can affect the biological characteristics of breast CSCs, which is related to CD44 and its downstream pathway[20,21]. As a widely distributed transmembrane glycoprotein, CD44 regulates the phosphoinosmde-3-kinase (PI3K)/protein-serine-threonine kinase (AKT)/mammalian target of rapamycin (mTOR) signaling pathway and participates in the migration of cancer cells. It is also highly expressed in CSCs and is one of the important markers of CSCs. Current studies have shown that the change of CD44 expression is consistent with the trend of HIF-2α expression[22-24], but the relationship between CD44 and HIF-2α and its regulation mechanism are still unknown. The aim of this study was to investigate the relationship between HIF-2α, CD44, and PI3K/AKT/mTOR signaling by using breast cancer cell line MDA-MB-231, and further analyze the mechanism of CSC activation in TNBC and its role in the malignant progression of TNBC.

MATERIALS AND METHODS

Patients and breast cancer tissues

A total of 49 female patients with primary breast cancer diagnosed at Cangzhou Central Hospital were enrolled in our study from 2016 to 2017. Among them are 29 cases of TNBC and 20 cases of lumen type breast cancer (non-TNBC). All the patients had never been treated with radiotherapy or chemotherapy and the diagnosis was confirmed pathologically by more than two pathologists. Patients who had recurrent or metastatic breast cancer were excluded. Tumor tissues from TNBC and non-TNBC patients obtained during surgery were fixed in 10% neutral buffered formalin and then embedded in paraffin wax for immunohistochemistry analysis. This study was approved by the Ethics Committee of Cangzhou Central Hospital.

Immunohistochemistry

The expression of HIF-2α and CD44 in breast cancer was measured by immunohistochemistry analysis. Briefly, sections of 4 μm thickness, obtained from patients with TNBC and non-TNBC, were subjected to deparaffinization, rehydration, and microwave antigen retrieval. The tissue sections were incubated in 0.3% H_2O_2 for 10 min and blocked using 1% BSA/PBS. The slides were then incubated with the following primary antibodies: anti-CD44 (dilution, 1:800) and anti-HIF-2α antibodies (dilution, 1:400; Abcam, Cambridge, MA, United States) overnight at 4 °C. Afterwards, the tissues were incubated with horseradish peroxidase-labeled secondary antibody (dilution, 1:1000; Santa Cruz Biotechnology, Inc) at 37 °C for 30 min and and stained with DAB, followed by haematoxylin counterstaning. The result was evaluated by pathologists based on the following criteria: >10% of cells stained represented positive expression and >30% of cells stained were considered as high expression.

Cell culture

Human breast cancer cell lines MDA-MB-231 and MCF-7 were obtained from American Type Culture Collection (ATCC, Manassas, VA, United States) and routinely cultured in Dulbecco's modified Eagle's medium-F12 medium containing 10% fetal bovine serum, 100 U/mL penicillin, and 100 μg/mL streptomycin (Gibco, Grand island, NY, United States). Cells were grown at 37 °C in a humidified incubator containing 5% CO_2 and the complete medium changed 24 h. Digestion and passage were performed and cells in exponential growth stage were harvested for various experiments. For hypoxia treatment, all cells were cultured in a constant-temperature incubator with 1%O_2, 5%CO_2, and 94%N_2.

Immunofluorescence

Cells were seeded on coverslides for 24 h and then fixed in 4% paraformaldehyde, followed by permeabilization with 0.2% Triton X-100. The nonspecific sites of samples were blocked with normal sheep serum at room temperature, and then the cells were stained with the primary antibody CD44-PE (dilution, 1:200) and rabbit anti-HIF-2α antibody (dilution, 1:600) provided by BD Biosciences overnight at 4 °C. Then, the samples were washed three times with PBS and incubated with the fluorophore-labelled goat anti-rabbit antibody for an additional 30 min at room temperature. After three washes with PBS, the samples were counterstained with 1 μg/mL 4',6-diamidino-2-phenylindole (Sigma, St. Louis, MO, United States) to visualize cell

nuclei and the stained cells were analyzed under a fluorescence microscope.

RNA interference and transfection

5×10^5 cells were seeded in 6-well plates containing antibiotic-free medium after enzyme digestion and cultured in a CO_2 incubator for 24 h. Transfection was performed in cells at 70%-80% confluence with small interfering ribonucleic acid (siRNA) using Lipofectamine 2000 (Invitrogen, United States) according to the manufacturer's instructions. siRNAs targeting HIF-2α were designed and synthesized by Sangon Biotech (Shanghai) Co., Ltd. Three siRNAs were tested and that with the highest efficiency of HIF-2α down-regulation was chosen. Briefly, siRNA and Lipofectamine 2000 were diluted with Opti-MEM medium (Invitrogen, United States) prior to the mixing and then cultured at room temperature for 20 min to allow the formation of a mixture of siRNA-Lipofectamine 2000. The mixture was added to each well, and culturing continued for 24 h. The medium was replaced with complete medium and incubated for an additional 24 h after hypoxia treatment. RNA was harvested to detect the expression of HIF-2α after 48 h by reverse transcription-PCR.

Real-time fluorescent quantitative PCR

Total RNA was isolated from MDA-MB-231 and MCF-7 cells with Trizol reagent (Invitrogen, United States) and the quality of RNA was detected by 1% agarose gel electrophoresis in strict accordance with the manual. 3μg of mRNA was used as template to reverse-transcribe into cDNA, and real-time fluorescent quantitative PCR was conducted utilizing Maxima SYB RGreen /ROX qPCR Master Mix (2X) (Fermentas, United States) and the ABI 7500 real-time PCR system. The $2^{-\Delta\Delta Ct}$ method was used to calculate the relative expression level of target genes. GAPDH as a housekeeping gene control was purchased from Sangon Biotech (Shanghai) Co., Ltd, and the specific primer sequences were designed using Primer 5. 0 software as follows: HIF-2α forward, 5′-GG TGAAAGTCTACAACAACTGCC-3′ and reverse, 5′-ATGGGTGCTGGATTGGTTC-3′; CD44 forward, 5′-CCAAGACACATTCCACCCCA-3′ and reverse, 5′-GCCAAGAGGGATGCCAAGAT-3′; GAPDH forward, 5′-TGGCACCCAGCACAATGAA-3′ and reverse 5′-CTAAGTCATAGTCCGC CTAGAAGCA-3′. The conditions for qPCR reactions were: 95 °C for 10 min, followed by 45 cycles of 15 s at 95 °C, 15 s at 57 °C, and 30 s at 72 °C. Melting curve analysis was performed to confirm the specificity of the target gene.

Flow cytometry

Briefly, MDA-MB-231 cells were washed once with PBS and enzymatically dissociated with trypsin-EDTA (Corning, Manassas, VA, United States). Detached cells were resuspended in PBS supplemented with 2% fetal bovine serum. The cell suspension at a density of 10^6 cells/100 μL were incubated with staining buffer containing monoclonal antibodies purchased from BD Biosciences (San Diego, CA, United States), including anti-human CD44-APC at a dilution of 1:40 and CD24-PE at a dilution of 1:40, for 30 to 40 min on ice, with IgG antibody labeled with APC and PE as isotype controls. Labeled cells were washed and resuspended in PBS, and analyzed on a Becton-Dickinson FACSCalibur flow cytometer. Specific CSC markers in control and HIF-2α siRNA transfected cells were detected.

TdT-mediated X-dUTP nick end labeling (TUNEL) assay

The effect of hypoxia treatment and downregulation HIF-2α on apoptosis of MDA-MB-231 cells was detected with a TUNEL assay kit following the manufacturer's instructions (Roche Molecular Diagnostics, Pleasanton, CA, United States). In brief, cells were seeded on glass coverslips, fixed with 4% paraformaldehyde in PBS, and permeated with 0.1% Triton X-100 in 0.1% sodium citrate for 2 min on ice, after which they were incubated with 50 μL reaction mixture in a humidified chamber at 37 °C for 1 h. Then, cells were washed with PBS three times and 4',6-diamidino-2-phenylindole staining was performed for 10 min at room temperature. Five random fields of each stained section were photographed under a fluorescence microscope (Olympus Corporation, Tokyo, Japan). The percentage of TUNEL-positive cells was determined by counting cells in at least eight fields and more than 500 cells in total.

Mammosphere formation assay

Following treatment, cells were harvested and dissociated into single cell suspension prior to filtration. Subsequently, cells were cultured in ultra-low attachment 96-well plates (Corning Incorporated, NY, United States) at a density of 1×10^5/mL. The serum-free DMEM/F-12 (HyClone, Logan, UT, United States) containing 2% B27 (Invitrogen, Carlsbed, CA, United States), 20 ng/mL b-FGF (Promega, United States), 20 ng/mL EGF (Promega, United States), and 5 μg/mL insulin was used for mammosphere culture. After culturing for 7-21 d, mammosphere were monitored and

the number of mammospheres was counted with an Olympus digital camera.

Western blot analysis

Cells were washed three times with ice-cold PBS and lysed in RIPA buffer (Beyotime, Shanghai, China) supplemented with 1% phosphatase inhibitor (Sigma-Aldrich), followed by centrifugation. The supernatant was harvested and protein concentration was determined using a bicinchoninic acid assay kit (Beyotime, Shanghai, China). Total proteins (10–30 μg) were subjected to 8%-15% sodium dodecyl sulfate-polyacrylamide gel electrophoresis. Then, the proteins were transferred to a polyvinylidene fluoride membrane (Millipore, United States), which was blocked with 5% BSA and then incubated with primary antibodies at 4 ˚C overnight. After washing, the membranes were incubated with an IgG antibody conjugated to horseradish peroxidase (dilution 1:2000) for 1 h at room temperature. Visualization of protein bands was performed with enhanced chemiluminescence solution (Thermo Fisher Scientific, Inc.), and GAPDH (Cell Signaling Technology, Danvers, United States) was used as a loading control. The primary antibodies were p-AKT (phosphor-ser473, dilution 1:500), AKT (dilution 1:500), p-mTOR (phosphor-ser2448, dilution 1:1000), and mTOR diluted to 1:1000 (Abcam, Cambridge, United Kingdom).

Statistical analysis

All data are represented as the mean ± standard deviation and analyzed with SPSS19.0 software. The independent *t*-test was used for two-group comparisons and one-way analysis of variance was applied to compare the means among three groups. Pairwise comparison was performed by the LSD test. $P < 0.05$ was considered to indicate a statistically significant difference.

RESULTS

Expression of HIF-2α and CD44 in different breast cancer patients

In this study, we analyzed HIF-2α and CD44 expression by immunohistochemical staining. The results showed that a high density of cancer cells positive for HIF-2α was observed in both TNBC and non-TNBC cells. CD44 was highly expressed in TNBC but lowly expressed in luminal breast cancer cells. The expression of HIF-2α in different molecular types of breast cancer cells was relatively consistent, while the expression of CD44 in different molecular types of breast cancer cells was different (Figure 1).

Immunofluorescent analysis for the expression of CD44 and HIF-2α in MCF-7 and MDA-MB-231 cells

After hypoxia treatment, immunofluorescence assay showed that HIF-2α was mainly expressed in the nucleus, while CD44 was mainly expressed on the cell membrane. It was found by image fusion that HIF-2α and CD44 were expressed almost in the same cell. The expression of HIF-2α and CD44 in MCF-7 was less than that in MDA-MB-231 cells (Figure 2).

HIF-2α and CD44 mRNA expression levels in MCF-7 and MDA-MB-231 cells after transfection

In contrast with normoxic control, the expression of HIF-2α and CD44 mRNAs in MDA-MB-231 cells was significantly increased after induction of hypoxia. HIF-2α siRNA transfection can lower the expression of HIF-2α and CD44 mRNAs in hypoxic cells, and the difference was statistically significant ($P < 0.05$). The expression of HIF-2α in MCF-7 cells treated with HIF-2α siRNA and hypoxia was higher than that in cells treated by hypoxia + negative-sequence control (NC), but there was no significant difference between the normoxic control and hypoxia cells ($P > 0.05$) (Figure 3).

HIF-2α silencing significantly reduces the $CD44^+/CD24^-$ population in MDA-MB-231 cells

To determine the effect of HIF-2α silencing on CSC properties, we assessed the percentage of CD44+/CD24− population in hypoxia with or without HIF-2α silencing by flow cytometry. As shown in Figure 4, the percentage of $CD44^+/CD24^-$ cells was 96.27% in the hypoxia group, and 84.02% in the hypoxia cells transfected with HIF-2α-siRNA. SiRNA-mediated HIF-2α depletion resulted in a reduction of $CD44^+/CD24^-$ population by 12.25%.

TUNEL assay to detect apoptotic cells

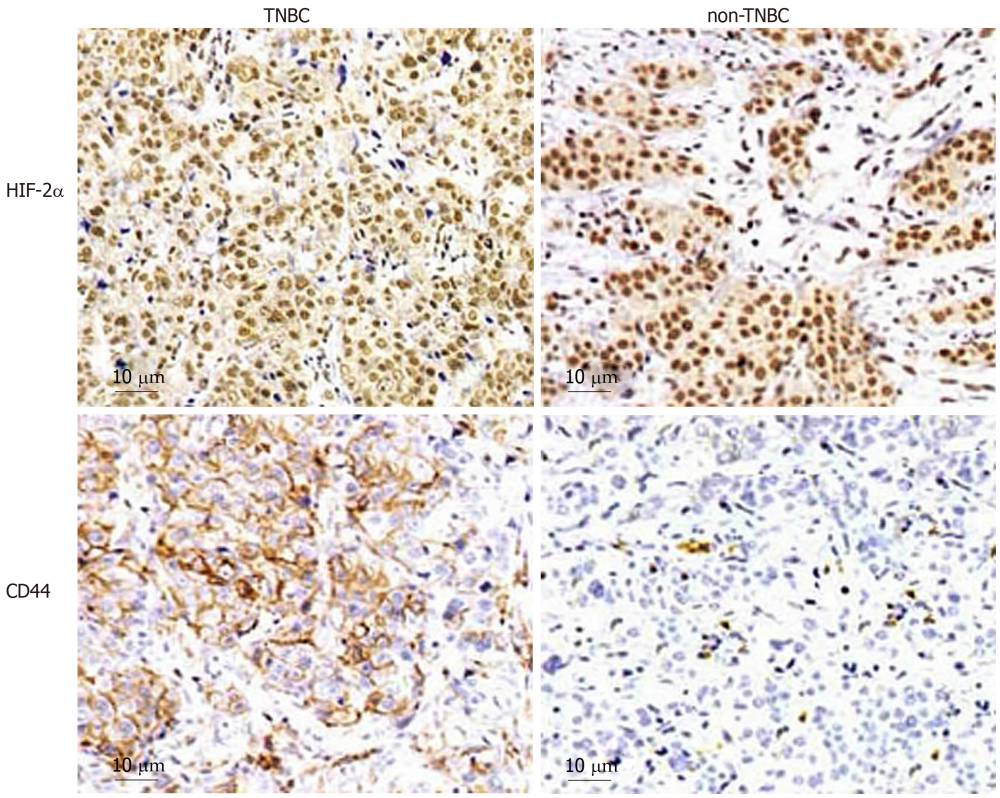

Figure 1 Expression of hypoxia-inducible factor-2α and CD44 in carcinoma tissues of triple-negative breast cancer and non-triple-negative breast cancer patients (×200). TNBC: Triple-negative breast cancer; HIF-2α: Hypoxia-inducible factor-2α.

To evaluate the effect of hypoxia and HIF-2α silencing on apoptosis *in vitro*, MDA-MB-231 cell apoptosis was detected using TUNEL assay. The results showed that the percentage of apoptotic cells was decreased under hypoxia compared to normoxic cells ($P < 0.05$). Further research found that transfection of HIF-2α–siRNA in MDA-MB-231 cells induced by hypoxia can increase the percentage of apoptotic cells than that in cells treated by hypoxia + NC, and the difference was statistically significant ($P < 0.05$), indicating that HIF-2α plays an important role in apoptosis of MDA-MB-231 cells (Figure 5).

Effect of HIF-2α on mammosphere formation efficiency (MFE) of MDA-MB-231 cells

From Figure 6, it is observed that mammospheres were successfully generated from MDA-MB-231 cells. In MDA-MB-231 cells, mammospheres appeared after 7 d of culture, and mammospheres of 100-200 μm in diameter formed and tended to attach after 21 d of culture. MFE of cells treated by hypoxia + NC and hypoxia + siRNA at 7 d was 0.32% ± 0.06% and 0.26% ± 0.05%, respectively. At the 21 d, MFE of the above cells was 0.33% ± 0.26% and 0.17% ± 0.09%, respectively, and the difference was statistically significant ($P < 0.05$). These data suggest that HIF-2α silencing significantly reduces mammosphere formation.

Effect of HIF-2α on the PI3K/AKT signaling pathway

PI3K/AKT/mTOR signaling is commonly activated in breast cancer and plays important roles in tumor invasion and metastasis. Therefore, in this study, the main signaling molecules of the PI3K-AKT-mTOR signaling pathway including AKT, mTOR, and their phosphorylation levels were identified by Western blot analysis. The results revealed that p-AKT and p-mTOR levels in MDA-MB-231 cells increased slightly under anoxic conditions, while decreased significantly with HIF-2α knockdown, and the difference was statistically significant ($P < 0.05$), which suggests that hypoxia could increase the HIF-2α level to promote stem phenotype conversion *via* the PI3K/AKT signaling pathway (Figure 7).

DISCUSSION

CSCs are considered as cells capable of highly proliferation, self-renewal, and multidirectional differentiation, which play an important role in tumorigenesis,

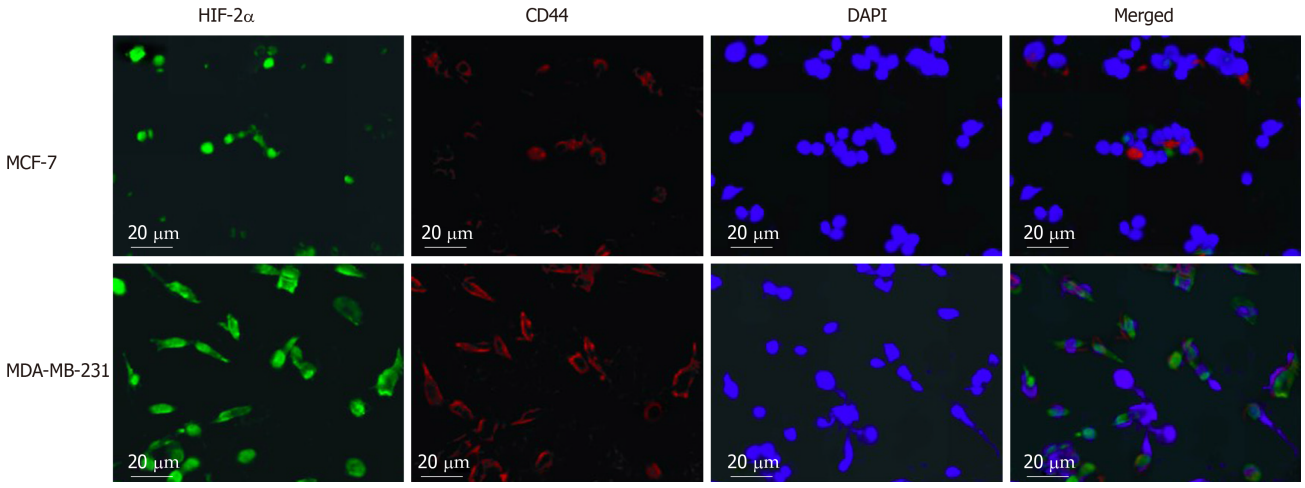

Figure 2 Expression of hypoxia-inducible factor-2α and CD44 in MCF-7 and MDA-MB-231 cells (×200). The expression of HIF-2α and CD44 in MDA-MB-231 cells was significantly higher than that in MCF-7 cells. HIF-2α: Hypoxia-inducible factor-2α; DAPI : 4',6-diamidino-2-phenylindole.

growth, invasion, metastasis, and recurrence[25-27]. Hypoxia can promote the dedifferentiation of differentiated cancer cells, enable cells to acquire stem cell characteristics, and enhance the invasiveness and tumorigenicity of cancer cells[28-30]. The expression of HIF-2α gene is positively correlated with the proliferation of breast cancer cells. A previous study found that HIFs and its target genes are highly expressed in TNBC[31]. Under hypoxic conditions, the expression of HIF-1α increased rapidly and generally decreased sharply within 2-12 h, while the expression of HIF-2α began to increase 48-72 h after hypoxia, and then continued to express steadily for about 2 wk[32-34]. Therefore, we believe that HIF-2α may play a more important role in tumors and other chronic hypoxic diseases. In this study, we found that HIF-2α was highly expressed in both TNBC and non-TNBC, and was higher in TNBC. This result is consistent with the findings of Goggins *et al*[35]. Further, clinical studies have shown that high expression of HIF-2α suggests a poor prognosis for both locally advanced breast cancer and early breast cancer patients[36-38].

The reduction of breast cancer recurrence rate and improvement of its cure rate in clinical practice are based on in-depth exploration of CSCs[39-41]. Therefore, this study analyzed the relationship between HIF-2α and CD44 by immunofluorescence after hypoxia treatment, and the results showed that HIF-2α and CD44 were expressed almost in the same cell, leading us to hypothesize that there is a close relationship between CD44 and HIF-2α. The latter may regulate the expression of the former, but the specific regulatory mechanism still needs to be further explored. Furthermore, RNA interference, flow cytometry, and TUNEL assays were applied to identify the effect of HIF-2α expression on the biological function of CSCs in breast cancer cells. In this experiment, it was found that the expression of HIF-2α mRNA in MDB-MB-231 and MCF-7 cells was significantly increased under hypoxic conditions, while significantly decreased after specific HIF-2α siRNA transfection, indicating successful cell transfection. Moreover, the results also showed that HIF-2α silencing can lower the expression of HIF-2α and CD44 mRNAs in hypoxic cells, suggesting that HIF-2α could affect the level of CD44.

In breast cancers, CSCs carry the phenotypic signature of being $CD24^{-}/CD44^{+}$[42]. Flow cytometry showed that the proportion of CD44 cells in hypoxia-induced cells was significantly lower than that in the hypoxia control group after HIF-2α down-regulation. The results confirmed that down-regulation of HIF-2α in hypoxic microenvironment can slow the formation of MDA-MB-231 tumor stem cells, and the results are consistent with those of Xie *et al*[43]. It is suggested that HIF-2α plays an important role in maintaining the stemness of CSCs. Alternatively, TUNEL assay showed that HIF-2α siRNA in MDA-MB-231 cells induced by hypoxia can increase the percentage of apoptotic cells, and high-level HIF-2α was believed to be linked to an increased risk of breast cancer recurrence and metastasis[44,45]. Invasion and metastasis are important factors affecting the prognosis of tumor patients. It was found that the percentage of apoptotic cells was decreased under hypoxic conditions, and increased after transfection of specific HIF-2α siRNA, which further confirms that HIF-2α can promote the migration and invasion of breast cancer cells and inhibit the apoptosis of breast cancer cells.

Activation of the PI3K/mTOR/mTOR signaling pathway is very common in breast cancer patients[46,47]. Whole-genome sequencing in ER-positive metastatic breast cancer

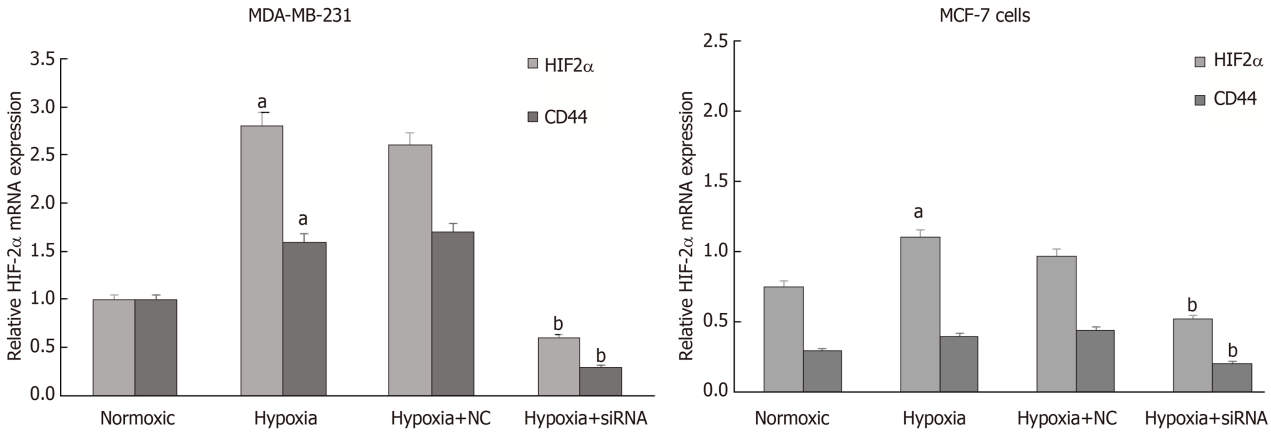

Figure 3 Expression of HIF-2α and CD44 mRNAs in human breast cancer cells after transfection. [a]*P* < 0.05 *vs* normoxia; *bP* < 0.05 *vs* hypoxia + NC. HIF-2α: Hypoxia-inducible factor-2α; NC: Negative-sequence control.

patients revealed frequent mutations in many genes. Sharma *et al*[48] showed that p7170, a dual inhibitor of PI3K/mTOR, has a strong inhibitory effect on proliferation of endocrine-sensitive and -resistant $ER^+/Her\text{-}2^-$ breast cancer cells. In this study, we hypothesized that HIF-2α silencing mediated by siRNA in human breast cancer MDA-MB-231 cells can inhibit the expression of CD44, thus inhibiting the expression of the intracellular p-AKT and p-mTOR, and the migration and invasion of cancer cells were suppressed.

In conclusion, down-regulation of HIF-2α expression can inhibit the stemness of human breast cancer MDA-MB-231 cells and promote apoptosis, and its mechanism may be related to the CD44/PI3K/AKT/mTOR signaling pathway, which is expected to be a target for the treatment of TNBC.

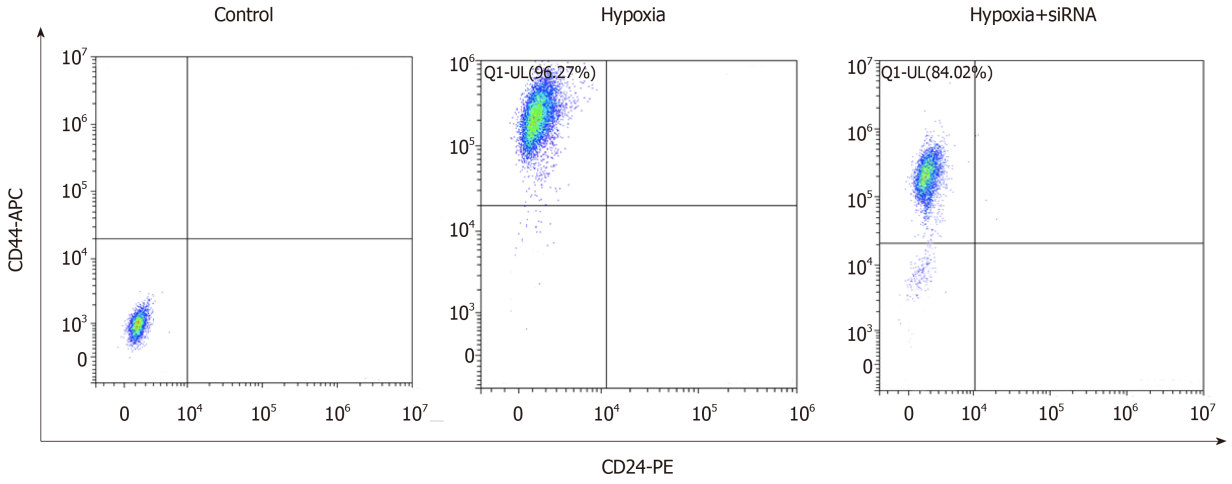

Figure 4 HIF-2α silencing reduces the CD44$^+$/CD24$^-$ population in MDA-MB-231 cells. Flow cytometry of the stem cell-associated cell surface markers CD44 and CD24 in hypoxia and HIF-2α-siRNA treated cells. HIF-2α: Hypoxia-inducible factor-2α.

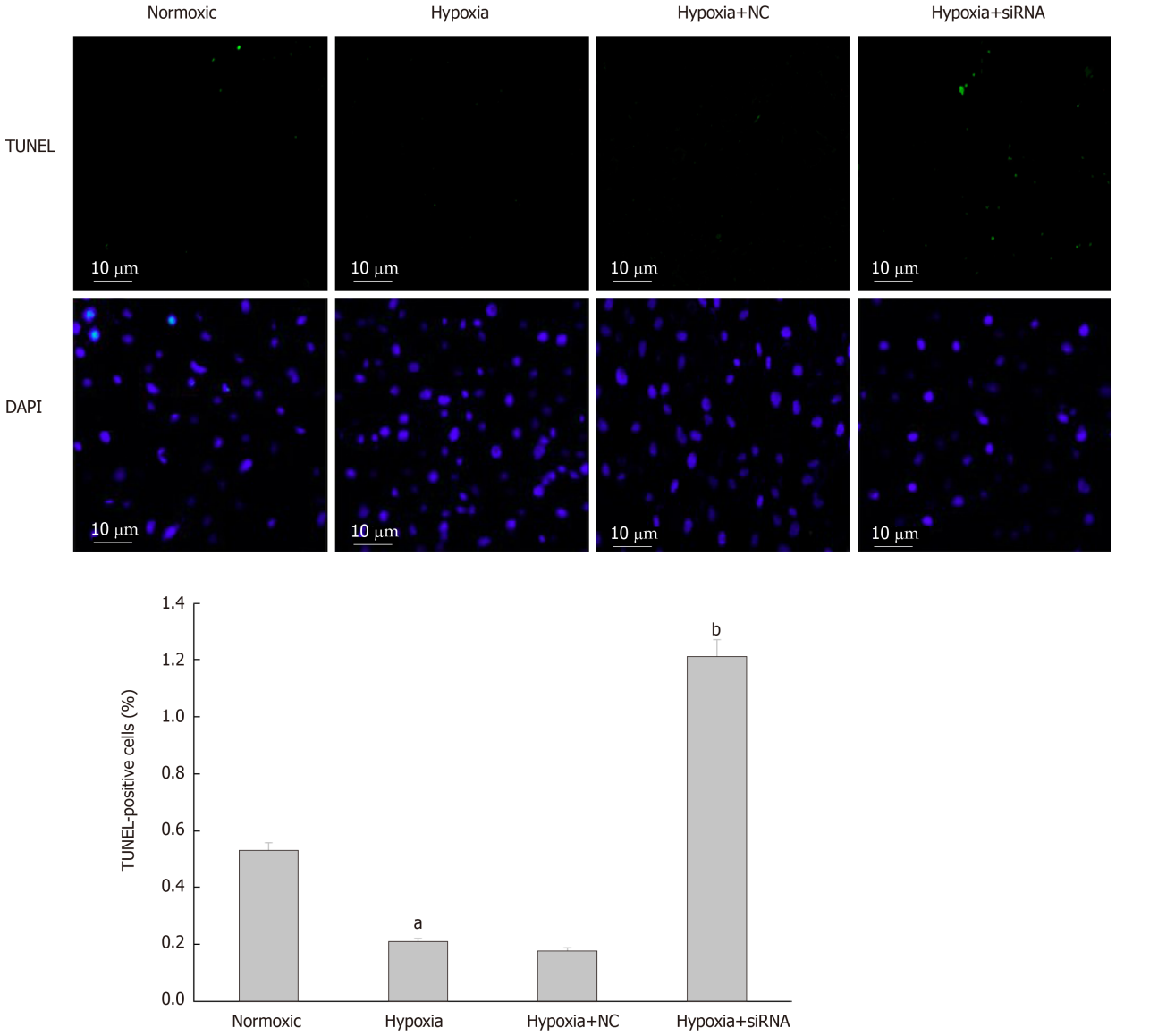

Figure 5 TUNEL assay of hypoxia-induced MDA-MB-231 cells after transfection (×200). Light green cells are TUNEL-positive staining cells. *aP* < 0.05 *vs* normoxia; *bP* < 0.01 *vs* hypoxia + NC. DAPI: 4',6-diamidino-2-phenylindole; NC: Negative-sequence control.

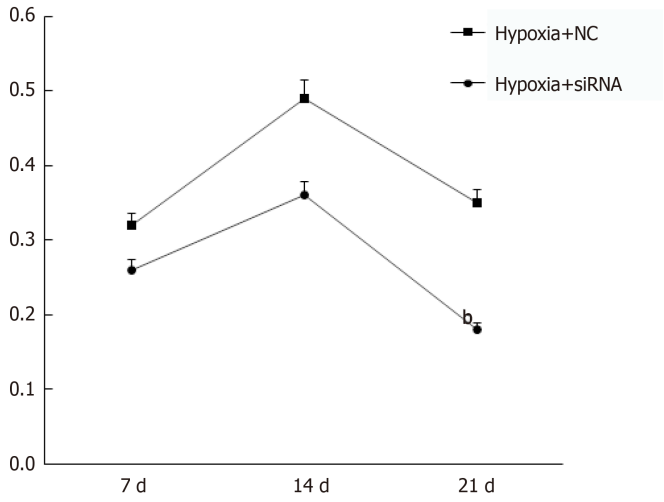

Figure 6 Quantification of mammosphere formation assay of MDA-MB-231 cells before and after transfection. Cells were cultured for 7-21 d under mammosphere culture conditions. *bP* < 0.01 *vs* hypoxia + NC. NC: Negative-sequence control.

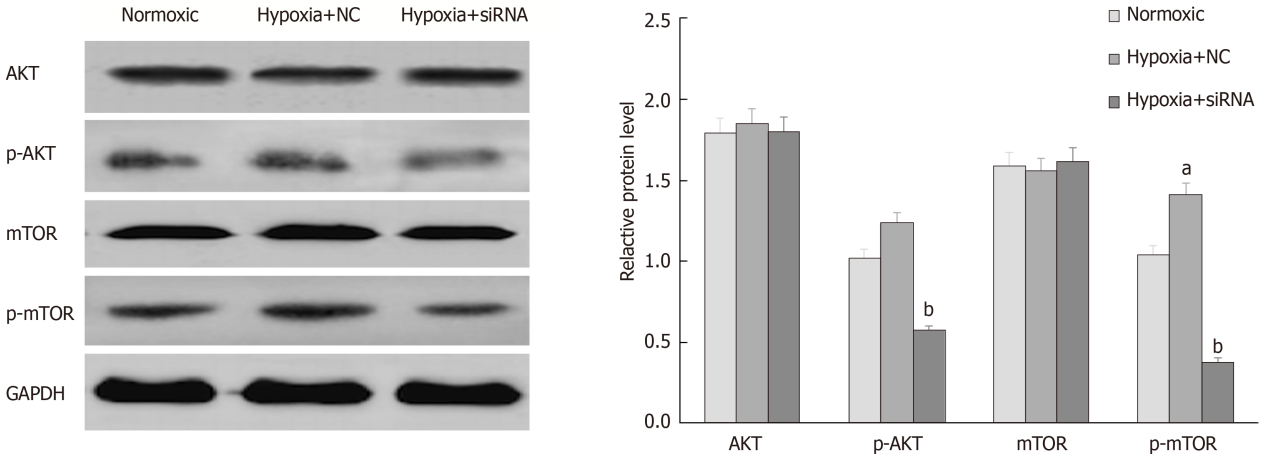

Figure 7 Effect of HIF-2α on the PI3K/AKT signaling pathway. In MDA-MB-231 cells induced by hypoxia, HIF-2α knockdown reduced the AKT and mTOR phosphorylation levels; *aP* < 0.05 *vs* normoxia; *bP* < 0.05 *vs* hypoxia + NC. PI3K: Phosphoinosmde-3-kinase; AKT: Protein-serine-threonine kinase; mTOR: Mammalian target of rapamycin; p-AKT: Phosphorylated AKT; p-mTOR: Phosphorylated mTOR; NC: Negative-sequence control.

ARTICLE HIGHLIGHTS

Research background

Breast cancer has a high degree of phenotype and functional heterogeneity, and the intratumoral variation is obvious. Traditional chemical and endocrine therapies are not effective in treating all cells in a tumor. Researchers have found a small group of highly tumorigenic cell populations in breast tumors. They have stem cell-like properties that are critical for tumorigenesis, progression, progression, and recurrence, and are closely associated with breast cancer metastasis. In the development of tumors, hypoxia-inducible factor-2α (HIF-2α) plays an important role in enhancing the drug resistance and migration of breast cancer stem cells. At present, whether the expression of cancer stem cells can be regulated by interfering with the expression of HIF-2α has not been reported in the literature.

Research motivation

Due to the rapid growth of triple-negative breast cancer (TNBC), and the lack of self-vascular supply to meet the needs of rapidly growing tumor cells, a hypoxic environment is gradually formed. In the long-term chronic hypoxia of tumors, the major regulatory factor is HIF-2α, which increases the malignant biological behavior of tumors by activating its downstream target genes. As a marker of breast cancer stem cells, CD44 is closely related to the invasion and metastasis of tumor cells. Previous studies have found that HIF-2α can regulate the expression of the cell adhesion molecule CD44, but the relationship between the two and the regulatory mechanism are not clear.

Research objectives
This study analyzed the relationship between the expression of HIF-2α and CD44 in patients with TNBC and non-TNBC. Then, the effects of HIF-2α on the expression of CD44 in human breast cancer cell lines MCF-7 and MDA-MB-231 and its possible mechanism were explored.

Research methods
We analyzed the expression of HIF-2α and CD44 in patients with TNBC (n = 29) and non-TNBC (n = 20) using immunohistochemistry. The co-expression of HIF-2α and CD44 in MDA-MB-231 cells and MCF-7 cells was characterized by double-labeling immunofluorescence. The impact of siRNA-mediated HIF-2α knockdown on the CSCs and apoptosis of MDA-MB-231 cells was detected by real-time fluorescent quantitative PCR, flow cytometry, TUNEL, and mammosphere formation assays. Data were statistically analyzed using the independent t-test and one-way analysis of variance followed by LSD pairwise comparison tests.

Research results
Our data showed that HIF-2α had a high level expression in both TNBC and non-TNBC, and HIF-2α and CD44 were located in the same cell. Functionally, HIF-2α silencing significantly reduced the expression of HIF-2α and CD44 mRNAs, but increased cell apoptosis. Flow cytometry and mammosphere formation assay results indicated downregulation of CD44+/CD24− population ($P < 0.05$) and mammosphere formation upon HIF-2α suppression in hypoxic MDA-MB-231 cells. Moreover, HIF-2α siRNA transfection could decrease the levels of phosphorylated protein-serine-threonine kinase (p-AKT) and phosphorylated mammalian target of rapamycin (p-mTOR) in MDA-MB-231 cells.

Research conclusions
HIF-2α plays an important role in the stemness and apoptosis of human breast cancer MDA-MB-231 cells *via* the CD44/PI3K/AKT/mTOR signaling pathway, thus emerging as a target for the treatment of TNBC.

Research perspectives
The molecular regulation mechanism of CSCs in TNBC tissues is still unclear. Inhibition of CSC activation or elimination of CSCs has become a difficult and critical step in the current treatment of TNBC. In this study, the effect of HIF-2α on CSCs was explored by clinicopathological specimens and *in vitro* experiments, and the mechanism of action was preliminarily analyzed. The conclusions of this study have important clinical and pathological significance for understanding the mechanism of CSC activation in TNBC tissues, blocking the signaling pathway of HIF-2α, inhibiting the malignant progression of TNBC, and improving the prognosis of patients.

REFERENCES

1 **Templeton AJ**, Ace O, McNamara MG, Al-Mubarak M, Vera-Badillo FE, Hermanns T, Seruga B, Ocaña A, Tannock IF, Amir E. Prognostic role of platelet to lymphocyte ratio in solid tumors: a systematic review and meta-analysis. *Cancer Epidemiol Biomarkers Prev* 2014; **23**: 1204-1212 [PMID: 24793958 DOI: 10.1158/1055-9965.EPI-14-0146]

2 **Neil-Sztramko SE**, Winters-Stone KM, Bland KA, Campbell KL. Updated systematic review of exercise studies in breast cancer survivors: attention to the principles of exercise training. *Br J Sports Med* 2019; **53**: 504-512 [PMID: 29162619 DOI: 10.1136/bjsports-2017-098389]

3 **Brandão T**, Schulz MS, Matos PM. Psychological adjustment after breast cancer: a systematic review of longitudinal studies. *Psychooncology* 2017; **26**: 917-926 [PMID: 27440317 DOI: 10.1002/pon.4230]

4 **Ennour-Idrissi K**, Maunsell E, Diorio C. Telomere Length and Breast Cancer Prognosis: A Systematic Review. *Cancer Epidemiol Biomarkers Prev* 2017; **26**: 3-10 [PMID: 27677729 DOI: 10.1158/1055-9965.EPI-16-0343]

5 **Lee JD**, Cai Q, Shu XO, Nechuta SJ. The Role of Biomarkers of Oxidative Stress in Breast Cancer Risk and Prognosis: A Systematic Review of the Epidemiologic Literature. *J Womens Health (Larchmt)* 2017; **26**: 467-482 [PMID: 28151039 DOI: 10.1089/jwh.2016.5973]

6 **Terranova CO**, Protani MM, Reeves MM. Overall Dietary Intake and Prognosis after Breast Cancer: A Systematic Review. *Nutr Cancer* 2018; **70**: 153-163 [PMID: 29308928 DOI: 10.1080/01635581.2018.1412478]

7 **Dent R**, Valentini A, Hanna W, Rawlinson E, Rakovitch E, Sun P, Narod SA. Factors associated with breast cancer mortality after local recurrence. *Curr Oncol* 2014; **21**: e418-e425 [PMID: 24940101 DOI: 10.3747/co.21.1563]

8 **Poggio F**, Bruzzone M, Ceppi M, Pondé NF, La Valle G, Del Mastro L, de Azambuja E, Lambertini M. Platinum-based neoadjuvant chemotherapy in triple-negative breast cancer: a systematic review and meta-analysis. *Ann Oncol* 2018; **29**: 1497-1508 [PMID: 29873695 DOI: 10.1093/annonc/mdy127]

9 **Li L**, Zhong Y, Zhang H, Yu H, Huang Y, Li Z, Chen G, Hua X. Association between oral contraceptive use as a risk factor and triple-negative breast cancer: A systematic review and meta-analysis. *Mol Clin Oncol* 2017; **7**: 76-80 [PMID: 28685080 DOI: 10.3892/mco.2017.1259]

10 **Dent R**, Trudeau M, Pritchard KI, Hanna WM, Kahn HK, Sawka CA, Lickley LA, Rawlinson E, Sun P, Narod SA. Triple-negative breast cancer: clinical features and patterns of recurrence. *Clin Cancer Res* 2007; **13**: 4429-4434 [PMID: 17671126 DOI: 10.1158/1078-0432.CCR-06-3045]

11 **Pindiprolu SKSS**, Krishnamurthy PT, Chintamaneni PK. Pharmacological targets of breast cancer stem cells: a review. *Naunyn Schmiedebergs Arch Pharmacol* 2018; **391**: 463-479 [PMID: 29476201 DOI: 10.1007/s00210-018-1479-3]

12 **Mansoori M**, Madjd Z, Janani L, Rasti A. Circulating cancer stem cell markers in breast carcinomas: a

systematic review protocol. *Syst Rev* 2017; **6**: 262 [PMID: 29258583 DOI: 10.1186/s13643-017-0660-y]
13 **Chen X**, Liu Q, Song E. Mammary stem cells: angels or demons in mammary gland? *Signal Transduct Target Ther* 2017; **2**: 16038 [PMID: 29263909 DOI: 10.1038/sigtrans.2016.38]
14 **Liu M**, Liu Y, Deng L, Wang D, He X, Zhou L, Wicha MS, Bai F, Liu S. Transcriptional profiles of different states of cancer stem cells in triple-negative breast cancer. *Mol Cancer* 2018; **17**: 65 [PMID: 29471829 DOI: 10.1186/s12943-018-0809-x]
15 **Ren D**, Zhu X, Kong R, Zhao Z, Sheng J, Wang J, Xu X, Liu J, Cui K, Zhang XH, Zhao H, Wong STC. Targeting Brain-Adaptive Cancer Stem Cells Prohibits Brain Metastatic Colonization of Triple-Negative Breast Cancer. *Cancer Res* 2018; **78**: 2052-2064 [PMID: 29567857 DOI: 10.1158/0008-5472.CAN-17-2994]
16 **Shi P**, Liu W, Tala, Wang H, Li F, Zhang H, Wu Y, Kong Y, Zhou Z, Wang C, Chen W, Liu R, Chen C. Metformin suppresses triple-negative breast cancer stem cells by targeting KLF5 for degradation. *Cell Discov* 2017; **3**: 17010 [PMID: 28480051 DOI: 10.1038/celldisc.2017.10]
17 **Lu H**, Samanta D, Xiang L, Zhang H, Hu H, Chen I, Bullen JW, Semenza GL. Chemotherapy triggers HIF-1-dependent glutathione synthesis and copper chelation that induces the breast cancer stem cell phenotype. *Proc Natl Acad Sci U S A* 2015; **112**: E4600-E4609 [PMID: 26229077 DOI: 10.1073/pnas.1513433112]
18 **Samanta D**, Gilkes DM, Chaturvedi P, Xiang L, Semenza GL. Hypoxia-inducible factors are required for chemotherapy resistance of breast cancer stem cells. *Proc Natl Acad Sci U S A* 2014; **111**: E5429-E5438 [PMID: 25453096 DOI: 10.1073/pnas.1421438111]
19 **Carroll VA**, Ashcroft M. Role of hypoxia-inducible factor (HIF)-1alpha versus HIF-2alpha in the regulation of HIF target genes in response to hypoxia, insulin-like growth factor-I, or loss of von Hippel-Lindau function: implications for targeting the HIF pathway. *Cancer Res* 2006; **66**: 6264-6270 [PMID: 16778202 DOI: 10.1158/0008-5472.CAN-05-2519]
20 **Kwak JH**, Lee NH, Lee HY, Hong IS, Nam JS. HIF2α/EFEMP1 cascade mediates hypoxic effects on breast cancer stem cell hierarchy. *Oncotarget* 2016; **7**: 43518-43533 [PMID: 27270657 DOI: 10.18632/oncotarget.9846]
21 **Kim RJ**, Park JR, Roh KJ, Choi AR, Kim SR, Kim PH, Yu JH, Lee JW, Ahn SH, Gong G, Hwang JW, Kang KS, Kong G, Sheen YY, Nam JS. High aldehyde dehydrogenase activity enhances stem cell features in breast cancer cells by activating hypoxia-inducible factor-2α. *Cancer Lett* 2013; **333**: 18-31 [PMID: 23174107 DOI: 10.1016/j.canlet.2012.11.026]
22 **Johansson E**, Grassi ES, Pantazopoulou V, Tong B, Lindgren D, Berg TJ, Pietras EJ, Axelson H, Pietras A. CD44 Interacts with HIF-2α to Modulate the Hypoxic Phenotype of Perinecrotic and Perivascular Glioma Cells. *Cell Rep* 2017; **20**: 1641-1653 [PMID: 28813675 DOI: 10.1016/j.celrep.2017.07.049]
23 **Covello KL**, Kehler J, Yu H, Gordan JD, Arsham AM, Hu CJ, Labosky PA, Simon MC, Keith B. HIF-2alpha regulates Oct-4: effects of hypoxia on stem cell function, embryonic development, and tumor growth. *Genes Dev* 2006; **20**: 557-570 [PMID: 16510872 DOI: 10.1101/gad.1399906]
24 **Koh MY**, Lemos R, Liu X, Powis G. The hypoxia-associated factor switches cells from HIF-1α- to HIF-2α-dependent signaling promoting stem cell characteristics, aggressive tumor growth and invasion. *Cancer Res* 2011; **71**: 4015-4027 [PMID: 21512133 DOI: 10.1158/0008-5472.CAN-10-4142]
25 **Luo M**, Clouthier SG, Deol Y, Liu S, Nagrath S, Azizi E, Wicha MS. Breast cancer stem cells: current advances and clinical implications. *Methods Mol Biol* 2015; **1293**: 1-49 [PMID: 26040679 DOI: 10.1007/978-1-4939-2519-3_1]
26 **Bettaieb A**, Paul C, Plenchette S, Shan J, Chouchane L, Ghiringhelli F. Precision medicine in breast cancer: reality or utopia? *J Transl Med* 2017; **15**: 139 [PMID: 28623955 DOI: 10.1186/s12967-017-1239-z]
27 **Lowry MC**, Gallagher WM, O'Driscoll L. The Role of Exosomes in Breast Cancer. *Clin Chem* 2015; **61**: 1457-1465 [PMID: 26467503 DOI: 10.1373/clinchem.2015.240028]
28 **Semenza GL**. Hypoxia-inducible factors: coupling glucose metabolism and redox regulation with induction of the breast cancer stem cell phenotype. *EMBO J* 2017; **36**: 252-259 [PMID: 28007895 DOI: 10.15252/embj.201695204]
29 **Schito L**, Rey S. Hypoxic pathobiology of breast cancer metastasis. *Biochim Biophys Acta Rev Cancer* 2017; **1868**: 239-245 [PMID: 28526262 DOI: 10.1016/j.bbcan.2017.05.004]
30 **Liu J**, Zhang C, Zhao Y, Yue X, Wu H, Huang S, Chen J, Tomsky K, Xie H, Khella CA, Gatza ML, Xia D, Gao J, White E, Haffty BG, Hu W, Feng Z. Parkin targets HIF-1α for ubiquitination and degradation to inhibit breast tumor progression. *Nat Commun* 2017; **8**: 1823 [PMID: 29180628 DOI: 10.1038/s41467-017-01947-w]
31 **Lv Y**, Chen C, Zhao B, Zhang X. Regulation of matrix stiffness on the epithelial-mesenchymal transition of breast cancer cells under hypoxia environment. *Naturwissenschaften* 2017; **104**: 38 [PMID: 28382476 DOI: 10.1007/s00114-017-1461-9]
32 **Schöning JP**, Monteiro M, Gu W. Drug resistance and cancer stem cells: the shared but distinct roles of hypoxia-inducible factors HIF1α and HIF2α. *Clin Exp Pharmacol Physiol* 2017; **44**: 153-161 [PMID: 27809360 DOI: 10.1111/1440-1681.12693]
33 **Shan C**, Zheng Y, Wang M, Lin S, Tian T, Deng Y, Xu P, Hao Q, Wu Y, Yang T, Guo Y, Dai Z. Polymorphisms in HIFs and breast cancer sutarsceptibility in Chinese women: a case-control study. *Biosci Rep* 2018; **38** [PMID: 30135144 DOI: 10.1042/BSR20180950]
34 **Påhlman S**, Lund LR, Jögi A. Differential HIF-1α and HIF-2α Expression in Mammary Epithelial Cells during Fat Pad Invasion, Lactation, and Involution. *PLoS One* 2015; **10**: e0125771 [PMID: 25955753 DOI: 10.1371/journal.pone.0125771]
35 **Goggins E**, Kakkad S, Mironchik Y, Jacob D, Wildes F, Krishnamachary B, Bhujwalla ZM. Hypoxia Inducible Factors Modify Collagen I Fibers in MDA-MB-231 Triple Negative Breast Cancer Xenografts. *Neoplasia* 2018; **20**: 131-139 [PMID: 29247885 DOI: 10.1016/j.neo.2017.11.010]
36 **Regan Anderson TM**, Ma SH, Raj GV, Cidlowski JA, Helle TM, Knutson TP, Krutilina RI, Seagroves TN, Lange CA. Breast Tumor Kinase (Brk/PTK6) Is Induced by HIF, Glucocorticoid Receptor, and PELP1-Mediated Stress Signaling in Triple-Negative Breast Cancer. *Cancer Res* 2016; **76**: 1653-1663 [PMID: 26825173 DOI: 10.1158/0008-5472.CAN-15-2510]
37 **Bharti SK**, Mironchik Y, Wildes F, Penet MF, Goggins E, Krishnamachary B, Bhujwalla ZM. Metabolic consequences of HIF silencing in a triple negative human breast cancer xenograft. *Oncotarget* 2018; **9**: 15326-15339 [PMID: 29632647 DOI: 10.18632/oncotarget.24569]
38 **Karousou E**, Misra S, Ghatak S, Dobra K, Götte M, Vigetti D, Passi A, Karamanos NK, Skandalis SS. Roles and targeting of the HAS/hyaluronan/CD44 molecular system in cancer. *Matrix Biol* 2017; **59**: 3-22

[PMID: 27746219 DOI: 10.1016/j.matbio.2016.10.001]
39 **Yang F**, Xu J, Tang L, Guan X. Breast cancer stem cell: the roles and therapeutic implications. *Cell Mol Life Sci* 2017; **74**: 951-966 [PMID: 27530548 DOI: 10.1007/s00018-016-2334-7]
40 **Schwarz-Cruz Y Celis A**, Espinosa M, Maldonado V, Melendez-Zajgla J. Advances in the knowledge of breast cancer stem cells. A review. *Histol Histopathol* 2016; **31**: 601-612 [PMID: 26715540 DOI: 10.14670/HH-11-718]
41 **Zhang L**, Wen X, Li M, Li S, Zhao H. Targeting cancer stem cells and signaling pathways by resveratrol and pterostilbene. *Biofactors* 2018; **44**: 61-68 [PMID: 29205560 DOI: 10.1002/biof.1398]
42 **Goyette S**, Liang Y, Mafuvadze B, Cook MT, Munir M, Hyder SM. Natural and synthetic progestins enrich cancer stem cell-like cells in hormone-responsive human breast cancer cell populations in vitro. *Breast Cancer (Dove Med Press)* 2017; **9**: 347-357 [PMID: 28579829 DOI: 10.2147/BCTT.S135371]
43 **Xie G**, Liu Y, Yao Q, Zheng R, Zhang L, Lin J, Guo Z, Du S, Ren C, Yuan Q, Yuan Y. Hypoxia-induced angiotensin II by the lactate-chymase-dependent mechanism mediates radioresistance of hypoxic tumor cells. *Sci Rep* 2017; **7**: 42396 [PMID: 28205588 DOI: 10.1038/srep42396]
44 **Fuady JH**, Gutsche K, Santambrogio S, Varga Z, Hoogewijs D, Wenger RH. Estrogen-dependent downregulation of hypoxia-inducible factor (HIF)-2α in invasive breast cancer cells. *Oncotarget* 2016; **7**: 31153-31165 [PMID: 27105516 DOI: 10.18632/oncotarget.8866]
45 **Shiraishi A**, Tachi K, Essid N, Tsuboi I, Nagano M, Kato T, Yamashita T, Bando H, Hara H, Ohneda O. Hypoxia promotes the phenotypic change of aldehyde dehydrogenase activity of breast cancer stem cells. *Cancer Sci* 2017; **108**: 362-372 [PMID: 28012234 DOI: 10.1111/cas.13147]
46 **Deng L**, Chen J, Zhong XR, Luo T, Wang YP, Huang HF, Yin LJ, Qiu Y, Bu H, Lv Q, Zheng H. Correlation between activation of PI3K/AKT/mTOR pathway and prognosis of breast cancer in Chinese women. *PLoS One* 2015; **10**: e0120511 [PMID: 25816324 DOI: 10.1371/journal.pone.0120511]
47 **Pierobon M**, Ramos C, Wong S, Hodge KA, Aldrich J, Byron S, Anthony SP, Robert NJ, Northfelt DW, Jahanzeb M, Vocila L, Wulfkuhle J, Gambara G, Gallagher RI, Dunetz B, Hoke N, Dong T, Craig DW, Cristofanilli M, Leyland-Jones B, Liotta LA, O'Shaughnessy JA, Carpten JD, Petricoin EF. Enrichment of PI3K-AKT-mTOR Pathway Activation in Hepatic Metastases from Breast Cancer. *Clin Cancer Res* 2017; **23**: 4919-4928 [PMID: 28446508 DOI: 10.1158/1078-0432.CCR-16-2656]
48 **Sharma VR**, Gupta GK, Sharma AK, Batra N, Sharma DK, Joshi A, Sharma AK. PI3K/Akt/mTOR Intracellular Pathway and Breast Cancer: Factors, Mechanism and Regulation. *Curr Pharm Des* 2017; **23**: 1633-1638 [PMID: 27848885 DOI: 10.2174/1381612823666161116125218]

Published By Baishideng Publishing Group Inc
7041 Koll Center Parkway, Suite 160, Pleasanton, CA 94566, USA
Telephone: +1-925-2238242
E-mail: bpgoffice@wjgnet.com
Help Desk: https://www.f6publishing.com/helpdesk
https://www.wjgnet.com